8-4-2015

Spectrally Based Material Color Equivalency: Modeling and Manipulation

Maxim W. Derhak

Spectrally Based Material Color Equivalency: Modeling and Manipulation

Maxim W Derhak

August 4, 2015
Version: 1.0

Rochester Institute of Technology

R·I·T | College of Science | MCSL

College of Science
Program of Color Science
Munsell Color Science Laboratory

PhD Dissertation

A Dissertation Submitted in
Partial Fulfillment of the Requirements for the
Degree of Doctorate of Science in Color Science

Spectrally Based Material Color Equivalency: Modeling and Manipulation

Maxim W Derhak

August 4, 2015

Signature of Author _____

Accepted by _____

Dr. Mark Fairchild Date

Graduate Program Director

Maxim W Derhak
Spectrally Based Material Color Equivalency: Modeling and Manipulation
PhD Dissertation, August 4, 2015
Advisor: Roy S. Berns
Committee Chair: David Ross
Committee Members: Mark Fairchild and Joe Geigel

Rochester Institute of Technology
College of Science
1 Lomb Memorial Dr
14623 and Rochester

COLLEGE OF SCIENCE
ROCHESTER INSTITUTE OF TECHNOLOGY
ROCHESTER, NEW YORK

CERTIFICATE OF APPROVAL

Ph.D. DEGREE DISSERTATION

The Ph.D. Degree Dissertation of Maxim W Derhak
has been examined and approved by the
committee as satisfactory for the
dissertation required for the
Ph.D. degree in Color Science

David Ross, Chair

Roy S. Berns, Advisor

Mark Fairchild

Joe Geigel

Date

“Some day we’ll find it – The rainbow connection – The lovers, the dreamers, and me”

— Kermit The Frog

Dedication

This dissertation is dedicated to my beloved wife, Staci, and my dearest children, Krystian, Kody, Auralia, Kameron, Karter, and Anya who have stood behind me and supported me in this nearly Quixotic adventure resulting in multiple cross-country moves with many, many evenings, weekends, and days where I was unavailable due to the pressures of school and/or work.

Abstract

A spectrally based normalization methodology (Wpt normalization) for linearly transforming cone excitations or sensor values (sensor excitations) to a representation that preserves the perceptive concepts of lightness, chroma and hue is proposed resulting in a color space with the axes labeled W, p, t. Wpt (pronounced “Waypoint") has been demonstrated to be an effective material color equivalency space that provides the basis for defining Material Adjustment Transforms that predict the changes in sensor excitations of material spectral reflectance colors due to variations in observer or illuminant. This is contrasted with Chromatic Adaptation Transforms that predict color appearance as defined by corresponding color experiments. Material color equivalency as provided by Wpt and Wpt normalization forms the underlying foundation of this doctoral research. A perceptually uniform material color equivalency space (“Waypoint Lab" or WLab) was developed that represents a non-linear transformation of Wpt coordinates, and Euclidean WLab distances were found to not be statistically different from $\Delta E^{\star}{}_{94}$ and ΔE_{00} color differences. Sets of Wpt coordinates for variations in reflectance, illumination, or observers were used to form the basis of defining Wpt shift manifolds. WLab distances of corresponding points within or between these manifolds were utilized to define metrics for color inconstancy, metamerism, observer rendering, illuminant rendering, and differences in observing conditions. Spectral estimation and manipulation strategies are presented that preserve various aspects of “Wpt shift potential" as represented by changes in Wpt shift manifolds. Two methods were explored for estimating Wpt normalization matrices based upon direct utilization of sensor excitations, and the use of a Wpt based Material Adjustment Transform to convert Cone Fundamentals to ”XYZ-like" Color Matching Functions was investigated and contrasted with other methods such as direct regression and prediction of a common color matching primaries. Finally, linear relationships between Wpt and spectral reflectances were utilized to develop approaches for spectral estimation and spectral manipulation within a general spectral reflectance manipulation framework – thus providing the ability to define and achieve “spectrally preferred" color rendering objectives. The presented methods of spectral estimation, spectral manipulation, and material adjustment where utilized to: define spectral reflectances for Munsell colors that minimize Wpt shift potential; manipulate spectral reflectances of actual printed characterization data sets to achieve colorimetry of reference printing conditions; and lastly to demonstrate the spectral estimation and manipulation of spectral reflectances using images and spectrally based profiles within an iccMAX color management workflow.

Acknowledgments

I would like to thank Dr. Roy S. Berns for first of all agreeing to be my advisor, and then helping me as a engineering practitioner to organize and present my ideas in an academic fashion. His patience with me has been greatly appreciated. I have learned much under his tutelage, and found his sage wisdom to be rock solid as I have often had to take basic ideas and start over in my approach at presenting things more academically.

I would like to thank the other members on my Ph.D. Committee – Mark Fairchild, Joe Geigel, and David Ross – for their understanding, support, and useful insights into making this dissertation a reality.

I would like to thank my parents who encouraged me in my intense curiosity about the world around me, enabling me to ask questions about how things work and relate to one another.

I'm thankful for Dr. Maria Helguera for believing in me enough to recommend me as a graduate candidate as I began pursing a Masters in Imaging Science at RIT.

I would like to thank Dr. Mitchell Rosen for believing in me and encouraging me to pursue a Ph.D. in Color Science.

I am extremely grateful for both the financial and moral support given to me by my employers and co-workers at Onyx Graphics Inc. Kendall Madsen was very supportive of me when I came in and proposed to move across the country, pursue a Ph.D. and still remain a productive member of the development team at ONYX. He believed it was possible and helped to ensure that I would receive continued support after he left the company. His successor – Jeff Despain – has also been gracious and supportive as well. Without their support I doubt this accomplishment would have been possible.

I'm thankful for Rohit Patil who helped me as a co-worker at Onyx in my first year in the MCSL Ph.D. program. He was very helpful in discussing things with me, reading papers, and offering helpful suggestions. I still think of him as a valuable friend and confidant even though he has moved on to pursue other interests.

I would like to thank all my friends and associates in the International Color Consortium (ICC) who have been very supportive and patient as I have hinted at what I was working on without

going into too many details. Many of the concepts that went into iccMAX during the official ICC meetings as well as after hour dinner discussions helped to provide focus for this research.

I would like to thank Jen Kruschwitz for finding the Latex template used for this dissertation.

I would like to thank Bob Hallam for providing me an image for spectral manipulation (even though it got cut out in the final version), and Mike Rodriguez for the spectral measurement data and reference printing colorimetry used for my spectral manipulation examples.

I would like to thank Sean McLeavy for graciously reviewing the entirety of this document and providing feedback.

I'm thankful for the knowledge and wisdom bestowed by the faculty and staff of the Munsell Color Science Lab and College of Imaging Science at RIT for instructing and preparing me to accomplish great things.

Finally, I would like to thank my friends and colleagues in the Munsell Color Science Laboratory for their often spontaneous comments, direction, inspirations, debates, and encouragement as I have ploddingly worked towards completion of this research. As this has been a part time venture for me, nearly two groups of students have passed through the program during the course of my studies.

Contents

List of Figures

List of Tables

Abbreviations

APC	**A**ctual **P**rinting **C**ondition
CAM	**C**olor **A**ppearance **M**odel
CAT	**C**hromatic **A**daptation **T**ransform
CCT	**C**orrelated **C**olor **T**emperature
CF	**C**one **F**undamental
CII	**C**olor **I**nconstancy **I**ndex
CMF	**C**olor **M**atching **F**unction
CMYK	**C**yan **M**agenta **Y**ellow Blac**k**
CR	**C**haracteristic **R**eflectance
HVS	**H**uman **V**isual **S**ystem
IRE	**I**lluminant **R**endering **E**quivalency
LUT	**L**ook **U**p **T**able
MAT	**M**aterial **A**djustment **T**ransform
MBC	**M**unsell **B**ook of **C**olor
MSP	**M**aterial **S**hift **P**otential
MMOCD	**M**ean **M**etameric **O**bject **C**olor **D**ifference
MOII	**M**ean **O**bject **I**nconstancy **I**ndex
OHSI	**O**bject **H**ue **S**imilarity **I**ndex
OMI	**O**bject **M**etamer **I**ndex
OCE	**O**bserving **C**onditions **E**quivalency
OME	**O**bserver **M**atching **E**quivalency
PCC	**P**rofile **C**onnection **C**onditions
PCS	**P**rofile **C**onnection **S**pace
PRD	**P**erfect **R**eflecting **D**iffusor
RGB	**R**ed **G**reen **B**lue
RPC	**R**eference **P**rinting **C**ondition
SAT	**S**ensor **A**djustment **T**ransform
SPD	**S**pectral **P**ower **D**istribution
SSF	**S**ensor **S**ensitvity **F**unction
WNME	**W**pt **N**ormalization **M**atrix **E**quivalency
WSM	**W**pt **S**hift **M**anifold

1 Introduction

1.1 Preface, Problem Statement, and Motivation

Colorimetry (and to a large part – color science) is based upon color matching experiments that led to the CIE 1931 Standard Observer for a two degree viewing field and the CIE 1964 Standard Observer for a ten degree viewing field [Wyszecki and Stiles, 2000]. Specifications of color for lighting, fabrication and manufacturing, color difference equations, color appearance models and color reproduction systems are all based on these standard observers. As will be discussed in the next section, tristimulus values that define standard colorimetry for objects result from the combination of lighting, surface reflectance, and observer color matching functions.

Sometime during the process that led up to this dissertation the following question (or something similar) was asked on a test: “If you were to start over and re-develop colorimetry (the measurement of color) - What would you do?" To some extent, this dissertation is an answer to this question in relationship to a second hypothetical question: “What if colorimetry was solely defined by surface reflectance?"

In absolute terms this second question is not achievable (as indicated by the following section as well as Chapter 2), but if it could be achieved then colorimetric values would not change due to differences in observer or lighting conditions as the values would be directly associated with surface reflectance. They could be attributed with perceptive concepts like lightness, chroma, and hue by association to a color ordering system, and differences in values for different surfaces would provide a measure of the perceptive differences in the surfaces. Lastly, correlations between the values and spectral reflectances could possibly be used to associate changes in these values with changes in spectral reflectances thus providing a way to manipulate surface reflectances.

The underlying premise of this dissertation is in finding and using a transformation or normalization of tristimulus or sensor values to realize a color equivalency representation (color coordinate system) that minimizes changes due to differences in observer or lighting conditions. Thus, the concepts of “material color" and “material color equivalency" [Logvinenko, 2013] (discussed in the next section as well as Chapter 2) are used to provide metrics for the designation of color in relationship to tristimulus or sensor values of reference material objects under reference observing conditions rather than using visual equivalency to combinations of primary light sources (which is the basis of color matching experiments) that relate to the perception of color. This results in an exploration of various impacted aspects of color science. Detailed literature

review as well as background information is therefore spread throughout this work as a result of the breadth of the topics considered.

Inventing an alternate way of defining color measurement that still has well defined relationships with existing colorimetry was not the original intent of the author as this dissertation work began. The author is a software developer of a company that provides software for large format digital output devices, and is deeply entrenched in the ICC Color Management community. Therefore, the initial focus of PhD research was to develop mechanisms to manipulate spectral reflectances in a spectral reproduction system driven by a spectrally based color management system (CMS). Additionally, it was also recognized that in defining such a CMS, a means of dealing with differences in observer and lighting conditions needed to be developed.

As the methods outlined in Chapter 7 were initially created, it was realized that a simple spectrally based mechanism was needed to provide a direct linear relationship between sensor based perceptive aspects of color and spectral reflectance. Therefore, one was developed that led to the sensor normalization process outlined in Chapter 2. However, rather than being based strictly on existing color matching function approaches, it utilizes the “similarity of color" defined by a select set of material colors that allows for the transformation of sensor values to provide perceptive aspects of color. Thus, a material color equivalency coordinate space (Wpt) arose through a process of normalizing relative to these material colors based on the spectral representations of observer, illumination, and object.

Upon further analysis of Wpt, it was soon found to be applicable to more than just spectral manipulation. It was shown to provide a fairly constant representation of surface colors for changes in observer and illuminant. Thus, Wpt could be used to transform sensor values between observer and illuminant conditions as well as provide the potential for representing differences in material color. However, Wpt is not perceptually uniform because it is the result of a linear transformation of sensor values. Therefore, an invertible non-linear transformation to a more perceptually uniform representation was investigated resulting in WLab. At this point it was realized that material color equivalency as expressed by Wpt and WLab had far greater applicability than simply the manipulation of spectral reflectance. Therefore, further areas of investigation were performed to explore applicability of Wpt and WLab including: color difference metrics using variability of observer, object, and/or illuminant; mechanisms of performing Wpt normalization based on direct sensor values; and the manipulation of sensor functions to achieve color matching functions with behavior similar to those of standard observers.

The result is an ecosystem of related color representations, comparisons and manipulations that are all based upon the principal of material color equivalency as represented by Wpt normalization (discussed in Chapter 2).

1.2 Introduction to Color Equivalency

A simple object-color system is made up of a light source (L), an object having a surface that interacts with the light (O), and a method of converting light energy (C) into channels of information (c_i) – here after referred to as sensor excitations to generalize the concept of tristimulus values, cone excitations or sensor values. The number of information channels is related to how many different kinds of light sensors there are. The human visual system has three types of chromatic sensors (cones) in photopic viewing conditions and is, therefore, trichromatic. The sensor excitations of the cones in the human visual system are further processed by various parts of the visual pathways to determine color appearance.

The resulting sensor excitations for each i^{th} sensor are often expressed mathematically using the following integral over wavelengths of light λ: [Wyszecki and Stiles, 2000]

$$c_i = \int_{\lambda} C_i\left(\lambda\right) O\left(\lambda\right) L\left(\lambda\right) d\lambda \tag{1.1}$$

This equation can be expanded to include fluorescence [Wyszecki and Stiles, 2000]. Thus integration over excitation wavelengths λ and reflected and emitted wavelengths ω results in:

$$\int_{\omega}\int_{\lambda} C_i\left(\omega\right) O\left(\omega,\lambda\right) L\left(\lambda\right) d\lambda d\omega \tag{1.2}$$

Eq. 1.2 can be represented as a linear matrix-vector equation when the color system is described using discrete steps of wavelength [Allen, 1966]. Such a representation preserves the transformative (transformance) nature of the color system [Mintz, 2009]. Thus:

$$\mathbf{c}_{x,y} = \mathbf{C}_x\mathbf{O}_y\mathbf{l}_x \tag{1.3}$$

where:
$\mathbf{c}$ defines a vector of resulting sensor excitations,
$\mathbf{C}$ defines a matrix containing sensitivity functions, cone fundamentals, or color-matching functions used to convert incident light to sensor excitations that may be scaled (normalized) to account for exposure or adjust sensor excitations to a desired range,
$\mathbf{O}$ defines a Donaldson matrix used to define how an object reflects and emits light at various wavelengths (with spectral reflectance factor defined along the diagonal), [Donaldson, 1954]
$\mathbf{l}$ defines a vector of the spectral power distribution of the illuminant,
x indicates a specific observing condition (i.e., the combination of observer and illumination), and
y indicates a specific object color.

For example: $\mathbf{c}_{src} = \mathbf{C}_{src}\mathbf{O}\mathbf{l}_{src}$ for src (source) observing conditions, $\mathbf{c}_{dst} = \mathbf{C}_{dst}\mathbf{O}\mathbf{l}_{dst}$ for dst (destination) observing conditions, $\mathbf{c}_{src,PRD} = \mathbf{C}_{src}\mathbf{O}_{PRD}\mathbf{l}_{src}$ for src observing conditions of a

perfect reflecting diffuser (PRD) defined by matrix $\mathbf{O}_{PRD}$, and $\mathbf{c}_{dst,PRD} = \mathbf{C}_{dst}\mathbf{O}_{PRD}\mathbf{l}_{dst}$ for dst observing conditions of a PRD defined by matrix $\mathbf{O}_{PRD}$.

It is often desirable to have a transform that predicts how the sensor excitations of a material object (or material color) change when the observing conditions change. The use of the general term “observing conditions" is intentional to indicate a possible change in either observer and/or illuminant as opposed to the more common term “viewing conditions" which is usually only associated with a change in lighting conditions (and is generally used in discussions of corresponding color or chromatic adaptation).

In this dissertation any generic transform that adjusts sensor excitation values shall be referred to as a Sensor Adjustment Transform (SAT), irrespective of how or why the adjustment is made. As an illustrative example, tristimulus values were calculated using Eq. 1.3 for a selection of Munsell colors for the CIE 1931 standard observer under Illuminants A, D65, and D100. The Munsell colors were defined by spectra corresponding to the Glossy edition at Values of 4, 6, and 8 and the neutral Value scale from 0 to 10 in 0.5 Value increments [Kohonen et al., 2006]. The spectra were corrected [Derhak and Berns, 2012] to achieve the exact Munsell renotation data for Illuminant C with the neutrals replaced with non-selective reflectances [Newhall et al., 1943]. The results are depicted in FIGURE 1.1 with sensor sensitivity normalized so that luminance factor, Y, is 100 for N10 (or perfect reflecting diffusor – PRD). The sensor excitations for the neutral colors have a linear relationship to one another for each illuminant, but go in different directions in XYZ coordinate space. The chromatic colors surround the neutrals and spread in different directions for each illuminant. Planes of constant Munsell Value are preserved, and generally parallel to one another. There is no correlation between the sensor excitation values for the different illuminants, which was expected since there is no illuminant-based normalization being performed. The perceptually uniform Munsell colors are not spaced uniformly in sensor excitation space.

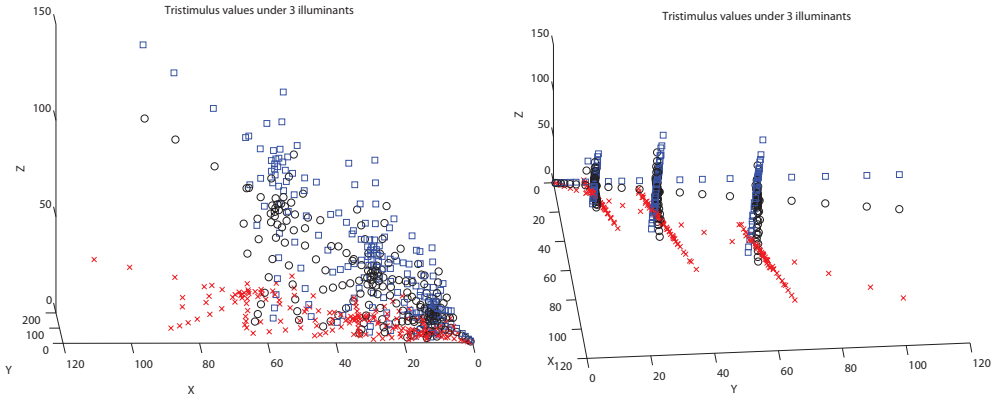

FIGURE 1.1. – Tristimulus values of various Munsell colors for the 1931 standard observer under Illuminants A (red x’s), D65 (black circles), and D100 (blue squares) with a viewing orientation of chroma planes (left) and a viewing orientation of planes of constant Munsell value (right).

One possible objective of a SAT would be to predict the sensor excitations of an object for a destination observing condition (dst) given the sensor excitations of the same object for a source observing condition (src). A typical approach is to perform a white balance adjustment that can be described by applying a linear von Kries-type transform matrix [vonKries, 1970] that utilizes the sensor excitations of a perfect reflecting diffuser ($\mathbf{O}_{PRD}$) under the source and destination observing conditions. Thus:

$$\mathbf{c}'_{dst} = \mathbf{M}_{vonKries}\mathbf{c}_{src} \tag{1.4}$$

$$\mathbf{M}_{vonKries} = \begin{bmatrix} \frac{d_1}{s_1} & 0 & 0 \\ 0 & \frac{d_2}{s_2} & 0 \\ 0 & 0 & \frac{d_3}{s_3} \end{bmatrix}$$

where:
$\mathbf{c}_{src}$ is a sensor excitation vector of an object ($\mathbf{O}$) for the src observing condition,
$\mathbf{c}'_{dst}$ is an estimated sensor excitation vector of an object ($\mathbf{O}$) for the dst observing condition,
s_j is the j^{th} sensor excitation of sensor vector $\mathbf{s} = \mathbf{c}_{src,PRD}$ for a PRD object for the src observing condition, and
d_j is the j^{th} sensor excitation of sensor vector $\mathbf{d} = \mathbf{c}_{dst,PRD}$ for a PRD object for the dst observing condition.

The assertion is made that the basis of the $\mathbf{M}_{vonKries}$ transform is the concept of a transformation into and out of an intermediate color equivalency representation space having a singularly defined representation for achromatic colors and white point with separate transforms for the source and destination illuminants. (Hereafter, the term color equivalency representation shall be used to refer to any coordinate system that is used to represent some form of color equivalency). Thus $\mathbf{M}_{vonKries}$ is equivalent to the following:

$$\mathbf{M}_{vonKries} = (\mathbf{U}_{dst})^{-1}\,\mathbf{U}_{src} \tag{1.5}$$

where:
$\mathbf{U}_x = \begin{bmatrix} \frac{1}{u_1} & 0 & 0 \\ 0 & \frac{1}{u_2} & 0 \\ 0 & 0 & \frac{1}{u_3} \end{bmatrix}$ for $x = src$ or $x = dst$, and
u_j is the j^{th} sensor excitation of sensor vector $\mathbf{u} = c_{x,PRD}$ for a PRD and observing condition x (using Eq. 1.3).

A visual representation of the intermediate space can be determined by applying an observing-condition specific $\mathbf{U}_x$ matrix to the sensor excitations:

$$\mathbf{e} = \mathbf{U}_x\mathbf{c}_x = \mathbf{U}_x\mathbf{C}_x\mathbf{Ol}_x \tag{1.6}$$

where:
$\mathbf{e}$ is a vector containing color equivalency coordinates.

The same set of tristimulus values for the Munsell colors for each observing condition was transformed to the intermediate color representation space ($\mathbf{e}$) using an appropriate matrix $\mathbf{U}_x$ with the results shown in FIGURE 1.2. In this example, the intermediate space has dimensions of X/Xn, Y/Yn, and Z/Zn. The differences between coordinates for the same object indicate differences in prediction of color equivalency. The neutral colors for each of the illuminants converge to the same locations along the diagonal from (0,0,0) to (1,1,1). The chromatic colors maintain their general relationships to the neutral axis, but the normalization does not result in the coordinates converging to the same location for each observing condition. This means that a SAT based on white point normalization does not predict sensor excitations for these Munsell colors. The reason is that white-point normalization does not account for the differences in sensor-excitation rotation, scaling, and shearing. (Additionally, because the normalization is based on tristimulus values, this also represents the color equivalency that can be expected for these illuminants within the CIELAB color space [McLaren, 1976]).

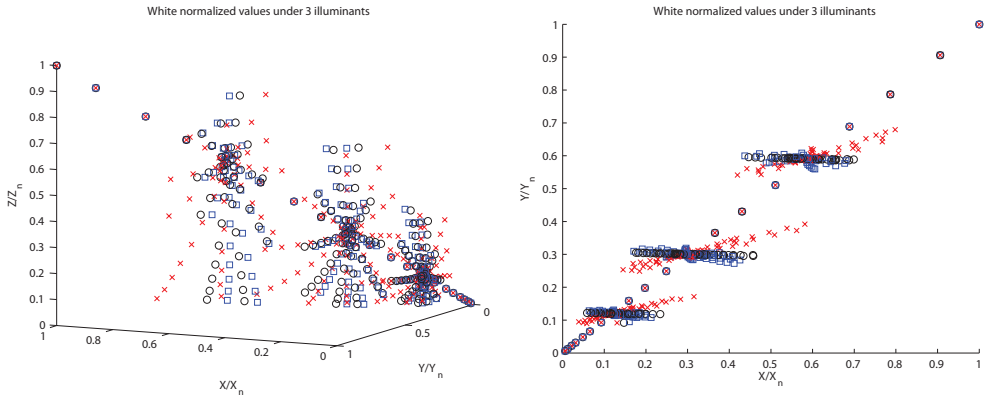

FIGURE 1.2. – White-normalized tristimulus values of various Munsell colors for the 1931 standard observer under Illuminant A (x's), D65 (dots), and D100 (squares) with a view orientation of chroma planes (left) and view orientation of planes of constant Munsell value (right).

Closer alignment of normalized sensor excitations result from the application of an additional transformation, often derived from optimized sensor excitations (i.e. sharpened cone fundamentals) rather than directly from color-matching functions or physiological cone fundamentals: [Susstrunk, 2005]

$$\mathbf{c}'_{dst} = \mathbf{S}^{-1}\mathbf{M}_{vonKries}\mathbf{S}\mathbf{c}_{src} \tag{1.7}$$

where $\mathbf{S}$ defines the matrix transformation from tristimulus values to sharpened-cone fundamentals. Eq. 1.7 can be written in the same form as Eq. 1.5:

$$c'_{dst} = \left(U_{dst}\right)^{-1}\left(U_{src}\right)c_{src} \tag{1.8}$$

The color equivalence coordinates are calculated by:

$$\mathbf{e} = \mathbf{S}^{-}1\mathbf{U}_x\mathbf{Sc}_x = \mathbf{S}^{-}1\mathbf{U}_x\mathbf{SC}_x\mathbf{Ol}_x \tag{1.9}$$

The results are plotted in FIGURE 1.3. In this case the neutral colors for each of the illuminants are also located along the diagonal from (0,0,0) to (1,1,1). The chromatic colors maintain their general relationships to the neutral axis, and there is better convergence between D65 points and D100 points, with improved but somewhat less convergence for illuminant A. Planes of constant Munsell Value are more orthogonal to the neutral axis. However, there is not complete convergence and thus, significant material color prediction differences persist.

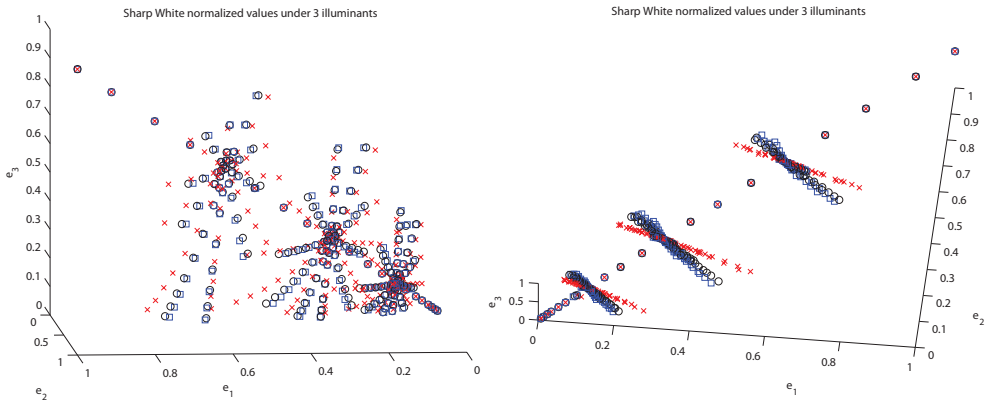

FIGURE 1.3. – White-normalized sharpened cone responses of various Munsell colors for the CIE 1931 standard observer under Illuminants A (x's), D65 (dots), D100 (squares) with a viewing orientation of chroma planes (left) and a viewing orientation of planes of constant Munsell Value (right).

The results shown in FIGURE 1.2 and FIGURE 1.3 are for changes in illuminant. Similar results occur with changes in sensitivity functions, that is, changes in $\mathbf{C}$ rather than changes in $\mathbf{l}$ in Eq. 1.6. This is shown in FIGURE 1.4 for three different sets of sensitivities under the same illuminant: the CIE 1931 standard observer, the CIE 2006 5°/ 45 year old cone fundamentals, [CIE170, 2006] and a CFA digital camera [Jiang et al., 2013]. The neutrals are nearly identical, but there are wildly varying results for the chromatic colors depending upon the rotational, scaling and shearing differences in sensor excitations resulting from differences in the sensor spectral sensitivities. White-balance normalization is a poor predictor of material color due to the effects of changing sensor sensitivities, that is, changes caused by changes in observer.

The figures and discussion in this section have all provided various examples of color equivalency representations where differences in coordinates of material objects are minimized to some extent for different observing conditions. However, in each case the explicit minimization of all the differences in transformed sensor excitations for material colors (material color equivalency) has not been performed. This is further explored in the next chapter and its applications are utilized throughout the remaining chapters.

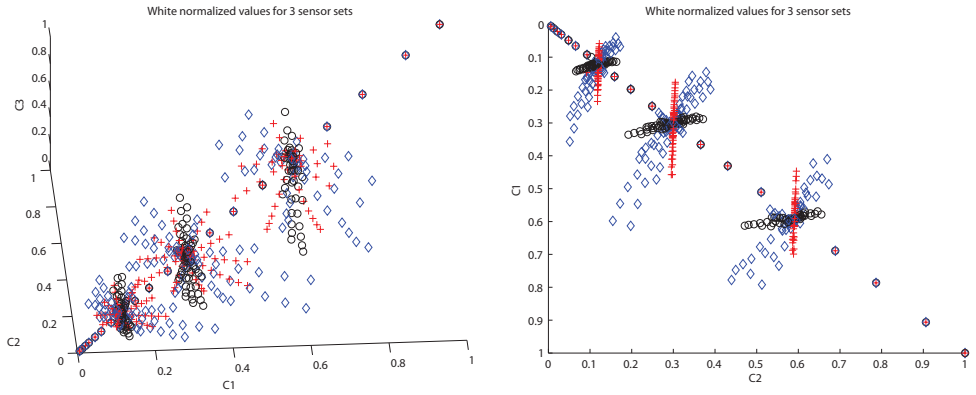

FIGURE 1.4. – White-normalized sensor excitation values of various Munsell color under D65 for the CIE 1931 observer (red pluses), CIE 2006 5° – 45 year-old cone fundamentals (black circles), and digital camera (blue diamonds) with a viewing orientation of chroma planes (left) and a viewing orientation of planes of constant Munsell Value (right).

1.3 Dissertation Structure

The central underlying thread throughout this dissertation is the realization of a material color equivalency representation (Wpt – pronounced “Waypoint") that largely predicts sensor excitations under various observing conditions. “Wpt material color equivalency" using a linear process of sensor excitation normalization is defined in Chapter 2, and is referred to throughout this dissertation as “Wpt Normalization". Each succeeding chapter utilizes or builds upon the concept of Wpt material color equivalency as defined by Wpt Normalization. The chapters each provide their own introduction and background as their topics have a different basis.

Chapter 2

The concept of color equivalency is further developed and explored – especially material color equivalency as described by Logvinenko [Logvinenko and Beer, 2012]. The contrast is made between the “similarity of color appearance" versus the “similarity of material color" along with their relationships to corresponding color experiments versus least-dissimilar color matching. This leads to the distinction between a Chromatic Adaptation Transform (CAT) and a separate form of SAT identified as a Material Adjustment Transform (MAT).

Wpt normalization is fully described. The resulting color coordinate system is identified by the axes (W, p, t) or Wpt (pronounced Waypoint) as it provides a waypoint for defining Material Adjustment Transforms. MATs based on “Wpt normalization" are presented, and comparisons to the results of Logvinenko as well as Chromatic Adaptation Transforms are provided.

The near constant alignment provided by Wpt normalization is demonstrated using Wpt coordinates that correspond to spectral reflectances of Munsell colors for different observers

and illuminants. Additionally, shifts in Wpt coordinates are found for different observers and illuminants due to the non-linear relationships between objects, observers, and illuminants that the linear minimization performed by Wpt normalization cannot account for.

Chapter 3

An invertible non-linear transform from Wpt to a perceptively uniform coordinate system (WLab) is derived and evaluated. A comparison is made between Wpt and existing color spaces by correlating the perceptive aspects of lightness, chroma and hue of these spaces to Munsell Value, Munsell Chroma, and Munsell Hue for colors from the Munsell Renotation color set. The non-uniform spacing of the Wpt lightness and chroma is clearly demonstrated. Then invertible equations are determined to achieve more perceptively uniform spacing of Wpt lightness and chroma for these Munsell Renotation colors with hue left unchanged. Additionally, a hue based correction of Wpt chroma spacing is determined that better correlates with color difference metrics provided by $\Delta E^{\star}{}_{94}$and ΔE_{00}.

WLab uniformity is compared to existing color spaces, and color differences defined by the Euclidean distances of WLab coordinates are compared to other color difference metrics. WLab is shown to not be statistically different from $\Delta E^{\star}{}_{94}$and ΔE_{00}under Illuminant C and performs better at predicting color difference experiments under Illuminant A. The perceptive uniformity and near constant alignment provided by Wpt normalization is demonstrated using WLab coordinates corresponding to spectral reflectances of Munsell colors for different observers and illuminants.

Chapter 4

A set of Wpt coordinates for variations of object, observer, and/or illuminant is identified as a Wpt Shift Manifold (WSM). Variations of object reflectance is enabled by a spectral estimation strategy that combines the concept of metameric black as defined by Wyszecki [Wyszecki, 1953] with the concept of principal or characteristic reflectance as defined by Chau [Chau, 1999]. Various aspects of WSMs are demonstrated through WSM visualizations.

Then metrics are derived and demonstrated that utilize differences of associated WLab coordinates for points within a single WSM as well as between corresponding points in separate Wpt shift manifolds. The extent of color inconstancy of a spectral reflectance (or appearance potential) is provided by the reflectance's WSM with varying observer and illuminance resulting in an object WSM. Comparing corresponding points between two object WSMs provides relative color difference metrics of two objects including minimum color difference, an index of metamerism (when the minimum distance is zero), and the average color difference (over all viewing conditions). A metric of the similarity of the color matching (discrimination) of two observers is derived by comparing corresponding WSM coordinates for two observers with varying objects and illuminants (thus demonstrating how well the Luther-Ives condition is satisfied). Finally, a metric comparing viewing conditions is proposed using WSM's.

Chapter 5

It is noted that the utility of Wpt and WLab is dependent on determining Wpt normalization matrices as outlined in Chapter 2. However, as this is based on Eq. 1.3, this requires a spectral understanding of both the observer and the illuminant. Two methods are explored for determining or estimating a Wpt matrix if a spectral understanding of one or the other is not available. The first method utilizes sensor excitations from one of several described calibration charts that can be acquired using an image capture system (digital camera). The second method utilizes sensor excitations of either a perfect reflecting diffuser (PRD) or a non-selective gray to estimate a Wpt normalization matrix when the spectral power distribution (SPD) of the illuminant is unknown. This is accomplished using the spectral sensitivity functions of the observer along with spectral power distributions(SPDs) of a wide selection of illuminants to directly estimate model coefficients for defining a Wpt matrix based on the direction of the gray axis in sensor excitation coordinates. Comparisons between actual and estimated Wpt normalization matrices are demonstrated.

Chapter 6

The use of Wpt based Material Adjustment Transforms is utilized as a mechanism for transforming cone fundamentals into color matching functions. The mathematical underpinnings defining the relationships between cone fundamentals and color matching functions are presented along with observations. The idea of the “sameness of color" from Chapter 2 is applied with relationship to the use of Wpt based MATs which relies on the “sameness of material color". This is compared and contrasted to methods of forming “XYZ-like" color matching functions from cone fundamentals that rely on the “sameness of tristimulus values" or the “sameness of primaries". It is proposed that the use of Wpt based MATs provides a good correlation between color matching functions that allows for the comparison of inter-observer color perception.

Chapter 7

The manipulation of spectral reflectance to achieve perceptive color adjustments based on Wpt is explored. This is discussed in terms of established color reproduction objectives with the proposal of a new objective – “Spectrally preferred color reproduction". A general framework for manipulating spectral reflectance is presented which allows for existing methods to be characterized. A specific implementation of the framework based on Wpt is proposed and utilized to estimated and manipulate spectral reflectances. This is demonstrated in two ways. First, the spectral reflectances of actual printed device characterization samples are manipulated to derive spectral reflectances for reference characterization data sets that are only defined colorimetrically. Second, Wpt based spectral estimation is used to define realistic spectral reflectances for Munsell Renotation colors that have minimal color inconstancy. Finally, the use of Wpt based spectral manipulation for performing spectral gamut mapping is described.

Chapter 8

Conclusions and summary of possible future research efforts is presented.

Appendix A

An early work that utilizes Matrix R to manipulate spectral reflectances is presented. Corrected

spectral reflectances corresponding to Munsell Renotation colors are demonstrated and used throughout the dissertation.

Appendix B

Equations used to convert from Wpt to WLab or WLab to Wpt are presented along with worked examples.

2 Introducing Wpt (Waypoint) – a Color Equivalency Representation for defining a Material Adjustment Transform

2.1 Sensor Adjustment Transform Approaches

In the previous chapter the concepts of sensor excitations, color equivalency, and Sensor Adjustment Transforms were introduced. A SAT defines a general transform that adjusts sensor excitations irrespective of the intent or mechanism used to define the transform. In this chapter, more specific cases of SATs are considered by answering the questions: “What does one want to accomplish using a SAT" and “What are various ways that a SAT can be defined?"

One of the most significant reasons for defining a SAT is to account for sensor excitation changes under different observing conditions for a specific object. The human visual system (HVS) “generally mitigates" these changes in sensor excitations to provide for a “more" consistent perceptual experience as objects undergo changing environmental conditions. Various visual experiments have been devised to characterize how and assess the degree to which the mechanisms of this mitigation operate in the HVS. These experiments generally involve asymmetric color matching using techniques including haploscopic viewing, short-term memory matching, or color estimation techniques [Foster, 2011].

The results of such experiments differ based upon what is asked of the observer when performing the color matching. When observers are instructed to identify an object independent color designation in one viewing condition that has the same appearance as the color of an object in a different viewing condition, one gets different results from when observers are instructed to identify an object color in one viewing condition that is made of the same material as the object under a different viewing condition (thus the objects are physically identical – like two halves of the same piece of paper) [Arend and Reeves, 1986]. These two kinds of results have led to two different approaches within the literature to what is hereafter referred to as “sameness of color”. The first approach focuses on sameness of appearance and results in corresponding color data that defines sensor excitations in one viewing condition that have the same appearance as the sensor excitations for an object in different viewing conditions (with a possible difference in object) [Luo, 2000]. The second approach focuses on sameness of material (or “material color constancy" where the term “color" is used to designate a singular

aspect of the material rather than to describe its appearance) with the direct prediction of sensor excitations for an object under one observing condition based upon the sensor excitations of the same object under different observing conditions (with a possible difference in appearance) [Foster, 2011]. The vast majority of object colors do not exhibit perfect apparent color constancy except spectrally non-selective samples. The transform used in FIGURE 1.3 was optimized to predict sameness of color appearance via corresponding colors, and therefore does not provide a prediction of material color constancy. If the transform predicted material color constancy, the colors would plot in nearly identical positions irrespective of the observing conditions. The neutral colors in FIGURE 1.3 exhibit material color constancy because their spectral reflectances are non-selective.

Logvinenko described a material color constancy experiment as a least dissimilar color matching experiment since the appearance of an object color under different viewing conditions may vary [Logvinenko and Tokunaga, 2011]. In other words, the observer is not able to discount the differences due to the change in illuminant. However, the observer is able to identify to some degree a material match despite the differences in appearance. Wright postulated that this could be indicative of secondary processing mechanisms in the visual system used to determine the match [Wright, 1981].

Color constancy research in the vision-science literature is mainly focused on the second approach with various methods of determining what adjustments are needed to transform sensor excitations for a scene to get a constant material color representation [Foster, 2011]. However, there are some challenges that will be encountered by any method used to predict material color constancy. Two object colors that are metameric (meaning that they have the same sensor excitations but different spectral reflectance characteristics) under one observing condition are not guaranteed to have the same sensor excitations with a change in viewing conditions. A transform that predicts a change for the first sensor excitations will not predict separate sensor excitations for the second viewing condition.

SATs can be defined based on either of the two color transform approaches utilizing different observations or data points with different kinds of resulting predictions. A SAT based on the first approach is a chromatic adaptation transform, or CAT. An effective CAT relies on visual experiments that result in corresponding colors data, and therefore a CAT predicts to some degree the sameness of color appearance [Foster, 2011]. A SAT based on the second approach would be used to predict material constancy or how sensor excitations for an object color change with changes in observing conditions [Logvinenko, 2013]. This second type of SAT shall hearafter be referred to as a Material Adjustment Transform, or MAT.

Because both sameness of appearance and material color constancy are sometimes associated with “sameness of color”, the distinction between them is often confused in the literature, and therefore in some cases, what should be identified as a MAT is often referred to as a CAT. Additionally, it is generally inappropriate to use a CAT to predict differences in sensor excitations between different observers because a CAT is optimized to predict corresponding color which only predicts an individual or average human’s visual adaptation with no reference to how

appearance differs between observers. A MAT is more appropriate in this case for predicting sensor excitations between different observers since it can be defined in terms of the same material colors.

The classification of SATs into MATs and CATs is dependent on the intention and optimization method used to define the SAT. Also, SATs should be evaluated against the relevant observations or data points that were used to establish the SAT, and since a SAT is defined in the most general terms, not every SAT will be classified as a MAT or CAT.

The use of a sharpening matrix to define a SAT as in Eq. 1.7 can be classified as a CAT when the sharpening matrix is optimized so that the SAT predicts experimentally derived corresponding-colors data. This is the case in FIGURE 1.3 where the CAT02 transform, which is the basis of the CIECAM02 color appearance model, was used [Moroney et al., 2002].

Kang discussed four ways of adjusting tristimulus values to account for differences in illumination [Kang, 2006]. These methods are not directly related to how the HVS adapts as they do not take corresponding color data into consideration, and therefore Kang described these SAT methods as white point conversion methods, useful in image processing applications to account for differences in illumination. Since the intent of these transforms is the prediction of sensor excitations these methods could be considered MATs.

Another form of SAT is a camera color correction transform that converts directly from sensor excitations to tristimulus values. The transform is formed by capturing a physical test target with color fields of known colorimetry and then using regression or nonlinear optimization to form a matrix that predicts colorimetry from the captured sensor excitations. In this case, corresponding color and a color equivalency representation are not used [Adams et al., 1998]. Other direct methods of determining a SAT that predicts sensor excitations of materials have been proposed by Finlayson [Finlayson et al., 2003]. When the actual relationship between the sensor excitations is only approximate the resulting linear transform will be dependent upon the training data used. Since such a direct transform is based upon measurements and capture of a material objects, such a transform could be considered a MAT.

Mirzaei and Funt proposed a method of predicting color stimulus change under an illuminant change [Mirzaei and Funt, 2011] by mapping LMS cone responses under an illuminant to coordinates of Logvinenko's color atlas [Logvinenko, 2009] which provides a spectral representation of the sensor excitations that can be used to arrive at LMS responses under a different illuminant. Though this approach does not use a linear transform, such a transform could be considered a MAT as it has no direct relationship to corresponding color.

Oleari has proposed a color equivalency representation that he defines as the "main-reference frame" (that is defined by "main tristimulus values" A, B, and C), which was derived by satisfying requirements of applying perceptually uniform steps defined by Weber fractions of these tristimulus values to equidistant colors from the OSA-UCS color order system for the CIE 1964 10° observer under D65 illumination [Oleari, 2005]. Based on this main-reference frame he has

developed color difference metrics [Oleari et al., 2009] as well as two methods of defining Sensor Adjustment Transforms [Oleari et al., 2011] by converting from cone excitations or colorimetric XYZ values for an alternate observer or illuminant to his main tristimulus values ABC for the 10° observer under D65 illumination.

The first method Oleari used to define SATs combines pairs of matrices as in Eq. 1.5 that are optimized using a conversion of XYZ tristimulus values with various observing conditions for 99 color samples from the Gretag-Macbeth (now Xrite) ColorChecker SG color rendition chart to his main tristimulus ABC values and minimized based upon differences in applying a log function to ratios of the ABC values [Oleari et al., 2011]. This is an example of a direct minimization between sensor excitations. Since all samples including white are involved in the optimization, there is variability in the preservation of neutral or white colors. Oleari provided optimized matrices for conversion between D65 with the 10° standard observer and D65, D50, CIE Illuminants A, C, and F11 for both the 2° and 10° observers. Additionally, Oleari provided functions based on color temperature for defining entries of adjustment matrices for black body radiators, and daylight illuminants for both 2° and 10° CIE observers based upon a similar minimization methodology. Oleari identified these transformations as CATs. However, since these SATs were optimized using direct minimization between sensor excitations (without any direct relationship to corresponding color data) they should more properly be identified as MATs (hereafter referred to as Oleari MATs).

Oleari has also recently proposed a method for determined SATs that were optimized utilizing various corresponding color data sets [Oleari, 2014]. Oleari provided comparisons and contrasts between the “usual” approach based upon Eq. 1.9 and his approach. His approach utilized the same color equivalency representation or main reference frame and objective function for minimization as his previous method. However, the data used for minimization came from corresponding color experiments. The colorimetry was first adjusted, as needed for the data sets that were not based on the standard 10° observer under D65 illumination, using an Oleari based MAT discussed in the previous paragraph to this reference observing condition. The resulting transformations therefore combine an Oleari based MAT with an additional transform that is optimized to predict corresponding colors as “adapted tristimulus values” in an “adaptation reference frame” or an adapted color equivalency representation. It is felt that such combined transforms should be categorized as CATs because they are minimized based upon corresponding color data. Though Oleari provided CATs that make predictions for various corresponding color data sets, he concluded that a general formula could not sufficiently be defined using his approach due to the lack of extensive and consistent corresponding color data for a wide variety of viewing conditions to define the relationships between Oleari based MATs and the additional transforms needed to predict corresponding colors.

Brill has also pointed out that using a pair of transformations that map cone space values into and out of a color equivalency representation can be used to define a CAT [Brill and Oleari, 2014]. As an example, Brill introduced the idea of combining an Oleari MAT with the inverse of an Oleari based MAT in like fashion to Eq. 1.5. In this case the tristimulus values for the standard 10° observer and D65 illuminant are being used as the color equivalency representation. Brill

identified such a combined transform as a CAT, but the resulting combined transforms should be identified as a MAT since the Oleari MATs were being referenced. However, Brill's general idea of using separate transforms to form a CAT would be appropriate as long as corresponding color data is used to optimize one or more of the transforms being combined, as in the case of the Oleari CATs [Oleari, 2014].

Pridmore proposed a very different approach that predicts color constancy by applying adaptation to hue, chroma and lightness (derived from Yxy) rather than to cone excitations [Pridmore, 2010]. The method presented by Pridmore is more conceptual than computational, and therefore an exact classification of SAT is not warranted. However, he did advocate for adaptation/adjustment of lightness, chroma, and hue separately.

2.2 Deriving a Material Adjustment Transform

An effective MAT will utilize a color-equivalent representation where changes in observing conditions lead to nearly identical coordinates. Deriving the matrix requires a set of surface colors that are representative of object colors. A subset of the Munsell glossy-edition samples described above was selected consisting of the 40 Munsell Hues at an intermediate lightness and chroma of Value 5 and Chroma 6. Their measured spectra were adjusted, as described previously. Two additional samples were selected: a perfect reflecting diffuser (PRD) and a vivid [Berns, 2014] yellow near unique yellow [Shamey et al., 2010]. These 42 samples were selected for both their spectral and visual characteristics. As physical samples, their spectra generally typify absorbing and scattering colorants. Visually, they have perceptive aspects [Tonnquist, 1986] of white (PRD sample), lightness, chroma, and hue, useful for an equivalency color representation, explained below. The Munsell samples are listed in TABLE 2.1, their reflectances plotted in FIGURE 2.1, and visualized as an image in FIGURE 2.2.

TABLE 2.1. – Munsell samples used to derive material adjustment transforms.

N10 (PRD)	3.75Y 8/14	2.5R 5/6	5R 5/6	7.5R 5/6	10R 5/6	2.5YR 5/6
5YR 5/6	7.5YR 5/6	10YR 5/6	2.5Y 5/6	5Y 5/6	7.5Y 5/6	10Y 5/6
2.5GY 5/6	5GY 5/6	7.5GY 5/6	10GY 5/6	2.5G 5/6	5G 5/6	7.5G 5/6
10G 5/6	2.5BG 5/6	5BG 5/6	7.5BG 5/6	10BG 5/6	2.5B 5/6	5B 5/6
7.5B 5/6	10B 5/6	2.5PB 5/6	5PB 5/6	7.5PB 5/6	10BP 5/6	2.5P 5/6
5P 5/6	7.5P 5/6	10P 5/6	2.5RP 5/6	5RP 5/6	7.5RP 5/6	10RP 5/6

The purpose of deriving a color equivalency representation was to achieve orthogonality between lightness and chromaticness, and if possible have linear loci of constant hue and circular contours of constant chroma. Colors that lead to uniform scales of lightness, chroma, and hue do not have to maintain uniform spacing, hence the use of Tonnquist's perceptive concepts of lightness, chroma, and hue rather than Munsell descriptions of Value, Chroma, and Hue [Tonnquist, 1986]. Intermediate Munsell Value and Chroma samples were used because a dependable representation of constant perceptive lightness and chroma for all hues is essential to establish

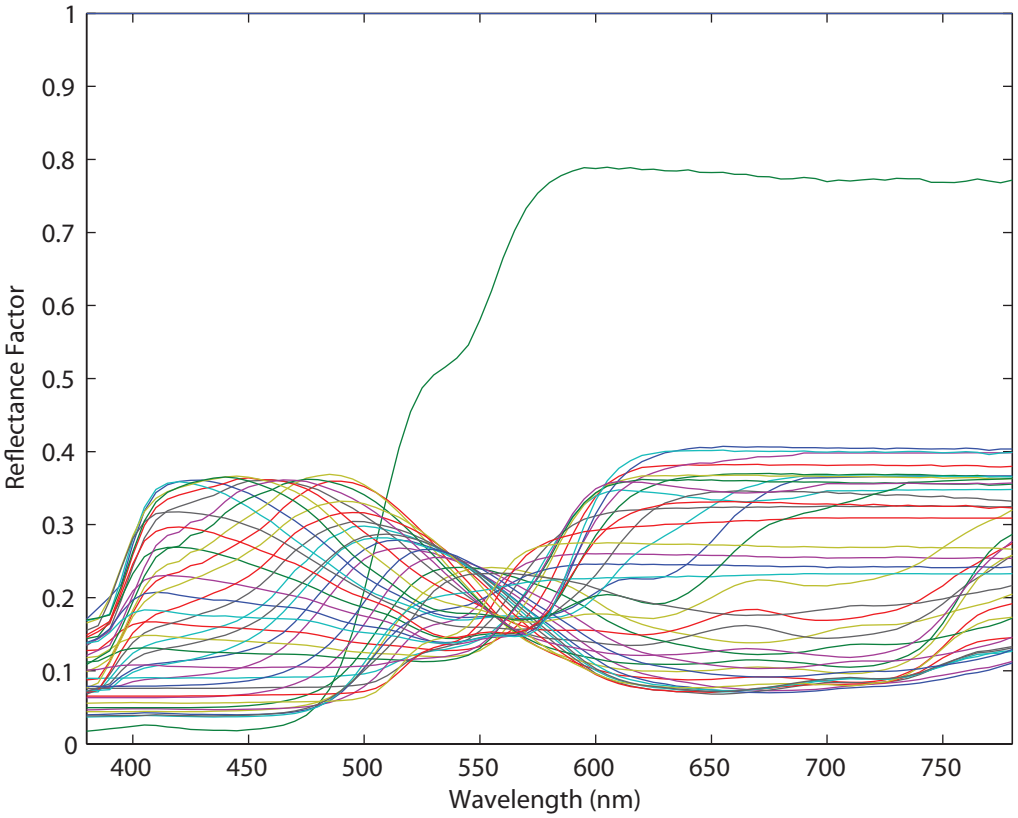

FIGURE 2.1. – Reflectance spectra of samples used for Wpt normalization.

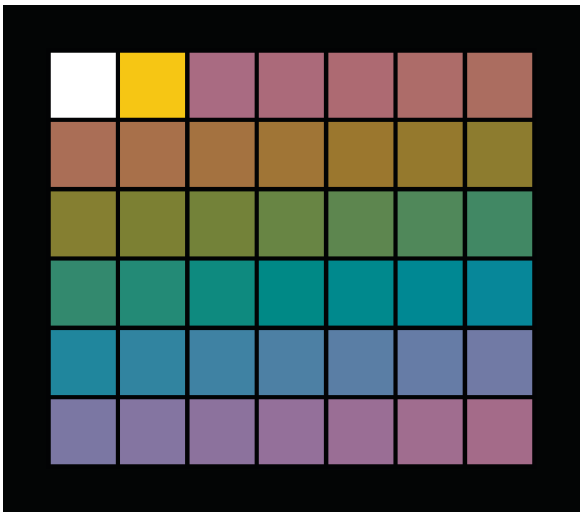

FIGURE 2.2. – Visualization of samples used for Wpt normalization (encoded using sRGB).

the equivalency color representation. Because the chosen colors are in the center of the Munsell system, it is believed that they are more likely to represent constant perceptive lightness and chroma and less likely to have observational and color formulation variability than colors near the edges of the Munsell renotation system [Newhall, 1940].

The coordinates of the derived representation are (W, p, t) or Wpt, pronounced "Waypoint." The identification "Waypoint" (with an uppercase "W") was a deliberate choice because this color equivalency representation forms a waypoint (a general term) between source and destination observing conditions. W coordinates represent perceptive lightness while p and t represent the dimensions of the perceptive chromaticness plane. A complete color system that utilizes such a transform is expressed with the following linear equation:

$$\begin{bmatrix} W \\ p \\ t \end{bmatrix} = \mathbf{ACOl} \tag{2.1}$$

where:
W represents perceptive lightness,
p, t represent perceptive chromaticness, i.e., a combination of perceptive chroma and hue at constant perceptive lightness,
$\mathbf{A}$ represents a linear transform matrix that converts from sensor excitations to coordinates (W, p, t), and
$\mathbf{C}$, $\mathbf{O}$, $\mathbf{l}$ are the same as previously defined in Chapter 1.

When deriving matrix $\mathbf{A}$, the following properties were desirable. The transformation should be linear. Non-selective spectral reflectances must always be co-linear with the W axis. Colors that have constant perceptive lightness should have constant W values. Colors with constant perceptive chroma and perceptive lightness should correspond to a constant distance from the lightness axis. The orientation of various hues should be similar to CIELAB with unique yellow plotting along the positive t axis. Colors that have chromaticities falling on a line intersecting white on a chromaticity diagram should fall on a plane that includes the W axis. In other words it should preserve hue as defined by dominant (complementary) wavelength. Finally, the perceptive concepts of hue, lightness, and chroma should be preserved. It is not expected that colors with uniformly spaced hue, lightness, and chroma, such as samples from the Munsell Book of Color, will maintain such spacing in Wpt since a linear transform connects sensor excitations and Wpt.

Matrix $\mathbf{A}$ is a function of observing conditions, that is, the specific sensor functions $\mathbf{C}$ and specific illuminant $\mathbf{l}$:

$$\mathbf{A} = T(\mathbf{C}, \mathbf{l}) \tag{2.2}$$

where $T(\mathbf{C}, \mathbf{l})$ is a function that finds matrix A using the proposed methodology for the observing condition defined by $\mathbf{C}$ and $\mathbf{l}$. The methodology has two variations. The first is for defining a transform for a reference observing condition with a standard 2° observer under Illuminant C, and the second is for defining a transform for alternate observing conditions.

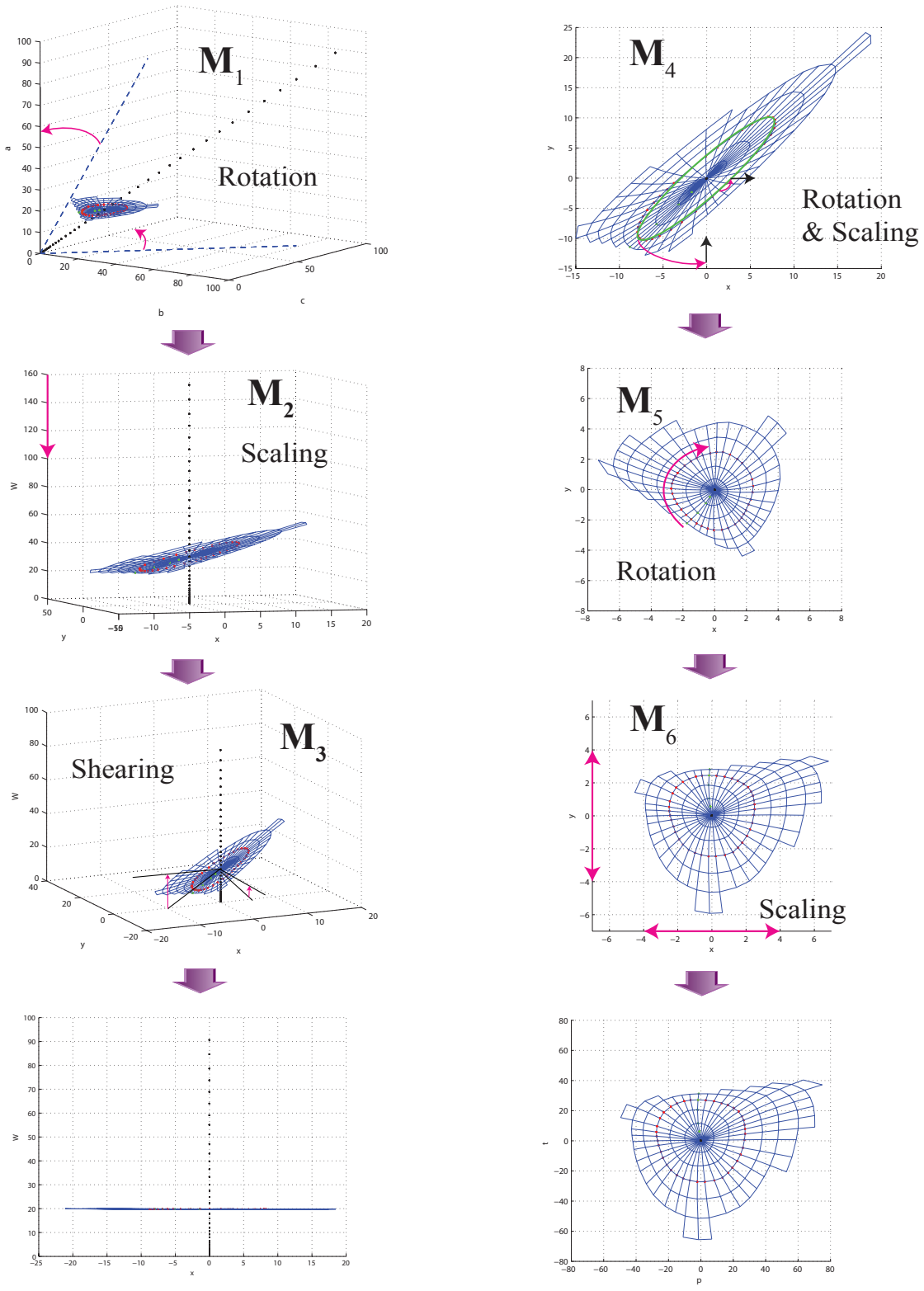

FIGURE 2.3. – Visualization of transformation steps used for Wpt normalization of Reference Observing Conditions.

The process of deriving transformation matrix A for the reference observing condition involves deriving a series of successive linear transformations depicted in FIGURE 2.3, essentially equivalent to a unique computational method of adjusting lightness, chroma, and hue separately as advocated by Pridmore [Pridmore, 2010]. The following are the steps to derive a transformation for the reference condition:

First, rotate the sensor excitations for the PRD to align with the first axis ($\mathbf{M}_1$). This is accomplished by rotating around the first axis, and then rotating around the second axis. As a result, the first axis will correspond to perceptive lightness (W). Scale the first axis so the PRD has a value of 100 (matrix $\mathbf{M}_2$). The rotation and scaling operations can be concatenated as single transformation matrix.

Second, apply the matrix resulting from the first step to get (W, c_1, c_2) coordinates for the forty colors having constant Munsell Value and constant Munsell Chroma. Fit these points with an equation for a plane ($a_0c_1 + a_1c_2 + a_2W = 0$), and use $-a_0$ and $-a_1$ in the W line of a matrix to form a shearing matrix ($\mathbf{M}_3$) that can be concatenated to the matrix resulting from the first step. This results in the forty chromatic reflectances having nearly constant value for W.

Third, fit the results for the same forty colors having constant Munsell chroma with the parametric representation of an ellipse centered on the origin to estimate an ellipse with axis scalars a and b having a rotational angle θ by minimizing for d as follows:

$$\begin{aligned} \varphi_i &= atan2\left(c_{2,i}, c_{1,i}\right) \\ x &= a\cos\varphi_i\cos\theta - b\sin\varphi_i\sin\theta \\ y &= a\cos\varphi_i\sin\theta + b\sin\varphi_i\cos\theta \\ d &= \sum_i \left(\left(c_{1,i} - x_i\right)^2 + \left(c_{2,i} - y_i\right)^2\right)^{\frac{1}{2}} \end{aligned} \tag{2.3}$$

where:
$c_{1,i}$ and $c_{2,i}$ represent chromatic coordinates of the i^{th} chromatic Munsell color after applying the first two steps,
x_i and y_i represent estimated chromatic coordinates for i^{th} chromatic Munsell color using parametric representation of a fitted ellipse, and
d represents the total sum of the differences between the actual and estimated chromic coordinates of the fitted Munsell colors.

After minimizing d to find constants a, b, and θ, a transformation matrix ($\mathbf{M}_4$) that rotates around the W axis by -θ is applied followed by a transformation matrix that scales the first chromatic axis by b/a and the second chromatic axis by a/b. This step may need to be repeated several times until the difference in d between iterations becomes negligible. The rotation and scaling matrices from this process are concatenated to the matrix resulting from step two to form a transformation matrix that additionally establishes approximately constant chroma for the forty chromatic Munsell colors.

At this point the orientation of the chromatic axes is arbitrary, and for normalization purposes a standard orientation is desired. Therefore, to get a similar orientation as CIELAB, the fourth step is to rotate the results around the W axis for the vivid yellow to align with the positive third axis (t) and flip the first axis (as needed by scaling by -1) so that reddish hues align with the positive second axis (p) using a matrix transform ($\mathbf{M}_5$).

Fifth, scale both the p and t axes by the same factor so the vivid yellow sample has a distance of 100 from the W axis using a matrix transform ($\mathbf{M}_6$).

The concatenation of all the transforms determined in these steps results in a single transformation matrix $A = \mathbf{M}_6\mathbf{M}_5\mathbf{M}_4\mathbf{M}_3\mathbf{M}_2\mathbf{M}_1$. The colors used to derive the reference transformation are plotted in Wpt, shown in FIGURE 2.4.

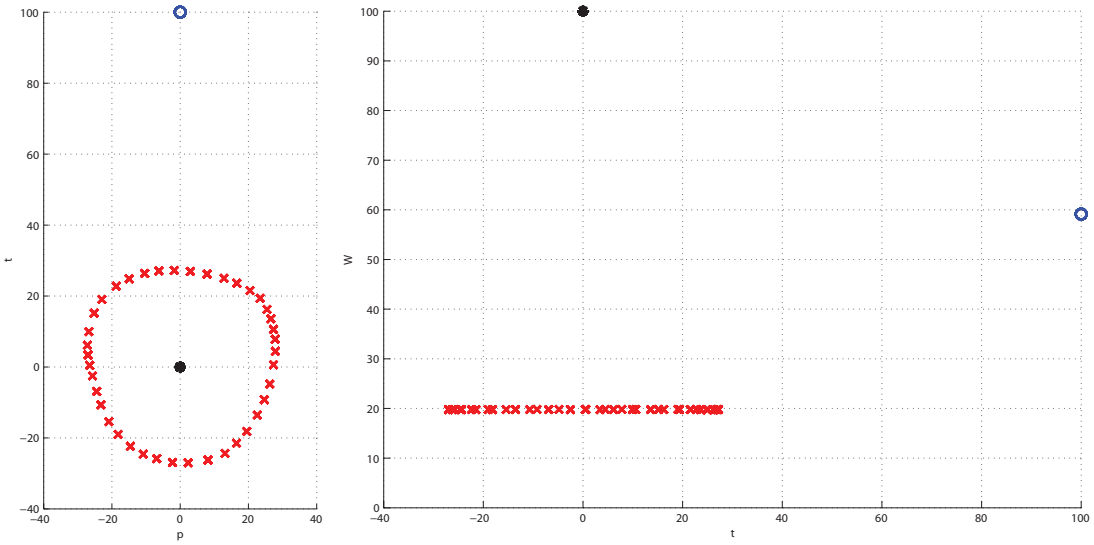

FIGURE 2.4. – Visualization of Table I samples plotted as Wpt coordinates. Black asterisk is PRD, Blue circle is vivid yellow. Red 'x's represent colors with constant Munsell Chroma and Value.

The above procedure works well for establishing a Wpt normalization matrix $\mathbf{A}$ for the reference standard 2° observer and reference illuminant C, and could potentially also be used for other observing conditions. However, the description of hue and chroma in steps three through five are dependent upon the sensor excitations of the vivid yellow. Since this sample may not exhibit material constancy, skewing relative to the other colors may result. A separate approach that addresses these issues uses direct regression to minimize the differences in p and t coordinates for an alternate observing condition and those found using the above procedure for the reference observing condition. Thus, the first approach is necessary to provide reference Wpt positions for minimization purposes. This results in the following approach for defining a Wpt normalization matrix for alternate observers and illuminants which uses the first two steps from the above approach and then replaces steps three through five as follows:

Third, use linear regression to find a matrix that minimizes the Euclidean distances in the p and t chromatic plane between the new and reference conditions. This results in general preservation of both hue and chroma while allowing for tradeoffs in accuracy due to differences in material constancy.

Finally, concatenate the transformations into a single transformation matrix $\mathbf{A}$. Matlab code as well as an Excel spreadsheet for establishing a Wpt normalization matrix can be found at (https://www.rit.edu/cos/colorscience/re_WptNormalization.php).

With reference p and t values for the forty chromatic Munsell colors determined this second approach can be used for any observer and illuminant (including the reference conditions). Additionally, this second approach can easily be extended to work with more than three sensors by extending the first step to rotate around the first, second and successive axes until the second to last axis, using an equation of a multidimensional plane to determine shearing constants for the remaining chromatic dimensions in the second step, and performing linear regression from the sheared multidimensional chromatic plane to the two dimensions of p and t.

Note: These procedures require that the dimensionality of the resulting sensor excitations is at least three because there is minimization of three dimensions: lightness, chroma, and hue. Thus, failures in the prediction of Wpt normalization matrices are likely if either there are fewer than three sensor types or the illuminant does not contain a combination of long, medium, and short wavelengths.

Examples of resulting Wpt normalization matrices using the second approach for the standard 10° and 2° observers with illuminant C, D65, D50, illuminant A, illuminant E, and a fluorescent F11 illuminant can be found in TABLE 2.2. Each matrix can be used to convert colorimetry for the observer and illuminant expressed as XYZ column vectors to Wpt coordinates where a PRD has a luminance factor, Y, equal to 100.

The matrices in TABLE 2.2 were all used as a matrix $\mathbf{A}$ in Eq. 2.1 with the complete set of Munsell spectral reflectances to determine Wpt coordinates for each of the observing conditions. These coordinates are simultaneously plotted in FIGURE 2.5; the variability in Wpt coordinates is generally minimized for differences in illuminant and observer with most Wpt coordinates for the same Munsell reflectances for different observing conditions converging to nearly the same location even though only 42 of Munsell colors were used to establish these matrices. The variability between the 2° and 10° observers is very minimal, and the greatest variability occurs for illuminant F11, and to a lesser extent, illuminant A.

Matrices were derived for the same three sensor spectral sensitivities used to evaluate MATs based on white normalization as plotted in FIGURE 1.4: the CIE 1931 standard observer, the CIE 2006 5°/ 45 year old cone fundamentals, and a CFA digital camera. The results are shown in FIGURE 2.6. There is very noticeable convergence between all of the sensor sets and a marked improvement compared with FIGURE 1.4. Thus, Wpt is a reasonable color equivalency representation (or waypoint) for changes in both illuminant and observer.

TABLE 2.2. – Matrices to convert XYZ column vectors to Wpt coordinates for various observing conditions

	Standard 10° Observer			Standard 2° Observer		
	0.07837	0.99300	-0.06271	0.02964	0.97487	-0.00280
D65	5.12107	-5.27209	0.38828	4.83916	-4.73122	0.12117
	0.78225	1.13989	-1.75315	0.54248	1.30671	-1.67368
	0.04888	1.02268	-0.06047	0.00000	1.00000	0.00000
C	5.14072	-5.36078	0.30964	4.84591	-4.80280	0.04258
	0.75497	1.15250	-1.62468	0.51873	1.30963	-1.53805
	-0.03390	1.06622	-0.04107	-0.06265	1.03839	0.02669
D50	4.98326	-5.37826	0.68588	4.68561	-4.82563	0.37293
	0.48282	1.35138	-2.23437	0.28350	1.50053	-2.15101
	-0.04091	1.08336	-0.04246	-0.07407	1.05436	0.01971
E	4.89821	-5.31600	0.41832	4.61340	-4.78331	0.16986
	0.59264	1.24324	-1.83561	0.37630	1.40421	-1.78050
	-0.36233	1.37188	0.08758	-0.33810	1.30006	0.20048
A	4.76102	-5.94588	1.85883	4.40232	-5.32134	1.36425
	-0.29792	2.07286	-4.94818	-0.41103	2.17849	-4.85343
	-0.13853	1.11178	0.04893	-0.12366	1.05659	0.10608
F11	4.73751	-5.27217	0.53588	4.38611	-4.63611	0.32299
	0.47386	1.20030	-2.57966	0.37476	1.29098	-2.59413

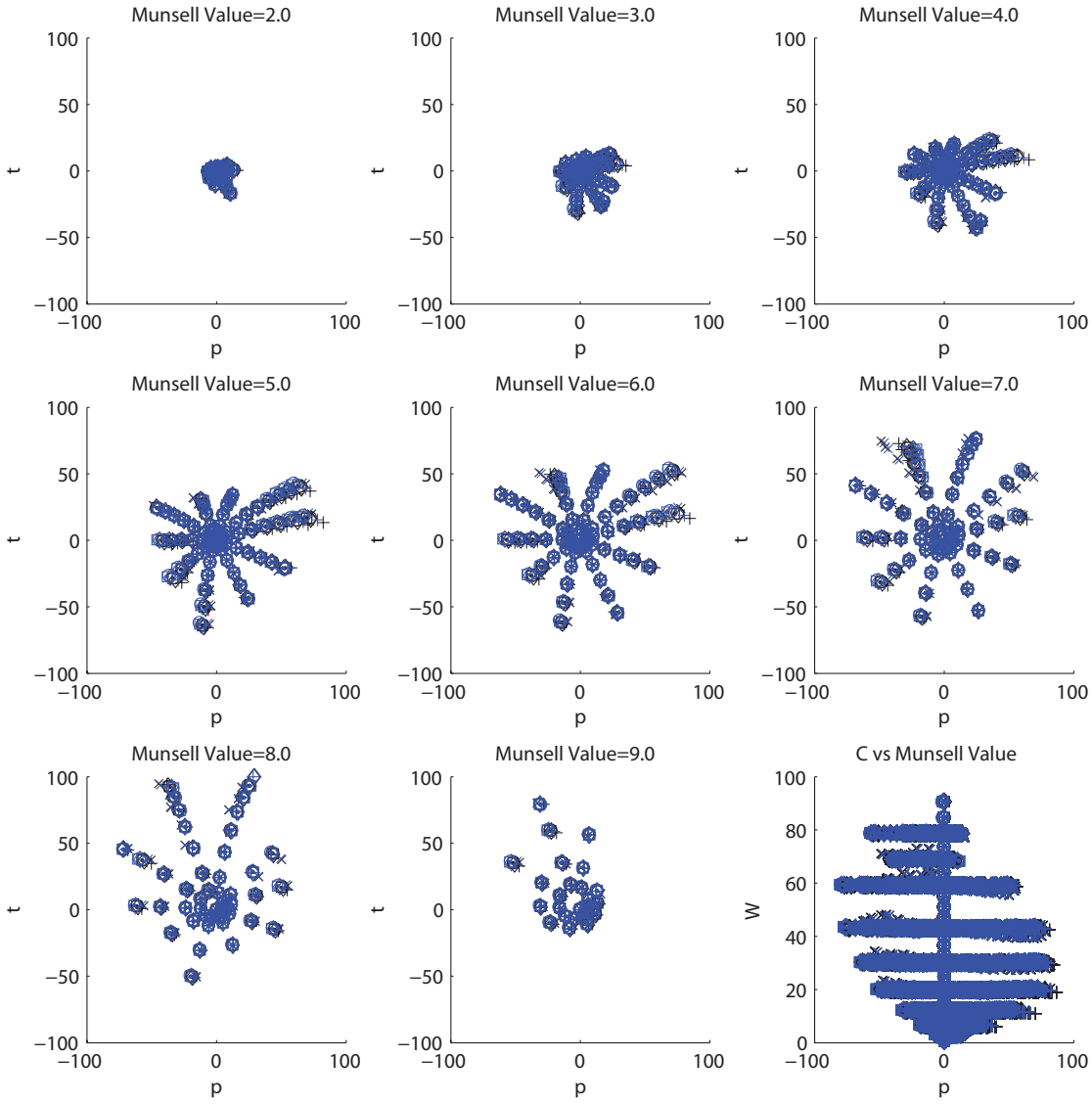

FIGURE 2.5. – Wpt coordinates for a selected set of "corrected" glossy Munsell reflectances. Illuminants are depicted by shape (D65: squares, D50: diamonds, A: pluses '+', C: points, E: circles, F11: crosses 'x') and observers are depicted by color (black: 2° observer, blue: 10° observer).

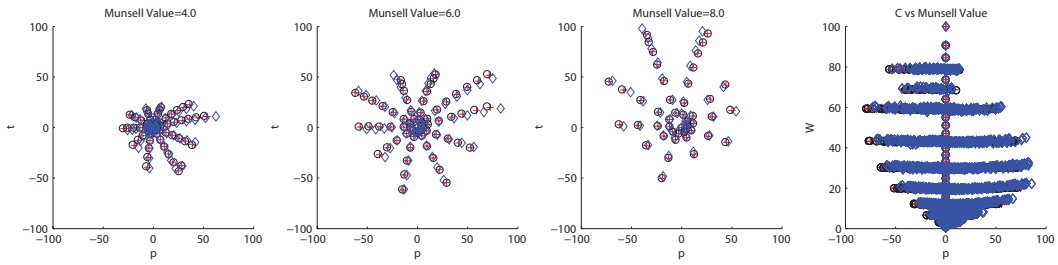

FIGURE 2.6. – Wpt normalized sensor excitation values of various Munsell reflectances under a D65 illuminant for standard 2° observer (red pluses), CIE 2006 5° – 45 year-old cone fundamentals (black circles), digital camera (blue diamonds).

There are three key features that make Wpt unique and advantageous as a color space. First, differences due to changes in illuminant or observer are minimized as part of the Wpt normalization process. Thus, Wpt provides a singular material color equivalency representation that is appropriate for defining Material Adjustment Transforms. Second, it can be experimentally shown that Wpt normalization using different observers that satisfy the same Luther-Ives conditions [Ives, 1915; Luther, 1927] results in different normalization matrices that transform sensor excitations to identical Wpt coordinates. Thus, Wpt coordinates are unique for an observer independent of whether color matching functions or cone fundamentals are used. And third, Wpt preserves the linear relationships of sensor excitations and the polar form of Wpt preserves the perceptive aspects of lightness, chroma, and hue. Therefore, Wpt normalization adjustments for differences in observing conditions are always represented as positive lightness, chroma, and hue even though the corresponding sensor excitations may have negative values.

A key limitation of Wpt is that it is not perceptually uniform because Wpt is based upon a linear transformation of sensor excitations. Therefore, constant differences in Wpt coordinates do not represent constant perceptual differences. A non-linear transform of Wpt coordinates is needed to achieve more perceptual uniformity, and will be discussed as part of Chapter 3.

2.3 Material Color Equivalency

The differences in convergence in FIGURE 2.5 and FIGURE 2.6 represent material color shifts as described by Logvinenko [Logvinenko, 2013]. By his reasoning, the differences in convergence in FIGURE 2.5 can be attributed to differences in color rendering by the illuminants. By similar reasoning the differences in convergence in FIGURE 2.6 are attributed to differences in color matching by the observers. Additionally, color inconstancy of the objects due to illuminant or observer metamerism may be a factor in both figures as well. Metamerism is not a factor in these figures as none of spectral reflectances involved have a colorimetric match under the observing conditions.

It is asserted that Wpt normalization as used in Eq. 2.1 represents an embodiment of a material color mapping of object colors to material colors as proposed by Logvinenko [Logvinenko, 2013]. Logvinenko defined object colors [Logvinenko, 2009] as the combination of an object's spectral reflectance representation (object) and an illuminant representation (light) in the form of a cross product with the combination of all possible object/light pairs forming an object color manifold [Logvinenko, 2013]. He further asserted that a material color mapping assigns object/light pairs from an object color manifold to material colors that can be represented using three dimensions, and object/light pairs that have the same material color can be said to belong to the same "$\sim$m equivalence class" which can be experimentally described by least dissimilar color matching.

A Wpt transformation as used in Eq. 2.1 maps a bispectral representation of an object with a spectral representation of an illuminant for an observer to a three dimensional representation that minimizes differences due to changes in both illuminant and observer. A point of note is that this extends the concepts proposed by Logvinenko to also include a representation of variability in the observer. Thus the material color equivalency mapping that Wpt normalization provides is relative to both a reference illuminant as well as to a reference observer. Thus, object colors (as object/light pairs) are extended to include information about the observer thus defining colors as object color observations (as object/light/observer triplets).

Because it is asserted that Wpt normalization represents a form of "$\sim$m equivalency" mapping as described by Logvinenko, and Logvinenko asserts that "$\sim$m equivalency" can be described by least dissimilar color matching, the least dissimilar color matching experiments of Logvinenko [Logvinenko and Tokunaga, 2011] were duplicated using Wpt normalization transforms. Wpt transforms were determined for the CIE 1931 standard 2° observer with each of the six light sources plotted in FIGURE 2.7 that are similar to those described by Logvinenko.

Tristimulus values for the standard 2° observer were determined under each of the light sources (test observing conditions) for the spectral reflectances of the same set of 22 Munsell colors used by Logvinenko: 5RP 5/12, 10P 4/12, 5P 4/12, 10PB 4/12, 5PB 5/12, 10B 5/12, 5B 5/10, 10BG 5/10, 5BG 6/10, 10G 5/10, 5G 5/10, 10GY 6/12, 5GY 7/12, 10Y 8.5/12, 5Y 8/14, 10YR 7/14, 5YR 7/14, 10R 5/16, 5R 4/14, 10RP 5/14, N 5, and N 1. The tristimulus values of the 22 samples for each test light source were transformed using an appropriate Wpt based MAT to visualization observing conditions using the 1931 standard observer and D65 illuminant using Eq. 2.4, and a visualization under the reference observing conditions is shown in FIGURE 2.8.

$$\mathbf{c}'_{vis} = (\mathbf{A}_{vis})^{-1} (\mathbf{A}_{test}) \, \mathbf{c}_{test} \tag{2.4}$$

where:
$\mathbf{c}_{test}$ is a vector of colorimetry of a patch under test observing conditions,
$\mathbf{A}_{test}$ is a Wpt normalization matrix relative to test observing conditions,
$\mathbf{A}_{vis}$ is a Wpt normalization matrix relative to the standard 2° observer illuminant and D65, and
$\mathbf{c}'_{vis}$ is a vector of colorimetry under the visualization observing conditions.

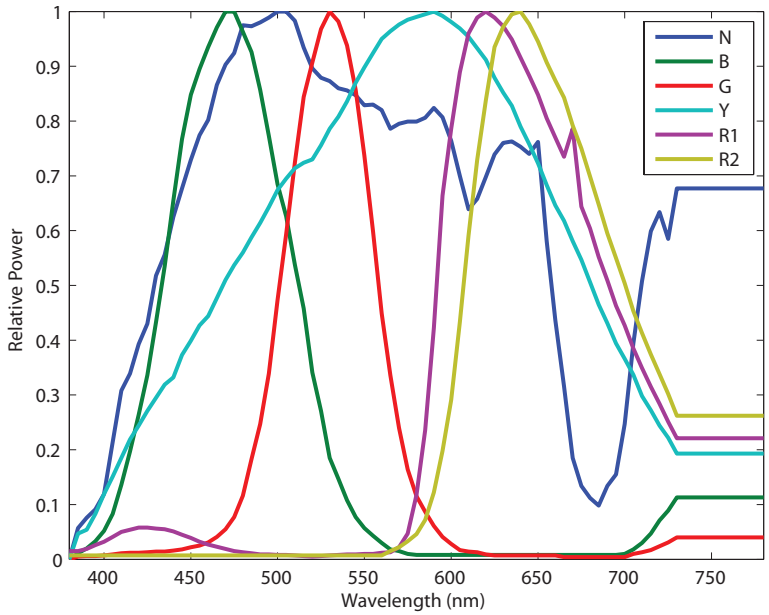

FIGURE 2.7. – Spectral power distributions of illuminants used to evaluate least dissimilar color matching.

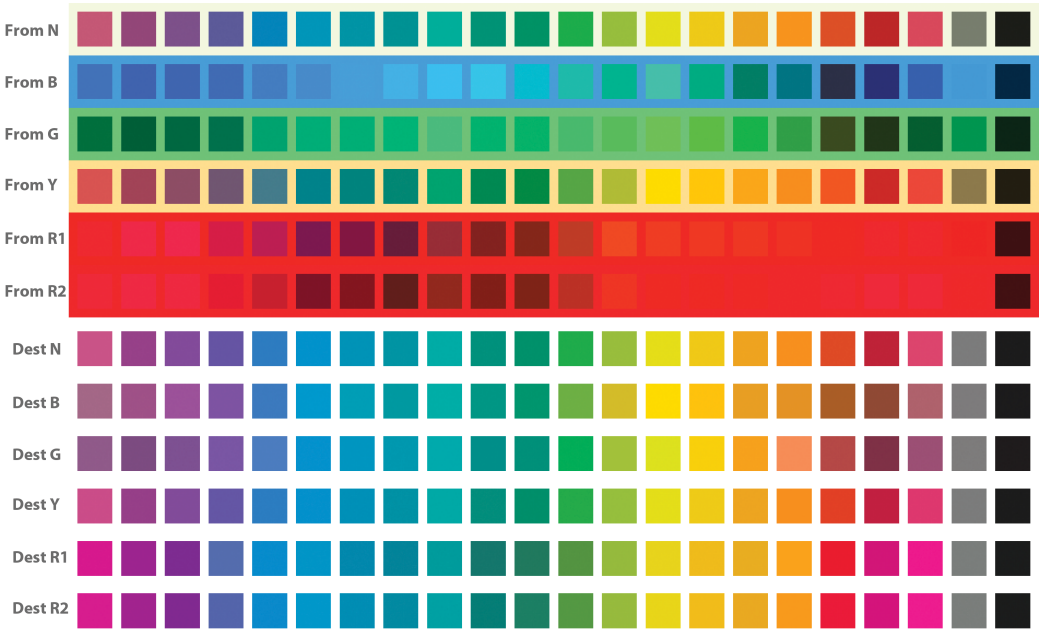

FIGURE 2.8. – Visualization of least dissimilar color matching patches under test illuminations (top) and adjusted to a D65 representation using Wpt based MATs for each illuminant (bottom). (Note: Mapping has been performed to some colors in this visualization as they are outside the output-rendering gamut).

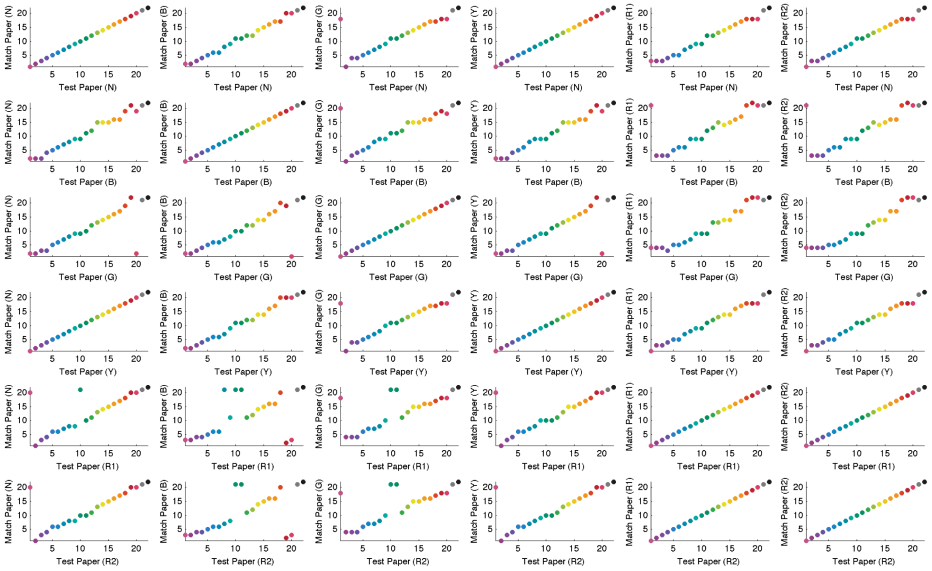

FIGURE 2.9. – Results of using Wpt normalization transforms to predict least dissimilar color matches for illuminants in Logvinenko's experiment.

A non-linear transformation of Wpt coordinates that results in a more perceptually uniform representation would be preferable for the purposes of performing least dissimilar color matching because Wpt is perceptually non-uniform. However, for the purposes of this demonstration, minimizing simple Euclidean distances of Wpt coordinates was performed to find matches. The Wpt coordinates for the patches under the test conditions were determined by applying Eq. 2.1 with the appropriate $\mathbf{A}_{test}$ matrices found using Eq. 2.4.

The results of the matching process are shown in FIGURE 2.9. Exact matches are represented by predictions along the diagonal. Deviations from the diagonal represent prediction mismatches. There appears to be greatest confusion between the **B** or **G** illuminants and the other illuminants. However, the average confusion is less than two Munsell steps from the actual.

TABLE 2.3 contains Logvinenko's reported results of percentage of exact matches averaged across all observers compared to exact match rates corresponding to the results in FIGURE 2.9. These results compare very favorably – exceeding the match rates of those found by Logvinenko with actual human observers in all cases, thus suggesting that Wpt normalization provides a material color mapping to a material color equivalency representation as described by Logvinenko.

TABLE 2.3. – Logvinenko's reported percentages of exact matches averaged across all the observers (upper), Wpt based exact match rates (lower) with best in each case identified by *italics*.

		N	B	G	Y	R1	R2
N	Log	92	39	42	77	31	27
	Wpt	*100*	*59*	*68*	*100*	*64*	*68*
B	Log	40	84	31	28	18	16
	Wpt	*72*	*100*	*59*	*64*	*37*	*37*
G	Log	56	30	78	41	17	11
	Wpt	*68*	*59*	*100*	*64*	*37*	*37*
Y	Log	80	27	41	93	39	28
	Wpt	*100*	*50*	*72*	*100*	*64*	*73*
R1	Log	32	18	18	41	76	59
	Wpt	*68*	*50*	*32*	*73*	*100*	*100*
R2	Log	30	14	19	30	62	75
	Wpt	*82*	*45*	*64*	*73*	*100*	*100*

2.4 Comparisons to other Sensor Adjustment Transforms

An evaluation of sensor adjustment transforms was performed using a data set of 5162 spectral reflectances gathered from 762 flowers in the FReD database [Arnold et al., 2010]; X-Rite Color checker patches; X-Rite Color Checker SG patches; X-Rite Color Checker DC patches; as well as Munsell Matte, Munsell glossy, Natural, Forest, Paper, Candy, Lumber and Agfa IT8.7/2 reflectances from the spectral database from the University of Eastern Finland, Spectral Color Research Group [Kohonen et al., 2006]. Tristimulus values were calculated for both the standard 2° and 10° observers under illuminants C, A, D65, D50, and F11. Oleari's published MATs [Oleari et al., 2011], CIECAT02, and Wpt based MATs were used to predict tristimulus values for these different source illuminants and observers. Oleari's reference conditions of the 10° observer and D65 were used as the destination conditions for all of the comparisons, the results shown in TABLE 2.4 where ΔE_{00} was used as an error metric. In all cases the Wpt based MATs predictions were, on average, closest to the actual. Generally, the Oleari MATs have better prediction than CAT02. However, the CAT02 transform is not a MAT and these results were expected. Another distinction is that Oleari MATs do not generally predict the observing condition white points.

A contrast to the results of TABLE 2.4 can be found by applying the same SATs to the Color Science Association of Japan (CSAJ) corresponding color data [Nayatani et al., 2002]. Tristimulus values for the test data set were transformed with the above SATs going from Illuminant A to D65. A plot of the CSAJ corresponding color colorimetry under D65 compared to the predicted colorimetry

TABLE 2.4. – Comparisons of mean ΔE_{00} between actual and predicted colorimetry using different SATs for 5162 Test with best in **bold** and second-best in *italics*.

	D65,10°	C,10°	D50,10°	A,10°	F11,10°	D65,2°	C,2°	D50,2°	A,2°	F11,2°
Wpt MAT	0.00	**0.10**	**0.35**	**1.24**	**1.41**	**0.61**	**0.63**	**0.92**	**1.72**	**1.68**
CAT02	0.00	*0.16*	0.57	*2.35*	2.25	1.77	2.01	2.01	3.35	3.22
Oleari MAT	0.00	0.79	*0.56*	2.51	*1.89*	*0.91*	*1.38*	*1.42*	*2.63*	*1.95*

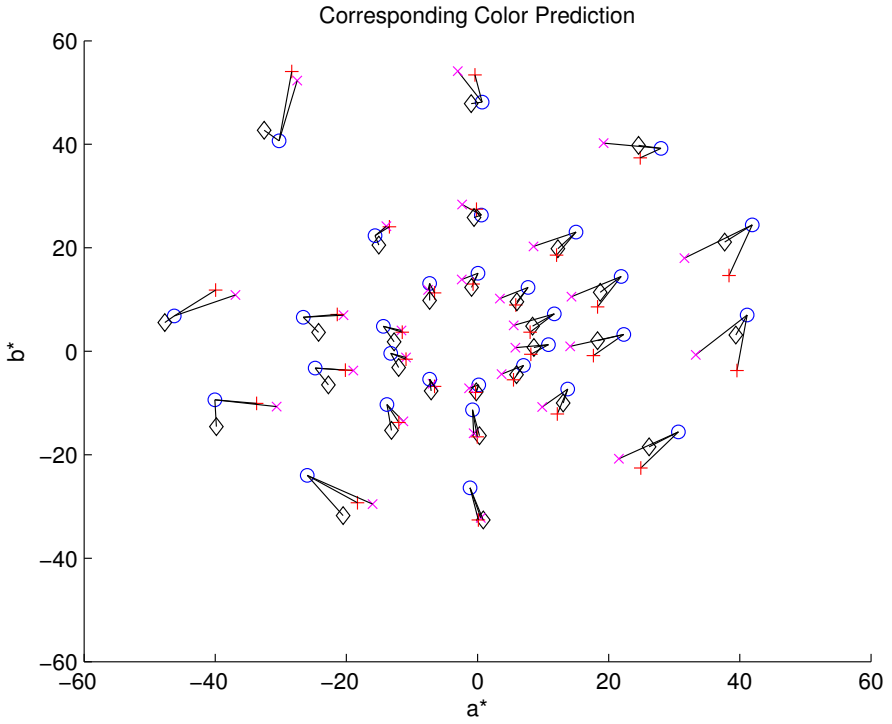

FIGURE 2.10. – Corresponding color prediction of various SATs (o's represent experimentally derived corresponding color, diamonds represent prediction by CAT02, +'s represent Wpt MAT predictions, x's represent Oleari MAT predictions)

using the SATs is shown in FIGURE 2.10. The mean color differences for each of the SATs are found in TABLE 2.5. The MATs do not predict the corresponding color data as well as a CAT02 based CAT. This is because the MATs are not derived with corresponding color data in mind. These results show that CATs and MATs predict different things related to appearance and material color constancy. A CAT predicts corresponding color and doesn't generally predict material constancy, while a MAT predicts material constancy and doesn't generally predict corresponding colors.

TABLE 2.5. – Mean ΔE_{00} difference between SAT predictions and actual CSAJ corresponding color data

CAT02	Wpt MAT	Oleari MAT
3.82	4.88	5.18

2.5 Conclusions

A classification system of Sensor Adjustment Transforms (SATs) has been presented with a distinction being made between Chromatic Adaptation Transforms (CATs) and Material Adjustment Transforms (MATs). A CAT models appearance constancy via corresponding color experiments while a MAT models material constancy via least dissimilar color matching. A method of determining a MAT was presented that uses a color equivalency representation named Wpt (pronounced waypoint) based on a normalization of sensor excitations. The Wpt normalization process preserves the white point as well as independently preserves the perceptive concepts of lightness, chroma, and hue.

Least dissimilar color matching using Wpt normalization and Wpt based MAT prediction of material color were both presented. However, these cases are only basic examples of areas where Wpt based normalization and MATs have merit. Further analysis of using Wpt based MATs for estimating the degree of metamerism, evaluating color rendering, categorizing observers, and converting cone fundamentals to color matching functions as well as investigating various differences and applications between the use of existing CATs and MATs for sensor adjustment transformation, color system analysis, and color modeling can be the subjects of future research.

The concept of a transformation from Wpt coordinates to be more perceptually uniform was introduced as part of the discussion related to performing least dissimilar color matching. However, an investigation of making Wpt more perceptually uniform and its application for estimating color differences is the subject of Chapter 3.

Finally, the proposed methods of determining a Wpt normalization transform require a spectral understanding of both the observer and the illuminant. Often only sensor excitations are available, and it would be useful to have a method to approximately define Wpt normalization transforms that minimize differences due to changes in illumination in these conditions. Alternatively, the

use of the spectral power distribution of the white point of a display to define a Wpt normalization matrix might result in undesirable transformations of the display's colors due to the sharpness of the display's primaries. In such cases an estimated Wpt normalization matrix from the sensor excitations of an illuminant can be found by establishing functional relationships between the entries of Wpt normalization matrices associated with well defined illuminants and the sensor excitations of those illuminants. This is the subject of Chapter 5.

3 Introducing WLab– Going from Wpt (Waypoint) to a Uniform Material Color Equivalency Space

3.1 Introduction

In Chapter 1 transforms were considered going between sensor excitations and adjusted sensor excitations. Generic transforms between sensor excitations without a stated purpose or method were designated as simply Sensor Adjustment Transforms (SAT). It was demonstrated that SATs (like the vonKries transform) [vonKries, 1970] can often be defined as the concatenation of two matrix transforms that utilize an intermediate color equivalency representation. SATs were then differentiated based upon the color equivalency representation utilized and the mechanisms used to determine the transform.

In Chapter 2 it was recognized for one designation that a Chromatic Adaptation Transform (CAT), long utilized in color and vision sciences, is often used for different purposes with conflicting meaning. CATs have been optimized to predict experimentally derived corresponding color data and therefore they utilize an intermediate color equivalency representation that preserves a sense of color appearance. Thus a CAT predicts for a single observer the sensor excitations under one viewing condition (illumination) having the same appearance as sensor excitations under different viewing conditions. Therefore, it was stated that it is inappropriate to use a CAT for relating sensor excitations of colors between different physical observers.

A different transform type was also recognized and given a designation that instead estimates the sensor excitations of a material object under one set of observing conditions (illumination and observer) based on the sensor excitations of the same material object under different observing conditions. Such a transform was designated as a Material Adjustment Transform (MAT) that predict the results of material matching or least dissimilar color matching experiments [Logvinenko and Tokunaga, 2011; Logvinenko and Beer, 2012]. Thus, a MAT utilizes an intermediate color equivalency representation that preserves or estimates material color, and therefore, it is appropriate to use a MAT for relating sensor excitations of colors for changes in illuminant and/or observer.

A normalization methodology was then proposed and demonstrated that linearly transforms sensor excitations (or linear transforms of sensor excitations) into a material color equivalency

representation that can be used as a waypoint for defining Material Adjustment Transforms. The normalization process adjusts for the white point and independently preserves the perceptive aspects of lightness, chroma, and hue [Tonnquist, 1986] resulting in an opponent like coordinate system designated by the axes W, p, and t.

Calculation of Wpt (pronounced Waypoint) coordinates for an object is shown in Eq. 3.1:

$$\begin{bmatrix} W \\ p \\ t \end{bmatrix} = \mathbf{ACOl} \tag{3.1}$$

where:
W represents perceptive lightness,
p, t represent perceptive chromaticness, i.e., a combination of perceptive chroma and hue at constant perceptive lightness,
$\mathbf{A}$ represents a linear transform matrix that converts from sensor excitations to coordinates (W, p, t),
$\mathbf{C}$ defines a matrix containing sensitivity functions, cone fundamentals, or color-matching functions used to convert incident light to sensor excitations that may be scaled (normalized) to account for exposure or to adjust sensor excitations to a desired range,
$\mathbf{O}$ defines a Donaldson matrix used to define how an object reflects and emits light at various wavelengths (with spectral reflectance factor defined along the diagonal) [Donaldson, 1954], and
$\mathbf{l}$ defines a vector of the spectral power distribution of the illuminant.

Matrix $\mathbf{A}$ in Eq. 3.1 is found using a function of the *observing conditions*, that is, the specific sensor functions $\mathbf{C}$ and illuminant $\mathbf{l}$. Thus:

$$A = T\left(\mathbf{C}, \mathbf{l}\right) \tag{3.2}$$

where $T\left(\mathbf{C}, \mathbf{l}\right)$ is a function that determines matrix $\mathbf{A}$ using the Wpt normalization methodology from Chapter 2 for the observing condition defined by $\mathbf{C}$ and $\mathbf{l}$.

A basic overview of the sequence of linear operations that are concatenated to form matrix $\mathbf{A}$ is as follows. First, sensor excitation coordinates are rotated for a perfect reflecting diffuser so that they are co-linear with the first axis (to become W). Then these excitations are scaled so that their W value is 100. Then a plane of sensor excitation coordinates for reflectances of Munsell colors having constant Munsell value and chroma is fitted and sheared to be orthogonal to the W axis. And finally, rotation and scaling is performed around the W axis so that differences in distances from the W axis of the same set of Munsell reflectances are minimized as well as their angular alignment with axes p and t are roughly similar to those used by CIELAB a* and b* axes. Matrix $\mathbf{A}$ therefore represents a transformation of sensor excitations to a coordinate system that preserves the independent perceptive concepts of Munsell value (lightness), chroma and hue.

The polar notation of p, t coordinates provides a representation of chroma (c_{pt}) and hue (h_{pt}). Polar coordinates (c_{pt}, h_{pt}) are found from general Cartesian coordinates (p, t), as follows:

$$\begin{aligned} c_{pt} &= \sqrt{p^2 + t^2} \\ h_{pt} &= tan^{-1}\,(t, p) \end{aligned} \tag{3.3}$$

And, conversion from polar notation back to Cartesian coordinates is determined as follows:

$$\begin{aligned} p &= c_{pt} \cos h_{pt} \\ t &= c_{pt} \sin h_{pt} \end{aligned} \tag{3.4}$$

There are three key features that make Wpt unique and advantageous as a color space. First, differences due to changes in illuminant or observer are minimized as part of the Wpt normalization process. Thus, Wpt provides a singular material color equivalency representation [Logvinenko and Beer, 2012]. Second, it can be experimentally shown that replacing matrix $\mathbf{C}$ in Eq. 3.1 and 3.2 with a linear (invertible) transformation of $\mathbf{C}$ always results in identical Wpt coordinates (which is a result of the minimization performed to establish the associated matrix $\mathbf{A}$ in each case). Thus, resulting Wpt coordinates are unique for an observer independent of whether color matching functions or cone fundamentals are used. Third, Wpt preserves the linear relationships of tristimulus values and the polar form of Wpt preserves the perceptive [Tonnquist, 1986] aspects of lightness, chroma, and hue. Therefore, Wpt normalization adjustments for differences in observing conditions are always represented as positive lightness, chroma, and hue even though the corresponding sensor excitations may have negative values.

However, equal distances of Wpt coordinates do not correspond to equal perceptual differences. This is because Wpt normalization is defined using a linear transformation of sensor excitations, and uniform color spaces such as CIELAB [CIE15, 2004] CIECAM02 [Moroney et al., 2002] and CAM02-UCS [Luo et al., 2006] require non-linear transformations of tristimulus values (which are linear transforms of sensor excitations) to achieve some form of perceptual uniformity.

The Munsell color order system was used as a rubric for evaluating and adjusting the perceptual uniformity of Wpt because the Munsell system is a reasonable representation of perceptually uniform colors [Newhall, 1940; Newhall et al., 1943]. Polar representations of Wpt, CIELAB, and CAM02-UCS coordinates were determined for corrected reflectances of the 1600 glossy Munsell Book of Color sample (Appendix A) for illuminant C and the 1931 standard 2° observer and plotted against actual Munsell value, chroma and hue to demonstrate various aspects of color space uniformity with the results found in FIGURE 3.1. Ideally, having all the points on a straight line is indicative of the consistency with the perceptual uniformity provided by the Munsell color order system. Thus, the degree of convergence of points onto a line, either linear or non-linear, indicates the level of perceptual independence of lightness chroma and hue, and the degree of linearity indicates the level of correlation with Munsell value, chroma, or hue.

There is nearly perfect convergence in lightness for both Wpt and CIELAB in FIGURE 3.1. This is because Munsell value planes are based upon CIE Y, and Wpt W is essentially the same as Y for the reference observing conditions and CIELAB L* is based on Y. CAM02-UCS has slightly

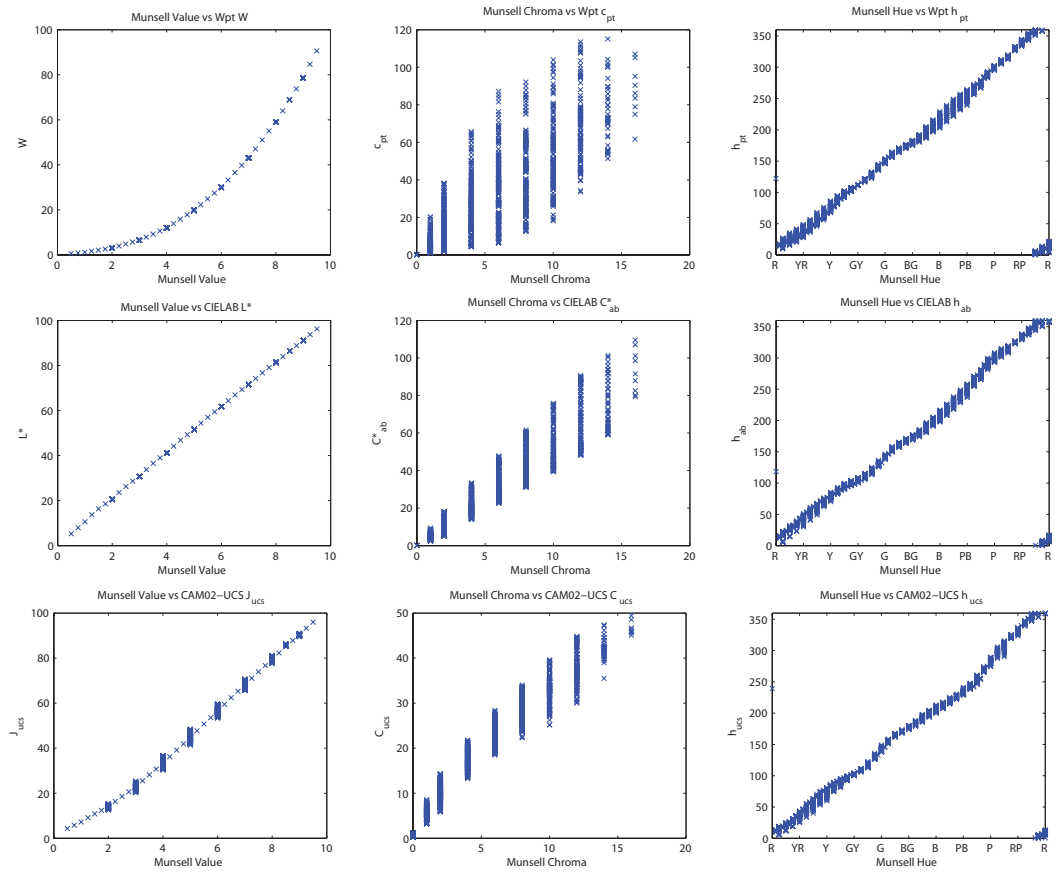

FIGURE 3.1. – Correlation Plots between Munsell and Wpt (top), CIELAB (middle), CAM02-UCS (bottom) with correlations between Munsell Value and space lightness (left), Munsell Chroma and space chroma (center), and Munsell Hue and space hue (right)

less convergence due to a dependency that J has on chroma. Although both CIELAB and CAM02-UCS have fairly linear relationships with Munsell value, the relationship between Wpt W (lightness) and Munsell value is not linear and thus, is non-uniform in lightness. CIELAB and CAM02-UCS both show tighter convergence for chroma than Wpt, but complete convergence does not generally occur, possibly indicating that Munsell chroma is not entirely independent of lightness and hue for these color spaces. CIELAB and CAM02-UCS both exhibit a fairly linear relationship within the level of convergence to Munsell chroma with a slight upward bow for CAM02-UCS due to optimizations that better predict supra-threshold level color difference experiments. Wpt exhibits very little convergence of chroma, which is indicative of significant non-uniformity of chroma with large dependences that Wpt chroma has on lightness and hue. Additionally, it is difficult to discern any linear relationship between Wpt chroma and Munsell chroma. Thus, Wpt is not perceptually uniform in chroma. All three color spaces in FIGURE 3.1 have nearly a linear relationship between their hue and Munsell hue, yet each has some lack of convergence in hue, but not to a great degree. This is indicative of slight dependencies of hue on lightness and/or chroma for the color spaces in relationship to the Munsell color order system. In summary, Wpt W is well correlated with Munsell value, but is non-linear (therefore non-uniform) in lightness. Wpt chroma has very poor correlation with Munsell chroma and its linearity is difficult to assess. Wpt hue is reasonably correlated and linear with Munsell hue.

3.2 Making Wpt More Perceptually Uniform

Only non-linear transforms of Wpt W, and c_{pt} were developed to get better perceptual uniformity. No further adjustments to h_{pt} were deemed necessary because of the linearity and relative convergence of h_{pt} in FIGURE 3.1. This had the additional benefit of maintaining the direct correlation between h_{pt} and dominant/complimentary wavelength because Wpt is a linear transformation of sensor excitations.

The application of the developed non-linear transforms of (W, p, t) coordinates results in perceptually uniform coordinates (L_w, a_w, b_w) which define a color space that shall hereafter be referred to as WLab (or *Waypoint-Lab*). These transformations are based upon modifying the polar notation of Wpt – thus modifying coordinates of (W, c_{pt}, h_{pt}). A few guiding principles that were used in developing these transforms are as follows:

First, the transforms should be mathematically invertible between (W, p, t) and (L_w, a_w, b_w) coordinates.

Second, L_w should be independent of chroma and hue, and have a linear relationship with Munsell value.

Third, dependencies of chroma on lightness and hue should be minimized with general agreement with the large-scale uniformity defined by the Munsell color order system.

Fourth, small distances in chroma without changes in lightness and hue should be adjusted to approximate color differences as determined by a well defined color difference formula like $\Delta E^{\star}{}_{94}$ [Berns, 1993] or ΔE_{00} [Luo et al., 2001]. Thus, small Euclidean distances of WLab coordinates should reasonably predict the results of supra-threshold color difference experiments.

A fifth, optional objective (that conflicts with the fourth objective, and cannot be simultaneously achieved) is that a linear relationship should exist between adjusted chroma and Munsell chroma.

The second objective was achieved using the CIE Y to CIE L* formulas [CIE15, 2004] to directly translate between W and L_w since W is equivalent to CIE Y for the standard 2° observer and illuminant C, and is also independent of chroma and hue. Thus:

$$L_w = 116 f\left(W\right) - 16 \tag{3.5}$$

where:

$$f\left(v\right) = \begin{cases} v^{1/3}, & \text{if } v > \left(\frac{6}{29}\right)^3 \\ \left(\frac{1}{3}\right)\left(\frac{29}{6}\right)^2 v + \frac{4}{29}, & \text{otherwise} \end{cases}$$

The first objective (mathematical invertibility) as well as the second objective (reduced dependence of chroma on lightness and hue) were achieved by separating the investigation and correction of chroma's dependence of lightness and hue into two separate steps. In FIGURE 3.2, the maximum Wpt chroma values for each Munsell chroma ring are plotted as 'x' marks relative to each ring's L_w value. Dependency relationships between L_w and Wpt chroma were then evaluated by connecting lines between the points for rings that have the same Munsell chroma. Ideally, if chroma was independent of lightness the lines would all be straight and horizontal. However, as can be seen in FIGURE 3.2, Wpt chroma (for rings that have the same Munsell chroma) increases as L_w increases although there is general similarity between the lines. The spacing between the chroma lines is also nearly uniform when the rings have a Munsell value 5/ L_w approximately equals 50). Finally, the curve with Munsell chroma /6 represents the median curve of the bottom five curves that all have similar shape.

The scaled curves having the same general exponential shape can be described as a function of L_w. This is shown in FIGURE 3.3 by scaling each of the chroma curves in FIGURE 3.2 by the Wpt chroma values for the rings when Munsell value equals 5/.

An estimation of a relative curve scale factor (s) was determined by using the chroma line points having Munsell chroma /6 (the median curve) as a general representative for all the curves. The fitted curve representing this scale factor is also depicted in FIGURE 3.3 as a function of L_w and is defined by the following:

$$s = \frac{e^{(g_0(L_w - g_1))}}{g_2} \tag{3.6}$$

where g_0 =0.0267, g_1=51.5762, g_2=0.4589.

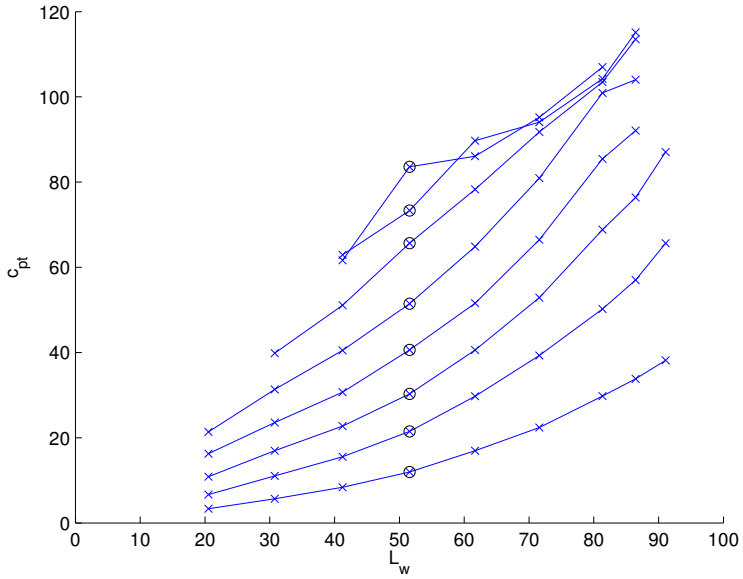

FIGURE 3.2. – Relationships between L_w and maximum Wpt chroma values for chroma rings with the same Munsell chroma. Circles represent maximum Wpt chroma values for chroma rings that have Munsell value 5/

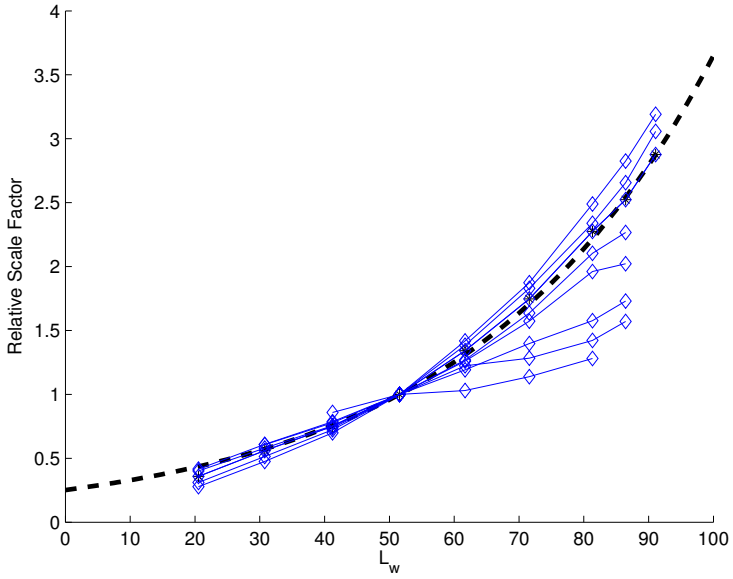

FIGURE 3.3. – Relative chroma scaling for chroma lines depicted in FIGURE 3.2. Dashed line represents fit for Munsell chroma /6.

The dependence of Wpt chroma on L_w was then minimized, assuming that s is a lightness dependent scale factor, by dividing the Wpt chroma (c_{pt}) by *s* as follows:

$$c_{mod} = \frac{c_{pt}}{s} \tag{3.7}$$

where:
c_{mod} represents a modified chroma that has reduced dependence on lightness,
c_{pt} represents the initial Wpt based chroma, and
s is the lightness scaling correction factor defined in Eq. 3.6.

The relationship between lightness corrected chroma and color difference formulas was then evaluated before evaluating dependencies between chroma and hue. This was accomplished by using a function $\Delta E_{\Delta c}$ that determines a ΔE color difference for a small increase of corrected Wpt chroma as follows:

$$\Delta E_{\Delta c}\left(L_w, c_{mod}, h\right) = \Delta E\left(g\left(L_w, c_{mod}, h\right), g\left(L_w, c_{mod} + \Delta c, h\right)\right) \tag{3.8}$$

where:
ΔE is a color difference formula of two CIELAB values,
L_w represents a perceptually corrected Wpt lightness value,
c_{mod} represents a lightness corrected Wpt chroma value,
h represents a Wpt hue angle, and
$g\left(\right)$ is a function that converts perceptually corrected (L_w, c_w, h_w) coordinates to CIELAB coordinates, and was implemented using the inverse of Eq. 3.7 and Eq. 3.5, and then Eq. 3.4 to get Wpt coordinates. Then an inverse of $\mathbf{A}$ in Eq. 3.1 was applied to the Wpt coordinates to get tristimulus XYZ values. These were then converted to CIELAB using standard XYZ to CIELAB formulas [CIE15, 2004].

Next, color difference chroma values for the k^{th} increment of Δc were expressed as the chroma value for the $(k-1)^{th}$ increment plus the mean of all the color differences over the range $(k-1)\Delta c$ to $k\Delta c$ using the following discrete recurrence relationship:

$$\begin{gathered} C_{\Delta E}\left(0\right) = 0 \\ C_{\Delta E}\left(k\Delta c\right) = C_{\Delta E}\left(\left(k-1\right)\Delta c\right) + \frac{\sum_{i=1}^{n}\sum_{j=1}^{m}\Delta E_{\Delta c}(L_{w,i},(k-1)\Delta c,h_j)}{nm} \end{gathered} \tag{3.9}$$

where:
$C_{\Delta E}\left(k\Delta c\right)$ is a discrete color difference chroma estimation for modified Wpt chroma value of $k\Delta c$,
k is a whole number greater than or equal to zero,
Δc represents a small change in modified Wpt chroma value, and
$\Delta E_{\Delta c}$ represents the function defined in Eq. 3.8, $L_{w,i}$ represents the i^{th} perceptually corrected Wpt lightness value that varies in n steps over range 0 to 100 for calculation of the mean, and h_j represents the j^{th} Wpt hue value that varies in m steps over range 0 to 360.

Various ΔE formulas were evaluated for the purposes of scaling modified Wpt chroma using color differences. However, because using ΔE_{00} was found to result in various large-scale spacing deformities (whereas using $\Delta E^{\star}{}_{94}$ did not) and because the scaling of the chroma term in ΔE_{00} formulas is identical to that of $\Delta E^{\star}{}_{94}$, the $\Delta E^{\star}{}_{94}$ color difference metric was ultimately used for correcting modified Wpt chroma. Thus, there was a conscious trade-off made in this case between large-scale and small-scale color difference uniformity. A plot of c_{mod} versus ΔE using the $\Delta E^{\star}{}_{94}$ color difference formula for ΔE in Eq. 3.9 is presented in FIGURE 3.4 where uniform lightness corrected chroma was found to have a logarithmic relationship to the color difference based chroma. This relationship was fitted and the results of this fit are also shown in FIGURE 3.4.

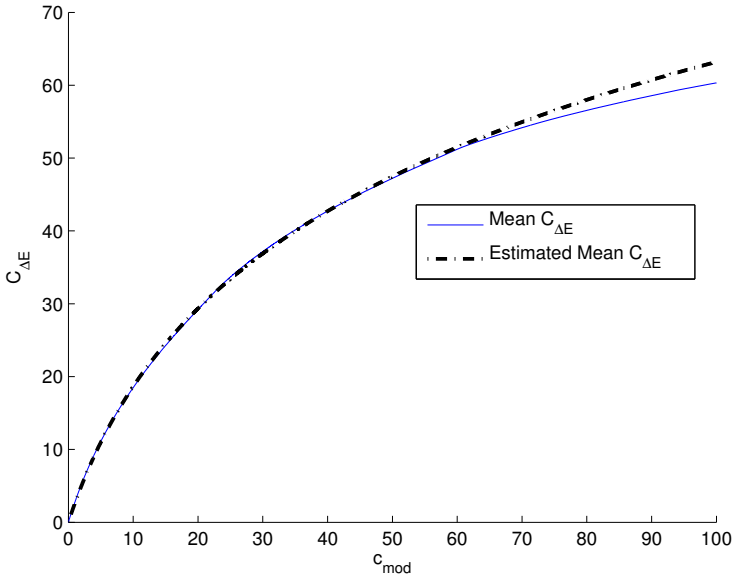

FIGURE 3.4. – Relationship between lightness corrected chroma and color difference chroma as defined by $\Delta E^{\star}{}_{94}$color difference equations (solid line), and fitted estimation using a logarithmic function (dot-dashed line)

The fitted equation for this relationship is as follows:

$$c_w = d_0 \left[\ln \left(\frac{c_{mod}}{80} + d_1 \right) - \ln (d_1) \right] \tag{3.10}$$

where:
c_{mod} represents a lightness corrected chroma using Eq. 3.7,
d_0=24.9523, and
d_1=0.1104.

However, this ignores the possible dependency on hue because the dependencies of chroma on hue are combined into the term determining the mean $\Delta E_{\Delta c}$ in Eq. 3.9. The approach was modified to determine hue specific chroma difference curves by only taking the mean of the

incremental color differences over the lightness range and making hue a variable of the function as follows:

$$C_{\Delta E}(0) = 0$$
$$C_{\Delta E}(k\Delta c, h) = C_{\Delta E}((k-1)\Delta c, h) + \frac{\sum_{i=1}^{n} \Delta E_{\Delta c}(L_{w,i},(k-1)\Delta c,h)}{n} \tag{3.11}$$

where:
$C_{\Delta E}(k\Delta c, h)$ is a color difference based chroma estimator for a discrete modified Wpt chroma value of $k\Delta c$ having Wpt hue h,and
n, Δc, ΔE, g, and $L_{w,i}$ are the same as in Eq. 3.9.

Color difference chroma curves were then determined for individual hues and plotted in FIGURE 3.5 in addition to the curves shown in FIGURE 3.5. The color difference chroma curves for the yellows have the greatest slope, and the color difference chroma curves for the blues have the least slope.

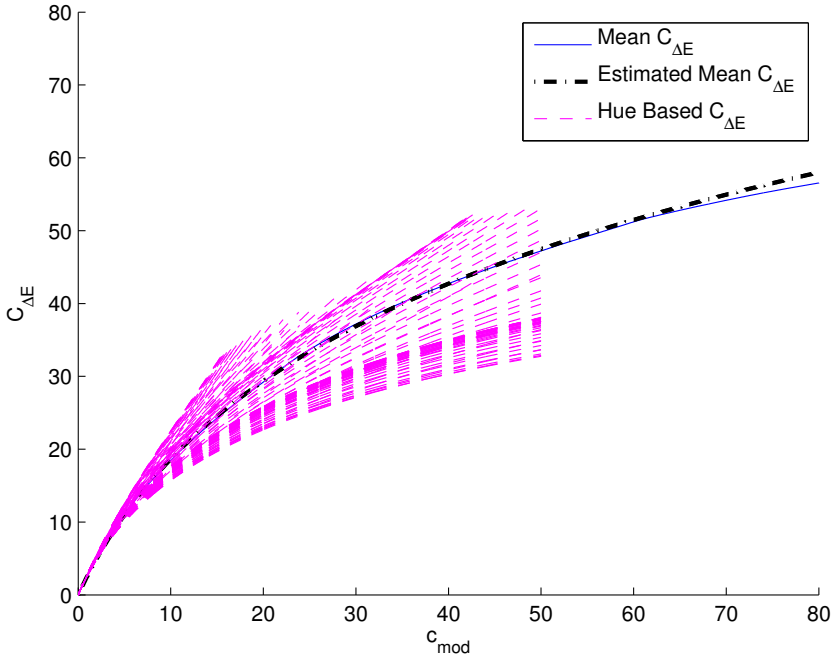

FIGURE 3.5. – Relationship between lightness corrected chroma and color difference chroma as defined by $\Delta E^{\star}{}_{94}$color difference equations (solid line), and fitted estimation using a logarithmic function (dot-dashed line)

Each of the hue based $C_{\Delta E}(k\Delta c, h)$ curves in FIGURE 3.5 were then fitted using Eq. 3.10 to solve for constants d_0 and d_1 as a function of hue. These results were then plotted and fitted in FIGURE 3.6 showing values for both d_0 and d_1 coefficients in terms of *h*. The curves for coefficients d_0 and d_1 in FIGURE 3.6 both have the same general shape and differ only in scale and vertical offset.

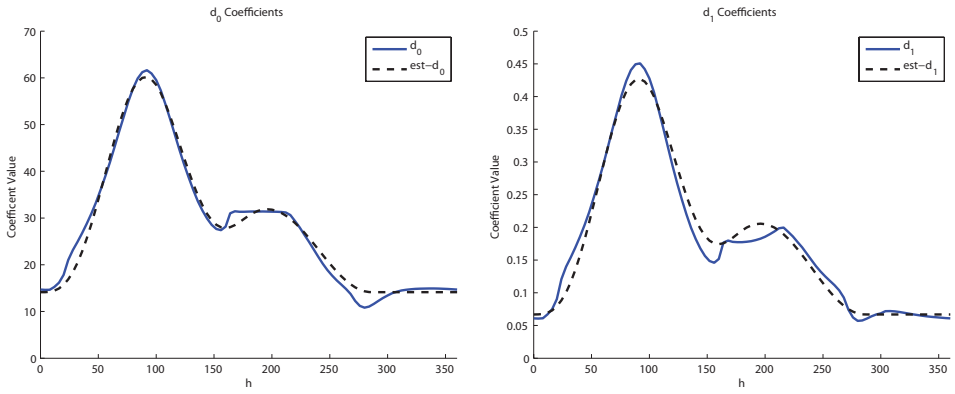

FIGURE 3.6. – Hue based d_0 (left) and d_1 (right) coefficients to be used in Eq. 3.10. Solid lines represent curves fitted to dashed lines in FIGURE 3.5. Dashed lines represented estimated fit as function of h.

A general function of h was determined for the general shape and coefficient functions were fitted to approximate each of the curves that is smooth joining at 0/360°. This resulted in hue specific definitions for coefficients d_0 and d_1 that can be used in Eq. 3.10 to provide both reduced chroma dependency on hue as well as a reasonable approximation of $\Delta E^{\star}{}_{94}$ difference for small differences of chroma with no change in lightness or hue. The fitted hue specific coefficients equations are as follows:

$$
\begin{aligned}
r_1 &= \begin{cases} [\sin h - 1]^3, & \text{if } h > 1 \text{ and } h < 181 \\ 0, & \text{otherwise} \end{cases} \\
r_2 &= \begin{cases} 0.39\,[\cos{(h - 14)}]^2, & \text{if } h > 104 \text{ and } h < 284 \\ 0, & \text{otherwise} \end{cases} \\
d_0 &= 62\,(r_1 + r_2 + 0.31) \\
d_1 &= 0.36\,(r_1 + r_2 + 0.19)
\end{aligned}
\tag{3.12}
$$

A complete process was then defined for converting Wpt coordinates to (L_w, a_w, b_w) coordinates once the method of hue based correction of chroma using Eq. 3.11 and Eq. 3.12 was established. The actual equations used to convert between Wpt and WLab are presented in Appendix B for the convenience of the reader.

The entire process can be stated as follows. First, Wpt is converted to polar form using Eq. 3.3. Then L_w is found using Eq. 3.5. Lightness based correction of chroma is then performed by applying Eq. 3.7 using the lightness based coefficient found by Eq. 3.6. Then, hue based color difference correction of chroma is performed by applying Eq. 3.10 using the hue based coefficients d_0 and d_1 found by Eq. 3.12. And finally, polar $(L_w,\ c_w,\ h_w)$ coordinates are converted to Cartesian $(L_w,\ a_w,\ b_w)$ coordinates using Eq. 3.3. Hereafter, the conversion of

Wpt to WLab shall be referred to as the function $u_w\left(\right)$ that converts a Wpt vector to a WLab vector as follows:

$$\begin{bmatrix} L_w \\ a_w \\ b_w \end{bmatrix} = u_w \left(\begin{bmatrix} W \\ p \\ t \end{bmatrix} \right) \tag{3.13}$$

3.3 Defining the inverse transform

A complete process was also defined for converting (L_w, a_w, b_w) coordinates to Wpt coordinates. This process involves applying the inverse of the transforms from the previous section in reverse order. First WLab is converted to polar notation (L_w, c_w, h_w using an equation similar to Eq. 3.4.

The functions that determine the coefficients used in the equations that adjust for chroma dependency DO NOT need to be inverted because they are independent functions of lightness and hue. Only the equations that use the coefficients are inverted. This greatly simplifies the process of inversion. The coefficients for inversion are calculated directly, since both L_w and h_w are both known, using Eq. 3.12 and Eq. 3.6.

The hue based chroma correction is undone using the coefficients based on *h* from Eq. 3.12 with the following equation, which is the logical inverse of Eq. 3.10:

$$c_{mod} = 80 \left[e^{\left(\frac{c_w}{d_0} + \ln(d_1) \right)} - d_1 \right] \tag{3.14}$$

where d_0 and d_1 are defined in Eq. 3.12.

The inverse of Eq. 3.7 is then applied to undo the correction that reduces the dependency of chroma on lightness as follows:

$$c_{pt} = s c_{mod} \tag{3.15}$$

where s is the same scalar coefficient defined in Eq. 3.6.

Next, the inverse of Eq. 3.5 is applied to convert from L_w to W as follows:

$$W = 100 f^{-1} \left(\frac{L_w + 16}{116} \right) \tag{3.16}$$

where:

$$f^{-1}\left(v\right) = \begin{cases} v^3, & \text{if } v > \frac{6}{29} \\ 3\left(\frac{2}{29}\right)^2 \left(v - \frac{4}{29}\right), & \text{otherwise} \end{cases}$$

Finally, polar (W, c_{pt}, h_{pt}) coordinates are converted to Cartesian (W, p, t) coordinates by applying Eq. 3.4. Likewise, the conversion of WLab to Wpt can be referred to as a function $u_w^{-1}()$ that converts a WLab vector to a Wpt vector as follows:

$$\begin{bmatrix} W \\ p \\ t \end{bmatrix} = u_w^{-1} \left(\begin{bmatrix} L_w \\ a_w \\ b_w \end{bmatrix} \right) \tag{3.17}$$

3.4 Comparisons and Analysis

Differences between WLab and standard color spaces like CIELAB[CIE15, 2004], DIN99o[Klein, 2010], CIECAM02[Moroney et al., 2002], CAM02-UCS[Luo et al., 2006] and others are inevitable because of differences in how they are derived. The following process, in general terms, is used to convert sensor excitations to these other color spaces. First, white point adjustment or chromatic adaptation is applied to sensor excitations (or tristimulus values). These adjusted sensor excitations are then transformed using a non-linear (power) function to get a perceptually uniform spacing. Then the adjusted uniform sensor excitations are transformed using some fixed linear transformation to derive lightness and opponent channels, which may be further modified to derive appearance correlates or achieve color difference metrics.

The order of operations when converting from sensor excitations to WLab is necessarily different because Wpt normalization is first performed before non-linear perceptual uniformity is applied. Wpt normalization involves first white point adjustment by rotation and scaling of sensor excitations, then constant lightness planes are established by regression and shearing, and finally opponency chroma separation as well as hue assignment are determined using minimization. These functions are all performed at the same time within a single observer/illuminant specific Wpt normalization matrix before WLab perceptual uniformity is applied. The net result is that the relationships between hue and chroma are different for WLab than they are for other color spaces. Additionally, because Wpt normalization is relative to the observing conditions (observer and illuminant) the lightness and opponent channel relationships to sensor excitations are variable for WLab rather than fixed (which is not the case for color spaces like CIELAB, DIN99o, and CIECAM02).

The question then is “Do the manipulations performed to get to WLab provide for a sufficiently stable prediction of perceptive color correlates (lightness, chroma, and hue) with a reasonably uniform prediction of color and color differences such that WLab can be used with confidence in situations were other standard color spaces are typically applied?” It is affirmed that the answer to this question is “Yes"! Comparisons to Munsell perceptual uniformity as well as comparisons to color difference equations were performed to arrive at this answer.

The results of FIGURE 3.1 were repeated as a first order comparison replacing the Wpt results with those of WLab, and are shown in FIGURE 3.7. The WLab lightness linearity and convergence

are practically identical to CIELAB, and there is greater convergence in WLab chroma indicative of reduced dependence on lightness and hue. With this convergence of chroma there is also a greater linear relationship between WLab chroma and Munsell chroma with a slight upward bow. It is hypothesized that this slight non-linearity is possibly indicative of using a color difference equation to optimize chroma by hue. There are no differences between the Wpt hue plot in FIGURE 3.1 and the WLab hue plot in FIGURE 3.7 since no changes were made to hue.

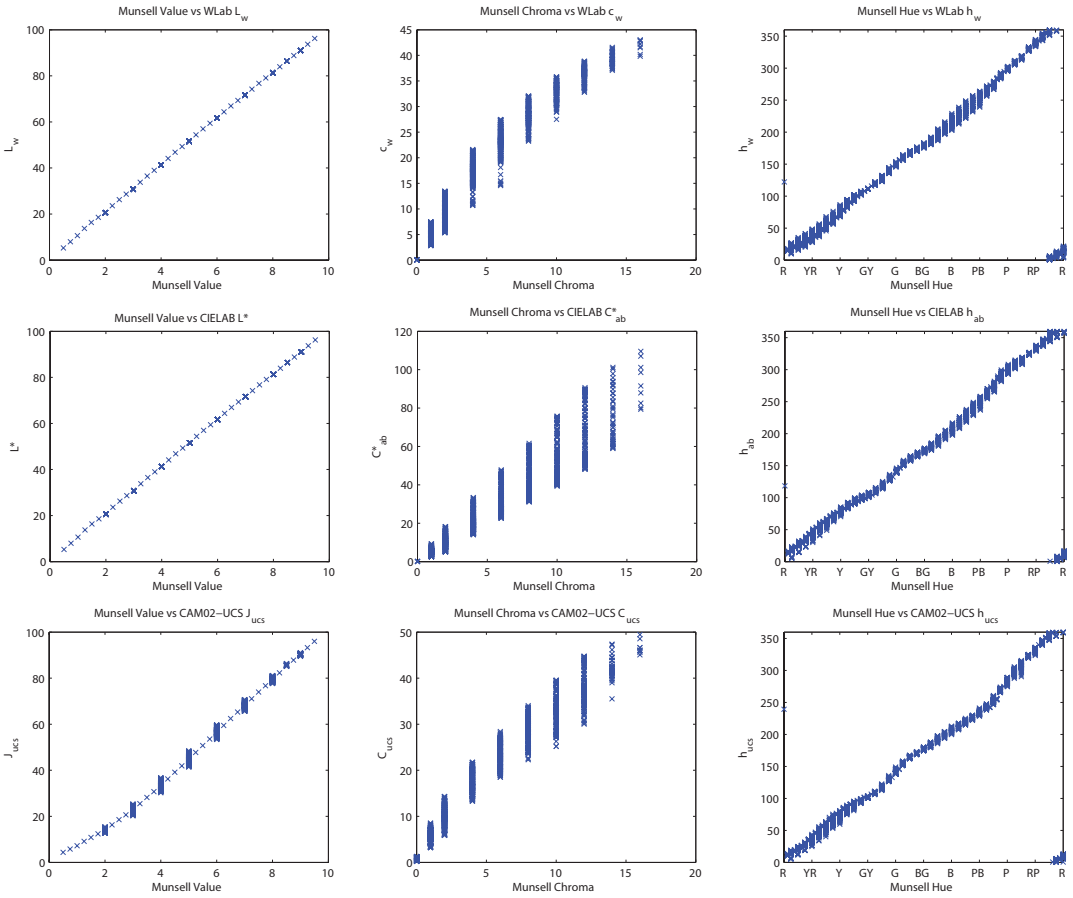

FIGURE 3.7. – Correlation Plots between Munsell and WLab (first row) CIELAB (second row), CIECAM02-UCS (bottom) with correlations between Munsell Value and space lightness (left), Munsell Chroma and space chroma (center), and Munsell Hue and space hue (right).

Alternatively, a hue based correction without applying a correction for color difference based chroma can be achieved by additionally applying the inverse of the mean chroma correction (Eq. 3.14 with the non-hue specific d_0 and d_1 coefficients that were found and presented with Eq. 3.10) directly after applying the hue specific correction (Eq. 3.10 with d_0 and d_1 coefficients found using Eq. 3.12). The resulting color space from this additional step shall hereafter be designated as LSWLab (for *Large-Scale Waypoint Lab*). A side side-by-side comparison of the correlations between Munsell and WLab and LSWLab was made, shown in FIGURE 3.8. The additional step employed by LSWLab results in closer linearity to Munsell chroma, and has a

chroma correlation that is more similar in shape to CIELAB's (though different in scale). With LSWLab there is also a change resulting in more convergence for less chromatic colors and slightly lesser convergence for more chromatic colors.

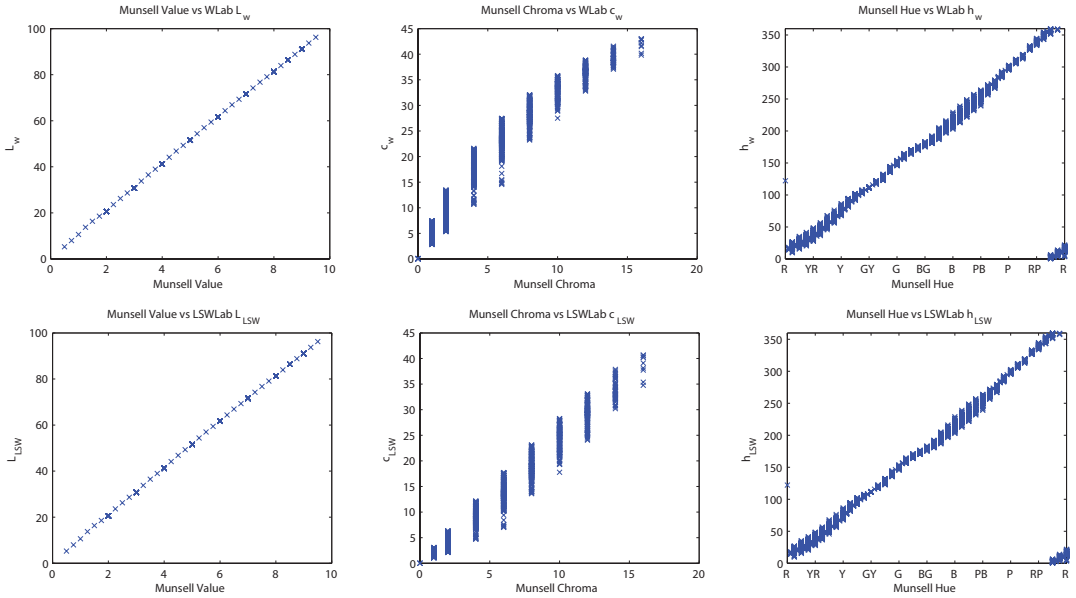

FIGURE 3.8. – Correlation Plots between Munsell and WLab (top) LSWLab (bottom) with correlations between Munsell Value and space lightness (left), Munsell Chroma and space chroma (center), and Munsell Hue and space hue (right).

A second method of evaluating perceptual uniformity of color spaces relative to Munsell colors was performed by plotting lines between coordinates for adjacent chroma and hue in various value planes as well as plotting chroma versus lightness relationships. The following three evaluation criteria are important when evaluating perceptual uniformity in these plots (assuming that Munsell colors are perceptually uniform for the 1931 two degree observer and Illuminant C). First, planes of constant Munsell value in a lightness versus chroma plane should form lines that are perpendicular to the achromatic axis and be evenly spaced. Second, rings of constant chroma should form circles centered on the origin and be evenly spaced. And lastly, lines of constant hue should be straight meeting at the origin and be evenly spaced. The degree to which these criteria are not met is an indication of perceptual non-uniformity of either the color space or the Munsell color order system, or both.

In FIGURE 3.9 three Munsell value planes were determined along with a side view showing the relationships that Munsell colors have with the color spaces' lightness and chroma axes. The ideal criteria described in the previous paragraph were generally approximated in FIGURE 3.9 by each of the color spaces with various deviations, and the extent of the variations are due to both the transforms involved in defining the color spaces as well as the criteria that were used to optimize them. The determination of which one is "best" is left to the reader as the use cases for each vary.

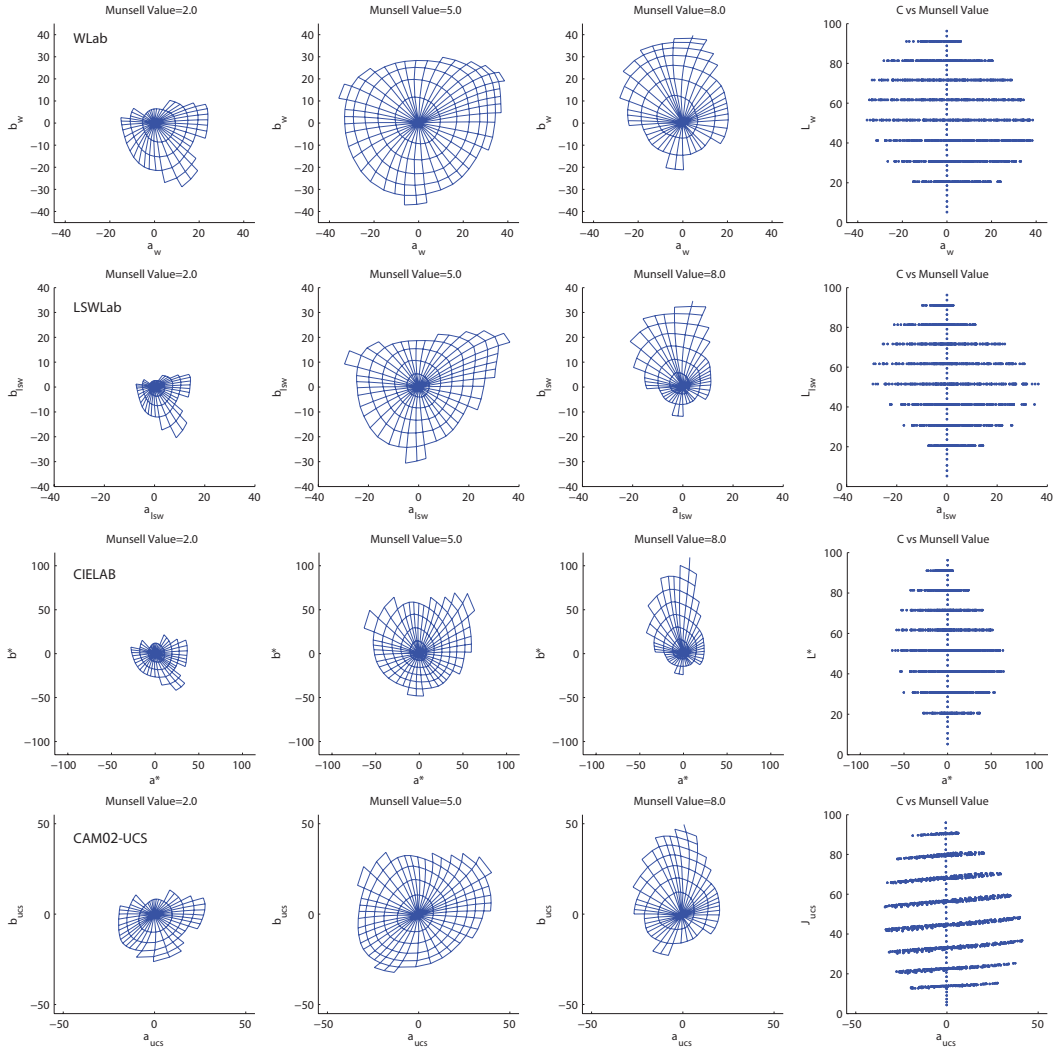

FIGURE 3.9. – Comparison of Munsell colors as represented by WLab(top), LSWLab(second row), CIELAB (third row), CAM02-UCS (bottom) for Munsell Value 2/ (left), Munsell Value 5/ (second column), Munsell Value 8/ (third column), and lightness vs chroma (right).

However, there are noteworthy differences in FIGURE 3.9 between the chroma rings in WLab and LSWLab. The LSWLab chroma rings appear more evenly spaced than the chroma rings for WLab (as there appears to be compression in chroma with WLab as chroma increases). But, the WLab rings appear to be rounder (more circular) than the LSWLab rings. It is postulated that these differences may be due to differences in perception of large-scale and small-scale color differences with large-scale color differences having a more linear relationship to sensor excitations and small-scale color differences having a more logarithmic relationship to sensor excitations.

Based on FIGURE 3.7 and FIGURE 3.9, it is generally reasonable to conclude that WLab is generally about as perceptually uniform, in comparison to the Munsell color order system, as CIELAB and CAM02-UCS.

3.5 Color differences using WLab

Color differences using WLab are determined using Euclidean differences of WLab coordinates as follows:

$$\begin{aligned} \Delta E_w &= \sqrt{\Delta L_w^2 + \Delta a_w^2 + \Delta b_w^2} \\ \Delta E_w \left(\begin{bmatrix} L_{w,1} \\ a_{w,1} \\ b_{w,1} \end{bmatrix}, \begin{bmatrix} L_{w,2} \\ a_{w,2} \\ b_{w,2} \end{bmatrix} \right) &= \sqrt{\left(L_{w,2} - L_{w,1}\right)^2 + \left(a_{w,2} - a_{w,1}\right)^2 + \left(b_{w,2} - b_{w,1}\right)^2} \end{aligned} \tag{3.18}$$

The following equation identifies various ways to determine WLab coordinates. Thus any i^{th} WLab vector can be arrived at by using any of the following equivalent terms:

$$\begin{bmatrix} L_{w,i} \\ a_{w,i} \\ b_{w,i} \end{bmatrix} = u_w \left(\begin{bmatrix} W_i \\ p_i \\ t_i \end{bmatrix} \right) = u_w \left(\mathbf{A}_i \mathbf{s}_i \right) = u_w \left(\mathbf{A}_i \mathbf{C}_i \mathbf{O}_i \mathbf{l}_i \right) \tag{3.19}$$

where:
$L_{w,i}$, $a_{w,i}$, $b_{w,i}$ represent the i^{th} resulting WLab coordinates,
W_i, p_i, t_i represent the i^{th} initial Wpt coordinates,
$u_w\,()$ is a function that converts Wpt to WLab (same as Eq. 3.13),
$\mathbf{A}_i$ represents a Wpt normalization matrix that converts sensor excitation vectors to Wpt vectors for the i^{th} observing condition using Eq. 3.2 with the observer described by matrix $\mathbf{C}_i$ and the illuminant described by vector $\mathbf{l}_i$,
$\mathbf{s}_i$ represents the i^{th} sensor excitation vector, and
$\mathbf{C}_i$, $\mathbf{O}_i$, $\mathbf{l}_i$ are the same as $\mathbf{C}$, $\mathbf{O}$, $\mathbf{l}$ in Eq. 3.1.

An analysis was performed using the “standardized residual sum of squares" (STRESS) index which employs multidimensional scaling techniques that allows for inferences on the statistical significance of two color-difference formulas with respect to a given set of visual data [Garcia et al.,

2007; Huang et al., 2012]. The STRESS analysis was performed to compare the usefulness of Euclidean WLab distances for determining color differences. The analysis used supra-threshold color difference pairs that have a Euclidean CIELAB $\Delta E^{\star}{}_{ab}$ difference between 0.01 and 9.0 from an extended RIT/MCSL dataset [Berns et al., 1991; Hou, 2010; Chen, 2011] as well as the Alder color difference dataset [Alder et al., 1982]. Both of these datasets employed experimental conditions based on the 10-degree standard observer and D65 illuminant. The Alder color difference dataset also included additional pair differences based on the 10-degree standard observer and illuminant A of which all pairs were used as part of this analysis. Color space coordinates were determined for the colors in each of the datasets for the observing conditions, and these were used to find STRESS values for ΔE_w as well as $\Delta E^{\star}{}_{ab}$, $\Delta E^{\star}{}_{94}$, ΔE_{00}, and Euclidean Cartesian distances of DIN99o, CIECAM02, CAM02-UCS, and scaled CAM02-SCD. The results of the STRESS calculations can be found in TABLE 3.1 with items in bold indicating the lowest (best prediction of the dataset) STRESS values. Interestingly, the ΔE_w color difference metric had the lowest STRESS value for the Alder dataset under Illuminant A despite the fact that chroma in the WLab equations was optimized using Illuminant C for the 2° standard observer. The low STRESS results of ΔE_w in this instance is attributed to Wpt normalization.

TABLE 3.1. – Color difference STRESS comparisons (**bold** indicates lowest stress or best prediction of dataset)

	ΔE_w	$\Delta E^{\star}{}_{ab}$	$\Delta E^{\star}{}_{94}$	ΔE_{00}	DIN99o	CIECAM -02	CAM02 -UCS	CAM02 -SCD
STRESS RIT/MCSL D65	24.99	35.59	23.29	**22.09**	24.00	37.75	27.69	28.51
STRESS Alder D65	27.76	44.69	27.24	**23.39**	25.12	39.67	26.63	24.77
STRESS Alder Ill. A	**28.54**	47.94	32.25	30.51	31.87	40.31	30.42	29.19

An F-test analysis [Garcia et al., 2007] was also performed to evaluate the statistical difference between each of the color metrics based on the STRESS values in TABLE 3.1. The results are found in TABLE 3.2. The items in bold indicate that there is no significant difference between the two color difference methods within a 95% confidence level. The values in TABLE 3.3 provide the degrees of freedom and critical values used to determine significant difference in TABLE 3.2. Clearly, the Euclidean WLab color differences are not statistically different from $\Delta E^{\star}{}_{94}$, ΔE_{00}, and CAM02-SCD equations as well as Euclidean distances of DIN99o, and CAM02-UCS for the color pairs compared in the datasets. Therefore, it can be concluded that WLab is a reasonable color space for estimating differences in color under the observing conditions involved in this analysis.

TABLE 3.2. – F-test analysis results comparing statistical differences between each of the color difference metrics (bold indicates that comparison between color difference metrics is not statistically different.

		ΔE_w	$\Delta E^\star_{ab}$	$\Delta E^\star_{94}$	ΔE_{00}	DIN99o	CIECAM -02	CAM02 -UCS	CAM02 -SCD
ΔE_w	**RIT**		1.42	**0.93**	**0.88**	**0.96**	1.51	**1.11**	**1.14**
	AIdD65		1.61	**0.98**	**0.84**	**0.90**	1.43	**0.96**	**0.89**
	AId II.A		1.68	**1.13**	**1.07**	**1.12**	1.41	**1.07**	**1.02**
$\Delta E^\star_{ab}$	**RIT**	0.70		0.65	0.62	0.67	**1.06**	0.78	**0.80**
	AIdD65	0.62		0.61	0.52	0.56	**0.89**	0.60	0.55
	AId II.A	0.60		0.67	0.64	0.66	**0.84**	0.63	0.61
$\Delta E^\star_{94}$	**RIT**	**1.07**	1.53		**0.95**	**1.03**	1.62	**1.19**	**1.22**
	AIdD65	**1.02**	1.64		**0.86**	**0.92**	1.46	**0.98**	**0.91**
	AId II.A	**0.88**	1.49		**0.95**	**0.99**	1.25	**0.94**	**0.91**
ΔE_{00}	**RIT**	**1.13**	1.61	**1.05**		**1.09**	1.71	**1.25**	1.29
	AIdD65	**1.19**	1.91	**1.16**		**1.07**	1.70	**1.14**	**1.06**
	AId II.A	**0.94**	1.57	**1.06**		**1.04**	1.32	**1.00**	**0.96**
DIN99o	**RIT**	**1.04**	1.48	**0.97**	**0.92**		1.57	**1.15**	**1.19**
	AIdD65	**1.11**	1.78	**1.08**	**0.93**		1.58	**1.06**	**0.99**
	AId II.A	**0.90**	1.50	**1.01**	**0.96**		1.27	**0.95**	**0.92**
CIECAM -02	**RIT**	0.66	**0.94**	0.62	0.59	0.64		0.73	0.76
	AIdD65	0.70	**1.13**	0.69	0.59	0.63		0.67	0.62
	AId II.A	0.71	**1.19**	0.80	0.76	0.79		0.75	0.72
CAM02 -UCS	**RIT**	**0.90**	1.29	**0.84**	**0.80**	**0.87**	1.36		**1.03**
	AIdD65	**1.04**	1.68	**1.02**	**0.88**	**0.94**	1.49		**0.93**
	AId II.A	**0.94**	1.58	**1.06**	**1.00**	**1.05**	1.33		**0.96**
CAM02 -SCD	**RIT**	**0.88**	**1.25**	**0.82**	0.77	**0.84**	1.32	**0.97**	
	AIdD65	**1.12**	**1.80**	**1.10**	**0.94**	**1.01**	1.60	**1.08**	
	AId II.A	**0.98**	1.64	**1.10**	**1.05**	**1.09**	1.38	**1.04**	

TABLE 3.3. – Color difference equality F-test critical values

	Deg. of Freedom	Lower Critical Value	Upper Critical Value
RIT	250	0.78	1.28
AId D65	506	0.84	1.19
AId II.A	475	0.84	1.20

However, comparisons between WLab coordinates determined from various other observing conditions also have significant meaning because all WLab coordinates are based on Wpt normalization, and they therefore have a common reference for comparison purposes. But, the meaning of the comparisons change based upon the observers, illuminants, and objects used Eq. 3.13 to determine the WLab coordinates.

This is demonstrated in the simultaneous plot of WLab coordinates in FIGURE 3.10 for a select set of corrected Munsell reflectances under six illuminants (Illuminant C, D65, D50, Illuminant A, F11, and Illuminant E), and 2 observers (Standard 2° observer and Standard 10° observer) resulting in 12 combinations of observing conditions with each condition having an associated Wpt normalization matrix. Generally, there is a high degree of correlation between the observing conditions. The noticeable differences between observing conditions in FIGURE 3.10 are the result of material color shifts [Logvinenko and Beer, 2012], and are minimized as the relationships between physical samples maintain their uniform perceptual spacing. Thus the conclusion is that the ΔE_w color difference between colors having the same observing condition will generally remain constant as long as the material color shifts are constant. In other words, ΔE_wdefines a material color difference rather than the apparent color difference.

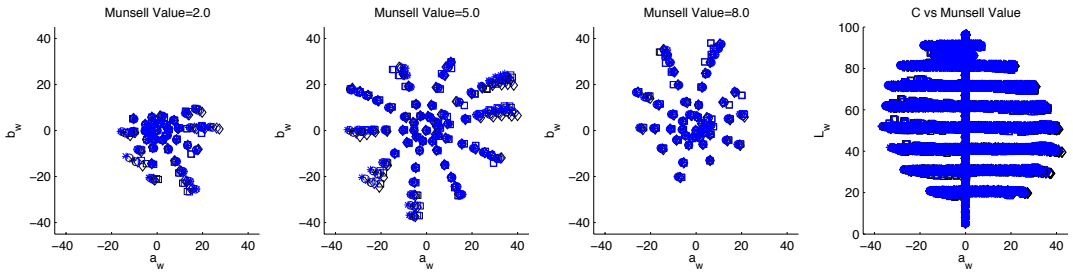

FIGURE 3.10. – Scatter plots for spectral reflectances of "corrected" Munsell glossy colors for two observers (black = Standard 2°observer, blue = Standard 10°observer) and six illuminants (x = Illum C, + = D65, o = D50, diamond = Illum A, square = F11, dot = Illum E).

Additionally, different observing conditions can be represented as comparisons of WLab coordinates utilizing changes in observer and/or illuminant. Therefore, it is affirmed that ΔE_w can potentially provide insight into such concepts as color inconstancy or metamerism due to observer and illuminant; color rendering characteristics of illuminants; color matching characteristics of observers; and classification of observers. This will be further explored in Chapter 4.

3.6 Conclusions about WLab

Transformations between Wpt and WLab have been presented and evaluated. Both perceptual uniformity analysis and color difference metrics were performed with evidence of perceptual

uniformity and equivalence with existing color difference metrics indicated for the reference observing conditions. WLab can therefore be considered as a perceptually uniform space with the ability to use Euclidean distances of WLab $\Delta E_w$to determine differences in color under various observing conditions.

WLab is different from existing uniform color spaces because it provides a perceptually uniform representation of material color as a result of being based upon Wpt normalization which predicts material color. WLab therefore defines a different kind of color space than either a color appearance model that is based upon chromatic adaptation that predicts corresponding color, or spaces such as CIELAB (which is often used as an appearance space) that derive color equivalency through vonKries normalization of white point tristimulus values. Examples of chromatic adaptation based appearance spaces include CAM02-UCS that provides a perceptually uniform representation of color appearance, or CAM02-SCD that allows for color differences to be determined that represent differences in color appearance. Additionally, the transformation into WLab is accomplished in a manner that avoids mathematical inconsistencies that are often present with color appearance models, and consistent relationships are maintained for material colors that are not physically realizable.

WLab should therefore properly be referred to as a “perceptually uniform material color equivalency space” (a first of its kind) with both perceptive aspects of color (lightness, chroma, and hue) and color differences being defined relative to the reference observing conditions. Thus, ΔE_w differences represent material color differences rather than differences in appearance with material color differences remaining fairly constant for changes in observing conditions and providing various relevant meanings for changes in objects, observers, and/or illuminants. Therefore, for the purposes of process or quality control, ΔE_w material color differences can potentially provide more desirable characteristics and metrics.

4 Wpt Shift Manifolds

4.1 Background and Introduction

A normalization method was introduced in Chapter 2 that transforms sensor excitations into a material equivalency representation [Logvinenko, 2013] which forms a color space described by the coordinates W, p, t. Wpt material color equivalency coordinates represent a normalization of sensor excitations resulting from the combined transformation of a physical color system that is comprised of an observer, object, and light source [Mintz, 2009]. The determination of Wpt coordinates for an arbitrary observer, object, and illuminant (or light source) is as follows:

$$\mathbf{w}_{i,j,k} = \begin{bmatrix} W \\ p \\ t \end{bmatrix}_{i,j,k} = \mathbf{A}_{i,k}\mathbf{C}_i\mathbf{O}_j\mathbf{l}_k \tag{4.1}$$

where:
i is an identifier for the i^{th} observer,
j is an identifier for the j^{th} object,
k is an identifier for the k^{th} illuminant,
$\mathbf{w}_{i,j,k}$ represents a Wpt vector for the i^{th} observer, j^{th} object, and k^{th} illuminant,
$\mathbf{A}_{i,k}$ represents a Wpt normalization matrix specific to the i^{th} observer and k^{th} illuminant,
$\mathbf{C}_i$ represents a matrix defining the sensor sensitivities or color matching functions for the i^{th} observer,
$\mathbf{O}_j$ represents a spectral reflectance matrix for the j^{th} object, and
$\mathbf{l}_k$ represents vector for the spectral power distribution (SPD) of the k^{th} illuminant.

A collection or set of Wpt coordinates can be formed by varying one or more of the observer, object, or illuminant in Eq. 4.1 (represented by varying the enumeration identifiers) while at the same time holding zero or more the other color system elements constant (represented by using constant enumeration identifiers). Riemann identified any set of points that describe the “positions of perceived objects" as a *manifold*, and also pointed out that color as described by color space coordinates would also constitute a manifold. Or in other words, a set of color space coordinates forms a *color manifold* [Riemann and Clifford, 1873]. Therefore, a set of Wpt points that is associated with multiple objects, observers and/or illuminants shall be hereafter referred to as a *Wpt Shift Manifold* or (WSM). (Note: The reason for the word “shift" is explained in section 4.1.1).

The use and comparison of WSMs is the subject of this chapter. Only a few manifold combinations formed by varying observers, objects, and illuminants are discussed in detail in this research for the purposes of comparing objects (4.3.1), illuminants (4.3.2), observers (4.3.3), and observing conditions (4.3.4).

Variability in object and illuminant are common in every day experience, and object variability as it relates to the composition of spectral reflectances is discussed in greater detail in the next few sections. Observer variability is an active area of research. However, an extensive discussion of the various reasons for observer variability is beyond the scope of the present work, and only a summary review is briefly mentioned.

Variation in human observer color matching can generally be attributed to one or more of the following factors: locational retinal variability in light sensitivity, variability in wavelength opacity of the optical system, and variability in pigment encoding (wavelength sensitivity) of the light sensor types [Fairchild and Heckaman, 2013]. The first two can affect a single observer due to changes in field size and age. Changes in color matching due to field size are attributed to: variations in density of various cones and rods by location on the retina; and parts of the retina are covered by the macula (which is a yellow pigmented layer) that changes the spectral power distribution of light getting to the sensors that the macula covers. As a person ages the optical density of the lens changes resulting in changes to the wavelengths of light transmitted through the system. The last factor in observer variability is due to differences in genetic encoding of the pigments used to determine wavelength sensitivity of the light sensors in the eye. There are light sensor pigment encoding variations in the general population for both color normal and color deviant (colorblind) observers [Stockman et al., 1999; Stockman and Sharpe, 1999; Stockman and Sharpe, 2000].

Image capture devices such as cameras can also be thought of as “observers" that have variability in their sensitivity functions. However, the process of defining and measuring camera sensitivities is beyond the scope of the present research. For this research, observer variability (whether it be human or otherwise) is simply assumed as a fact and existing methods from the literature that define various observer sensitivity functions are utilized for comparison and manipulation without thought or discussion to how they are determined. The comparison of observers relative to Wpt shift manifolds is discussed in 4.3, and the manipulation of cone fundamentals and color matching functions without changing the color discriminability (matching) of the observer is discussed in Chapter 6.

4.1.1 Object based Material Color Shifts

Logvinenko introduced the concepts of “material color equivalency spaces" and the resulting “material color shifts" due to changes in illuminant when discussing what he defined as Object Color Manifolds [Logvinenko, 2013]. For this research it is asserted that material color shifts also result due to changes in observer as well – though Logvinenko did not specifically discuss this. Material color shifts due to both illuminant and observer can clearly be demonstrated using

a manifold of Wpt points or a *Wpt shift manifold*. This is because Wpt normalization results in defining a material equivalency space by linearly minimizing differences due to variability of both observer and illuminant, and shifts in Wpt coordinates for differences in observer an illuminant are the result of the nonlinear relationships between observer, object and illuminant.

Metamers are objects that have the same sensor excitations for one observing condition but have different surface spectral reflectances [Wyszecki and Stiles, 2000]. Therefore, the sensor excitations are likely to be different for alternate observing conditions. It is shown in section 4.2 that metamers result in differences in Wpt shift manifolds which are the result of the differences in the spectral reflectances of the objects.

In section 4.1.2, various approaches of spectral reflectance deconstruction are reviewed leading to methods that are also used throughout this research. In section 4.2, Wpt shift manifolds are shown to be useful for the purpose of understanding the extent and character of material color shifts that can occur for an object. In section 4.3, comparisons between Wpt shift manifolds are discussed to determine metrics for comparing spectral reflectance qualities of objects.

4.1.2 Spectral Decomposition

The basis of spectral decomposition is that spectral reflectances can be decomposed into a sum of spectral reflectances. Various methods of decomposing and recomposing spectral reflectances have been introduced in the literature, and eigenvector analysis is the typical method utilized for defining the decomposition of spectral reflectances. An excellent overview and generalization of spectral reflectances using eigenvectors has been provided by Peyvandi [Peyvandi and Amirshahi, 2011]. However, for the present research the use of eigenvector decomposition was limited only to the spectral decomposition of metameric blacks.

Wyszecki made the hypothesis that a spectral reflectance could be decomposed into visible and invisible components [Wyszecki, 1953]. Cohen later described these as fundamental and metameric black components with fundamental curves being defined that have a special relationship with color matching functions or cone fundamentals [Cohen, 2001]. However, for the purposes of this research the concept of fundamental curves will not be pursued as it is felt by the author that any spectral reflectance can be considered to convey visual information, and metameric blacks simply provide additional invisible information.

4.1.3 Decomposing Metameric Blacks

A metameric black has positive and negative reflectance factor values over the observed spectrum that results in zero sensor excitations for a specified observer and illuminant (observing condition). The Wyszecki Hypothesis results in the ability to add a metameric black to a spectral reflectance with no apparent change in color for the observing condition(s) under which the metameric black results in zero sensor excitations. In terms of Wpt coordinates, the relationship

between two objects with distinct spectral reflectances that appear the same for a specified observing condition (metamers) can be described by the following equation:

$$\begin{gathered}\mathbf{O}_1 = \mathbf{O}_2 + \mathbf{B} \\ \text{and} \\ \mathbf{w}_{\text{obs},1,\text{ill}} = \mathbf{w}_{\text{obs},2,\text{ill}}\end{gathered} \tag{4.2}$$

where:
$\mathbf{O}_1$ is a reflectance matrix for the first object,
$\mathbf{O}_2$ is a reflectance matrix for the second object,
$\mathbf{B}$ is a metameric black reflectance representing the residual difference between $\mathbf{O}_1$ and $\mathbf{O}_2$,
$\mathbf{w}_{\text{obs},1,\text{ill}}$ represents a Wpt vector for $\mathbf{O}_1$ as defined by Eq. 4.1 for a given observer and illuminant, and
$\mathbf{w}_{\text{obs},2,\text{ill}}$ represents the Wpt vector for $\mathbf{O}_2$ as defined by Eq. 4.1 for the second object with the same observer and illuminant as the first object.

There are several methods identified in the literature for generating metameric blacks [Cohen, 2001; Wyszecki and Stiles, 2000]. However, the set of metameric black basis vectors determined for the purposes of this research used a method similar to that previously proposed by the author for the purposes of spectral gamut mapping [Derhak and Rosen, 2004] as follows:

$$\begin{aligned}\mathbf{E} &= \mathbf{R} \cdot pinv\left(\mathbf{W}\right) \\ \mathbf{B}_w &= \mathbf{R} - \mathbf{E}\mathbf{W} \\ \mathbf{B} &= eigenvectors\left(\mathbf{B}_w\mathbf{B}_w^T\right)\end{aligned} \tag{4.3}$$

where:
$\mathbf{E}$ is an array of estimated spectral reflectance vectors $\mathbf{r}_{\text{est},1} \ldots \mathbf{r}_{\text{est},n}$ $\mathbf{R}$ is an array of reflectance vectors $\mathbf{r}_1 \ldots \mathbf{r}_n$,
$pinv\left(\right)$ represents a function that applies a matrix pseudo-inverse, [Derhak and Rosen, 2004]
$\mathbf{W}$ is an array of Wpt vectors $\mathbf{w}_{\text{obs},1,\text{ill}} \ldots \mathbf{w}_{\text{obs},n,\text{ill}}$ for a reference observer and illuminant,
$\mathbf{B}_w$ in array of metameric black residual difference vectors between estimated and actual reflectances having the same Wpt coordinates, and
$eigenvectors\left(\right)$ represents a function that determines the eigenvectors of a square matrix [Hotelling, 1936].

The reflectances from the Munsell Glossy Database from the University of East Finland [Orava, 2012] were used for $\mathbf{R}$ and corresponding Wpt coordinates $\mathbf{W}$ were determined using Eq. 4.3 to find the metameric black basis vectors for this research.

4.1.4 Decomposing Visual Reflectances

In a similar vein to the Wyszecki Hypothesis, Chau proposed as part of his doctoral dissertation (hereafter referred to as the Chau Hypothesis) that a spectral reflectance can be decomposed into two components – a wavelength invariant non-selective component, and a wavelength

selective component [Chau, 1999]. Thus an arbitrary reflectance matrix $\mathbf{O}_{\text{any}}$ can be defined as follows:

$$\mathbf{O}_{\text{any}} = g\mathbf{I} + s\mathbf{O}_{\text{select}} \tag{4.4}$$

where:
$\mathbf{O}_{\text{any}}$ is an arbitrary spectral reflectance matrix for an object,
$\mathbf{I}$ is the identity matrix,
$\mathbf{O}_{\text{select}}$ defines a matrix that selectively adjusts light based on wavelength (thus $min\left(\mathbf{O}_{\text{select}}\right) \neq max\left(\mathbf{O}_{\text{select}}\right)$),
g is a scalar that adjusts the non-selective (gray) portion of the spectral reflectance, and
s is a scalar that adjusts the selective (saturation) portion of the spectral reflectance.

The selection matrix $\mathbf{O}_{\text{select}}$ is arbitrary but Chau showed that it can be normalized such that $min\left(\mathbf{O}_{\text{select}}\right) = 0$ and $max\left(\mathbf{O}_{\text{select}}\right) = 1$. When normalized, Chau referred to the result as the primary reflectance. The determination of the primary or *characteristic* reflectance matrix to use as $\mathbf{O}_{\text{select}}$ is shown as follows:

$$\begin{aligned} &\mathbf{O}_{\text{select}} = P\left(\mathbf{O}_{\text{any}}\right) \\ &P\left(\mathbf{O}_{\text{any}}\right) = \begin{cases} \dfrac{\mathbf{O}_{\text{any}} - min\left(\mathbf{O}_{\text{any}}\right)}{max\left(\mathbf{O}_{\text{any}}\right) - min\left(\mathbf{O}_{\text{any}}\right)}, & \text{if } \left(max\left(\mathbf{O}_{\text{any}}\right) - min\left(\mathbf{O}_{\text{any}}\right)\right) > 0 \\ zero, & \text{otherwise} \end{cases} \end{aligned} \tag{4.5}$$

where:
O_{select} is the same as in Eq. 4.4, and
$P\left(\mathbf{O}_{\text{any}}\right)$ is a function that determines the characteristic reflectances of a reflectance defined by matrix $O_{\textbf{any}}$.

It is the primary or *characteristic* reflectance in Eq. 4.4 that defines both hue and chroma. This can be shown by substituting the right hand side of Eq. 4.4 for $\mathbf{O}$ in Eq. 4.1 resulting in the following equation:

$$\mathbf{w}_{\text{obs,any,ill}} = g\mathbf{w}_{\text{obs,identity,ill}} + s\mathbf{w}_{\text{obs,select,ill}} \tag{4.6}$$

where:
$\mathbf{w}_{\text{obs,any,ill}}$ is the Wpt vector of “any" object for the observing condition defined by the observer matrix $\mathbf{C}_{\text{obs}}$ and illuminant vector $\mathbf{l}_{\text{ill}}$,
$\mathbf{w}_{\text{obs,identity,ill}}$ is the Wpt vector associated with a PRD for the observing condition defined by the observer matrix $\mathbf{C}_{\text{obs}}$ and illuminant vector $\mathbf{l}_{\text{ill}}$, and
$\mathbf{w}_{\text{obs,select,ill}}$ is the Wpt vector associated with the characteristic reflectance of object “any" for the observing condition defined by the observer matrix $\mathbf{C}_{\text{obs}}$ and illuminant vector $\mathbf{l}_{\text{ill}}$.

The vector $\mathbf{w}_{\text{obs,identity,ill}}$ contains zero values for the p, and t entries because the identity $\mathbf{I}$ reflectance results in scaling the illuminant and the Wpt coordinates are collinear with the gray axis. Only the $\mathbf{w}_{\text{obs,select,ill}}$ vector has non-zero values for p and t. Thus, Wpt hue and chroma are entirely defined by $\mathbf{O}_{\text{select}}$.

It is proposed that compositions of spectral reflectance metamers can be defined by combining the Wyszecki Hypothesis with the Chau Hypothesis as follows:

$$\mathbf{O}_{\text{any}} = g\mathbf{I} + s\mathbf{O}_{\text{select}} + b\mathbf{B} \tag{4.7}$$

where:
$\mathbf{O}$ is an arbitrary spectral reflectance matrix for an object,
$\mathbf{I}$ is the identity matrix,
$\mathbf{O}_{\text{select}}$ defines a matrix that selectively adjusts light based on wavelength (thus $min\left(\mathbf{O}_{\text{select}}\right) \neq max\left(\mathbf{O}_{\text{select}}\right)$),
$\mathbf{B}$ is a metameric black for the given observing conditions,
g is a scalar that adjusts the non-selective (gray) portion of the spectral reflectance,
s is a scalar that adjusts the selective (saturation) portion of the spectral reflectance, and
b is a scalar that adjusts the metameric black component.

It will be shown in the next section that both the $\mathbf{O}_{\text{select}}$ and $\mathbf{B}$ vectors define the shape and orientation of the Wpt shift manifold.

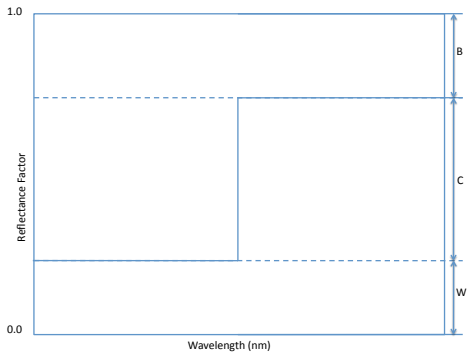

FIGURE 4.1. – Ostwald defined idealized spectral reflectances as the sum of three color regions where $W + B + C = 1$.

Interestingly, Eq. 4.7 has similarities to the method of defining spectral reflectances proposed by Ostwald which defines spectral reflectances based on the equation $W + B + C = 1$ which is graphically depicted in FIGURE 4.1 [Foss et al., 1944]. Ostwald defined spectral reflectances that had rectangular curve shapes made up of three regions: the lower white (W) region, the middle “fullcolor" (C) region, and the upper black (B) region. This is especially the case when b is set to zero, $\mathbf{O}_{\text{select}}$ is defined as a rectangular curve with a minimum of 0 and a maximum of 1, and $g + s \leq 1$.

Eq. 4.7 can also be considered a spectral generalization of the Coloroid Color System that defines colors as the sum of three colorimetric vectors as follows: [Nemcsics, 2002]

$$\mathbf{c} = p\mathbf{h} + w\mathbf{w} + s\mathbf{s} \tag{4.8}$$

where:
$\mathbf{c}$ is the resulting output color vector,
$\mathbf{h}$ defines the color content (which has specific colorimetry for each hue defined by a dominant/opponent wavelength), vector $\mathbf{w}$ defines the white content, vector $\mathbf{s}$ defines the black content, and the sum of the scalars is equal to one, thus $p + w + s = 1$.

By similar reasoning, the object color manifold spectral reflectances defined by Logvinenko can also be generalized by Eq. 4.7 [Logvinenko, 2013]. In this case, the B matrix is set to zero and direct translations of Logvinenko's reflectance definitions result in specific values for $\mathbf{O}_{\text{select}}$ and the scalars g and s.

There are three significant differences between Eq. 4.7 and those of Ostwald, Nemcsics, and Logvinenko. Firstly, the $\mathbf{O}_{\text{select}}$ is arbitrary while those of Ostwald, Nemcsics and Logvinenko have specific values for each hue, and secondly the sum of the scalars is not limited to the value of one. Lastly, the metameric black $\mathbf{B}$ in Eq. 4.7 provides no colorimetric information for the reference observer and illuminant. Thus, Eq. 4.7 allows for both physically realizable as well as physically non-realizable spectral reflectances to be defined.

4.2 Visualizing Object Wpt Shift Manifolds

A visualization of an object's WSM was performed by first determining the set of points belonging to the manifold and then plotting them as Wpt coordinates. The set of Wpt points in the manifold is determined for an object using Eq. 4.1 holding the object matrix $\mathbf{O}_j$ constant and varying for all combinations of $\mathbf{C}_i$ out of a set of observers and $\mathbf{l}_k$ out of a set of illuminants. The reference observing conditions for Wpt Normalization uses the 1931 Standard Observer with Illuminant C (as discussed in Chapter 2).

TABLE 4.1. – Observers used for Wpt shift manifold generation

1931 Standard 2°			1964 Standard 10°			
2006 20yo, 1°	2006 30yo, 1°	2006 40yo, 1°	2006 50yo, 1°	2006 60yo, 1°	2006 70yo, 1°	2006 80yo, 1°
2006 20yo, 2°	2006 30yo, 2°	2006 40yo, 2°	2006 50yo, 2°	2006 60yo, 2°	2006 70yo, 2°	2006 80yo, 2°
2006 20yo, 3°	2006 30yo, 3°	2006 40yo, 3°	2006 50yo, 3°	2006 60yo, 3°	2006 70yo, 3°	2006 80yo, 3°
2006 20yo, 4°	2006 30yo, 4°	2006 40yo, 4°	2006 50yo, 4°	2006 60yo, 4°	2006 70yo, 4°	2006 80yo, 4°
2006 20yo, 5°	2006 30yo, 5°	2006 40yo, 5°	2006 50yo, 5°	2006 60yo, 5°	2006 70yo, 5°	2006 80yo, 5°
2006 20yo, 6°	2006 30yo, 6°	2006 40yo, 6°	2006 50yo, 6°	2006 60yo, 6°	2006 70yo, 6°	2006 80yo, 6°
2006 20yo, 7°	2006 30yo, 7°	2006 40yo, 7°	2006 50yo, 7°	2006 60yo, 7°	2006 70yo, 7°	2006 80yo, 7°
2006 20yo, 8°	2006 30yo, 8°	2006 40yo, 8°	2006 50yo, 8°	2006 60yo, 8°	2006 70yo, 8°	2006 80yo, 8°
2006 20yo, 9°	2006 30yo, 9°	2006 40yo, 9°	2006 50yo, 9°	2006 60yo, 9°	2006 70yo, 9°	2006 80yo, 9°
2006 20yo, 10°	2006 30yo, 10°	2006 40yo, 10°	2006 50yo, 10°	2006 60yo, 10°	2006 70yo, 10°	2006 80yo, 10°

Only variability in field size and age were considered for the purposes of visualizing Wpt shift manifolds in this research (thus representing the extent to which a single "normal" physical observer might see material shift changes in color matching over the space of a lifetime). However, it is also possible to apply identical techniques with other observer color matching

functions or cone fundamentals defined by methods in the literature [Sarkar et al., 2011; Fairchild and Heckaman, 2013; Asano et al., 2014].

The members of the set of observers that were used for visualizing Wpt shift manifolds are identified in TABLE 4.1, [Wyszecki and Stiles, 2000; CIE170, 2006], and a view of the sensor excitation curves (normalized so the area under each curve is one for visual comparison purposes) is found in FIGURE 4.2. The members of the illuminants are identified in TABLE 4.2 with a relative spectral power distribution for the illuminants shown in FIGURE 4.3.

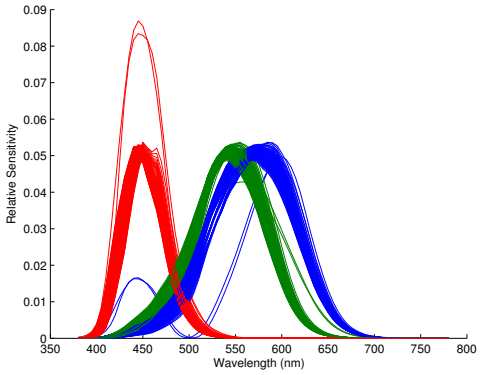

FIGURE 4.2. – Normalized Spectral Sensitivities of Observers used to determine Wpt shift manifolds

TABLE 4.2. – Illuminants used for Wpt shift manifold generation

Ill C	Ill F9	Daylight 5750K	Daylight 8500K	Daylight 11250K	Daylight 14000K	Blackbody 4250K	Blackbody 7000K	Blackbody 9750K
Ill A	Ill F10	Daylight 6000K	Daylight 8750K	Daylight 11500K	Blackbody 1750K	Blackbody 4500K	Blackbody 7250K	Blackbody 10000K
Ill E	Ill F11	Daylight 6250K	Daylight 9000K	Daylight 11750K	Blackbody 2000K	Blackbody 4750K	Blackbody 7500K	Blackbody 10250K
Ill F1	Ill F12	Daylight 6500K	Daylight 9250K	Daylight 12000K	Blackbody 2250K	Blackbody 5000K	Blackbody 7750K	Blackbody 10500K
Ill F2	Daylight 4000K	Daylight 6750K	Daylight 9500K	Daylight 12250K	Blackbody 2500K	Blackbody 5250K	Blackbody 8000K	Blackbody 10750K
Ill F3	Daylight 4250K	Daylight 7000K	Daylight 9750K	Daylight 12500K	Blackbody 2750K	Blackbody 5500K	Blackbody 8250K	Blackbody 11000K
Ill F4	Daylight 4500K	Daylight 7250K	Daylight 10000K	Daylight 12750K	Blackbody 3000K	Blackbody 5750K	Blackbody 8500K	Blackbody 11250K
Ill F5	Daylight 4750K	Daylight 7500K	Daylight 10250K	Daylight 13000K	Blackbody 3250K	Blackbody 6000K	Blackbody 8750K	Blackbody 11500K
Ill F6	Daylight 5000K	Daylight 7750K	Daylight 10500K	Daylight 13250K	Blackbody 3500K	Blackbody 6250K	Blackbody 9000K	Blackbody 11750K
Ill F7	Daylight 5250K	Daylight 8000K	Daylight 10750K	Daylight 13500K	Blackbody 3750K	Blackbody 6500K	Blackbody 9250K	Blackbody 12000K
Ill F8	Daylight 5500K	Daylight 8250K	Daylight 11000K	Daylight 13750K	Blackbody 4000K	Blackbody 6750K	Blackbody 9500K	White LED

Wpt shift manifolds were generated for visualization purposes for objects defined using various combinations of the terms in Eq. 4.7. The visualizations of the Wpt shift manifolds that follow only depict the variability that occurred in the chromatic plane (although shifts also occurred in the W axis). This is because it was felt that visualization of the shifts in the chromatic plane was adequate for demonstrating the various properties of Wpt shift manifolds.

In the first case, a non-selective reflectance over all wavelengths with 50% of the light being reflected was used and is shown in the upper left (G1) of FIGURE 4.4. Additional reflectances were also generated for visualization purposes by adding metameric black reflectances to this base non-selective reflectance to demonstrate variations in material shift between gray metamers. The spectral reflectances for these metamers are shown on the right side of FIGURE 4.4.

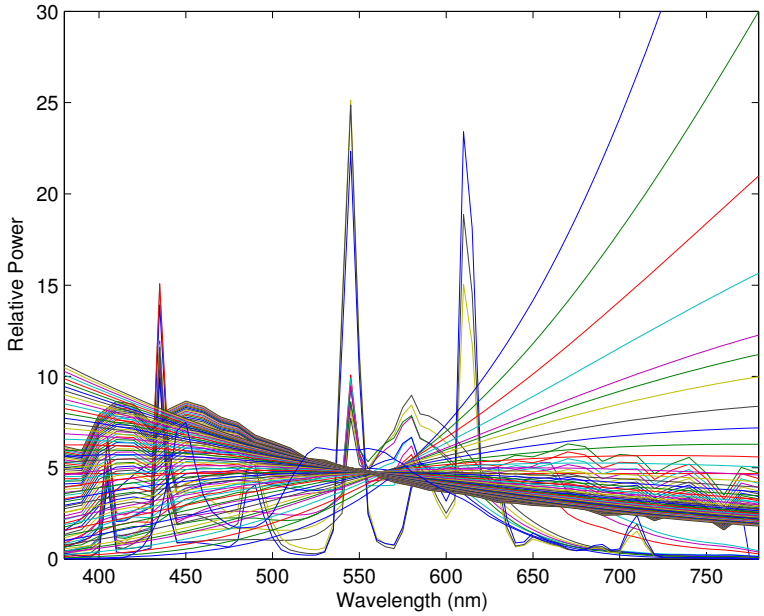

FIGURE 4.3. – Spectral Power Distributions of Illuminants used to determine Wpt shift manifolds

Wpt points for each of these spectral reflectances were determined by varying the observer from TABLE 4.1 and illuminant from TABLE 4.2 resulting in 7000 points in each object's Wpt shift manifold. A visualization of Wpt shift manifolds for each of the reflectances is found on the right side of FIGURE 4.4. The point associated with the reference observing conditions (1931 Standard Observer under Illuminant C) are indicated by a red '+' mark in the sub-figures.

There are several observations that can be made from the Wpt shift manifolds in FIGURE 4.4. First, all of the (p, t) coordinates under the reference observing conditions are located at (0,0) thus indicating that the reflectances are metamers for the reference observing conditions. Second, all the points in the Wpt shift manifold for the non-selective spectral reflectance are located at the same point thus indicating that the spectral reflectance has relative color constancy for all of the observers and illuminants. Third, the addition of different metameric blacks to the non-selective reflectance results in different material shifts for various observer and illuminant combinations. This is an indication of color inconstancy for the spectral reflectances and the nature of the inconstancy is unique for each of the spectral reflectances.

In the second case of material shift manifold visualization, various scale factors of the metameric black labeled G6 in FIGURE 4.4 were added to the same non-selective gray (which is equivalent to defining spectral reflectances using Eq. 4.7 and setting both s and $\mathbf{O}_{\text{select}}$ to zero). The resulting reflectances are shown on the left in FIGURE 4.5 with the corresponding material shift manifolds for each reflectance shown on the right. In this case the shapes and orientations of the manifolds (hereafter referred to as the "material shift potential") remain the same while the size of each manifold is scaled in proportion to the amount of the metameric black added to

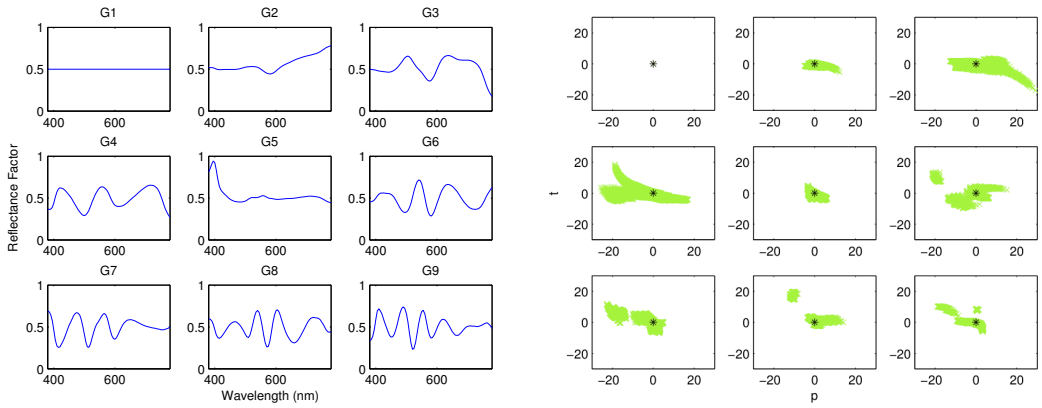

FIGURE 4.4. – Metameric gray spectral reflectances for the CIE 1931 Standard observer under Illuminant C (left), Material Shift Manifolds for the metameric gray spectral reflectances (right) with red '+' indicating position for reference observing conditions.

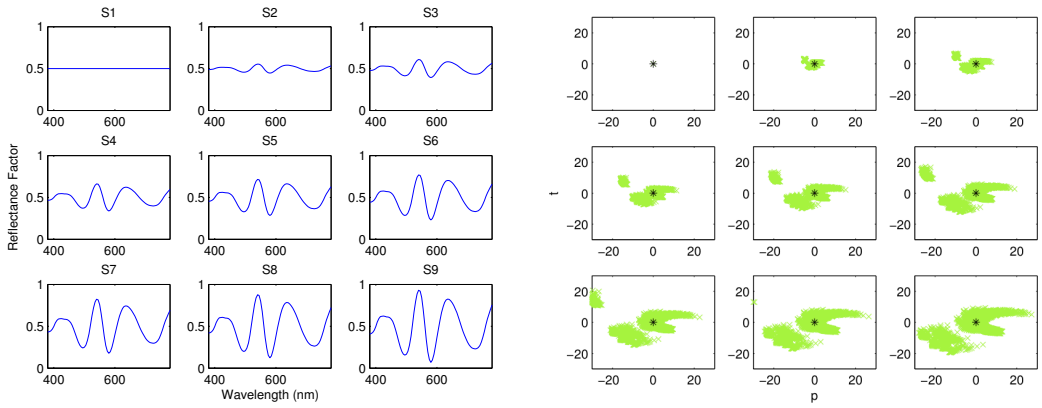

FIGURE 4.5. – Metameric gray spectral with scaled metameric black reflectances for the CIE 1931 Standard observer under Illuminant C (left), Material Shift Manifolds corresponding to these scaled reflectances (right) with red '+' indicating position for reference observing conditions.

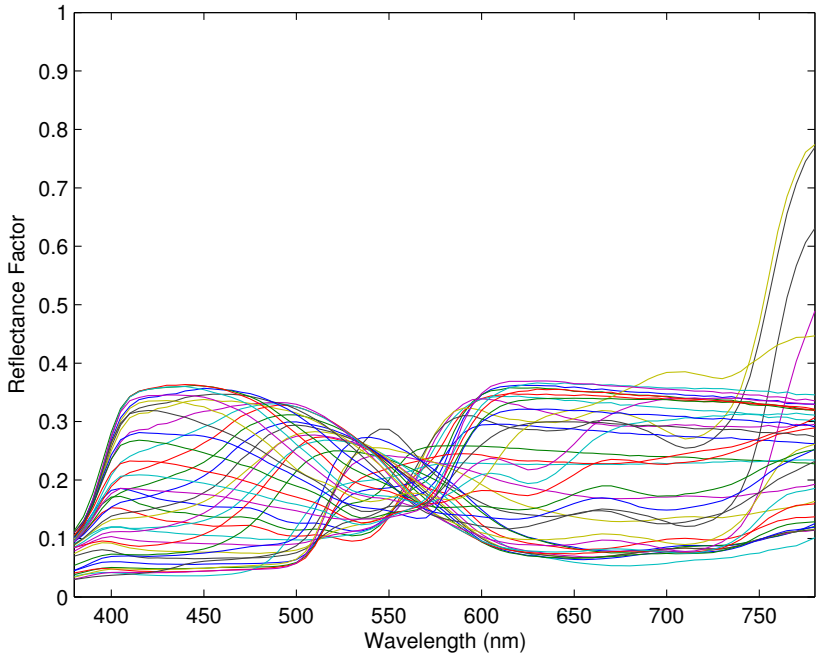

FIGURE 4.6. – Spectra reflectances for Munsell hues having Munsell Value 5 and Munsell Chroma 6

the non-selective gray. Thus the resulting material shift potential associated with the object is preserved (as the Wpt hue of corresponding points in the material shift manifolds remains is the same).

In the third case, Wpt shift manifolds were determined and visualized for the spectral reflectances corresponding to 40 Glossy Munsell chromatic hues each having Munsell value of 5 and Munsell chroma of 6 [Orava, 2012]. This is an example of varying matrix $\mathbf{O}_{\text{select}}$ in Eq. 4.7 to demonstrate material shifts for different hues. The reflectances can be found in FIGURE 4.6 and material shift manifolds for each of the spectral reflectances are shown in FIGURE 4.7. The Wpt shift manifolds were plotted using polar Wpt coordinates (WCh) which allows for the direct visualization of how shifts in hue and chroma occur for each of the Munsell hues. Wpt Normalization involves minimization to get the best overall Wpt coordinate constancy for these specific spectral reflectances. Horizontal shifts correspond to changes in hue, and vertical shifts correspond to changes in chroma. Overall the Munsell P, PB, and B hues have the greatest overall material color constancy as they exhibit the smallest manifold sizes. Y, GY, G and BG hues appear to have the widest shifts in hue.

It is postulated that the shifts in hue depicted in FIGURE 4.7 are due to the non-linear relationships between the illuminants, observers and objects. The systemic nature of the shifts in FIGURE 4.7 is demonstrated by simultaneously plotting the same data as aggregate Wpt coordinates. This is shown in FIGURE 4.8. The exponential changes in the illuminants at higher wavelengths as

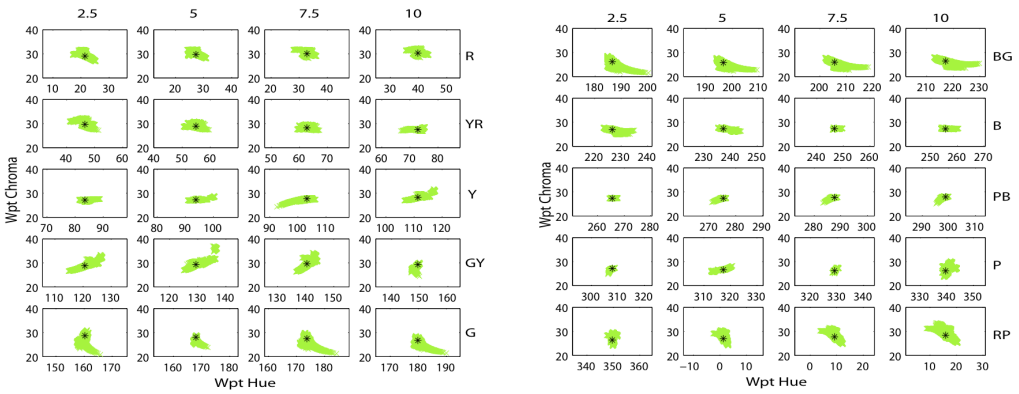

FIGURE 4.7. – Material Shift Manifolds for various Munsell hues

the CCT becomes lower provide a major component to the material shifts. Since P, PB, and B spectra have fairly low reflectance factor values for these higher wavelengths they are therefore less affected by the material shift for the illuminants with lower CCT. Overall there is a general shift in p with lesser shifts in t. Further analysis related to factors that result in material shifts, and how they cause shifts are left as a future research effort.

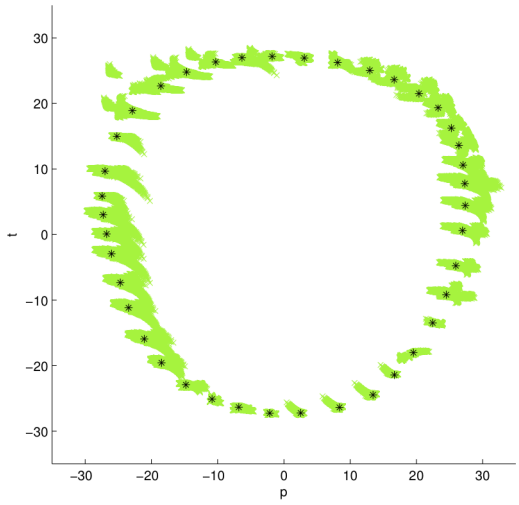

FIGURE 4.8. – Aggregated Material Shift Manifolds for various Munsell hues in Wpt

The next example of Object WSMs involves Munsell spectral reflectances for Munsell colors that have the same hue. In FIGURE 4.9 spectral reflectances for each of the chips in the Munsell 5Y Hue Plane are shown alongside corresponding Wpt shift manifolds for each of the spectral reflectances. Two observations can be made from this figure. The first is that there is significant variability to the shapes of the Wpt shift manifolds (in other words the material shift potential is not preserved). This would imply that as observing conditions change there will be significant variability in the resulting relationships between the colors, or in other words there

is no consistency between them in their color inconstancy. The second observation is that for spectral reflectances that have similar overall shapes there is similarity in the Wpt shift manifolds. This would lead to the hypothesis that getting consistent spectral shapes (thus preserving material shift potential) and will lead to more consistent inter-color color inconstancy.

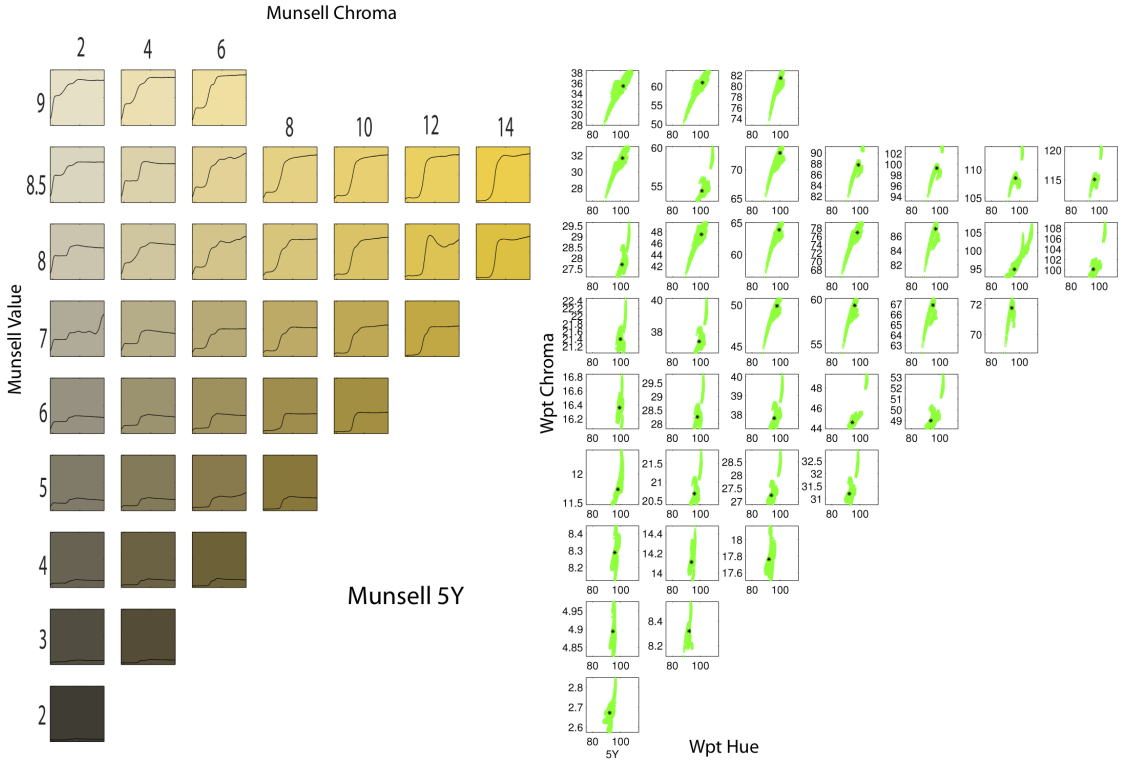

FIGURE 4.9. – Reflectances (left) and Shift Manifolds (right) for 5Y Munsell Plane

A hint that this can be accomplished is demonstrated in FIGURE 4.10 where Eq. 4.4 was used with the primary or characteristic reflectance of Munsell 5Y 8.5/12 to define yellowish reflectances that have identically shaped Wpt shift manifolds. In this case the material shift potential is preserved, and the use of this technique to get more consistent inter-color color inconstancy for defining reflectances for Munsell Renotation colors will further be investigated in Chapter 7.

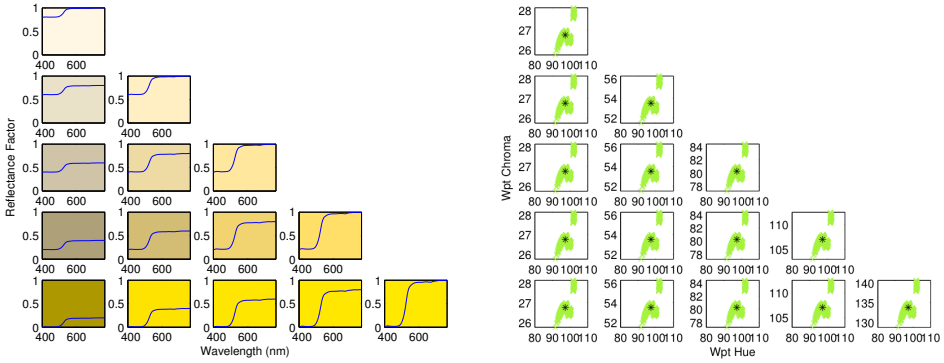

FIGURE 4.10. – Reflectances (left) and Shift Manifolds (right) for Yellow reflectances defined using Eq. 4.4 with characteristic reflectance from 5Y 8.5/12 in FIGURE 4.9

4.3 Comparing Wpt Shift Manifolds

Various Wpt Shift Manifolds were visualized in the previous section which provide a means of performing a visual comparison between manifolds. In this section metrics that provide quantitative comparisons of corresponding points between manifolds are considered. However, extensive analysis along with comparisons to other possible metrics has been left as a future research effort.

Manifolds involving observer variability allow for quantification and characterization of both observer based inconstancy and metamerism which will prove to be important in Chapter 7 for the manipulation of color in ways that account for changes in observer and illuminant. Three types of manifolds can be established by holding the object, illuminant or observer constant. Then comparisons can be made between points within a single manifold or between corresponding points between two manifolds that have different objects, illuminants or observers held constant. In the latter case this provides metrics of similarity between the objects, illuminants or observers.

A ΔE_{Wpt} color difference metric was used for making quantitative comparisons that first involves a conversion to WLab because the spacing between Wpt coordinates is not perceptually uniform. Wpt coordinates are converted to WLab coordinates using the u_w function defined in Eq. 3.19 of Chapter 3, and then the Euclidean distance is determined between these WLab coordinates using the ΔE metric defined by Eq. 3.18 in the same chapter. Thus relative color differences of indexed Wpt vectors defined in Eq. 4.1 can be described as follows:

$$\Delta E_{\text{Wpt}}\left(\mathbf{w}_{i_1,j_1,k_1}, \mathbf{w}_{i_2,j_2,k_2}\right) = \Delta E_w\left(u_w\left(\mathbf{w}_{\text{observer}_1,\text{object}_1,\text{illum}_1}\right), \left(\mathbf{w}_{\text{observer}_2,\text{object}_2,\text{illum}_2}\right)\right) \quad (4.9)$$

where:
ΔE_{Wpt} determines the color difference between two indexed Wpt vectors,
ΔE_w is same as defined in Eq. 3.18, and

$u_w\,()$ is the function that converts Wpt coordinates to WLab coordinates defined in Eq. 3.19 and described in Appendix B.

4.3.1 Object Shift Manifold Difference Metrics

The first type of object based Wpt shift manifold difference metric compares WLab coordinates within a single Wpt shift manifold to the WLab coordinate for a reference observing condition. This provides a measure of color inconstancy for the object. The Mean Object Inconstancy Index (MOII) for an object defined by matrix $\mathbf{O}_x$ is determined by Eq. 4.10 and an example of MOII values is shown in FIGURE 4.11 which corresponding to MOII values for the Wpt shift manifolds in FIGURE 4.7. These MOII values provide quantitative support to the visual assessment made previously of FIGURE 4.7 (that the B, BP, and P colors have the least color inconstancy). Also notice that the mean ΔE_w from the reference condition is generally below 1.0 indicating that Wpt normalization on average does a good job of minimizing Wpt differences due to changes in observer and illuminant.

$$MOII\,(\mathbf{O}_x) = \frac{\sum_i \sum_k \Delta E_{Wpt}\left(\mathbf{w}_{i,x,k}, \mathbf{w}_{\text{ReObserver},x,\text{RefIlluminant}}\right)}{ik} \tag{4.10}$$

where:
x identifies the object,
$\mathbf{w}_{i,x,k}$ defines the Wpt coordinate using Eq. 4.1 of object x for the i^{th} observer and the k^{th} illuminant, and
$\mathbf{w}_{\text{RefObserver},x,\text{RefIlluminant}}$ defines the Wpt coordinate using Eq. 4.1 of object x for a reference observer and a reference illuminant.

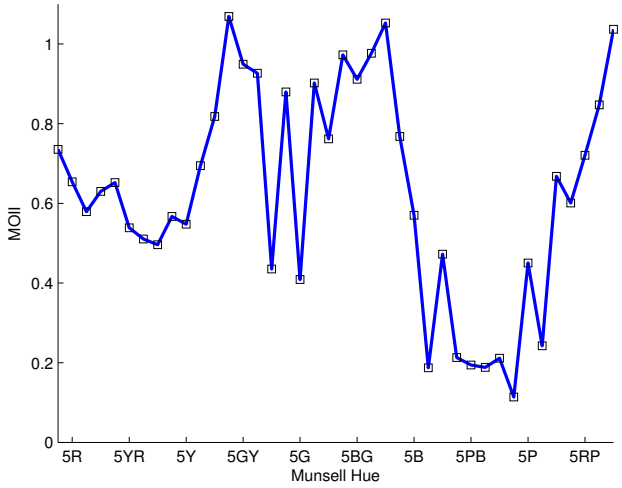

FIGURE 4.11. – Mean Object Inconstancy Index (MOII) values for reflectances for 40 Munsell Hue colors

The next type of object metric compares corresponding Wpt coordinates for Wpt shift manifolds of two separate object reflectances. The Mean Metameric Object Color Difference (MMOCD) of two objects is determined using Eq. 4.11 and provides both a mean index of metamerism (if the objects are metamers) as well as a general sense of overall color difference between two objects that are not metamers while factoring in color inconstancy of the two objects.

$$MMOCD\left(\mathbf{O}_{\text{batch}}, \mathbf{O}_{\text{std}}\right) = \frac{\sum_i \sum_k \Delta E_{\text{Wpt}}\left(\mathbf{w}_{i,\text{batch},k}, \mathbf{w}_{i,\text{std},j}\right)}{ik} \tag{4.11}$$

where:
O_{batch} identifies the batch object reflectance matrix,
O_{std} identifies the standard object reflectance matrix,
$\mathbf{w}_{i,\text{batch},k}$ defines the Wpt coordinate using Eq. 4.1 of batch object for the i^{th} observer and the k^{th} illuminant, and
$\mathbf{w}_{i,\text{std},k}$ defines the Wpt coordinate using Eq. 4.1 of standard object for the i^{th} observer and the k^{th} illuminant.

Objects that are spectrally identical will have a MMOCD value of zero. As one example, MMOCD values were determined for combinations of the reflectances in FIGURE 4.4, and the results are found in TABLE 4.3. These MMOCD values provide an indication of relative differences in Wpt shift manifolds – thus providing a measure of metamerism because these reflectances are all metamers. In TABLE 4.4 the reflectances in FIGURE 4.4 were scaled down by 0.5% and compared using MMOCD to the reflectances in FIGURE 4.5. These MMOCD values provide both an indication of relative differences in Wpt shift manifolds and an overal indication of color differences. The lowest values are not zero (G1' vs S1) and (G6' vs S5) because the reflectances are not metamers. However, the MMOCD metric alone cannot distinguish between low metamerism and overall color difference.

TABLE 4.3. – MMOCD comparisons between reflectances in FIGURE 4.4. Lower values indicate fewer differences due to metamerism.

MMOCD	**G1**	**G2**	**G3**	**G4**	**G5**	**G6**	**G7**	**G8**	**G9**
G1	0.00	1.26	3.96	5.01	1.93	2.52	2.59	1.69	1.92
G2	1.26	0.00	2.79	6.08	2.94	2.88	2.94	1.88	2.08
G3	3.96	2.79	0.00	8.85	5.64	5.41	4.91	3.78	4.44
G4	5.01	6.08	8.85	0.00	3.33	3.97	5.76	6.03	5.03
G5	1.93	2.94	5.64	3.33	0.00	1.74	4.05	3.41	2.53
G6	2.52	2.88	5.41	3.97	1.74	0.00	3.83	3.21	2.33
G7	2.59	2.94	4.91	5.76	4.05	3.83	0.00	2.17	2.80
G8	1.69	1.88	3.78	6.03	3.41	3.21	2.17	0.00	2.40
G9	1.92	2.08	4.44	5.03	2.53	2.33	2.80	2.40	0.00

TABLE 4.4. – MMOCD comparisons between reflectances in FIGURE 4.4 scaled down by 0.5% and FIGURE 4.5. Lower values indicate fewer differences in color inconstancy combined with differences in color.

MMOCD	**G1'**	**G2'**	**G3'**	**G4'**	**G5'**	**G6'**	**G7'**	**G8'**	**G9'**
S1	0.15	1.27	3.95	5.02	1.94	2.54	2.62	1.68	1.94
S2	0.69	1.50	4.26	4.62	1.68	1.87	2.82	1.94	1.76
S3	1.31	1.91	4.60	4.32	1.60	1.24	3.09	2.30	1.77
S4	1.92	2.38	4.99	4.12	1.59	0.64	3.43	2.72	1.97
S5	2.51	2.87	5.40	3.99	1.73	0.15	3.84	3.19	2.34
S6	3.08	3.37	5.81	3.91	2.06	0.59	4.29	3.68	2.77
S7	3.63	3.88	6.23	3.89	2.47	1.13	4.76	4.18	3.23
S8	4.17	4.38	6.65	3.91	2.92	1.66	5.23	4.68	3.70
S9	4.69	4.87	7.07	3.98	3.39	2.18	5.70	5.18	4.17

Using the minimum of the differences determined in Eq. 4.11 provides an Object Metamer Index (OMI) which indicates how close a pair of objects are to being metamers for some observing condition. This is expressed by the operations found in Eq. 4.12.

$$\begin{aligned} \mathbb{D}_{\text{batch,std}} &= \{\Delta E_{\text{Wpt}}\left(\mathbf{w}_{i,\text{batch},k}, \mathbf{w}_{i,\text{std},j}\right) | \forall i, \forall k\} \\ OMI\left(\mathbf{O}_{\text{batch}}, \mathbf{O}_{\text{std}}\right) &= min\left(\mathbb{D}_{\text{batch,std}}\right) \end{aligned} \tag{4.12}$$

where:
$\mathbb{D}_{\text{batch,std}}$ defines a set of corresponding Wpt color differences between manifolds for a batch and a standard object,
O_{batch} identifies the batch object reflectance matrix,
O_{std} identifies the standard object reflectance matrix,
$\mathbf{w}_{i,\text{batch},k}$ defines the Wpt coordinate using Eq. 4.1of the batch object for the i^{th} observer and the k^{th} illuminant, and
$\mathbf{w}_{i,\text{std},k}$ defines the Wpt coordinate using Eq. 4.1 of the standard object for the i^{th} observer and the k^{th} illuminant.

If the OMI value is zero then the two objects are metamers for one or more observing conditions, and low but non-zero OMI values (≤ 1) would be indicative that the objects are paramers. Larger values provide an indication of how minimally different the colors of two objects are for all the observing conditions considered. OMI values were determined for the same reflectances used for finding MMOCD values in TABLE 4.4. The results are shown in TABLE 4.5. The values are all non-zero but small which is indicative of that the reflectances being compared are paramers.

The last type of proposed object metric compares two objects by the Wpt shift manifolds of their characteristic reflectances (found using Eq. 4.5) using the MMOCD metric (from Eq. 4.11) to provide an Object Hue Similarity Index (OHSI) as shown in Eq. 4.13. This metric is useful

TABLE 4.5. – OMI comparisons between reflectances in FIGURE 4.4 scaled down by 0.5% and FIGURE 4.5. Lower values indicate fewer differences in color inconstancy combined with differences in color.

OMI	**G1'**	**G2'**	**G3'**	**G4'**	**G5'**	**G6'**	**G7'**	**G8'**	**G9'**
S1	0.15	0.12	0.02	0.15	0.15	0.07	0.15	0.15	0.08
S2	0.08	0.06	0.02	0.15	0.15	0.09	0.15	0.15	0.12
S3	0.01	0.05	0.02	0.12	0.09	0.08	0.15	0.06	0.05
S4	0.03	0.05	0.04	0.09	0.01	0.07	0.15	0.04	0.04
S5	0.05	0.04	0.06	0.03	0.02	0.15	0.15	0.08	0.03
S6	0.05	0.05	0.10	0.15	0.04	0.08	0.07	0.04	0.05
S7	0.05	0.07	0.11	0.12	0.06	0.01	0.15	0.04	0.08
S8	0.05	0.06	0.12	0.07	0.08	0.03	0.11	0.10	0.07
S9	0.06	0.05	0.14	0.05	0.05	0.05	0.14	0.15	0.15

because the characteristic reflectance uniquely defines the hue of an object under various observing conditions.

$$OHSI\left(\mathbf{O}_{\text{batch}}, \mathbf{O}_{\text{std}}\right) = MMOCD\left(P\left(\mathbf{O}_{\text{batch}}\right), P\left(\mathbf{O}_{\text{std}}\right)\right) \tag{4.13}$$

where:
O_{batch} identifies the batch object reflectance matrix,
O_{std} identifies the standard object reflectance matrix,
$P\left(O_{\text{batch}}\right)$ uses Eq. 4.5 to determine the characteristic reflectance for the batch object reflectance matrix,
$P\left(O_{\text{std}}\right)$ uses Eq. 4.5 to determine the characteristic reflectance for the standard object reflectance matrix, and
$MMOCD\left(\right)$ uses Eq. 4.11 to determine the Mean Metameric Object Color Difference.

As an example, OHSI values were determined for the same set of reflectances used in TABLE 4.5 with the results shown in TABLE 4.6. There are large OSHI values when comparing non-selective reflectances to those that are wavelength selective. This is due to the characteristic reflectance being zero for non-selective reflectances. The comparisons between S2-S9 with G1'-G9' are all the same because the reflectances of S2-S9 all have the same characteristic reflectance curve. The OHSI for the S1 vs G1' and the S5 vs G6' comparisons are zero as a result of the characteristic reflectances of the curves being compared being the same.

A final example demonstrates the simultaneous use of the MMOCD, OMI, and OHSI metrics. MMOCD, OMI and OHSI values were determined by comparing reflectances from FIGURE 4.9 with the reflectance for Munsell 5Y 7/12 and are provided in TABLE 4.7. The MMOCD and OMI values are all fairly similar with the OMI value being much larger that zero. This indicates that the colors are not metamers and that the MMOCD value largely determines the general color difference between the reflectances. Variability in the OHSI is somewhat indicative of

TABLE 4.6. – OHSI comparisons between reflectances in FIGURE 4.4 scaled down by 0.5% and FIGURE 4.5. Lower values indicate that reflectances have similar hue characteristics for different observing conditions with a value of zero indicating that characteristic reflectances are the same.

OHSI	**G1'**	**G2'**	**G3'**	**G4'**	**G5'**	**G6'**	**G7'**	**G8'**	**G9'**
S1	0.0	48.3	85.6	82.2	41.0	76.1	79.6	79.0	77.9
S2	76.1	30.0	14.1	9.8	36.7	0.0	8.8	7.6	5.3
S3	76.1	30.0	14.1	9.8	36.7	0.0	8.8	7.6	5.3
S4	76.1	30.0	14.1	9.8	36.7	0.0	8.8	7.6	5.3
S5	76.1	30.0	14.1	9.8	36.7	0.0	8.8	7.6	5.3
S6	76.1	30.0	14.1	9.8	36.7	0.0	8.8	7.6	5.3
S7	76.1	30.0	14.1	9.8	36.7	0.0	8.8	7.6	5.3
S8	76.1	30.0	14.1	9.8	36.7	0.0	8.8	7.6	5.3
S9	76.1	30.0	14.1	9.8	36.7	0.0	8.8	7.6	5.3

the variations in the Wpt shift manifolds in FIGURE 4.9. However, as the OHSI is based on the mean it merely provides insight into the general distribution and is not entirely expressive of the relative shape and extent of differences in the manifolds.

TABLE 4.7. – Shift Manifold Metrics for 5Y Munsell Plane for Munsell Values (vertical) and Munsell Chromas (horizontal) with metrics MMOCD (top), OMI (middle) and OHSI (bottom) relative to 5Y 7/12

	2	4	6	8	10	12	14
	30.9	25.5	22.2				
9	30.3	24.5	21.6				
	26.4	17.7	12.0				
	28.1	22.0	18.1	16.0	15.2	15	15.1
8.5	27.7	21.5	17.5	15.7	14.8	14.7	14.9
	26.0	17.2	10.3	6.3	3.5	2.0	1.6
	25.7	18.8	14.1	11.4	10.1	10.1	10.1
8	25.1	18.0	13.5	10.1	9.5	9.3	9.7
	25.3	16.5	9.6	5.9	2.6	3.4	1.7
	23.7	15.6	9.7	5.4	2.1	0.0	
7	23.1	14.8	9.3	5.2	1.9	0.0	
	27.8	12.4	7.1	2.6	2.0	0.0	
	25.7	18.6	13.9	11.5	10.5		
6	25.0	17.8	13.1	10.8	9.6		
	21.2	10.3	4.0	1.7	1.8		
	31.6	25.9	22.8	21.5			
5	30.3	25.0	21.9	20.6			
	16.4	5.8	9.4	2.0			
	39.4	35.4	33.5				
4	38.5	34.6	32.6				
	12.3	2.2	2.4				
	49.2	46.3				MMOCD	
3	48.3	45.8				OMI	
	7.2	2.5				OHSI	
	59.1						
2	58.0						
	3.8						

4.3.2 Illuminant Shift Manifold Difference Metric

There is an abundance of literature related to the characterization of the qualities of light sources and illuminants in terms of how they make objects appear. *Color rendering* of a light source is a measure of the degree to which the perceived colors of objects illuminated by the source conform to those of the same objects illuminated by a standard source, for specified observing conditions [Nickerson, 1960]. A color rendering index quantifies color rendering (color rendition). Both Rea and Royer provide background and understanding related to the state of art in this field [Rea and Freyssinier, 2010; Royer et al., 2012].

The dominant color rendering index (CRI) defined by the CIE [CIE13, 1995] uses a vonKries chromatic adaptation to convert colorimetry of a set of select reflectances for a standard observer under a test illuminant to colorimetry under a reference illuminant. Others have pointed out limitations of this approach while proposing other metrics that use gamut volume, color appearance models, or more perceptually uniform color spaces for determining color rendering metrics. In most cases these metrics all rely on the principle of color equivalency as provided by some form of chromatic adaptation.

As was pointed out in Chapter 2, chromatic adaptation provides a sense of color equivalency that preserves to some extent a “similarity of appearance". As Wpt normalization provides a “similarity of material color equivalency" that minimizes differences due to observer and illuminant it is proposed that Wpt based MATs or Wpt shift manifolds could possibly be used to define metrics related to the color rendering of illuminants. This is meant only as an introduction to the possibilities, and an extensive analysis and comparison is left as a future research effort.

One initial method would be to use a Wpt based Material Adjustment Transform (MAT) in conjunction with already published methods of determining metrics of color rendering. However, this line of research is left as a future effort.

Relative to the present research, a different metric that provides insight into the color equivalency of using two illuminants is proposed. This proposed illuminant metric compares corresponding Wpt coordinates between Wpt shift manifolds varying both the object and observer. For visualization purposes, a set of reflectances along with the previous set of observers defined in TABLE 4.1 and FIGURE 4.2 under the two separate illuminants were used to define Wpt shift manifolds for comparison purposes. The set of spectral reflectances consisted of corrected reflectances from the Glossy Munsell Book of Color as described in Appendix A. The Illuminant Rendering Equivalency (IRE) for two illuminants is determined using Eq. 4.14. This metric also factors in the equivalence of illuminants relative to variations in observer (which other color rendering indices like CRI do not account for). This is because a Wpt shift manifold is defined by the aggregate of the variations in object, observer and illuminant.

$$IRE\left(\mathbf{l}_{\text{test}}, \mathbf{l}_{\text{alternate}}\right) = \frac{\sum_i \sum_j \Delta E_{\text{Wpt}}\left(\mathbf{w}_{i,j,\text{test}}, \mathbf{w}_{i,j,\text{alternate}}\right)}{ij} \tag{4.14}$$

where:
$\mathbf{l}_{\text{test}}$ is a vector that identifies the SPD of the test illuminant,
$\mathbf{l}_{\text{alternate}}$ is a vector that identifies the SPD of an alternate illuminant,
$\mathbf{w}_{i,j,\text{test}}$ defines the Wpt coordinate using Eq. 4.1 of the j^{th} object for the i^{th} observer and under the test illuminant, and
$\mathbf{w}_{i,j,\text{alternate}}$ defines the Wpt coordinate using Eq. 4.1 of the j^{th} object for the i^{th} observer under the alternate illuminant.

Twelve CIE F illuminants and a white LED light source were used as test illuminants to determine IRE values for demonstration purposes. The relative spectral power distributions of these illuminants is shown in FIGURE 4.12. The IRE values were determined by comparing to reference illuminants made up of daylight illuminants (with CCTs from 4000K to 14000K) and black body radiators (with CCTs from 1750K to 12000K) all from the set of illuminants defined in TABLE 4.2. The resulting IRE values are visualized as curves for each test illuminant in FIGURE 4.13 while minimum points are identified in TABLE 4.8.

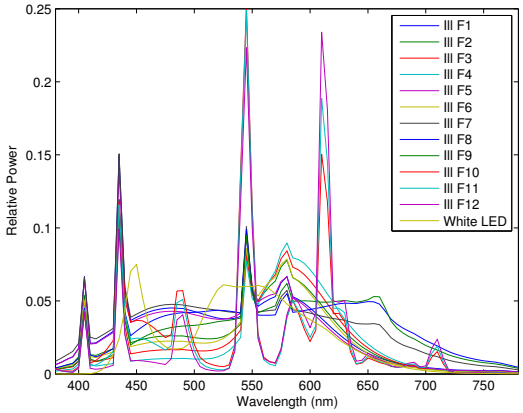

FIGURE 4.12. – IRE Test Illuminants

The horizontal position on the curve corresponds to the comparison of the test illuminant to a reference blackbody or daylight illuminant with a CCT of a specific temperature. The vertical position indicates the mean WLab distance between corresponding points in the Wpt shift manifolds for the reference and test illuminant. The larger the average distance is the greater the difference is in rendering of the test and reference illuminants. Each of the IRE curves has a minimum IRE point that indicates the CCT of the "closest" reference illuminant and the mean difference between Wpt color renderings.

In TABLE 4.8 the closest CCT for blackbody illuminants doesn't necessary correspond to the closest CCT for the test daylight illuminants. In some cases the CCT range for blackbody illuminants goes lower than it does for daylight illuminants and the minimum is out of range. In other cases there is just a difference in how blackbody and daylight illuminants render into Wpt. IRE values are solely determined by the rendering of the colors by the illuminant rather than the color of the illuminant because Wpt normalization causes the illuminants' white points to

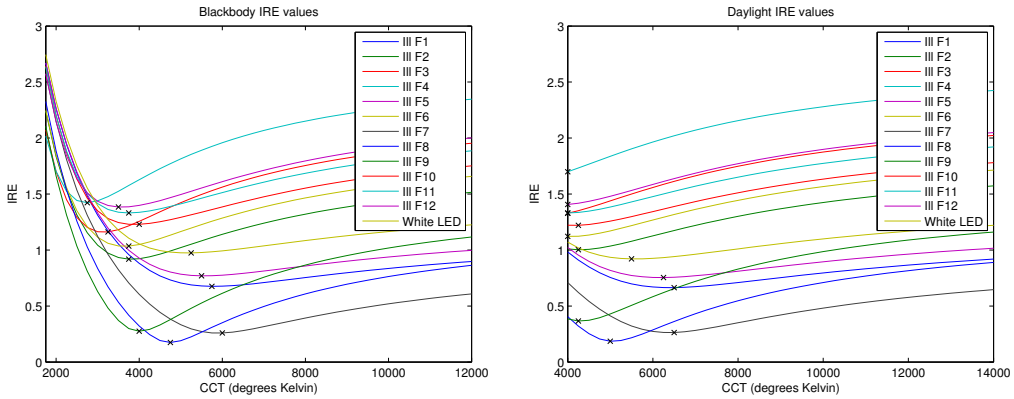

FIGURE 4.13. – IRE Results for Test Illuminants compared to blackbody (left) and daylight (right) reference illuminants. The minimum point for each test illuminant are marked with an 'x'.

TABLE 4.8. – Illuminants and IRE values for minimum points on curves in FIGURE 4.13. Minimum IRE values identified in *italics*.

Test (T)	Closest Blackbody (B)	T-B IRE	Closest Daylight (D)	T-D IRE
F1	Blackbody 5750K	0.68	Daylight 6500K	*0.66*
F2	Blackbody 3750K	*0.92*	Daylight 4250K	1.00
F3	Blackbody 3250K	*1.16*	Daylight 4000K	1.33
F4	Blackbody 2750K	*1.42*	Daylight 4000K	1.70
F5	Blackbody 5500K	0.77	Daylight 6250K	*0.75*
F6	Blackbody 3750K	*1.04*	Daylight 4000K	1.12
F7	Blackbody 6000K	*0.26*	Daylight 6500K	*0.26*
F8	Blackbody 4750K	*0.17*	Daylight 5000K	0.19
F9	Blackbody 4000K	*0.27*	Daylight 4250K	0.37
F10	Blackbody 4000K	1.23	Daylight 4250K	*1.22*
F11	Blackbody 3750K	*1.33*	Daylight 4000K	*1.33*
F12	Blackbody 3500K	*1.38*	Daylight 4000K	1.41
White LED	Blackbody 5250K	0.97	Daylight 5500K	*0.92*

all align to the same Wpt point. Therefore the minimum IRE may not correspond to the CCT determined by the illuminants' colorimetry.

The lowest IRE curve minimum values occur for test illuminants F8, F7, and F9 which correspond to "broadband" full-spectrum light sources. The highest minimum curve value occurs for test illuminant F4 which was used by the CIE to calibrate the CRI formula. Illuminants F12, F11, and F10 have the next highest minimum curve values which correspond to narrow-band emission (energy efficient) light sources. The minimum curve value for the White LED falls in the mid to upper range of the IRE values for the test illuminants indicating that the color rendering equivalency of this particular White LED is not particularly close to the blackbody or daylight reference illuminants. Overall, the IRE results for the F series illuminants are fairly consistent with general color rendering observations found in the literature. As such, it is reasonable to conclude that the use of Wpt shift manifolds for characterizing illuminant rendering has potential. However, further analysis, comparison, and extrapolation is left as a future research effort.

4.3.3 Observer Equivalency Metric

The Luther-Ives condition [Luther, 1927; Ives, 1915] can be simply stated that two observers have identical color discrimination (ability to match colors) if the sensor sensitivity functions or color matching functions of the first observer can be expressed as a linear combination of the second observer, or as an equation the following always holds true:

$$\mathbf{C}_1 = \mathbf{M}\mathbf{C}_2 \tag{4.15}$$

where:
$\mathbf{C}_1$ and $\mathbf{C}_2$ are matrices defining sensor sensitivity functions or color matching functions for the first and second observer, and
$\mathbf{M}$ is a linear non-singular transformation matrix.

If identical object matrices and light source vectors are applied to both sides of Eq. 4.15 then the Luther-Ives condition is expressed in terms of sensor excitations as follows:

$$\mathbf{C}_1\mathbf{O}_j\mathbf{l}_k = \mathbf{M}\mathbf{C}_2\mathbf{O}_j\mathbf{l}_k \tag{4.16}$$

where:
$\mathbf{C}_1$, $\mathbf{C}_2$, and $\mathbf{M}$ are the same as in Eq. 4.15, and
$\mathbf{O}_j$ and $\mathbf{l}_k$ are the same as in Eq. 4.1.

It is asserted that matrix $\mathbf{M}$ in Eq. 4.16 can be defined using a Wpt based MAT, and the Luther-Ives condition therefore holds if the Wpt coordinates are the same. Thus, their difference is a null vector. This is shown by first substituting Wpt normalization matrices in similar fashion as Eq. 2.4 for the MAT in Eq. 4.16; shifting the Wpt normalization matrix to the left side, substituting

Wpt vectors as in Eq. 4.1; and finally subtracting the right side from the left side resulting in a null vector as follows:

$$\begin{gathered}\mathbf{C}_1\mathbf{O}_j\mathbf{l}_k = \left(\left(\mathbf{A}_{1,k}\right)^{-1}\mathbf{A}_{2,k}\right)\mathbf{C}_2\mathbf{O}_j\mathbf{l}_k \\ \mathbf{A}_{1,k}\mathbf{C}_1\mathbf{O}_j\mathbf{l}_k = \mathbf{A}_{2,k}\mathbf{C}_2\mathbf{O}_j\mathbf{l}_k \\ \mathbf{w}_{1,j,k} = \mathbf{w}_{2,j,k} \\ \text{or} \\ \mathbf{w}_{1,j,k} - \mathbf{w}_{2,j,k} = \oslash\end{gathered} \tag{4.17}$$

The results of Eq. 4.17 indicate that the difference of Wpt coordinates provides an indication of how well the Luther-Ives condition is met. This leads to the following metric that provides insight into the color matching equivalency of two observers. The proposed Observer Matching Equivalency (OME) metric compares corresponding Wpt coordinates for Wpt shift manifolds varying both the object and illuminant as follows:

$$ORE\left(\mathbf{C}_{\text{test}}, \mathbf{C}_{\text{alternate}}\right) = \frac{\sum_j \sum_k \Delta E_{\text{Wpt}}\left(\mathbf{w}_{\text{test},j,k}, \mathbf{w}_{\text{alternate}j,k}\right)}{jk} \tag{4.18}$$

where:
$\mathbf{C}_{\text{test}}$ is a matrix that identifies the sensor sensitivities/color matching functions of the test observer,
$\mathbf{C}_{\text{alternate}}$ is a matrix that identifies the sensor sensitivities/color matching functions of the alternate observer,
$\mathbf{w}_{\text{test},j,k}$ defines the Wpt coordinate using Eq. 4.1 of j^{th} object for the k^{th} illuminant and under the test illuminant, and
$\mathbf{w}_{\text{alternate},j,k}$ defines the Wpt coordinate using Eq. 4.1 of j^{th} object for the k^{th} observer under the alternate illuminant.

For visualization purposes, Wpt shift manifolds were determined for a set of reference reflectances under D65, D50, Illuminant A, Illuminant E, and the CIE F illuminants (1-12) from TABLE 4.2 and FIGURE 4.3 for the Standard 10° observer, Standard 2° observer, and Judd-Vos modified 2° observer [Vos, 1978; Wyszecki and Stiles, 2000] as well as CIE2006 observers varying by field size in 0.5° steps and age by steps of 5 years. The set of spectral reflectances utilized was from the Corrected Glossy Munsell Book of Color as described in Appendix A. The set of illuminants was intentionally limited from previous metric visualizations to limit computational complexity since many observers were being compared. The OME metric of Eq. 4.18 was used to compare the Standard 10° observer, Standard 2° observer, and Judd-Vos modified 2° observer [Vos, 1978; Wyszecki and Stiles, 2000] to each of the CIE2006 observers.

The results of the observer comparisons are shown in FIGURE 4.14. Equivalent numeric values for the Std 10° observer are found in TABLE 4.9, and from both the figure and this table the closest color observer equivalency match for the Standard 10° observer is the CIE2006 10° 40 year old. Additionally, for the 10° observer, the OME has a value of 0.036 which is indicative that the color matching is on average nearly identical between these two observers.

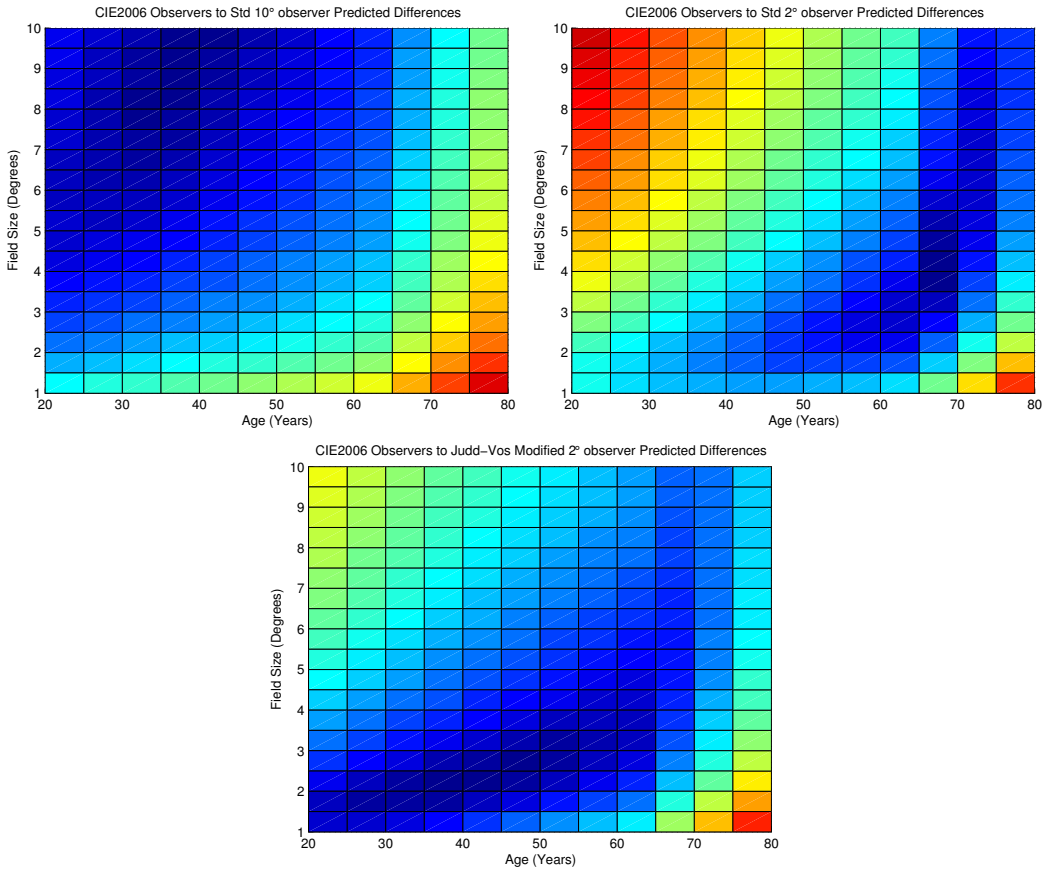

FIGURE 4.14. – Observer Matching Equivalency (OME) results comparing CIE2006 Cone Fundamentals to 10° standard observer (top-left), 2° standard observer (top-right), and Judd-Vos modified 2° observer (bottom). Dark blue represents lowest values and red represents highest values with intermediate colors representing intermediate values. Actual corresponding numeric values can be found in TABLE 4.9, TABLE 4.10, TABLE 4.11.

TABLE 4.9. – Observer Matching Equivalency (OME) results comparing 10° standard observer to CIE2006 Cone Fundamentals with Field size (vertical) and Age (horizontal) with OME value for closest (best) match shown in ***bold-italics***.

	20yo	25yo	30yo	35yo	40yo	45yo	50yo	55yo	60yo	65yo	70yo	75yo	80yo
10.0°	0.166	0.120	0.077	0.040	***0.036***	0.072	0.114	0.157	0.200	0.343	0.484	0.623	0.759
9.5°	0.156	0.111	0.067	0.033	0.041	0.079	0.122	0.165	0.209	0.352	0.493	0.631	0.767
9.0°	0.147	0.101	0.058	0.029	0.049	0.089	0.132	0.175	0.218	0.361	0.501	0.639	0.775
8.5°	0.136	0.092	0.051	0.032	0.059	0.099	0.142	0.185	0.229	0.371	0.511	0.649	0.784
8.0°	0.126	0.082	0.045	0.039	0.071	0.111	0.154	0.197	0.240	0.382	0.522	0.659	0.794
7.5°	0.116	0.075	0.046	0.051	0.084	0.125	0.167	0.210	0.253	0.394	0.534	0.671	0.806
7.0°	0.107	0.071	0.052	0.065	0.100	0.140	0.182	0.224	0.267	0.408	0.547	0.683	0.818
6.5°	0.101	0.071	0.063	0.082	0.117	0.157	0.198	0.240	0.282	0.423	0.561	0.697	0.831
6.0°	0.098	0.077	0.078	0.101	0.136	0.175	0.216	0.258	0.300	0.439	0.577	0.712	0.846
5.5°	0.099	0.088	0.097	0.123	0.157	0.196	0.236	0.278	0.319	0.458	0.595	0.730	0.863
5.0°	0.107	0.104	0.120	0.147	0.181	0.219	0.259	0.300	0.341	0.478	0.615	0.749	0.882
4.5°	0.120	0.126	0.145	0.173	0.207	0.245	0.285	0.325	0.366	0.502	0.638	0.772	0.904
4.0°	0.141	0.153	0.175	0.204	0.238	0.275	0.314	0.354	0.394	0.530	0.665	0.798	0.930
3.5°	0.169	0.185	0.210	0.239	0.273	0.310	0.349	0.388	0.428	0.563	0.697	0.830	0.961
3.0°	0.205	0.225	0.251	0.281	0.315	0.352	0.390	0.429	0.469	0.602	0.736	0.868	0.999
2.5°	0.251	0.274	0.301	0.332	0.366	0.403	0.441	0.480	0.519	0.652	0.784	0.916	1.047
2.0°	0.312	0.337	0.365	0.397	0.431	0.467	0.505	0.544	0.583	0.715	0.847	0.978	1.108
1.5°	0.391	0.418	0.448	0.481	0.515	0.551	0.589	0.627	0.666	0.797	0.929	1.059	1.190
1.0°	0.499	0.527	0.558	0.592	0.626	0.663	0.700	0.738	0.777	0.907	1.038	1.169	1.298

TABLE 4.10. – Observer Matching Equivalency (OME) results comparing 2° standard observer to CIE2006 Cone Fundamentals with Field size (vertical) and Age (horizontal) with OME value for closest (best) match shown in ***bold-italics***.

	20yo	25yo	30yo	35yo	40yo	45yo	50yo	55yo	60yo	65yo	70yo	75yo	80yo
10.0°	0.840	0.785	0.731	0.678	0.626	0.575	0.525	0.475	0.427	0.281	0.176	0.191	0.298
9.5°	0.827	0.772	0.719	0.666	0.614	0.562	0.512	0.463	0.414	0.268	0.166	0.191	0.304
9.0°	0.814	0.759	0.705	0.652	0.600	0.549	0.498	0.449	0.401	0.254	0.155	0.193	0.310
8.5°	0.799	0.744	0.691	0.638	0.585	0.534	0.483	0.434	0.386	0.239	0.145	0.195	0.317
8.0°	0.783	0.729	0.675	0.622	0.570	0.518	0.468	0.418	0.370	0.223	0.135	0.199	0.325
7.5°	0.766	0.712	0.658	0.605	0.552	0.501	0.450	0.401	0.352	0.206	0.126	0.204	0.335
7.0°	0.748	0.693	0.639	0.586	0.534	0.482	0.432	0.382	0.334	0.187	0.118	0.211	0.346
6.5°	0.728	0.673	0.619	0.566	0.514	0.462	0.412	0.362	0.313	0.167	0.113	0.220	0.359
6.0°	0.707	0.652	0.598	0.545	0.492	0.441	0.390	0.340	0.291	0.145	0.112	0.232	0.375
5.5°	0.683	0.628	0.574	0.521	0.468	0.417	0.366	0.316	0.267	0.122	0.117	0.248	0.393
5.0°	0.657	0.602	0.548	0.495	0.442	0.391	0.340	0.290	0.241	0.097	0.127	0.267	0.414
4.5°	0.629	0.574	0.520	0.466	0.414	0.362	0.311	0.261	0.212	0.073	0.145	0.290	0.439
4.0°	0.597	0.542	0.487	0.434	0.381	0.329	0.278	0.228	0.180	***0.059***	0.170	0.320	0.469
3.5°	0.561	0.505	0.451	0.398	0.345	0.293	0.243	0.193	0.145	0.071	0.204	0.355	0.505
3.0°	0.519	0.464	0.410	0.357	0.305	0.254	0.204	0.158	0.116	0.106	0.248	0.400	0.550
2.5°	0.472	0.418	0.364	0.312	0.262	0.215	0.172	0.136	0.112	0.160	0.305	0.456	0.606
2.0°	0.420	0.368	0.319	0.273	0.231	0.195	0.167	0.149	0.147	0.234	0.379	0.529	0.677
1.5°	0.379	0.335	0.296	0.262	0.234	0.215	0.206	0.209	0.223	0.331	0.475	0.624	0.771
1.0°	0.374	0.343	0.317	0.299	0.290	0.290	0.299	0.316	0.341	0.460	0.603	0.750	0.896

TABLE 4.11. – Observer Matching Equivalency (OME) results comparing 2° Judd-Vos modified observer to CIE2006 Cone Fundamentals with Field size (vertical) and Age (horizontal) with OME value for closest (best) match shown in ***bold-italics***.

	20yo	25yo	30yo	35yo	40yo	45yo	50yo	55yo	60yo	65yo	70yo	75yo	80yo
10.0°	0.719	0.674	0.631	0.589	0.549	0.512	0.477	0.445	0.415	0.350	0.357	0.433	0.543
9.5°	0.705	0.660	0.617	0.575	0.536	0.499	0.464	0.432	0.403	0.341	0.355	0.435	0.547
9.0°	0.690	0.645	0.602	0.561	0.521	0.485	0.450	0.419	0.390	0.332	0.352	0.438	0.553
8.5°	0.674	0.629	0.586	0.545	0.506	0.469	0.435	0.404	0.376	0.323	0.350	0.441	0.559
8.0°	0.656	0.611	0.568	0.528	0.489	0.452	0.419	0.388	0.362	0.313	0.349	0.445	0.567
7.5°	0.637	0.592	0.550	0.509	0.470	0.434	0.401	0.371	0.346	0.303	0.349	0.451	0.575
7.0°	0.616	0.572	0.529	0.489	0.450	0.415	0.382	0.353	0.328	0.294	0.349	0.457	0.585
6.5°	0.594	0.550	0.507	0.467	0.429	0.394	0.362	0.334	0.310	0.285	0.352	0.466	0.596
6.0°	0.570	0.525	0.483	0.443	0.405	0.371	0.339	0.312	0.291	0.277	0.356	0.476	0.609
5.5°	0.543	0.498	0.456	0.416	0.379	0.345	0.315	0.290	0.270	0.271	0.362	0.489	0.624
5.0°	0.513	0.469	0.427	0.387	0.351	0.318	0.289	0.265	0.249	0.268	0.373	0.504	0.642
4.5°	0.480	0.436	0.394	0.355	0.319	0.287	0.260	0.239	0.227	0.269	0.387	0.524	0.663
4.0°	0.443	0.399	0.358	0.319	0.284	0.254	0.229	0.212	0.207	0.277	0.407	0.547	0.689
3.5°	0.401	0.357	0.316	0.278	0.244	0.216	0.196	0.187	0.193	0.294	0.433	0.577	0.720
3.0°	0.352	0.308	0.268	0.232	0.201	0.177	0.166	0.172	0.196	0.323	0.468	0.614	0.759
2.5°	0.296	0.253	0.215	0.182	0.158	0.147	0.157	0.185	0.222	0.364	0.514	0.663	0.808
2.0°	0.235	0.197	0.166	0.145	***0.141***	0.159	0.191	0.230	0.273	0.424	0.576	0.726	0.873
1.5°	0.193	0.169	0.157	0.164	0.188	0.223	0.264	0.307	0.352	0.507	0.660	0.811	0.958
1.0°	0.210	0.211	0.227	0.256	0.292	0.333	0.377	0.422	0.468	0.622	0.776	0.927	1.074

Equivalent numeric values for the Std 2° observer are found in TABLE 4.10, and from both the figure and this table the closest color observer equivalency match for the Standard 2° observer is the CIE2006 4° 65 year old. Additionally, for the Std 2° observer, the OME has a value of 0.059 which is indicative that the color matching is on average nearly identical between these two observers.

The analysis of the Judd-Vos modified 2° observer was included to ensure correctness of the OME metric, in which equivalent numeric values for the Judd-Vos modified 2° observer are found in TABLE 4.10. From both the figure and this table the closest color observer equivalency match for the Judd-Vos modified 2° observer is the CIE2006 2° 40 year old. However, for the Judd Vos 2° observer, the OME has a value of 0.141 which is indicative that the color matching is very close between these two observers.

As a second example, the 1000 observer cone fundamentals statistically derived by Fairchild and Heckaman [Fairchild and Heckaman, 2013] were each compared to the CIE2006 observers using the same comparison metrics used to derive FIGURE 4.14 and TABLE 4.9. These comparisons were used to find the closest CIE2006 observer for each of the Fairchild-Heckaman observers. An observer categorization distribution was obtained from these results which are shown in FIGURE 4.15. As can be seen from this figure the Fairchild-Heckaman observers have a reasonably normal distribution over all field sizes for 20 year old observers. It is believed that the Fairchild-Heckaman set includes data for observers younger than 20 years thus resulting in the large bump for 20 year old observers in FIGURE 4.15. The distribution also diminishes as the observers' age increases indicative of a drop off in the size of the population of older people. This set also appears to have greatest concentration of observers around a 4° field of view with practically no observers with a field of view greater than 7° that are older than 30 years old. It is postulated that the Luther-Ives condition will therefore likely be relevant when converting to color matching functions based on the Standard 2°observer (which also most closely matches the

CIE2006 4°observer). However, it is also postulated that the Luther-Ives condition will likely not hold well when trying to convert this dataset to color matching functions based on the Standard 10°observer, thus resulting in various material shifts in tristimulus values (see Chapter 6).

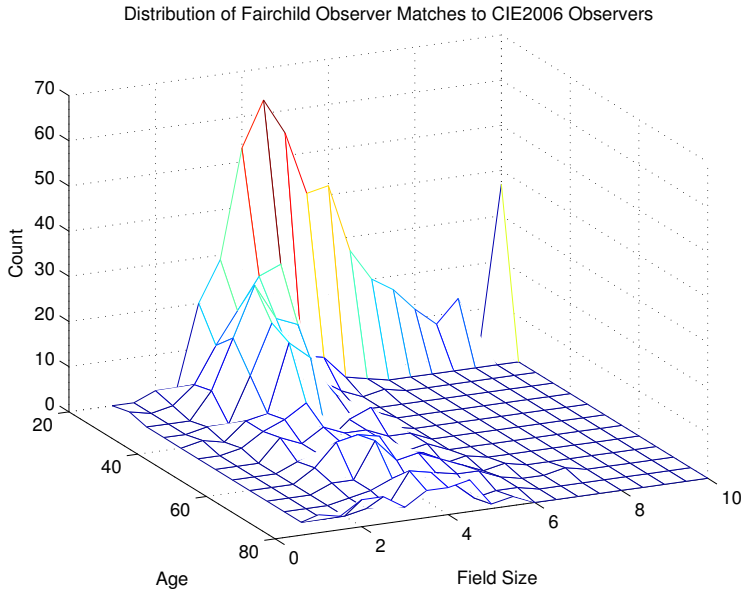

FIGURE 4.15. – Distribution of Fairchild-Heckaman observers when compared to the CIE2006 observers using OME values.

As a third example of observer comparisons, OME values were determined by comparing a database of spectral sensitivities for digital cameras [Jiang et al., 2013] to the Std 2° Observer for the same illuminants and reflectances used to determine the OME values in TABLE 4.9. The results are shown TABLE 4.12. All of the cameras in the first column have OME values less than one indicating that on average the perceptual difference in matching between the cameras and the Std 2° Observer is negligible. However, further analysis of results such as these are left as a future research effort.

TABLE 4.12. – Sorted comparison of Observer Matching Equivalency (OME) results for various digital cameras when compared to Std 2° Observer

OME	Camera	OME	Camera
0.60	Canon 50D	0.83	Canon 40D
0.61	Canon 60D	0.84	Canon 300D
0.62	Canon 500D	0.84	Nikon D3X
0.67	Nikon D40	0.85	Nikon D200
0.69	Canon 600D	0.88	Nikon D5100
0.73	Canon 5DMarkII	0.90	Nikon D90
0.73	SONY NEX-5N	0.95	Nikon D300s
0.78	Nikon D50	0.98	Olympus E-PL2
0.78	Pentax K-5	1.03	Canon 20D
0.79	Nokia N900	1.07	Nikon D80
0.80	Canon 1DMarkIII	1.18	Phase One
0.80	Nikon D700	1.37	Point Grey Grasshopper2 14S5C
0.80	Pentax Q	1.41	Hasselblad H2
0.82	Nikon D3	2.93	Point Grey Grasshopper 50S5C

4.3.4 Observing Conditions Shift Manifold Difference Metric

Throughout this research the combination of observer and illuminant has been referred to as an observing condition (which becomes the basis of Wpt normalization). It is therefore appropriate to propose a metric that provides insight into the color equivalency of using two observing conditions. The proposed Observing Conditions Equivalency (OCE) metric for two observing conditions compares the corresponding Wpt coordinates between Wpt shift manifolds of varying object reflectances for two different observer and illuminant combinations, and is determined using the following equation:

$$OCE\left(\mathbf{C}_{\text{test}}, \mathbf{l}_{\text{test}}, \mathbf{C}_{\text{alternate}}, \mathbf{l}_{\text{alternate}}\right) = \frac{\sum_j \Delta E_{\text{Wpt}}\left(\mathbf{w}_{\text{test},j,\text{test}}, \mathbf{w}_{\text{alternate}j,\text{alternate}}\right)}{j} \tag{4.19}$$

where:
$\mathbf{C}_{\text{test}}$ is a matrix that identifies the sensor sensitivities/color matching functions of the test observing condition observer,
$\mathbf{l}_{\text{test}}$ is a vector that identifies the SPD of the test observing condition illuminant,
$\mathbf{C}_{\text{alternate}}$ is a matrix that identifies the sensor sensitivities/color matching functions of the alternate observing condition observer,
$\mathbf{l}_{\text{alternate}}$ is a vector that identifies the SPD of an alternate observing condition illuminant,
$\mathbf{w}_{\text{test},j,\text{test}}$ defines the Wpt coordinate using Eq. 4.1 of the j^{th} object for the test observing condition, and

$\mathbf{w}_{\text{alternate},j,\text{alternate}}$ defines the Wpt coordinate using Eq. 4.1 of the j^{th} object for the alternate observing condition.

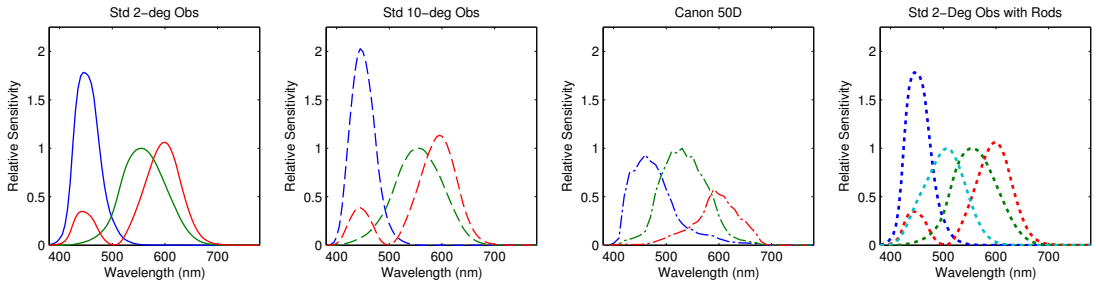

FIGURE 4.16. – Observers used for determining Observing Conditions Equivalency (OCE) results in FIGURE 4.17

Eq. 4.19 was used for visualization purposes to determine OCE values comparing a single observing condition made up of the 1931 Standard Observer (Std 2° observer) under a D65 illuminant to observing conditions made up of a several of observers under blackbody illuminants. Calculations were performed for CCT values at intervals of 250K. The results are shown in FIGURE 4.17. The set of comparison observers consisted of the Std 2° observer, the Std 10° observer, a Canon 50D camera, and the Std 2° observer plus the inclusion of the rod sensitivities. Spectral sensitivities for these observers are shown in FIGURE 4.16. The set of spectral reflectances used were from the Corrected Glossy Munsell Book of Color as described in Appendix A.

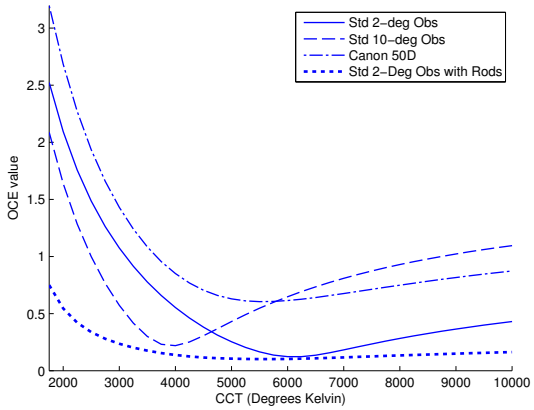

FIGURE 4.17. – Observing Conditions Equivalency (OCE) results comparing the observing condition Wpt shift manifold for Std 2° observer under D65 to the observing condition Wpt shift manifolds for several observers (see Legend) under blackbody illuminants

Each point in the curves in FIGURE 4.17 represents an OCE comparison of a single observing condition (defined by the curve's associated observer under a black body illuminant with the CCT of the point) and a fixed observing condition (defined by the Std 2° observer under D65).

The minimum of each of the curves represents the point at which there is a minimal mean material color shift between the observer with a blackbody illuminant and the fixed observing condition. In other words, these are observing conditions that are most similar in Wpt rendering to fixed observing condition. Remarkably, the CCTs of the illuminants for the minimal OCE points do not correspond to the CCT of the fixed observing conditions, and can be found in TABLE 4.13. The OCE values for the Std 2° observer are fairly flat near 6500K, and the slight difference is attributable to differences in black-body and daylight illuminant rendering being a bit better for a slightly lower CCT. For the other observing conditions it is believed that the reason for this difference in best matching CCT is that the differences in observer color matching is being compensated for by the shift in CCT of the illuminant. It is important to remember that an OCE comparison is a measure of the differences in observing conditions (illuminant plus observer) rather just the differences in illuminant.

TABLE 4.13. – Most equivalent observing conditions (blackbody illuminant/observer) to the observing conditions defined by a Std 2° observer under D65 (corresponding to the minimum points in OCE curves in FIGURE 4.17).

Blackbody CCT	Observer
6000K	Std 2-deg Obs
4000K	Std 10-deg Obs
5500K	Canon 50D
5500K	Std 2-Deg Obs with Rods

Interestingly, the lowest overall curve in FIGURE 4.17 corresponds to observing conditions that were defined by the Std 2° observer color matching function plus the inclusion of the rods. Comparing this curve to the observing conditions curve associated with only the Std 2° observer shows that there is a significant lowering of material color shift by including the rods – thus resulting in a more constant material color equivalency relationship with the fixed observing conditions. It is thought that this is because the rods provide an extra degree of freedom in the Wpt Normalization process to compensate for the exponential increase of light in the higher wavelengths of the SPD of blackbody illuminants as the CCT drops. Light sources such as firelight and candle light are modeled well using blackbody illuminants with low CCT values and generally the light intensity in such conditions is low enough to allow for rod interaction (mesopic vision) [McCann, 2006]. If the visual system were to use something like Wpt normalization as part of the adaptation process then including the rods would provide a mechanism for reducing differences in apparent color. At this point this is only conjecture and further research is needed to refute/validate any such possibility.

4.4 Conclusions about Wpt Shift Manifolds

In conclusion, various Wpt shift manifolds have been introduced showing that WSMs have the potential to provide a powerful mechanism for defining various metrics for comparing colors.

With such metrics, material color differences due to changes in illuminant and observer are minimized. Wpt shift manifolds simultaneously encompass changes in object, illuminant and observer thus allowing the possible scope of appearance that an object can have to easily be represented. From this, metrics of object color and comparisons of color between objects were more fully described and demonstrated. Additionally, Wpt shift manifolds have been used to define metrics for understanding and comparing illuminants, observers, and observing conditions. However, only initial descriptions and demonstrations of such metrics have been presented, and research to further understand and optimize such metrics has been left as a future endeavor.

5 Direct Wpt

5.1 Introduction

In Chapter 2 a method was introduced to normalize cone excitations, sensor values, or tristimulus values into an opponency-like coordinate system (Wpt) that provides a color equivalency representation for defining a material adjustment transform (MAT). In Chapter 3 a method was introduced to transform colors between Wpt coordinates and WLab $[L_w, a_w, b_w]$ coordinates which provide a more perceptually uniform representation of material color suitable for determining color differences.

It is believed that Wpt and WLab possibly provide benefits for the purposes of camera color correction and computer vision because differences in color are minimized due to changes in illumination, and perceptive uniformity is achieved for adjusting colors. The proposed Wpt normalization methodology requires a spectral characterization of both the observer and illuminant. However, for many imaging applications the spectral characterization of the illumination is not known. What is known is the sensor excitation values for colors in the captured scene, and possibly the spectral characteristics of the observer/capture device.

Two methods are proposed in this chapter for using the cone/sensor excitations values in the scene to approximately determine a Wpt normalization transform matrix. Such matrices can then be used to either establish material color equivalency aspects of the scene sensor data by the application of Wpt based material adjustment transforms as well as determine perceptively uniform material color attributes of lightness, chroma, and hue using WLab.

Validation of these methods was performed in like fashion to the metrics proposed in Chapter 4. Mean differences in Wpt coordinates determined by actual and estimated Wpt Normalization matrices for the illuminants in TABLE 4.2 and the Corrected Munsell Glossy reflectances provide a metric to the equivalency of two Wpt normalization matrices. Thus a Wpt Normalization Matrix Equivalency (WNME) metric is determined as follows:

$$WNME\left(\mathbf{A}_{\text{est}}, \mathbf{A}_{\text{actual}}\right) = \frac{\sum_j \sum_k \Delta E_{\text{Wpt}}\left(\mathbf{A}_{\text{est}}\mathbf{CO}_j\mathbf{l}_k, \mathbf{A}_{\text{actual}}\mathbf{CO}_j\mathbf{l}_k\right)}{jk} \tag{5.1}$$

5.2 Background

As described in Chapter 2, Wpt normalization transforms cone excitations or sensor values (referred to as sensor excitations) into a lightness-opponency representation (Wpt coordinates) that is minimized to be independent of observer and illumination. A Wpt normalization transform matrix is determined by performing linear geometrical operations to sensor excitations based on a set of material colors with specific spectral reflectances that have Munsell color designations with constant perceptive characteristics of lightness and chroma and vary evenly in hue. Wpt coordinates provide a useful waypoint or color equivalency representation (material color) for converting sensor excitations between different capture systems and/or different viewing conditions because Wpt represents the minimization of lightness, chroma, and hue variation due to illuminant and observer.

Often the term Chromatic Adaptation is used for any transform that makes predictions about how sensor excitation values change for an object as observing conditions change. The distinction is made in Chapter 2 between the general class of Sensor Adjustment Transform (SAT) and sensor transforms that have more specific meaning or relationships to experimental data. It was proposed that the definition of a Chromatic Adaptation Transform (CAT) be limited to sensor adjustment transforms that actually try to predict how the human visual system adapts under different lighting conditions with reference to psychophysically derived corresponding color data [Luo, 2000]. A sensor adjustment transform type was also proposed in Chapter 2 that tries to predict how sensor excitations vary for changes in illuminant or observer, and is referred to as a Material Adjustment Transform (MAT). In short – A CAT predicts color appearance, and a MAT predicts material color. In many cases these are two entirely different things, and having a clear distinction between MATs and CATs helps to distinguish between methods and intents for defining sensor adjustment transforms (SATs).

Wpt normalization provides a convenient color equivalency representation for defining a Material Adjustment Transform between sensor values for different observers or lighting conditions. A MAT differs from a CAT in that it is not necessarily directly based upon psychophysically derived corresponding color matches by human observers. For a single observer, a MAT may be experimentally defined by a Least Dissimilar Color Matching experiment [Logvinenko and Tokunaga, 2011]. For different observers it is proposed that the experimental basis of Least Dissimilar Color Matching be extended by using successive experiments with a common viewing condition for the observer which is analogous to the reference color equivalency representation used by a Wpt based MAT.

White balancing or camera color correction is often performed by rescaling the sensor values by the white point [Kang, 2006]. This is a form of SAT that differs from a CAT (since human adaptation is not involved), but can possibly be alternately defined using a MAT. Color correction in the literature is often associated with the concept of color constancy. However, aside from spectrally non-selective neutral colors, color constancy is only approximate, as two metamers

that have the same sensor excitations under one illuminant may have entirely different sensor excitations under a different illuminant [Wright, 1981].

In practice the spectral nature of the illumination at the time of image capture is not known and must be determined empirically from the image capture data [Smithson, 2005]. Various methods have been proposed including maximum pixel value, average pixel (grey world assumption), and other methods that are beyond the scope of the present work. Usually, the illuminant is determined to be a combination of sensor values, and these values are then used to determine a transform that factors out the influence of the illuminant. (Note: The methods of determining the white point of a captured scene are beyond the scope of this research. For the purposes of this research they are simply assumed to be externally determined).

As Wpt normalization minimizes differences due to sensor sensitivity functions (SSFs) and illuminant spectral power distributions (SPDs) it approximates color constancy and provides a means of quantifying inconstancy. It is therefore conceivably appropriate to use for camera color correction and computer vision where differences in material color under different lighting conditions are not desired. However, the method of Wpt normalization proposed in Chapter 2 requires a spectral model of the illuminant, sensor sensitivities, and surface reflectances of a set of reference colors to predict their sensor excitations. Because spectral information about the illuminant is often not known in the cases of color correction or computer vision, a separate form of Wpt normalization is needed in order for Wpt to be useful in these situations.

Two different approaches are proposed in the following sections to determine Wpt normalization transforms using various sensor excitation values. There is generally nothing novel in how they are implemented other than the fact that they provide a richer access to Wpt normalization matrices. The first approach uses one of four specialized physical color charts that can be included as part of the capture process to provide direct sensor excitation data that is used to determine an appropriate Wpt normalization transform. The second approach uses knowledge of the SSF of the of the capture system, spectral power distributions of a broad range of illuminants, and sensor excitation values captured or estimated for the illuminant (white point) to determine an appropriate Wpt normalization transform. This is similar in concept to the approach taken by Oleari in defining MATs based upon the CCT of the illuminant [Oleari et al., 2009]. However, the proposed method differs from that of Oleari in that sensor excitations for arbitrary illuminants (not just those defined by CCT for blackbody and Daylight illuminants) are used to estimate Wpt normalization matrices.

5.3 Wpt normalization from a Physical Chart

The proposed method of directly estimating a Wpt normalization matrix from sensor excitation values of a specialized color chart utilizes the same linear transform approach defined in Chapter 2. The significant difference is that actual sensor excitation values of a physical chart are used rather than estimated sensor excitation values for “corrected” Munsell Glossy reflectances. Four

different physical charts are proposed with increasing hue sampling frequency. The colors of the charts are defined using polar WLab coordinates L_w, c_w, h_w for the 1931 Standard Observer and CIE Illuminant C with corresponding CIEXYZ values. The proposed charts have been defined with one or more levels of non-selective grayscale patches along with chromatic patches that have constant WLab chroma and lightness and equal spacing of WLab hue h_w. TABLE 5.1 contains patch identifications and color values for various chart patch definitions. Several chart definitions were defined because it was felt that more patches might provide better results considering noise in the reproduction and capture process, but more patches may also be more difficult to accurately formulate with sufficient spectral variability. Only a single gray patch is needed to perform the Wpt normalization. However, additional gray patches in the larger charts can provide a means of determining and correcting for camera non-linearity.

The proposed method of determining a Wpt normalization matrix from sensor excitation values of the one of the charts defined in TABLE 5.1 is as follows:

(a) Rotate the sensor excitations for the non-selective gray reflectance with L_w=50 to align with the first axis. This is accomplished by first rotating around the first axis, and then rotating around the second axis. As a result the first axis will correspond to the attribute of lightness W.

(b) Scale the first axis so that adjusted non-selective grey reflectance with L_w=50 has a distance of 18.42 (i.e. the corresponding value for W) from the origin.

(c) Fit the adjusted sensor excitations for the chromatic patches (that have constant L_w) with an equation for a plane $(a_0c_1 + a_1c_2 + a_2W = 0)$, and use $-a_0$ and $-a_1$ in the W line of a matrix to form a shearing matrix that can be concatenated to the matrix resulting from the previous steps. This results in the chromatic patches having a nearly constant value for the first dimension W.

(d) Use direct linear regression to find a matrix that minimizes the distances between the transformed sensor excitation values of the patch colors and the actual p, t coordinates for the patches. This results in general preservation of both hue and chroma while allowing for trade-offs in accuracy due to differences induced by changes in observer and illuminant.

The creation of an actual physical target for demonstration and analysis has been left as a future research effort. For evaluation purposes spectral reflectances were estimated (see FIGURE 5.1) for each of the Wpt coordinates found in TABLE 5.1 using techniques that are established in Chapter 7. These were then used with the sensor functions for the set of digital cameras in TABLE 4.12 [Jiang et al., 2013] using Eq. 1.3 to estimate sensor excitations for the digital cameras under a D65 illuminant. Wpt normalization matrices were then determined using these estimated sensor excitations and the above steps. WNME differences were determined for each of the cameras and chart sizes which can be found in TABLE 5.2.

TABLE 5.1. – Desired chart target colors for direct Wpt normalization

10 Patch	15 Patch	24 Patch	42 Patch	L_w	c_w	h_w	p	t	CIE X	CIE Y	CIE Y
	1	1	1	97	0	0	0.0000	0.0000	90.66	92.44	109.29
	2	2	2	75	0	0	0.0000	0.0000	47.35	48.28	57.08
1	3	3	3	50	0	0	0.0000	0.0000	18.06	18.42	21.78
	4	4	4	25	0	0	0.0000	0.0000	4.33	4.42	5.22
	5	5	5	12	0	0	0.0000	0.0000	1.38	1.41	1.66
	6	6	6	3	0	0	0.0000	0.0000	0.33	0.33	0.39
2	7	7	7	50	22	0	24.4802	0.0000	23.10	18.42	23.47
			8	50	22	10	24.0938	4.2484	23.04	18.42	20.69
		8	9	50	22	20	22.8623	8.3212	22.81	18.42	17.97
			10	50	22	30	20.7387	11.9735	22.40	18.42	15.45
3	8	9	11	50	22	40	17.9395	15.0531	21.84	18.42	13.26
			12	50	22	50	14.7544	17.5836	21.20	18.42	11.40
		10	13	50	22	60	11.3141	19.5966	20.50	18.42	9.86
			14	50	22	70	7.6699	21.0729	19.76	18.42	8.65
4	9	11	15	50	22	80	3.8749	21.9758	18.99	18.42	7.80
			16	50	22	90	0.0000	22.2761	18.19	18.42	7.33
		12	17	50	22	100	-3.8727	21.9629	17.39	18.42	7.27
			18	50	22	110	-7.6588	21.0425	16.61	18.42	7.60
5	10	13	19	50	22	120	-11.2720	19.5237	15.86	18.42	8.34
			20	50	22	130	-14.6236	17.4277	15.15	18.42	9.46
		14	21	50	22	140	-17.6037	14.7713	14.53	18.42	10.98
			22	50	22	150	-20.0586	11.5809	14.00	18.42	12.88
6	11	15	23	50	22	160	-21.8251	7.9437	13.62	18.42	15.11
			24	50	22	170	-22.8250	4.0247	13.39	18.42	17.58
		16	25	50	22	180	-23.0911	0.0000	13.31	18.42	20.17
			26	50	22	190	-22.6928	-4.0014	13.37	18.42	22.79
7	12	17	27	50	22	200	-21.6582	-7.8830	13.56	18.42	25.38
			28	50	22	210	-20.0116	-11.5537	13.88	18.42	27.88
		18	29	50	22	220	-17.7900	-14.9276	14.32	18.42	30.22
			30	50	22	230	-15.0406	-17.9247	14.87	18.42	32.35
8	13	19	31	50	22	240	-11.8169	-20.4674	15.52	18.42	34.22
			32	50	22	250	-8.1779	-22.4686	16.25	18.42	35.77
		20	33	50	22	260	-4.1994	-23.8161	17.06	18.42	36.92
			34	50	22	270	0.0000	-24.3840	17.92	18.42	37.58
9	14	21	35	50	22	280	4.2497	-24.1012	18.80	18.42	37.69
			36	50	22	290	8.3727	-23.0039	19.66	18.42	37.27
		22	37	50	22	300	12.2401	-21.2005	20.46	18.42	36.37
			38	50	22	310	15.7356	-18.7529	21.19	18.42	35.02
10	15	23	39	50	22	320	18.7529	-15.7356	21.83	18.42	33.28
			40	50	22	330	21.2005	-12.2401	22.36	18.42	31.18
		24	41	50	22	340	23.0039	-8.3727	22.75	18.42	28.80
			42	50	22	350	24.1083	-4.2509	23.00	18.42	26.20

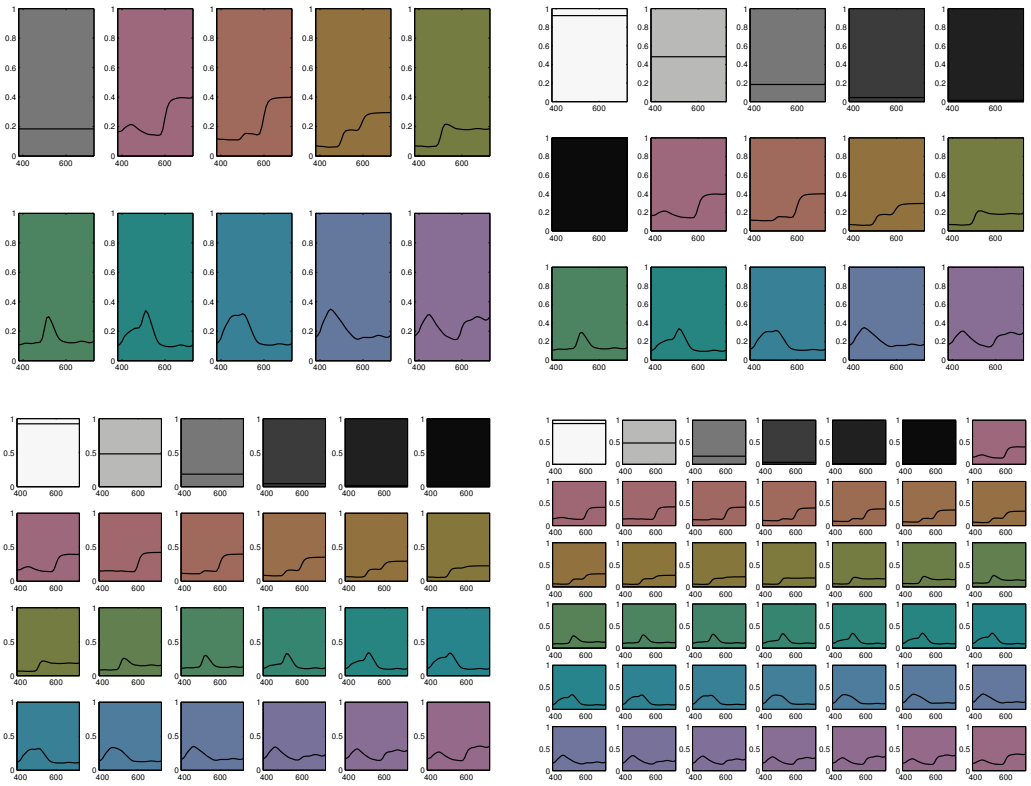

FIGURE 5.1. – Wpt Checker reflectances for 10 Patch (upper left), 15 Patch (upper right), 24 Patch (lower left), and 42 Patch (lower right) charts.

TABLE 5.2. – WNME differences between Wpt Matrices from targets vs method outlined in Chapter 2.

10 Patch/IIIA	24 Patch/IIIC	42Patch/IIIE	Camera
0.78	0.37	0.39	Canon 1DMarkIII
1.1	0.52	0.59	Canon 20D
0.65	0.27	0.34	Canon 300D
1.25	0.52	0.61	Canon 40D
1.02	0.27	0.36	Canon 500D
1.03	0.31	0.39	Canon 50D
1.15	0.42	0.51	Canon 5DMarkII
1.13	0.36	0.44	Canon 600D
1.05	0.3	0.4	Canon 60D
1.32	0.78	0.94	Hasselblad H2
0.71	0.34	0.33	Nikon D3X
0.73	0.46	0.44	Nikon D200
0.71	0.43	0.41	Nikon D3
0.74	0.39	0.39	Nikon D300s
0.65	0.38	0.4	Nikon D40
0.89	0.42	0.5	Nikon D50
0.76	0.52	0.48	Nikon D5100
0.75	0.4	0.38	Nikon D700
0.75	0.54	0.5	Nikon D80
0.72	0.39	0.38	Nikon D90
1.18	0.57	0.76	Nokia N900
1.06	0.47	0.57	Olympus E-PL2
0.9	0.43	0.46	Pentax K-5
1.33	0.59	0.7	Pentax Q
3.52	2.65	2.75	Point Grey Grasshopper 50S5C
1.75	1.06	1.21	Point Grey Grasshopper2 14S5C
0.45	0.83	0.79	Phase One
0.63	0.43	0.41	SONY NEX-5N

Initial calculations showed negligible differences between patch counts so different illuminants (Ill A, Ill C, and Ill E) were used for each patch count. Because the patches in FIGURE 5.1 have reflectances with different characteristic reflectances (see 4.1.2) there are differences in Wpt prediction that vary based upon the illuminant. However, the differences on average are small (near to or less than 1) except for cameras that have low correlation with the standard observer.

5.4 Wpt normalization from illuminant's sensor excitation values

The second proposed method of directly estimating a Wpt normalization matrix from sensor excitation values for a target illuminant utilizes the angular directions of the target illuminant's white point relative to the axes in sensor value coordinate space. These angles are used in nine separate functions to define each entry in a Material Adjustment Transform (MAT) that directly converts sensor excitations for the target illuminant to those of a reference illuminant. This MAT is then concatenated with the Wpt normalization matrix associated with the reference illuminant to form an estimated Wpt normalization matrix for the source illuminant.

Note: This is different from the "Color by correlation" strategy advocated by Finlayson which tries to determine unknown illuminant sensor values from known sensor excitation values from within an image rather than try to estimate unknown Wpt normalization matrix entries from known illuminant sensor excitations [Finllayson et al., 2001]. There is one conceptual similarity in the fact that a database of illuminants is used as part of the process, however how the database is used, and what is being modeled from the database is completely different. Additionally, it is possible to combine the results of any color constancy research (including that of Finlayson) that determines the sensor excitations of the illuminant with the proposed Wpt normalization estimation to define a MAT that better predicts material colors than that of a vonKries type SAT based upon the same sensor excitations of the illuminant.

5.4.1 Outline of Approach

The basic steps to estimate a Wpt normalization matrix from target illuminant sensor values are defined in two parts. The first part is performed just once and determines initialization values that are used by the second part. The second part estimates a Wpt normalization matrix for arbitrary source illuminant sensor values. The first part is defined as follows:

(a) Establish an illuminant set with known spectral power distributions (SPDs) that cover a "reasonably" broad range of illuminants.

(b) Use the set of illuminant SPDs established in (a) and the capture system's spectral sensitivities to derive sensor values for each illuminant.

(c) Determine illuminant sensor angles for each illuminant in the set by converting illuminant sensor values to an angular representation relative to one sensor axis. The G axis for RGB sensors is used as the reference axis for determining illuminant angles as follows:

$$\begin{aligned} \theta_{1,i} &= atan\left(c_{i,2}, c_{i,1}\right) \\ \theta_{2,i} &= atan\left(c_{i,2}, c_{i,3}\right) \end{aligned} \tag{5.2}$$

where:

$\begin{bmatrix} c_{i,1} \\ c_{i,2} \\ c_{i,3} \end{bmatrix} = \mathbf{c}_i$ represents sensor values of vector $\mathbf{c}_i$ for the i^{th} illuminant, and

$\theta_{1,i}$ and $\theta_{2,i}$ represent illuminant sensor angles for the i^{th} illuminant.

(d) Determine Wpt normalization matrices for the same set of illuminants used in step (b) with the capture system's spectral sensitivities by applying the Wpt normalization method established in Chapter 2.

$$\mathbf{A}_i = T\left(\mathbf{C}, \mathbf{l}_i\right) \tag{5.3}$$

where:
$\mathbf{A}_i$ represents the Wpt normalization matrix for the i^{th} illuminant,
$T\left(\right)$ represents the function to determine a Wpt normaliztion matrix described in Chapter 2,
$\mathbf{C}$ represents the capture system's spectral sensitivities used to determine sensor values, and
$\mathbf{l}_i$ represents a vector containing the SPD of the i^{th} illuminant.

Also do this for the reference illuminant (if not included in this set).

$$\mathbf{A}_{\text{ref}} = T\left(\mathbf{C}, \mathbf{l}_{\text{ref}}\right) \tag{5.4}$$

where: $T\left(\right)$, and $\mathbf{C}$ are the same as in Eq. 5.3,
$\mathbf{A}_{\text{ref}}$ represents the Wpt normalization matrix for the reference illuminant, and
$\mathbf{l}_{\text{ref}}$ represents a vector containing the SPD of the reference illuminant.

(e) Concatenate each illuminant's Wpt normalization matrix by the inverse of the reference illuminant's Wpt normalization matrix to determine a MAT that transforms sensor excitations for each illuminant sensor excitations for the reference illuminant.

$$\mathbf{M}_i = \left(\mathbf{A}_{\text{ref}}\right)^{-1} \mathbf{A}_i \tag{5.5}$$

(f) Establish a functional relationship between illuminant sensor angles found in Eq. 5.2 and entries of MAT matrices found in Eq. 5.5.

$$m_{j,i} = \sum_{k=1}^{n} a_{k,j} f_{k,j} \left(\theta_{1,i}, \theta_{2,i}\right) \tag{5.6}$$

where:

$\mathbf{M}_i = \begin{bmatrix} m_{1,i} & m_{2,i} & m_{3,i} \\ m_{4,i} & m_{5,i} & m_{6,i} \\ m_{7,i} & m_{8,i} & m_{9,i} \end{bmatrix}$,

$m_{j,i}$ represents the j^{th} coefficient of the i^{th} illuminant's MAT found using Eq. 5.5,
$a_{k,j}$ are coefficient constants that are solved for using regression,
$f_{k,j}$ is a function of two values associated with the k^{th} term of an estimation function for the j^{th} matrix coefficient, and
$\theta_{1,i}$, and $\theta_{2,i}$ represent illuminat sensor angles for the i^{th} illuminant found using Eq. 5.2.

(g) Use regression to solve for functional constants $a_{k,j}$ in Eq. 5.6.

The second part uses the Wpt normalization matrix $\mathbf{A}_{\text{ref}}$ and the functional coefficients $a_{k,j}$ determined during the first initialization stage along with sensor excitation values for a source illuminant $\mathbf{c}_{src}$ to estimate a Wpt normalization matrix as follows:

(h) Determine illuminant sensor angles for the source (*src*) illuminant.

$$\begin{aligned} \theta_{1,i} &= atan\left(c_{\text{src},2}, c_{\text{src},1}\right) \\ \theta_{2,i} &= atan\left(c_{\text{src},2}, c_{\text{src},3}\right) \end{aligned} \tag{5.7}$$

where:

$\begin{bmatrix} c_{\text{src},1} \\ c_{\text{src},2} \\ c_{\text{src},3} \end{bmatrix} = \mathbf{c}_{\text{src}}$ represents sensor values of vector $\mathbf{c}_{\text{src}}$ for the source illuminant, and

$\theta_{1,\text{src}}$ and $\theta_{2,\text{src}}$ represent illuminant sensor angles for the source illuminant.

(i) Apply source illuminant sensor angles $\theta_{1,\text{src}}$ and $\theta_{2,\text{src}}$ along with functional coefficients found in (g) in Eq. 5.6 to estimate a MAT that predicts sensor excitation values under the reference illuminant from sensor excitation values under the source illuminant.

$$\mathbf{M}_{\text{est}} = \begin{bmatrix} m_1 & m_2 & m_3 \\ m_4 & m_5 & m_6 \\ m_7 & m_8 & m_9 \end{bmatrix} \tag{5.8}$$

where:

$$m_k = \sum_{k=1}^{n} a_k f_k \left(\theta_{\text{src},1}, \theta_{\text{src},2}\right) \tag{5.9}$$

(j) Concatenate the reference illuminant's Wpt normalization matrix $\mathbf{A}_{\text{ref}}$ found in Eq. 5.4 with the matrix estimated in (i) to establish a Wpt estimation matrix for the source (*src*) illuminant.

$$\mathbf{A}''_{\text{est}} = \mathbf{A}_{\text{ref}}\mathbf{M}_{\text{est}} \tag{5.10}$$

(k) Adjust $\mathbf{A}''_{est}$to correctly predict white for the source illuminant. This is done by first scaling W so that sensor excitations for the source illuminant result in 100.

$$\mathbf{A}'_{\text{est}} = \begin{bmatrix} \left(\frac{100}{W''_{\text{est}}}\right) & 0 & 0 \\ 0 & 1 & 0 \\ 0 & 0 & 1 \end{bmatrix} \mathbf{A}''_{\text{est}} \tag{5.11}$$

where:

$\begin{bmatrix} W''_{\text{est}} \\ p''_{\text{est}} \\ t''_{\text{est}} \end{bmatrix} = \mathbf{A}''_{\text{est}}\mathbf{c}_{\text{src}}$ estimates Wpt coordinates for the source illuminant.

Then the p and t values are shifted to zero for the source illuminant resulting in an estimated Wpt normalization matrix for the source illuminant.

$$\mathbf{A}_{\text{est}} = \begin{bmatrix} 1 & \left(\frac{-p'_{\text{est}}}{100}\right) & \left(\frac{t'_{\text{est}}}{100}\right) \\ 0 & 1 & 0 \\ 0 & 0 & 1 \end{bmatrix} \mathbf{A}'_{\text{est}} \tag{5.12}$$

where:

$\begin{bmatrix} W'_{\text{est}} \\ p'_{\text{est}} \\ t'_{\text{est}} \end{bmatrix} = \mathbf{A}'_{\text{est}}\mathbf{c}_{\text{src}}$ estimates Wpt coordinates for the source illuminant.

5.4.2 Implementation and Results

The proposed set of training illuminants contains blackbody, daylight, CIE fluorescent illuminants as well as additional filtered illuminants. SPDs for the blackbody, daylight, and CIE fluorescent illuminants are shown in FIGURE 5.2.

The filtered illuminants are made up of key blackbody and daylight illuminants that have hue based filters applied resulting in pseudo-illuminants that have sensor angles that surround the sensor angle of each key filter. The purpose of using additional filtered illuminants was to broaden the sampling of the angular sensor space to allow for the prediction of Wpt normalization matrices for arbitrary illuminants that may lie outside the path of illuminants strictly defined by correlated color temperature (CCT). The hue based filters correspond to synthetic smooth

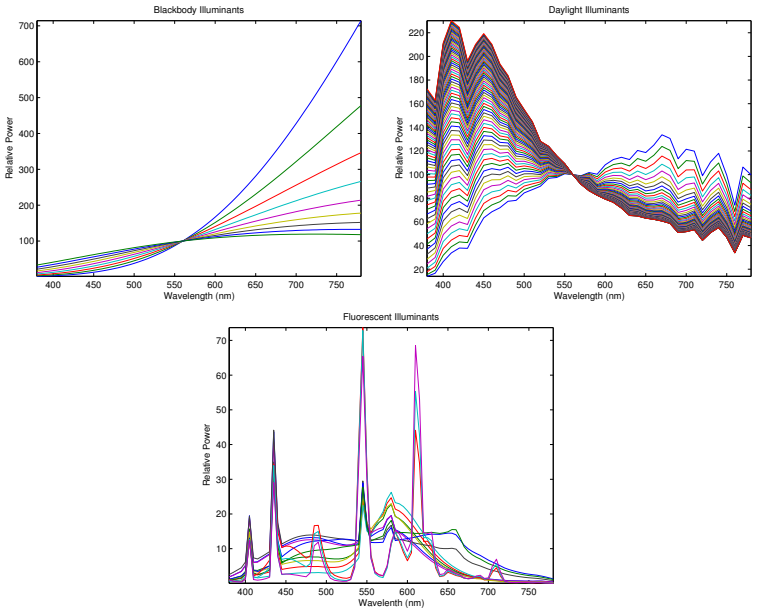

FIGURE 5.2. – Spectral Power Distributions of Illuminants used to determine Wpt shift manifolds

curves that were generated to be used as characteristic reflectances (Eq. 4.5) corresponding to the hues used to train Wpt normalization matrices. Two sets of hue filters were used: one set reduces light overall by 25% and the other set reduces light overall by 50%. The resulting filtered illuminants were determined by taking the scalar product of the filters and the SPD of the key illuminants.

A visualization of the filter sets, SPDs of the key illuminants, and the 25% filters applied to the D50 illuminant is shown in FIGURE 5.3.

The sensor value angles determined using Eq. 5.2 for the entire set of illuminants is shown FIGURE 5.4. The illuminants in the upper left of the figure correspond to the lowest CCT. As can be seen in this figure, variation due to the color temperature of the black body radiators and daylight illuminants occurs predominantly in the θ_2 axis.

Having an established illuminant set then allowed for various definitions of the functions in Eq. 5.9 to be experimented with for estimating Wpt Normalization matrices. It was found that having three degrees of freedom for each dimension were needed to fit the behavior of some of the Wpt matrix entries, and using exponentials allowed for better fit of illuminant behavior. Thus, one that was found to work reasonably well with relatively few terms (thus reducing data over-fitting) is as follows:

$$m_k = a_0\theta_1 + a_1\theta_2 + a_3e^{\theta_1} + a_4e^{\theta_2} + a_5log\left(\theta_1 + 0.01\right) + a_6log\left(\theta_2 + 0.01\right) + a_7 \tag{5.13}$$

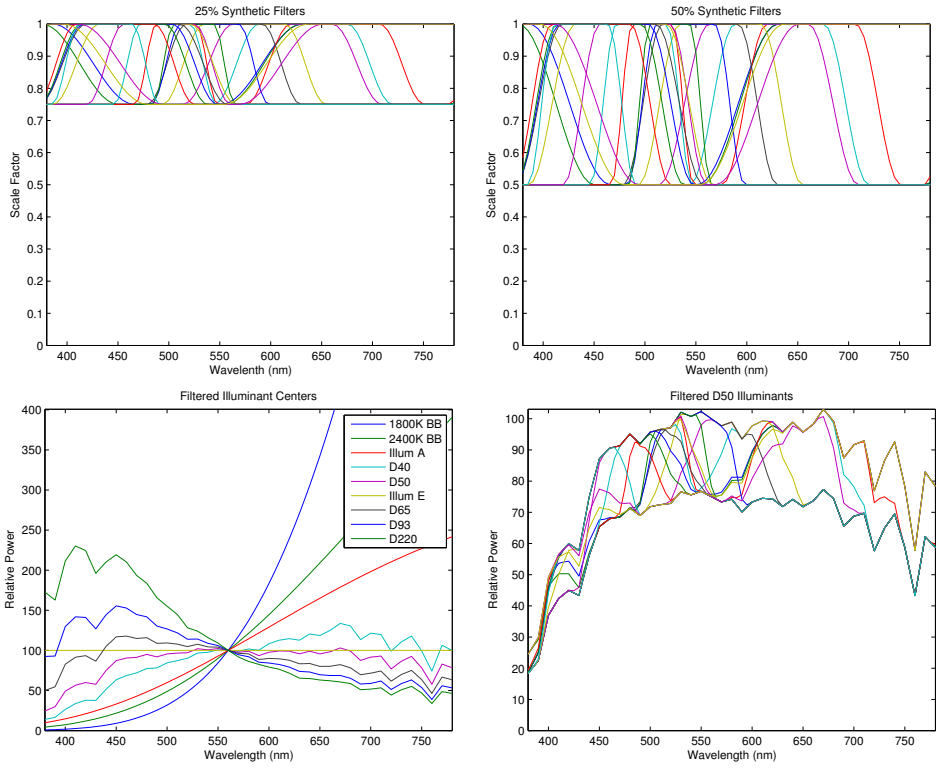

FIGURE 5.3. – Filters applied to Spectral Power Distributions of Key Illuminants used to determine Wpt shift manifolds

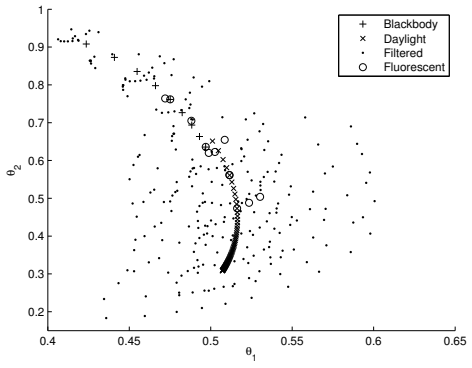

FIGURE 5.4. – Illuminant Sensor Angles for Wpt Normalization Estimation

where:
m_k represents the k^{th} entry in the estimated Wpt normalization matrix in Eq. 5.9, and
a_i represents the i^{th} coefficient of the function.

The steps in the previous section were then applied to determine coefficients for Eq. 5.13 for the standard observer. The resulting coefficients can be found in TABLE 5.3.

TABLE 5.3. – Regressed coefficients used in Eq. 5.13 to estimate Wpt Normalization matrices for the Std 2°observer

	a_1	a_2	a_3	a_4	a_5	a_6	a_7
m_1	-66.6554	1.9864	31.4265	-0.1399	10.2768	-1.3359	-13.3126
m_2	433.1594	-0.2539	-166.1655	1.7018	-75.3965	-1.601	7.4925
m_3	-218.8339	9.918	94.6744	-3.4107	36.6337	-3.329	-23.2365
m_4	119.3692	-1.5255	-44.7769	0.4135	-25.3575	0.6938	-1.3278
m_5	-573.6424	6.3285	228.5067	-2.8971	101.8594	-1.5272	-25.5693
m_6	434.6152	-14.0651	-164.911	6.4344	-85.6353	2.4952	-3.5686
m_7	558.814	-12.2939	-218.4081	5.3896	-101.3409	1.8065	10.9144
m_8	565.1291	-46.2234	-216.2978	22.1213	-105.4623	5.9515	-6.2344
m_9	-5687.4426	183.2996	2201.0449	-84.5904	1044.6302	-23.4846	-51.1272

A visualization of the estimated vs actual results for the training set of illuminants can be found in FIGURE 5.5. As can be seen in the figure the estimation is only approximate for some illuminants.

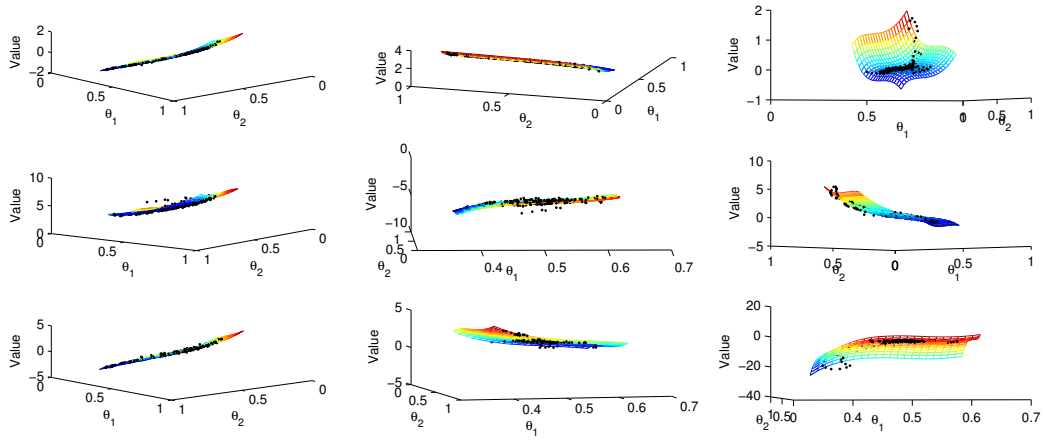

FIGURE 5.5. – Each of the 9 figures shows actual (points) versus estimated (surface) values for a Wpt Normalization Matrix based on illuminant sensor angles. Points not on surface represent estimation errors.

Estimated Wpt Normalization matrices were then determined for both the 2° and 10° standard observers under Illuminant A, Illuminant C, Illuminant E, D50, D65, and F12. These estimated

matrices were then compared to actual Wpt Matrices using a technique similar to those found in Chapter 4. Wpt manifolds for the set of Munsell Renotation colors were established using estimated and actual Wpt Normalization matrices, and the mean of the WLab color differences between corresponding points in the manifolds was determined for each observing condition. The results are found in TABLE 5.4

TABLE 5.4. – Mean ΔE_w between using estimated and actual Wpt Normalization Matrices with global illuminant regression

	Std 2	Std 10
A	1.06	1.04
C	1.41	1.19
E	2.83	2.69
D50	2.24	2.24
D65	1.20	1.04
F	1.93	2.20

It was hypothesized that limiting the illuminants used in the regression to just those closest in illuminant sensor angle might result in a regression with much better fit to the local characteristics of the actual matrix values. Wpt matrices were then estimated using illuminants in the regression with a θ_2 within ± 0.1 of the θ_2 of the target illuminant. The same comparisons were made between estimated and actual matrices, and the results are found in TABLE 5.5. In comparing these results to those in TABLE 5.4 one finds that using local illuminants in the regression provides much better results (with a mean ΔE_w much less than one – or the point where the difference is considered to be perceivably different). However, the improvement for the F11 illuminant is not as great. It is believed that this is because the sharp features in the F11 spectral power distribution are not as well characterized by the regression which includes many illuminants that have much smoother features. A view of the difference between actual and estimated WLab coordinates is found in FIGURE 5.6 where differences mainly occur in blues and reds, and are not generally extreme.

TABLE 5.5. – Mean ΔE_w between using estimated and actual Wpt Normalization Matrices with localized illuminant regression

	Std 2	Std 10
A	0.07	0.08
C	0.20	0.18
E	0.19	0.17
D50	0.11	0.25
D65	0.05	0.03
F	1.47	1.51

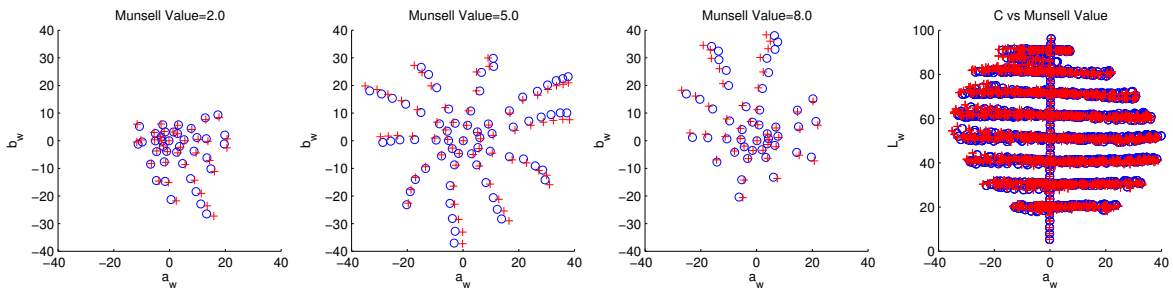

FIGURE 5.6. – Comparison of WLab coordinates using actual (blue 'o's) and estimated (red '+'s) Wpt Normalization matrices for Munsell Reflectances under F11

5.5 Conclusions

Two methods for estimating a Wpt Normalization matrix have been presented when spectral data of the illuminant are unavailable. The first method utilizes a special calibration target that is imaged to provide sensor excitation values that provides the data to perform Wpt normalization. This approach also has no requirement to have a spectral characterization of the observer's sensor sensitivity functions. It is believed that this would be most useful for performing camera calibration from a capture of a scene containing the special target. The resulting estimated Wpt normalization matrix provides a calibration for anything imaged under similar capture conditions resulting in an estimation of material color equivalency that minimizes differences due to the unknown illuminant SPD and camera sensitivities. Combining the estimated Wpt normalization matrix into a Wpt based MAT provides a means for rendering the captured scene to any desired observing condition.

The second method of estimating a Wpt Normalization matrix requires a spectral understanding of the observer, but has no requirement for a spectral understanding of the illuminant. Instead, it utilizes a suite of illuminants with known spectral sensitivities to establish a regression model that allows for the direct estimation of Wpt normalization matrices based upon the sensor excitations of an unknown illuminants. The regression model was found to be most effective for illuminants that have similar sensor illuminant angles to those that are modeled. This second method is more appropriate to use when the sensor sensitivity functions of the camera/observer are known. The utilization of this method is most appropriate in conjunction with “color constancy" algorithms that determine the illuminant sensor excitation values from pixels in a scene. From estimated illuminant excitation values, an estimated Wpt normalization matrix (from the second method) can be used to form a MAT that provides a material color equivalent rendering of the scene for any desired observing condition – which might prove useful for computer vision models. However, the practical application of such possibilities is left as separate research effort.

6 Manipulating Color Matching Functions

The primary focus of this chapter is the conversion of Cone Fundamentals (CFs) to Color Matching Functions (CMFs). Cone Fundamentals define the resulting physical spectral sensitivities of the visual sensors as light is imaged through the associated visual system. Cone Fundamentals therefore take into account the optical properties of the entire visual system. Color Matching Functions represent an indirect method of determining the color matching characteristics of the visual system's cone fundamentals without directly determining their sensitivities. Tristimulus values that result from applying either cone fundamentals or color matching functions provide a measure of color where having identical tristimulus values is an indication of a color match regardless of whether cone fundamentals or color matching functions are used. Thus, cone fundamentals are a special case of color matching functions, and color matching functions are not the same as cone fundamentals. Since color difference metrics and color appearance models have largely been defined in terms of tristimulus values based upon the Standard 2° and 10° color matching functions, it is hypothesized that the primary reason for converting cone fundamentals to XYZ-like color matching function is for the purpose of being able to relate to and compare color experiences of observers defined by cone fundamentals that cannot be expressed as an exact linear transformation of the standard observers.

In other words, the conversion of cone fundamentals to other forms of color matching functions represents an “optimized" conversion to a common numerical representation of color that allows for the color experiences of different observers to be defined and compared. Two existing approaches along with one additional proposed approach based upon Wpt normalization are identified that utilize different criteria and optimization for defining the conversion of cone fundamentals to color matching functions. In the process, the mathematical underpinnings defining the relationships between cone fundamentals and color matching functions are presented along with observations. It is asserted that the differences in the identified approaches have associated differences in meaning when comparing non-matching tristimulus values from the resulting color matching functions. This is especially important when assessing the meaning of differences in tristimulus values from different observers.

6.1 Relationships between cone fundamentals and color matching functions

As was stated in Chapter 1, Colorimetry (and to a large part – color science) is based upon color matching and color matching experiments that led to the CIE 1931 Standard Observer for a two degree viewing field and the CIE 1964 Standard Observer for a ten degree viewing field [CIE15, 2004; ISO, 2007]. Various methods have been established in recent years to define custom cone fundamentals based upon various physiological aspects of color vision [CIE170, 2006; Sarkar et al., 2011; Fairchild and Heckaman, 2013; Asano et al., 2014]. In order to apply such cone fundamentals in areas where either of the standard observers are used there needs to be transformation from cone fundamentals to XYZ-like color matching functions.

Normal human color vision is trichromatic – having only three types of photoreceptors (cones) for determining color perception. Additionally, the human visual system (HVS) has experimentally been determined (to a first approximation) to be linear and additive thus satisfying Grassmann's laws of additive color mixture [Wyszecki and Stiles, 2000]. The resulting sensor excitations of a light stimulus can be described as follows:

$$\mathbf{f} = \mathbf{F}\mathbf{s} \tag{6.1}$$

where:
$\mathbf{f}$ is a column vector representing the resulting sensor excitations,
$\mathbf{F}$ is a matrix representing the cone fundamentals of the observer, and
$\mathbf{s}$ is a column vector representing the light stimulus SPD.

An apparatus used to perform color matching can be described as having a view with a bipartite field that allows for a colored light in one field to be compared and matched with a combination of primary lights in the second field. A color match is determined with such an apparatus by an observer adjusting the intensities of the primaries until a match to the test stimulus is found (with negative primary intensities represented as intensities of the primaries added to the test stimulus). Such a color matching system is mathematically described as the resulting sensor excitations of the test stimulus being identical to the resulting sensor excitations from a linear combination of three primary lights used for color matching [Wyszecki and Stiles, 2000; Krantz, 1975]. Thus:

$$\begin{aligned} \mathbf{f}_{\text{test}} &= \mathbf{f}_{\text{match}} \\ \mathbf{F}\mathbf{s} &= \mathbf{F}\mathbf{P}\mathbf{c} \end{aligned} \tag{6.2}$$

where: $\mathbf{f}$, $\mathbf{F}$, and $\mathbf{s}$ are the same as in Eq. 6.1,
$\mathbf{f}_{\text{test}}$ is the resulting sensor excitations of the test stimulus and $\mathbf{f}_{\text{test}} = \mathbf{F}\mathbf{s}$,
$\mathbf{f}_{\text{match}}$ is the resulting sensor excitations of the matching stimulus and $\mathbf{f}_{\text{match}} = \mathbf{F}\mathbf{P}\mathbf{c}$,
$\mathbf{P}$ is a matrix containing column vectors with the SPD for each of the primary matching lights, and

$\mathbf{c}$ is a column vector that indicates the relative intensities of the primaries needed to obtain a visual match by the observer with cone fundamentals $\mathbf{F}$.

As colorimetry was developed, the direct determination of cone fundamentals was not performed. Instead combinations of chromatic primaries were determined in terms of color matches for single wavelengths of light (monochromatic) [Wright, 1982]. Thus:

$$\mathbf{F}\left[\mathbf{s}_{\lambda_1}\ldots\mathbf{s}_{\lambda_n}\right]=\mathbf{FP}\left[\mathbf{c}_{\lambda_1}\ldots\mathbf{c}_{\lambda_n}\right] \tag{6.3}$$

where:
$\mathbf{F}$, $\mathbf{P}$ are the same as in Eq. 6.2,
$\mathbf{s}_{\lambda_i}$ is the i^{th} column vector containing the SPD of the i^{th} test light that only has a “unit" amount of the wavelength of light defined by λ,
$\mathbf{c}_{\lambda_i}$ is the i^{th} column vector that indicates the relative intensities of the primaries needed to obtain a visual match of the i^{th} single wavelength of light defined by $\mathbf{s}_{\lambda_i}$.

The relationship between cone fundamentals and color matching functions is defined using the fact that $I=[\mathbf{s}_{\lambda_1}\ldots\mathbf{s}_{\lambda_n}]$ and $C=[\mathbf{c}_{\lambda_1}\ldots\mathbf{c}_{\lambda_n}]$ in Eq. 6.3 as follows:

$$\begin{aligned}&\mathbf{F}\left[\mathbf{s}_{\lambda_1}\ldots\mathbf{s}_{\lambda_n}\right]=\mathbf{FP}\left[\mathbf{c}_{\lambda_1}\ldots\mathbf{c}_{\lambda_n}\right]\\&\mathbf{FI}=\mathbf{FPC}\\&\therefore\\&\mathbf{F}=\mathbf{FPC}\end{aligned} \tag{6.4}$$

where:
$\mathbf{F}$, $\mathbf{P}$ are the same as in Eq. 6.2,
$\mathbf{s}_{\lambda_i}$ is a column vector containing the SPD of a test light that only has a “unit" amount of the i^{th} wavelength of light λ_i for each of the n wavelengths of light,
$\mathbf{c}_{\lambda_i}$ is a column vector that indicates the relative intensities of the primaries needed to obtain a visual match of a light defined by $\mathbf{s}_{\lambda_i}$, $\mathbf{I}$ is an identity matrix, and
$\mathbf{C}$ is a matrix defining color matching functions corresponding to the primaries defined by $\mathbf{P}$ for an observer with cone fundamentals defined by $\mathbf{F}$.

A logical interpretation of the result of Eq. 6.4 is that the color matching functions with associated color matching primaries $(\mathbf{PC})$ convert the SPD of the test light into a metamer of the test light for the observer with cone fundamentals defined by $\mathbf{F}$. A mathematical interpretation of Eq. 6.4 is that the term $(\mathbf{PC})$ acts as an identity operation when combined with $\mathbf{F}$.

The following useful observations can be inferred from Eq. 6.1 and Eq. 6.4.

1. The actual cone fundamentals are not needed to define a color match. Matches can instead be defined strictly in terms of the intensities of the primaries used [Wright, 1982]. This can be shown as follows:

$$\begin{aligned} \mathbf{F}\mathbf{s}_1 &= \mathbf{F}\mathbf{s}_2 \\ \mathbf{F}\mathbf{P}\mathbf{C}\mathbf{s}_1 &= \mathbf{F}\mathbf{P}\mathbf{C}\mathbf{s}_2 \\ \mathbf{C}\mathbf{s}_1 &= \mathbf{C}\mathbf{s}_2 \end{aligned} \tag{6.5}$$

2. As was discussed by Brainard and Stockman, color matching functions can also be expressed as a linear transform of the cone fundamentals [Brainard and Stockman, 2010]. Therefore, color matching functions can be used in place of cone fundamentals for defining relationships in color matching systems. This can be shown by multiplying both sides of Eq. 6.4 by $(\mathbf{FP})^{-1}$ and then swapping sides resulting in:

$$\mathbf{C} = (\mathbf{FP})^{-1}\,\mathbf{F} \tag{6.6}$$

   where:
   $\mathbf{C}$, and $\mathbf{F}$ are the same as in Eq. 6.4.

   Then substituting $\mathbf{M}$ for $(\mathbf{FP})^{-1}$ results in:

$$\mathbf{C} = \mathbf{M}\mathbf{F} \tag{6.7}$$

   where:
   $\mathbf{C}$ and $\mathbf{F}$ are the same as in Eq. 6.4, and $\mathbf{M}$ is an invertible square matrix.

3. Any non-singular transformation of the cone fundamentals doesn't change the color matching characteristics of the system – often called the Luther-Ives condition [Luther, 1927; Ives, 1915]. This can be shown by multiplying both sides of Eq. 6.4 by an arbitrary but invertible transformation matrix M as follows:

$$\begin{aligned} \mathbf{M}\mathbf{F} &= \mathbf{M}\mathbf{F}\mathbf{P}\mathbf{C} \\ (\mathbf{M}\mathbf{F}) &= (\mathbf{M}\mathbf{F})\,\mathbf{P}\mathbf{C} \end{aligned} \tag{6.8}$$

   where:
   $\mathbf{F}$, $\mathbf{P}$, and $\mathbf{C}$ are the same as in Eq. 6.4, and
   $\mathbf{M}$ is a arbitrary non-singular square matrix.

4. The choice of primaries and color matching functions is not unique. Any simultaneous manipulation of the primaries and color matching functions that result in transforming test

stimuli to metamers of the test stimuli for the observer can be used. This can be shown by manipulating Eq. 6.4 as follows:

$$\begin{aligned}
\mathbf{F} &= \mathbf{FPC} \\
\mathbf{F} &= \mathbf{FPM}^{-1}\mathbf{MC} \\
\mathbf{F} &= \mathbf{F}\left(\mathbf{PM}^{-1}\right)(\mathbf{MC}) \\
\mathbf{F} &= \mathbf{FP_M C_M}
\end{aligned} \tag{6.9}$$

where:
$\mathbf{F}$, $\mathbf{P}$, and $\mathbf{C}$ are the same as in Eq. 6.4
$\mathbf{M}$ is a arbitrary non-singular square matrix,
$\mathbf{P_M}$ represents an alternate set of color primaries, and
$\mathbf{C_M}$ represents an alternate set of color matching functions.

5. The pseudo-inverse of the color matching functions can be used as a satisfactory replacement of the primaries. This can be shown by manipulating Eq. 6.4 as follows:

$$\begin{aligned}
&\mathbf{F} = \mathbf{FPC} \\
&\mathbf{F} = \mathbf{FI} \\
&\therefore \\
&\mathbf{PC} \equiv \mathbf{I} \\
&\mathbf{P} \equiv \mathbf{C}^T\left(\mathbf{CC}^T\right)^{-1} = pinv\left(\mathbf{C}\right)
\end{aligned} \tag{6.10}$$

6. Conversely, the pseudo-inverse of the primaries can be used as a satisfactory replacement of the color matching functions. This is because the color matching functions predict the primaries (i.e. applying the color matching functions to the primaries results in the identity matrix) . Thus:

$$\begin{aligned}
&\mathbf{I} = \mathbf{CP} \\
&\mathbf{C} = \mathbf{P}^T\left(\mathbf{PP}^T\right)^{-1} = pinv\left(\mathbf{P}\right)
\end{aligned} \tag{6.11}$$

7. Building on observation 6, if the color matching functions of multiple observers all predict the same set of primaries then Eq. 6.11 can be utilized to determine the common primaries. Thus:

$$\begin{aligned}
&\begin{bmatrix} \mathbf{I}_1 \\ \mathbf{I}_2 \\ \vdots \\ \mathbf{I}_n \end{bmatrix} = \begin{bmatrix} \mathbf{C}_1 \\ \mathbf{C}_2 \\ \vdots \\ \mathbf{C}_n \end{bmatrix} \mathbf{P} \\
&\therefore \\
&\mathbf{P} = pinv\left(\begin{bmatrix} \mathbf{C}_1 \\ \mathbf{C}_2 \\ \vdots \\ \mathbf{C}_n \end{bmatrix}\right)\begin{bmatrix} \mathbf{I}_1 \\ \mathbf{I}_2 \\ \vdots \\ \mathbf{I}_n \end{bmatrix}
\end{aligned} \tag{6.12}$$

where:
$\mathbf{I}_i$ represents the i^{th} identity matrix,
$\mathbf{C}_i$ represents the i^{th} color matching function,
$\mathbf{P}$ contains column vectors representing the common color matching primary of all the observers, and
$pinv\left(\mathbf{X}\right)$ represents the pseudo-inverse function applied to a non-square matrix $\mathbf{X}$.

6.2 Transforming Cone Fundamentals to Color Matching Functions

Both Eq. 6.6 and Eq. 6.7 define color matching functions in terms of cone fundamentals. Two existing methods of transforming cone fundamentals to color matching functions use one of these two functions. The differences are due to what that is optimized or preserved in the process.

6.2.1 Transformation using “Sameness of Primaries" (Primary Based)

The first general approach for transforming an initial observer's cone fundamentals to color matching functions can be found by first applying Eq. 6.6 which defines color matches for a set of cone fundamentals for the initial observer relative to an arbitrary set of primaries with the match represented by intensity values for the primaries. Then, the same primaries are applied to these results followed by the application of a reference observer's color matching functions to complete the transformation of cone fundamentals to color matching functions. Conceptually, the reference observer with well defined color matching functions is predicting a match of the primary set match determined using the cone fundamentals of the first observer [Asano et al., 2014]. In this case the set of primaries is the “same" for both matches. The concatenation of these transforms results in the definition of color matching functions for the first observer's cone fundamentals as follows:

$$\mathbf{C}_{\text{alt}} = \mathbf{C}_{\text{ref}}\mathbf{P}\left(\mathbf{F}_{\text{alt}}\mathbf{P}\right)^{-1}\mathbf{F}_{\text{alt}} \tag{6.13}$$

where:
$\mathbf{C}_{\text{alt}}$ represents color matching functions for an alternate observer,
$\mathbf{F}_{\text{alt}}$ represents cone fundamentals for an alternate observer,
$\mathbf{P}$ represents an arbitrary set of color matching primaries, and
$\mathbf{C}_{\text{ref}}$ represents color matching functions for a reference observer.

Alternatively, a more direct conversion of cone fundamentals to color matching functions can be defined by using the fact that the implied primaries of the reference observer can be found

directly from the reference observer's color matching functions using Eq. 6.10. Applying this to Eq. 6.6 results in the following:

$$\begin{aligned} &\mathbf{C}_{\text{alt}} = \left(\mathbf{F}_{\text{alt}}\mathbf{P}_{\text{ref}}\right)^{-1}\mathbf{F}_{\text{alt}} \\ &\therefore \\ &\mathbf{C}_{\text{alt}} = \left(\mathbf{F}_{\text{alt}} pinv\left(\mathbf{C}_{\text{ref}}\right)\right)^{-1}\mathbf{F}_{\text{alt}} \\ &\mathbf{C}_{\text{alt}} = \left(\mathbf{F}_{\text{alt}}\mathbf{C}_{\text{ref}}^{T}\left(\mathbf{C}_{\text{ref}}\mathbf{C}_{\text{ref}}^{T}\right)\right)^{-1}\mathbf{F}_{\text{alt}} \end{aligned} \tag{6.14}$$

where:
$\mathbf{C}_{\text{alt}}$ represents color matching functions for an alternate observer,
$\mathbf{F}_{\text{alt}}$ represents cone fundamentals for an alternate observer,
$\mathbf{P}_{\text{ref}}$ represents color matching primaries for a reference observer, and
$\mathbf{C}_{\text{ref}}$ represents color matching functions for a reference observer.

This alternate method of matching primaries in Eq. 6.14 has the advantage of not having two matches being performed while a single set of primaries is used to define both the reference and alternate color matching functions.

An important point to consider is the meaning of tristimulus values using color matching functions that predict the same primaries and defined by either Eq. 6.13 or Eq. 6.14. The relevant meaning or equivalency basis of the tristimulus values using Eq. 6.13 is defined by the perception of the color matching performed by the reference observer via $\mathbf{C}_{\text{ref}}$. Thus, differences in tristimulus values from different observers represent the differences that the reference observer perceives in the combinations of primaries resulting from matches made by the observers (see FIGURE 6.1). This means that the perception of the observers is not not taken into account – only the perception of the matching of primaries as observed by the reference observer defines the meaning of the tristimulus values and their differences.

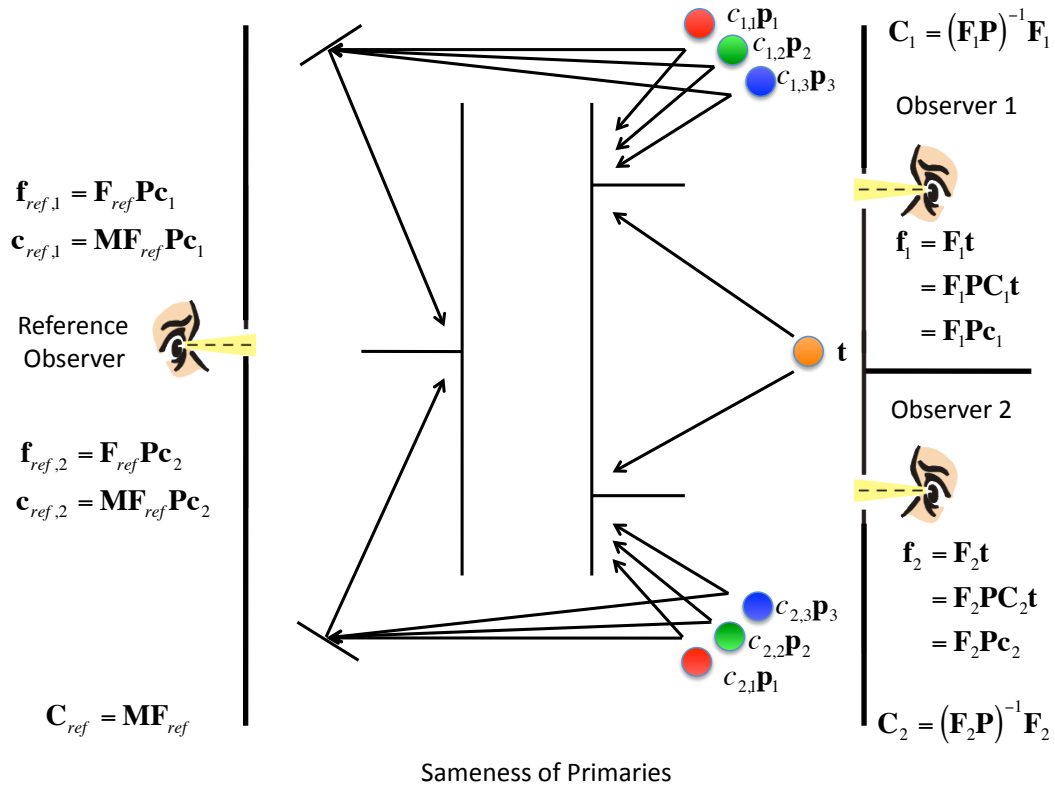

FIGURE 6.1. – Comparing matches made by two observers using “Sameness of Primaries". The primaries are the same everywhere.

6.2.2 Transformation using “Similarity of Tristimulus Values" (XYZ Based)

One approach that has been taken in the literature is to use Eq. 6.7 and then apply the pseudo-inverse of the cone fundamentals to both sides (direct regression) resulting in an estimation of matrix $\mathbf{M}_{\text{est}}$ that transforms the cone fundamentals into color matching functions [Alfvin and Fairchild, 1997; Brainard and Stockman, 2010]. Thus:

$$\begin{aligned} &\mathbf{M}_{\text{est}} = \mathbf{C}_{\text{ref}} pinv\left(\mathbf{F}_{\text{alt}}\right) \\ &\therefore \\ &\mathbf{C}_{\text{alt}} = \mathbf{C}_{\text{ref}} pinv\left(\mathbf{F}_{\text{alt}}\right) \mathbf{F}_{\text{alt}} \\ &\mathbf{C}_{\text{alt}} = \mathbf{C}_{\text{ref}} \mathbf{F}_{\text{alt}}^{T} \left(\mathbf{F}_{\text{alt}} \mathbf{F}_{\text{alt}}^{T}\right) \mathbf{F}_{\text{alt}} \end{aligned} \tag{6.15}$$

When this is done the resulting $\mathbf{C}_{\text{alt}}$ transforms input stimulus values into tristimulus values that are minimized to be as similar to the tristimulus values produced by $\mathbf{C}_{\text{ref}}$. Thus, the matrix $\mathbf{M}_{\text{est}}$ is providing a “Similarity of Tristimulus Values" by minimizing differences in tristimulus values produced by both sets of color matching functions. Matrix $\mathbf{M}_{\text{est}}$ can also be thought of as a transformation that is trying to minimize differences in spectral shape between the reference and alternate color matching functions.

An important consideration relative to Eq. 6.15 is that it does not preserve color matching primaries. This is because only tristimulus values or spectral shape of the color matching functions are being minimized. Conceptually this can be likened to picking different primaries to use for color matching for each observer that result in color matches of the same color having the same intensity values of their respective primaries even though the primaries differ in SPD (see FIGURE 6.2). The relevant meaning or equivalency basis of the tristimulus values using Eq. 6.15 is defined by the perception of the tristimulus values applied to the reference primaries by the reference observer. Thus, differences in tristimulus values from different observers represent the differences that the reference observer perceives in the differences of the tristimulus values as they are applied to the reference primaries by the reference observer. This means that the perception of the observers beyond the match is not taken into account as their perception is defined by the primaries that they are using for matching and not the primaries used by the reference observer. Only the perception of the tristimulus values as observed by the reference observer defines the meaning of the tristimulus values and their differences. However, when the spectral shapes of the color matching functions are similar then the perceived magnitude is such color differences can probably be considered to generally be the same between the observers and the reference observer.

As an additional note, applying the same $\mathbf{M}_{\text{est}}$ to multiple cone fundamental $\mathbf{F}_i$ (where i represents the i^{th} observer) does not ensure that the same color matching primaries are being used (which was the case in [Fairchild and Heckaman, 2013]). The resulting color matching functions will predict the same primaries only if each of the $\mathbf{F}_i$ cone fundamentals already predicted the same color matching primaries to begin with. This can be tested using Eq. 6.12.

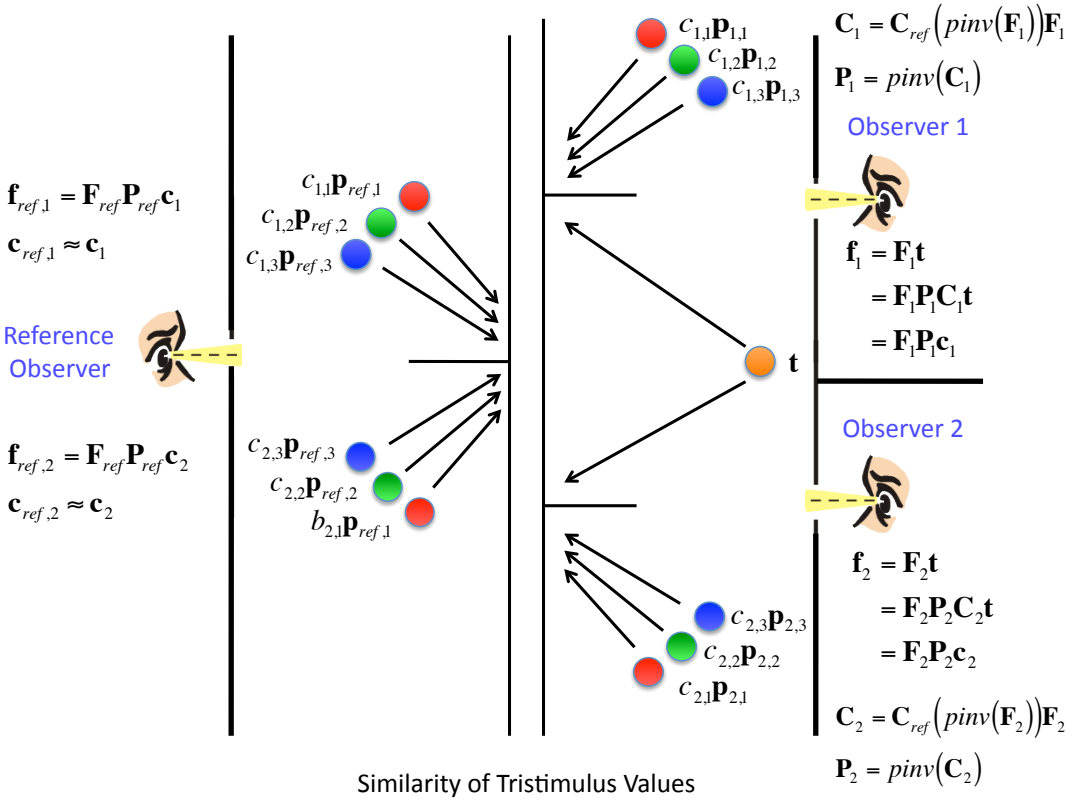

FIGURE 6.2. – Comparing matches made by two observers using "Similarity of Tristimulus Values". The tristimulus values of the observers are used by the reference observer to evaluate differences in observers matches. The primaries for each of the observers are adjusted so that they are similar to the reference observer's tristimulus values. Optimization use regression to approximate spectral match of color matching functions.

6.2.3 Transformation using “Sameness of material color" (Wpt Based)

It is proposed that using a Wpt based MAT (as defined in Chapter 2) for $\mathbf{M}$ in Eq. 6.7 provides a transformation from cone fundamentals to color matching functions that approximately preserves material color equivalency defined for a reference observing condition. Thus:

$$\mathbf{C}_{\text{alt}} = (\mathbf{A}_{\text{ref}})^{-1} \mathbf{A}_{\text{alt}} \mathbf{F}_{\text{alt}} \tag{6.16}$$

where:
$\mathbf{C}_{\text{alt}}$ is a matrix representing the estimated alternate color matching functions,
$\mathbf{F}_{\text{alt}}$ is a matrix representing the initial alternate cone fundamentals,
$\mathbf{A}_{\text{ref}}$ is a Wpt normalization matrix found by applying $\mathbf{A}_{\text{ref}} = T(\mathbf{C}_{\text{ref}}, \mathbf{l}_{\text{ref}})$ with $T()$ from Eq. 2.2 and the observer defined by color matching functions $\mathbf{C}_{\text{ref}}$ and the illuminant defined by $\mathbf{l}_{\text{ref}}$,
$\mathbf{A}_{\text{alt}} = T(\mathbf{F}_{\text{alt}}, \mathbf{l}_{\text{ref}})$ with $T()$ from Eq. 2.2 and the observer defined by cone fundamentals $\mathbf{F}_{\text{alt}}$ and the illuminant defined by $\mathbf{l}_{\text{ref}}$, and
$\mathbf{l}_{\text{ref}}$ establishes the reference illuminant for defining material color equivalency.

It is important to keep in mind that the choice of reference observing condition is arbitrary. It simply provides the material color basis for defining color equivalency when making comparisons of tristimulus values. Wpt normalization provides two criteria for making such comparisons. First, it establishes a set of tristimulus values that are identical for a PRD under the reference illuminant. Second, it establishes consistent scaling of tristimulus values so that perceptive differences in lightness, chroma, and hue are minimized relative to the reference observing conditions. A significant difference in using sameness of material color for conversion of color fundamentals to color matching functions is that the perceptive aspects of color for each of the observers is accounted for by the Wpt normalization matrices used to form the MAT (see FIGURE 6.3).

As such, the illuminant or light source used when determining tristimulus values with alternate color matching functions from Eq. 6.16 does not need to be the same as the reference illuminant used to determine the alternate color matching functions. This allows one to make relative comparisons of perceptive differences in illuminants between observers with different cone fundamentals. The examples in Section 6.3 can be used to illustrate this.

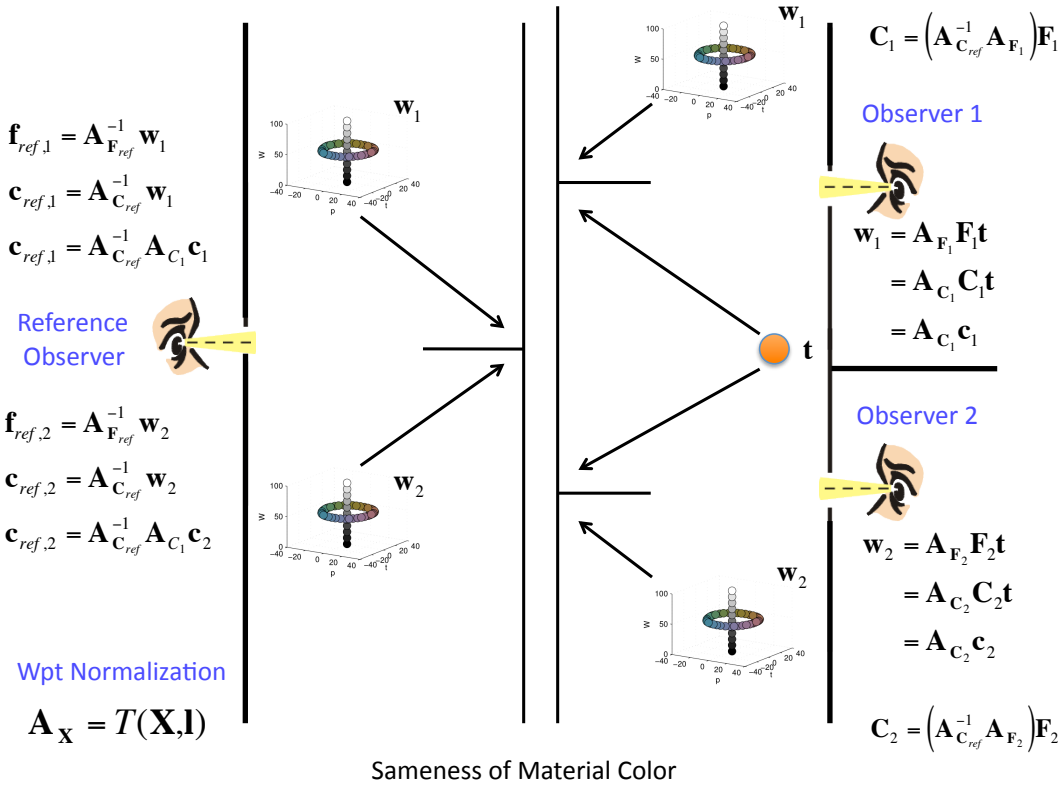

FIGURE 6.3. – Comparing matches made by two observers using "Sameness of Material Color". Wpt values are determined by applying a Wpt normalization matrix to the observers' cone fundamentals or tristimulus values. The inverse of the reference observer's Wpt normalization matrix is applied to Wpt values from the compared observers to determine sensor excitations or tristimulus values that are used to evaluate the differences in observers' matches.

6.2.4 Transform correction using “Sameness of White Point"

Unlike Wpt normalization, the methods of defining color matching functions in 6.2.1 and 6.2.2 both utilize no aspect of perception by the alternate observers. There is no reference that provides meaning for each observers' tristimulus values for the viewing illuminant. Nor is there any reference in place to allow for relative color appearance differences to be assessed.

One method commonly used in the literature is to perform a normalization or white balancing on the tristimulus values so that they match for a reference illuminant [Brainard and Stockman, 2010]. This can be done in conjunction with Eq. 6.15 or Eq. 6.14 by concatenating the results of either of these equations with a vonKries transform matrix based upon the ristimulus values of the illuminant using the color matching functions of both the reference and alternate observer as follows:

$$\mathbf{C}'_{\text{alt}} = \mathbf{V}\mathbf{C}_{\text{alt}} \tag{6.17}$$

where:

$$\mathbf{V} = \begin{bmatrix} \frac{x_1}{x_2} & 0 & 0 \\ 0 & \frac{y_1}{y_2} & 0 \\ 0 & 0 & \frac{z_1}{z_2} \end{bmatrix},$$

$$\begin{bmatrix} x_1 \\ y_1 \\ z_1 \end{bmatrix} = \mathbf{C}_{\text{ref}}\mathbf{l}_{\text{ref}} \tag{6.18}$$

$$\begin{bmatrix} x_2 \\ y_2 \\ z_2 \end{bmatrix} = \mathbf{C}_{\text{alt}}\mathbf{l}_{\text{ref}}, \qquad \text{and}$$

$\mathbf{l}_{\text{ref}}$ is a vector containing the SPD of the reference white.

To some this might be considered to be applying a chromatic adaptation. However, corresponding color information is not utilized in the definition of the transform. Therefore, it is more appropriate to refer to such normalization of CMFs as a white balancing SAT as discussed in Chapter 2.

Application of Eq. 6.17 after Eq. 6.15 or Eq. 6.14 to predict the same tristimulus values for a reference illuminant results in a scaling of the color matching primaries implied by the observer's color matching functions. This means that the maximum intensity of the color matching primaries has to change so that the relative intensity of the primaries can be the same for the observers. Thus, the chromaticity of the implied primaries remains the same since they are based upon relative primary values.

6.2.5 Scaling Primary Intensity

Tristimulus values obtained using the converted color matching functions in this section may only be approximately the same to that of the reference observer because the color discrimination of the cone fundamentals differ and the scaling of the sensitivities could vary widely. Performing the following additional step ensures that the scale of the prediction of the tristimulus Y primary is the same by scaling the estimated color matching functions uniformly. This is commonly done when calculating colorimetric tristimulus values using an integral [Wyszecki and Stiles, 2000]. The scaling in Eq. 6.19 results in no change in chromaticity and corresponds to a slight uniform change in intensity of all the primaries. This is done as follows:

$$\mathbf{C}'_{\text{alt}} = k\mathbf{C}_{\text{alt}} \tag{6.19}$$

where:

$$\begin{gathered} k = \left(\frac{Y_1}{Y_2}\right), \\ \begin{bmatrix} X_1 \\ Y_1 \\ Z_1 \end{bmatrix} = \mathbf{C}_{\text{ref}}\mathbf{p}_Y, \text{ and} \\ \begin{bmatrix} X_2 \\ Y_2 \\ Z_2 \end{bmatrix} = \mathbf{C}_{\text{alt}}\mathbf{p}_Y \end{gathered}, \tag{6.20}$$

and $\mathbf{p}_Y$ is a vector containing the SPD of the tristimulus Y primary used for scaling.

6.3 Observer Manipulation and Analysis

Five methods of transforming cone fundamentals to color matching functions were applied to two sets of cone fundamentals targeting the 1931 standard 2-degree observer for visualization purposes. The first transform method (XYZ Based) utilized Eq. 6.15 with Eq. 6.19 optimizing “similarity of tristimulus values." The second transform method (Primary Based) utilized Eq. 6.14 with Eq. 6.19 preserving “sameness of primaries." The third transform method (WB XYZ Based) utilized Eq. 6.15 with Eq. 6.17 preserving both the ‘similarity of tristimulus values" along with the “sameness of white point." The forth transform method (WB Primary Based) utilized Eq. 6.14 with Eq. 6.17 preserving both the ‘sameness of primaries" along with the “sameness of white point." The last transform method (Wpt Based) utilized Wpt normalization with Eq. 6.19 preserving the “sameness of material color." Illuminant E was used as the reference illuminant for the third, forth, and last transform methods. The set of cone fundamentals used for conversion to CMFs consisted of 1000 observers statistically derived by Fairchild and Heckaman (hereafter referred to simply as the Fairchild-Heckaman set) [Fairchild and Heckaman, 2013].

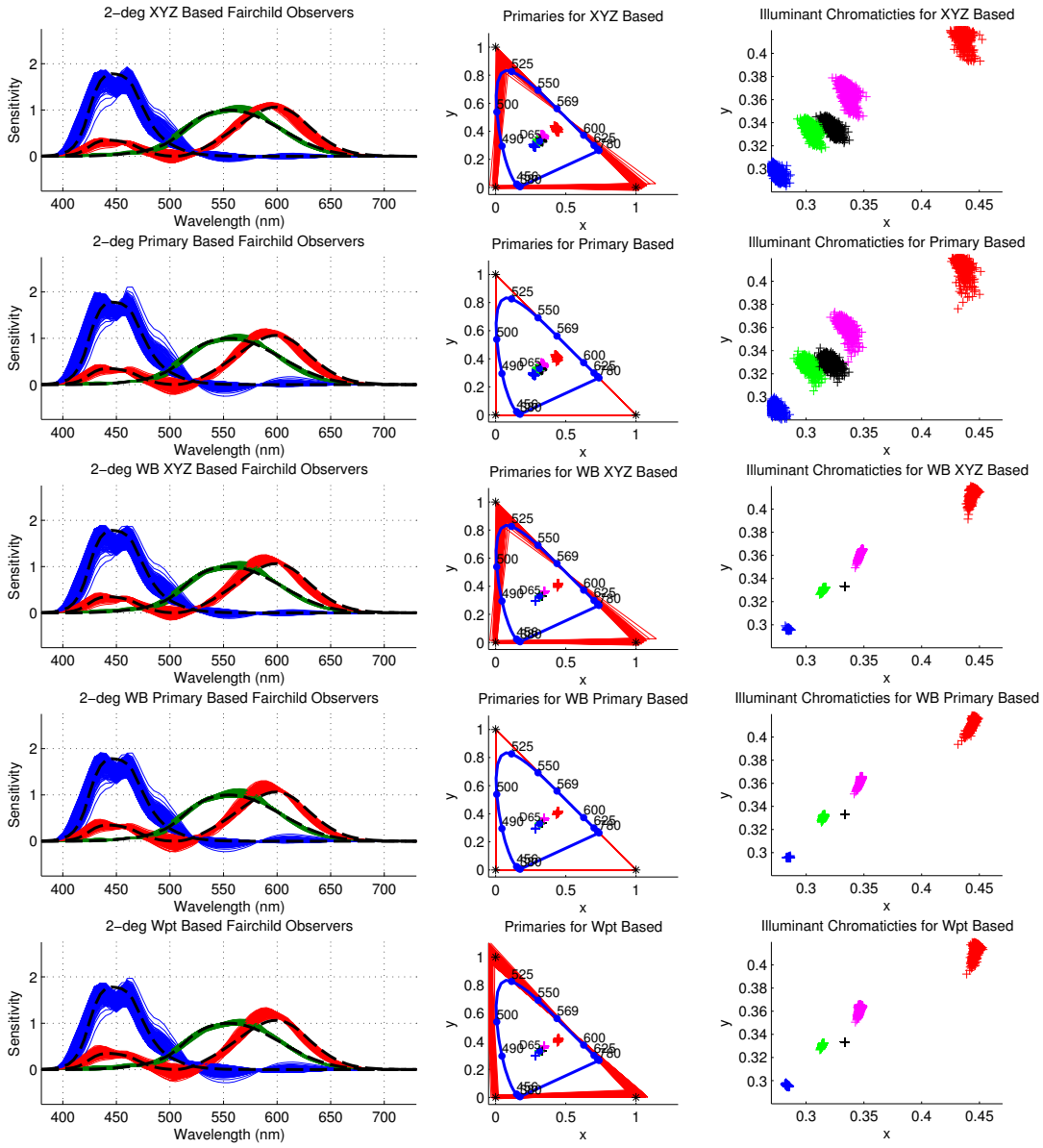

FIGURE 6.4. – 2° Fairchild-Heckaman CMFs (left column), Predicted Primaries (middle column) and Illuminant Chromaticities (right column) with minimizing tristimulus values (top row), predicting ref observers primaries (second row), minimizing tristimulus values with white balancing (third row), predicting ref observers primaries with white balancing (forth row), Wpt based CMFs (bottom row). Illuminant chromaticities visualized for D95 (blue '+'), D65 (green '+'), Illuminant E (black '+'), D50 (magenta '+'), Illuminant A (red '+').

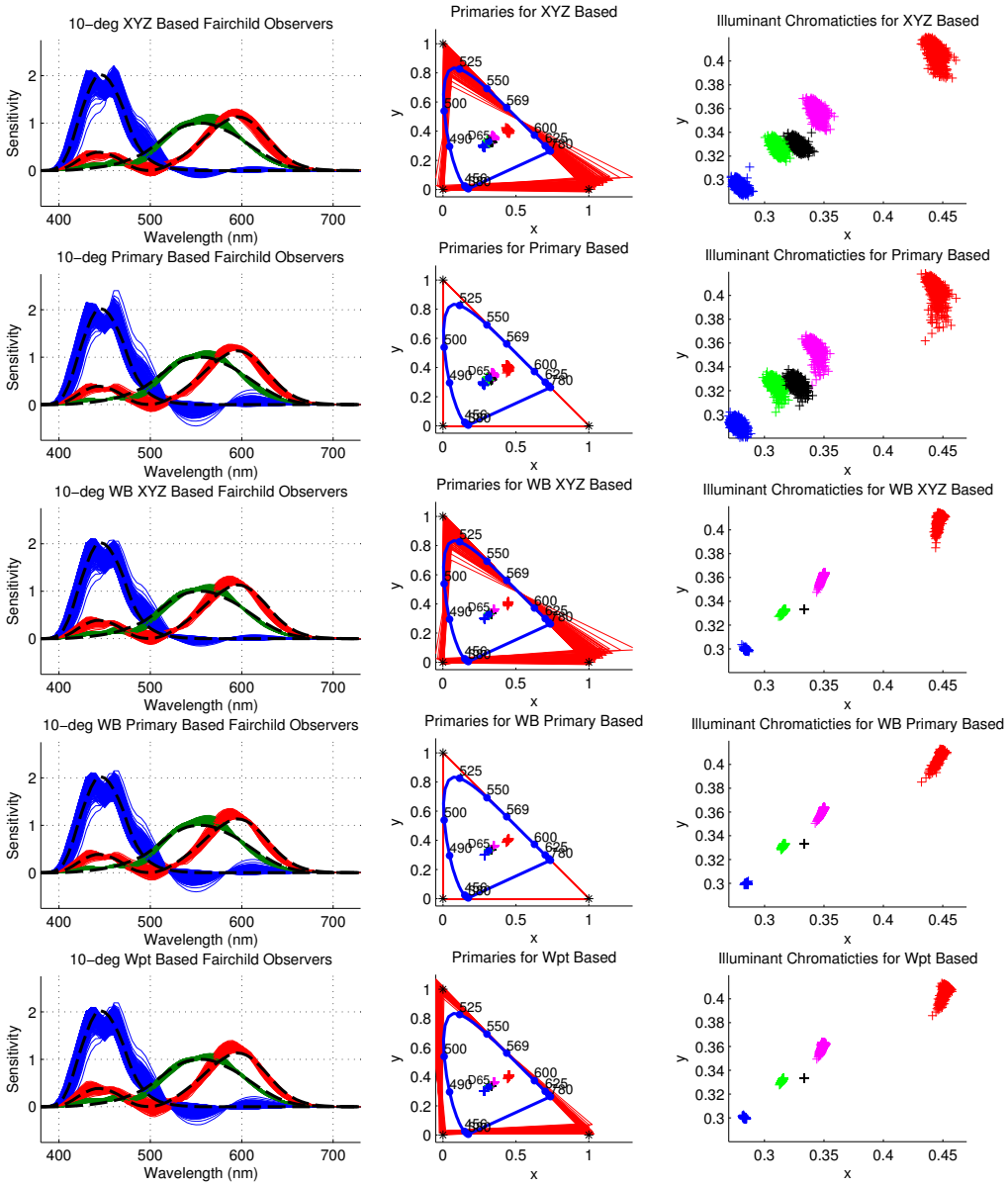

FIGURE 6.5. – 10° Fairchild-Heckaman CMFs (left column), Predicted Primaries (middle column) and Illuminant Chromaticities (right column) with minimizing tristimulus values (top row), predicting ref observers primaries (second row), minimizing tristimulus values with white balancing (third row), predicting ref observers primaries with white balancing (forth row), Wpt based CMFs (bottom row). Illuminant chromaticities visualized for D95 (blue '+'), D65 (red '+'), Illuminant E (black '+'), D50 (magenta '+'), Illuminant A (red 'x').

As was noted in Section 4.3.3 related to categorizing the Fairchild-Heckaman set as CIE2006 observers shown in FIGURE 4.15, the Fairchild-Heckaman set appears to be most closely related to the CIE2006 4° observers (which also matches the Std 2° observer Observer Equivalence Matching (OME) based categorizations). Therefore it was hypothesized that conversions of the Fairchild-Heckaman set CFs to CMFs targeting the Standard 2° observer will more closely satisfy the Luther-Ives condition (see Section 4.3.3). However, some of the results are also expected to vary based upon the minimization involved in the strategies used to make the conversions.

FIGURE 6.4 represents the visualization of the resulting converted CMFs from the Fairchild-Heckaman set targeting the Standard 2° observer, and FIGURE 6.5 represents the visualization of the resulting converted CMFs from the Fairchild-Heckaman set targeting the Standard 10° observer. As OME metrics resulting from Section 4.3.3 indicated, the conversion targeting the Std 10° observer is less likely to satisfy the Luther-Ives condition, and the outcomes of the 10° CFs to CMFs conversion are expected to vary somewhat more than those 2° CFs to CMFs conversions.

In FIGURE 6.4, the Color Matching Functions that preserve “similarity of tristimulus values" (XYZ based) through direct regression (top) are closest to the Standard 2° observer for the Z curves (blue), Y curves (green), and X curves (red), and to a lesser extent for the X curves white balancing is performed in addition to XYZ based conversion (third row). However, in these cases this results in the observers predicting drastically different chromaticities for the reference observer’s primaries than that of the reference observer, and the triangles of the predicted primaries cross significantly through the reference observers’s spectrum locus.

The color matching functions in the second and forth row corresponding to matching the same primaries as the reference observer have no noticable convergance for all observers at any particular wavelength. This is because the color matching primaries of the reference observer are not defined using monochromatic (single wavelength) light sources. However, the second and forth color rows’ matching functions both perfectly preserve the chromaticities of the primaries predicted by the reference observer, and the resulting CMFs have a larger spread of difference from the standard 2° CMFs than the XYZ based CMFs.

Comparing the first and second rows to the third and fourth rows shows that using white balancing with both XYZ based and Primary based CMFs results in more stable chromaticities for D95, D65, Illuminant E, D50, and Illuminant A. In the bottom row, the color matching functions based upon Wpt Normalization strike a middle ground between predicting the primaries (by not significantly crossing the referebce observer’s spectrum locus), and getting stable prediction of the illuminant chromaticities. The prediction of the illuminants in the bottom three rows appears to be fairly similar.

There are only a few noticeable differences between FIGURE 6.4 and FIGURE 6.5. First, there appears to be slightly greater spread in all of the color matching functions for the 10° observer. There is also greater spread for the 10° CMFs in the primary matching for both the XYZ based

conversion approaches. However, the primary matching in FIGURE 6.5 for the Wpt Based conversion remains outside the reference obervers's spectrum locus, and appears slightly reduced in spread. There are no appreciable differences in the illuminant chromaticities.

TABLE 6.1. – III E optimized Fairchild-Heckaman based CMFs ΔE_{00} comparisons to Std observer CMFs for Corrected Munsell Reflectances. Minimum ΔE_{00} values are in *italics*.

		Targeting 2° observer		Targeting 10° observer	
		Mean	**Max**	**Mean**	**Max**
	XYZ Based	1.31	*26.50*	*0.94*	*20.70*
III A	**Primary Based**	*1.19*	27.69	1.04	37.90
	Wpt Based	1.98	29.24	1.20	31.99
	XYZ Based	0.87	*10.72*	1.06	*11.70*
III C	**Primary Based**	0.79	12.58	0.92	18.53
	Wpt Based	*0.72*	12.16	*0.57*	14.77
	XYZ Based	0.90	*10.98*	0.96	*10.96*
IIIE	**Primary Based**	0.82	14.83	0.85	21.42
	Wpt Based	*0.76*	14.31	*0.57*	17.31
	XYZ Based	0.91	*11.82*	0.95	*10.94*
D50	**Primary Based**	*0.82*	15.36	0.85	22.23
	Wpt Based	0.86	14.82	*0.63*	17.85
	XYZ Based	0.85	*10.48*	0.99	*11.50*
D65	**Primary Based**	0.78	12.50	0.87	18.49
	Wpt Based	*0.75*	12.06	*0.58*	14.70
	XYZ Based	0.83	15.67	*0.75*	*16.52*
F11	**Primary Based**	*0.69*	23.46	0.87	33.14
	Wpt Based	1.08	22.98	0.85	27.48

Separate calculations were performed to compare tristimulus values of material colors using the color matching functions in FIGURE 6.4 and FIGURE 6.5 under a variety of illuminants. The 1600 corrected Munsell reflectances used in Chapter 4 were transformed to tristimulus values and then to CIELAB values under Illuminant A, Illuminant C, Illuminant E, D50, D65, and F11 for these color matching functions. These were then compared using ΔE_{00} to CIELAB values under the same illuminants for the Standard 2° and Standard 10° observers. Wpt Normalization matrices used to form the CMFs (Wpt based) were only optimized for the Standard 2° or Standard 10°

observer under a single illuminant (Illuminant E). The results of these calculations can be found in TABLE 6.1. Only white point balancing was performed for both XYZ based and Primary based CMF conversion since the CIELAB equations utilize a normalization of the white point.

The 2° results for the XYZ based CMFs had the largest mean values for all illuminants but Ill A and F11 while also having the lowest Maximum values for all the illuminants. This is indicative of direct regression used by XYZ based conversions resulting in spectral minimization rather than a perceptual minimization. The Wpt based CMFs have the lowest mean ΔE_{00} for Ill C, Ill E, and D65. Primary based CMFs have the lowest mean ΔE_{00} for Ill A, D50 and F11 – though the difference of the mean between the Primary based and Wpt based for D50 is very small. The large mean values for Wpt based CMFs under Ill A and F11 is indicative of the fact that the Wpt based CMFs were optimized for Ill E are therefore not optimal for Ill A and F11. The key to Wpt based conversion is that the color matching functions are tuned to get best results for the illuminant combined with the observer, and if the observers do not have a Luther-Ives relationship and illuminant varies widely then the prediction may not be as good.

Overall the maximum mean color difference results for the 10° Fairchild-Heckaman set CMFs are somewhat larger than the values for the 2° Fairchild-Heckaman set CMFs thus confirming the assertion that the Fairchild-Heckaman set has closer observer matching to the 2° observer than the 10° observer. In general the roles reversed between the 2° and 10°XYZ based CMFs and Primary based CMFs. The 10° XYZ based CMFs had the smallest Mean values for illuminants A and F11 while also having the lowest Maximum values for all the illuminants, and the 10° Primary based CMFs performed the most poorly. The 10°Wpt based CMFs also have the lowest mean ΔE_{00} for Ill C, Ill E, D50, and D65, and the difference between the Wpt Based Mean values and the other methods' mean values is much greater. Also, the large mean values for Wpt based CMFs under Ill A and F11 reinforces the notion that Wpt based CMFs optimized for Ill E are not optimal for Ill A and F11. However, the spread between the Wpt based mean values and the minimum mean values has significantly decreased.

Better mean results for Wpt based CMFs under Ill A and F11 can be accomplished by using illuminant specific MATs when generating the Wpt based CMFs as seen in TABLE 6.2. In some cases CMFs optimized for Ill E in TABLE 6.1 have slightly better mean values than for illuminant specific optimization. It is believed these slight variations are due to material shifts involved in optimizing for the various observing conditions. The 10° Fairchild-Heckaman CMFs generated using Wpt based conversion also show overall mean results that are much lower than for the similarly generated 2° CMFs while the maximum results are larger. The change in maximum results is attributed to the inherent difference in matching field size between the Fairchild-Heckman CMFs and the Standard 10° observer. It is postulated that the reduction in mean going from 2° to 10° field sizes is an indication of other unknown similarities between the Fairchild-Heckaman set and the Standard 10° observer.

TABLE 6.2. – Illuminant specific Wpt based Fairchild-Heckaman CMFs ΔE_{00} comparisons to Std Observer CMFs for 1600 Corrected Munsell Reflectances.

	Targeting 2° observer		Targeting 10° observer	
	Mean	**Max**	**Mean**	**Max**
IIIA:	0.73	14.87	0.52	17.82
IIIC:	0.73	13.93	0.58	16.81
IIIE:	0.76	14.31	0.57	17.31
DE50:	0.73	13.59	0.55	16.42
D65:	0.73	13.63	0.57	16.50
F11:	0.43	10.47	0.38	12.45

6.4 Conclusions

Three basic approaches to converting cone fundamentals to color matching functions have been discussed in light of a mathematical basis for describing relationships between cone fundamentals, color matching primaries and color matching functions. When the observers do not have a Luther-Ives condition relationship then non-linear relations exist between the observers and the conversion will result in differences in the color matching functions based upon the criteria used to make the conversion. These differences may have an associated meaning that should be kept in mind when evaluating differences in inter-observer color matching.

1. Color matching functions are optimized to predict “sameness of color matching primaries" (Primary based) using one of two approaches. The first uses an arbitrary set of primaries (possibly from a digital display) and the resulting color matching functions reflect the tristimulus values of a reference observer to the matches made by the alternate observers. The second approach for predicting color matching primaries makes a direct prediction of the reference observer’s primaries. Such a prediction utilizes a single reference set of primaries. However, the predicted primaries are actually metamers to the reference observer’s primaries. Additionally, comparisons of tristimulus values using predicted primaries represent how color matches of other observers appear to the reference observer, but do not provide a reference for describing inter-observer color perception. The magnitude of the differences involves both the differences between the observers as well as differences from the reference observer.

2. Direct regression is used to predict “similarity of tristimulus values" (XYZ based). Direct regression achieves overall similar tristimulus values, but provides no reference for making comparisons of relative perception between observers unless white balancing is performed. However, normalization of the white point does not provide a common reference for describing matches of arbitrary colors as it doesn’t account for the perception of the matches to the observers involved. Therefore, differences in tristimulus values for

CMFs generated using direct regression provides a magnitude estimation of the spectral differences between the observers involved, but directional comparisons of the differences may not reflect the actual perceptions of the observers.

3. Wpt normalization is used to define CMFs that predict material color equivalency of a basis observer under a specified illumination. Differences in tristimulus values based on Wpt based CMFs represent differences in material color as perceived by the observers involved. This is because they are optimized to get similar results for the same set of material colors. Thus, Wpt based CMFs provide a reference for comparing inter-observer tristimulus values. However, this optimization incorporates the interaction of the illuminant and is therefore not entirely optimal for matching the basis observer's tristimulus values across all illuminants due to the effects of material color shifts.

7 Manipulating Spectral Reflectance

7.1 Background and Introduction

In this chapter the concepts and principles of Chapter 4 are built upon to develop generalized methods of spectral reflectance estimation and manipulation. Color reproduction systems and their objectives are reviewed leading to the proposal of a new color reproduction objective – “Spectrally Preferred Reproduction". A general framework for spectral reflectance manipulation is then introduced along with examples of how it can be applied to existing approaches of spectral manipulation. A specific instance of this framework is then proposed using Wpt/WLab and the spectral decomposition method proposed in Section 4.1.2. Finally, examples of spectral estimation and manipulation are presented. Spectral estimation is used to determine spectral reflectances for Munsell Color System colors, and spectral manipulation is used to manipulate spectral reflectances of actual printed test colors to get realistic reflectances corresponding to reference printing conditions solely defined by colorimetry. Lastly, the techniques proposed in this chapter are used to estimate and manipulate spectral reflectances of an image using an iccMAX color management workflow.

7.1.1 Spectral Estimation

In Section 4.1.2 methods of spectral decomposition proposed by Wyszecki [Wyszecki, 1953] and Chau [Chau, 1999] were combined to define a general decomposition of spectral reflectances as follows:

$$\mathbf{O}_{\text{any}} = g\mathbf{I} + s\mathbf{O}_{\text{select}} + b\mathbf{B} \tag{7.1}$$

where:
$\mathbf{O}$ is an arbitrary spectral reflectance matrix for an object,
$\mathbf{I}$ is the identity matrix,
$\mathbf{O}_{\text{select}}$ defines a matrix that selectively adjusts light based on wavelength (thus $min\left(\mathbf{O}_{\text{select}}\right) \neq max\left(\mathbf{O}_{\text{select}}\right)$),
$\mathbf{B}$ is a metameric black for the given observing conditions,
g is a scalar that adjusts the non-selective (gray) portion of the spectral reflectance,
s is a scalar that adjusts the selective (saturation) portion of the spectral reflectance, and
b is a scalar that adjusts the metameric black component.

When b in Eq. 7.1 is set to zero the equation is identical to the spectral decomposition defined by Chau, and the $\mathbf{O}_{\text{select}}$ matrix defines a characteristic reflectance when $min\left(\mathbf{O}_{\text{select}}\right)$ is zero and $max\left(\mathbf{O}_{\text{select}}\right)$ is one.

Spectral reflectance estimation based upon a color description defined by lightness, chroma, and hue is performed by first establishing a relationship between hue and the characteristic reflectance; then a relationship needs to be established between the combination of lightness and chroma and the scalars g and s. With these relationships in place the values of lightness, chroma, and hue can be used to determine values for $\mathbf{O}_{\text{select}}$, g, and s. These values can then be applied in Eq. 7.1 with b set to zero to determine the spectral estimation corresponding to the lightness, chroma, and hue. As will be further discussed in Section 7.2.3, Chau defined one method of establishing these relationships. Domain specific relationships with Wpt based hue and direct linear relationships with Wpt lightness and chroma will be proposed in Section 7.3.

7.1.2 Material Shift Potential

Object Wpt shift manifolds were introduced in Chapter 4 that represent the extent to which material color shifts due to changes in observer and illuminant occur for an object's given spectral reflectances. It was also shown through the visualization of Object Wpt shift manifolds that both the $\mathbf{O}_{\text{select}}$ and $\mathbf{B}$ vectors in Eq. 7.1 define the shape and orientation of the Wpt shift manifold (also defined as the "Material Shift Potential" (MSP) of the object). Preserving MSP was identified to be the same as preserving Wpt hue, and it was shown that the MSP is preserved when both the $\mathbf{O}_{\text{select}}$ and $\mathbf{B}$ vectors are held constant and only the scalars are adjusted. These concepts can be applied in the context of defining color reproduction systems that preserve MSP.

7.1.3 Color Reproduction

A color reproduction system can be considered as a color system with additional control parameters provided to manipulate one or more of the elements in the following equation to achieve reproduction objectives.

$$\mathbf{d}_{i,j,k} = p\left(\mathbf{C}_i\mathbf{O}_j\mathbf{l}_k, \ldots\right) \tag{7.2}$$

where:
p is a function that takes sensor excitations as input (along with other possible inputs) and outputs a color description,
i is an identifier for the i^{th} observer,
j is an identifier for the j^{th} object,
k is an identifier for the k^{th} illuminant,
$\mathbf{d}_{i,j,k}$ is the resulting color description for the i^{th} observer, j^{th} object and k^{th} illuminant,
$\mathbf{C}_i$ represents the color matching function or sensor sensitivities of the i^{th} observer,
$\mathbf{O}_j$ represents the reflectance matrix for the j^{th} object, and
$\mathbf{l}_k$ represents the spectral power distribution for the k^{th} illuminant/light source.

A color system can be graphically represented as a workflow with representations of each of the terms in Eq. 7.2 having a “processing" step representative of the $p()$ function, a “capture" step representative of the $\mathbf{C}$ matrix, an “object" step representative of the $\mathbf{O}$ matrix, and a “light" step representative of the $\mathbf{l}$ vector. Variability in the terms is represented as stacked workflow steps. Figurative examples of both a generic color display system and a generic color printing system are depicted in FIGURE 7.1. Dotted lines in the figure are representative of information from one step being made available to the definition or operation of another step. Color management (which works outside the color system) utilizes relationships between color descriptions and control parameters (device values) to establish device values that achieve desired color rendering objectives.

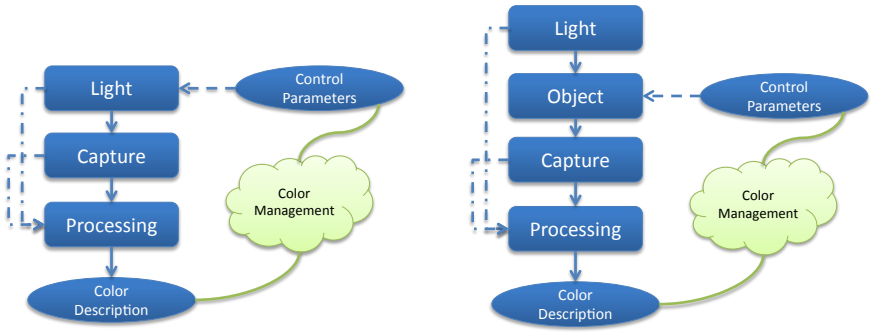

FIGURE 7.1. – Providing control parameters to a color system results in: (Left) a Generic Color Display System, (Right) a Generic Color Printing System. Color management systems control color utilizing relationships between color descriptions and control parameters.

If the color descriptions in Eq. 7.2 are represented as Wpt coordinates then the processing function in Eq. 7.2 is equivalent to applying a Wpt normalization matrix $\mathbf{A}$ and the resulting function is the same as the equation used to represent a point in a Wpt Shift manifold defined in Eq. 4.1. Thus:

$$\mathbf{w}_{i,j,k} = \begin{bmatrix} W_{i,j,k} \\ p_{i,j,k} \\ t_{i,j,k} \end{bmatrix} = \mathbf{A}_{i,k}\mathbf{C}_i\mathbf{O}_j\mathbf{l}_k \tag{7.3}$$

where:
$\mathbf{w}_{i,j,k}$ represents a Wpt vector for the i^{th} observer, j^{th} object, and k^{th} illuminant,
$\mathbf{A}_{i,k}$ represents a Wpt normalization matrix specific to the i^{th} observer and k^{th} illuminant,
i, j, k, $\mathbf{C}_i$, $\mathbf{O}_j$, and $\mathbf{l}_k$ are the same as in Eq. 7.2.

The primary focus of this chapter is spectral reflectance manipulation as it is related to spectral color reproduction. Hunt describes seven types color reproduction objectives including: spectral color reproduction, colorimetric color reproduction, exact color reproduction, equivalent color reproduction, corresponding color reproduction, and preferred color reproduction [Hunt, 2005]. The distinction between these reproduction objectives lies in the variability of the sub-systems

associated with a reference and reproduction color system, and therefore relationships between reproduction objectives can be expressed in terms of Wpt Shift Manifolds (WSMs) as described in Chapter 4.

It is expected that the color descriptions (or Wpt coordinates) for a spectral color reproduction between the two systems will match regardless of the observer or the light source. Thus the Object Wpt shift manifolds of the source (src) and reproduced (repro) objects will be the same. Thus:

$$\mathbf{w}_{i,\text{src},k} = \mathbf{w}_{i,\text{repro},k} \qquad \forall i,k \tag{7.4}$$

where both sides of the equation represent corresponding points in two separate WSMs.

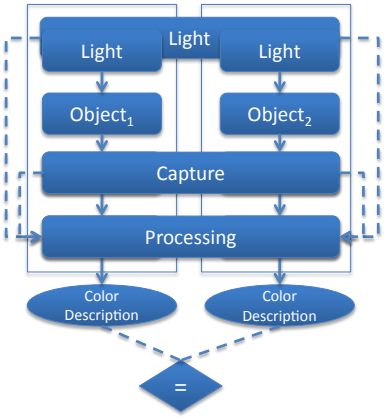

FIGURE 7.2. – Hunt's remaining reproduction objectives (excluding preferred reproduction) utilize metameric matching and processing adjustments to account for differences in lighting. The Light sub-systems may or may not be the same.

A metameric match occurs when the resulting color descriptions are the same for two color systems that have the same lighting and observer but different object elements [Berns, 2000]. Hunt's remaining reproduction objectives (except for preferred color reproduction) rely on the principle of metameric matching or appearance matching. Additionally, some of Hunt's reproduction objectives also incorporate processing adjustments made by the visual system to minimize perceptual differences between different lighting conditions. The general workflow for these reproduction objectives is depicted by the flow diagram in FIGURE 7.2 and described by Eq. 7.5.

$$\mathbf{d}_{\text{std,src,ref}} = \mathbf{d}_{\text{std,repro,ref}} \tag{7.5}$$

where:
color descriptions $\mathbf{d}_{\text{std,src,src}}$ represents the color description of a source object for a standard observer under a source illuminant,
$\mathbf{d}_{\text{std,repro,repro}}$ represents the color description of a reproduced object for a standard observer under a reproduction illuminant, and
these are found using Eq. 7.2 with function $p\,()$ defined to determine either a colorimetric or

appearance based color description. The source and reproduction illuminants may or may not be the same.

Hunt's final (and often most challenging) color reproduction objective is preferred reproduction. There are many factors that predicate preferred reproduction, but in some cases it is required due to differences in what colors can be achieved by different color reproduction systems. As a result, the matching of color description implied by Eq. 7.5 is either not possible, or just not desired in order to achieve some preferred objective. However, a partial preservation of color description is often utilized resulting in one or more of the color description attributes being preserved. Thus:

$$d_{1,m} \equiv d_{2,m} \tag{7.6}$$

where:
$\equiv$ represents an equivalence operation between color description attributes,
m is one or more members of the set of identifiers for color description attributes that are preserved,

$\begin{bmatrix} d_{1,1} \\ \vdots \\ d_{1,n} \end{bmatrix} = \mathbf{d}_{std,1,1}$ defines n color attributes for description 1 using Eq. 7.2, and

$\begin{bmatrix} d_{2,1} \\ \vdots \\ d_{2,n} \end{bmatrix} = \mathbf{d}_{std,2,2}$ defined n color attributes for description 2 using Eq. 7.2.

The essential aspect of preferred rendering is that the color description attributes are not completely the same but rather they have a preferred difference. A more specific example of a preferred rendering is the case of gamut mapping [Morovic, 2008] where the aspect of hue is the same (or very similar) and other attributes (like lightness and chroma) are modified to achieve the preferred reproduction. This case is shown in FIGURE 7.3.

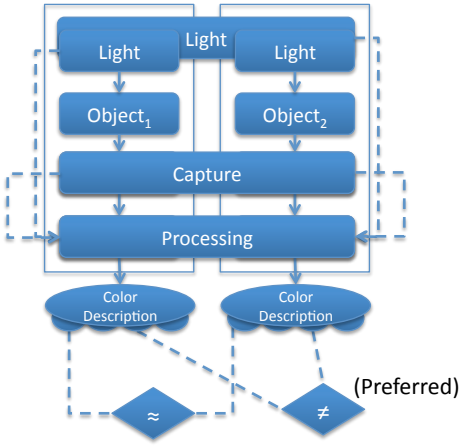

FIGURE 7.3. – Preferred color rendering with partial preservation of color description attributes. The Light sub-systems may or may not be the same.

7.1.4 Proposed Reproduction Objective

It is proposed that an additional color reproduction objective can be defined by combining aspects of spectral reproduction with preferred reproduction to define a spectrally preferred reproduction. In this case only a subset of the color description attributes are preserved for all observers and illuminants.

$$d_{1,m} \equiv d_{2,m} \tag{7.7}$$

where:
$\equiv$ represents an equivalence operation between color description attributes,
m is one or more members of the set of identifiers for color description attributes that are preserved,
$\begin{bmatrix} d_{1,1} \\ \vdots \\ d_{1,n} \end{bmatrix} = \mathbf{d}_{i,\text{src},k}$ defines n color description characteristics using Eq. 7.2 or a source (src) object for all observers i and light sources k,
$\begin{bmatrix} d_{2,1} \\ \vdots \\ d_{2,n} \end{bmatrix} = \mathbf{d}_{i,\text{repro},k}$ defined by Eq. 7.2 of a reproduction (dst) object for all observers i and light sources k.

A workflow diagram for spectrally preferred reproduction is shown in FIGURE 7.4.

An example of this is a spectrally based gamut mapping system where the hue matches between the two objects regardless of how the hue changes for different lighting or capture characteristics. Thus, the material shift potential is preserved. Two important questions arise

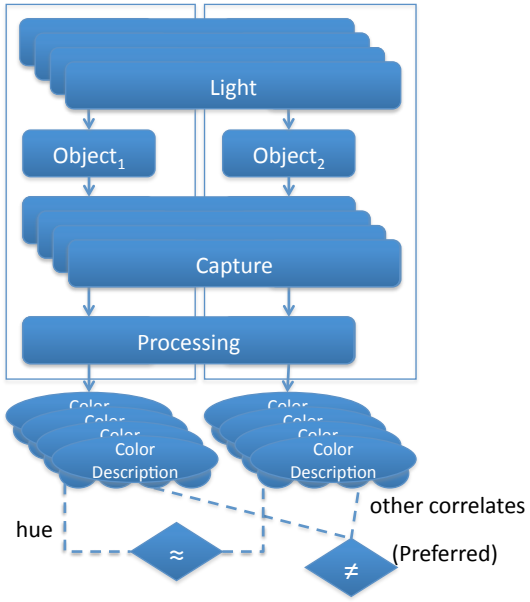

FIGURE 7.4. – Spectrally Preferred Reproduction with partial preservation of appearance potential attributes.

when considering implementation of a reproduction system that achieves spectrally preferred reproduction objectives:

1. How do you manipulate the spectral representation of an object to get observer-preferred results?

2. How do you maintain color description attributes as you manipulate the spectral representation of an object?

These questions are addressed in the next section.

7.2 Spectral Reflectance Manipulation

7.2.1 Framework

A general spectral reflectance manipulation framework is shown in FIGURE 7.5 and represents a generalization of the approach proposed to perform paramer correction used when calculating an index of metamerism for paramers [Berns, 2000; Li and Berns, 2007]. On the left of the figure is the workflow and on the right is depicted the data flow. In the data flow diagram the rectangles represent states of color information and the rounded rectangles represent operational steps or transformations of information.

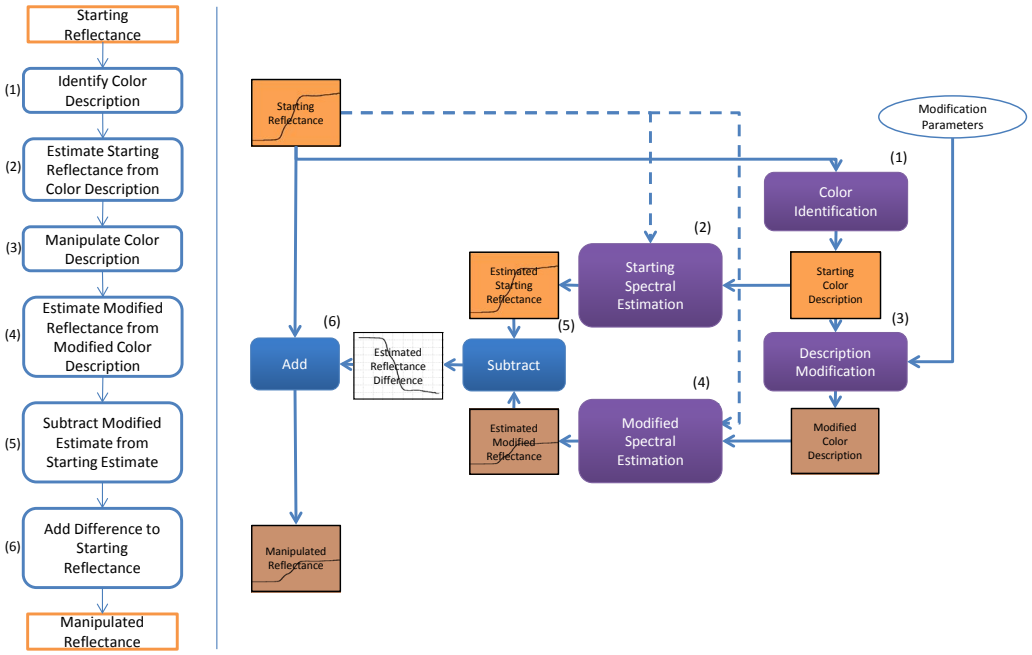

FIGURE 7.5. – This general "spectral manipulation framework" allows for the manipulation of spectral reflectances through the modification of color description attributes with workflow (left), data flow (right).

The workflow steps within this framework are described as follows:

1. A color identification step is applied to the starting reflectance to determine color description attributes for the starting spectral reflectance.

2. A spectral estimation step is applied to the color description attributes for the starting reflectance to derive an estimated starting reflectance.

3. The starting color description attributes are modified by a description modification step using modification parameters to get a modified color description.

4. A spectral estimation step is applied to the modified color description to derive an estimated modified reflectance.

5. The difference between the estimated modified reflectance and the estimated starting reflectance is determined. This represents just the delta spectral reflectance associated specifically with the change in color description.

6. This difference is then added to the starting reflectance to derive the modified reflectance. Thus the essence of the starting reflectance is preserved as only the delta reflectance involves spectral estimation.

[Note: In the data flow diagram dotted lines indicate that information about the starting spectral reflectance may or may not be utilized by either of the spectral estimation steps].

Additionally, applying a color identification step (similar to the one used to get the starting color description) to the final modified reflectance provides a color description that can be compared to the modified color description to verify that it exactly matches.

7.2.2 Preliminary Implementation

An implementation of the spectral manipulation framework in FIGURE 7.5 defines specific implementations for the following: the two spectral estimation steps, color identification step, color description attributes used, and a method of modifying the color description attributes. As the framework is general, the two spectral estimation steps may or may not use the same implementation. A simple example where the estimation steps are not the same is the case where the framework is used to describe the replacement of a spectral reflectance with a spectral reflectance determined solely by an estimated reflectance. In this case the first estimation step simply uses the starting spectral reflectance, and the second estimation step determines the actual estimated reflectance.

An example implementation of a spectral manipulation system was developed [Derhak and Berns, 2012] to manipulate the spectral reflectances of the University of Eastern Finland (UEF –

formerly Joensuu University) Glossy Munsell Reflectance database to get spectral reflectances that correspond to the colorimetry defined by the Munsell Renotation system and is described fully in Appendix A. Eq. 1.3 is used to define the color identification model with the CIE 1931 2° observer, and the spectral power distribution of the CIE Illuminant C applied. The color description attributes involved were tristimulus colorimetric values. The spectral estimation technique used the same Matrix R spectral estimation technique defined by Cohen [Cohen, 2001] as proposed by Berns for paramer correction when calculating an index of metamerism for paramers [Berns, 2000]. The resulting spectral reflectances have the correct colorimetry under Illuminant C for the standard observer, but there are no guarantees related to the appearance potential of the resulting spectral reflectances [Derhak and Berns, 2012].

In fact, the general nature of the framework in FIGURE 7.5 does not provide any guarantees related to the preservation of color description attributes for changes in observer or illuminant or “material shift potential." Such preservation requires that the implementation of the color identification and spectral estimation steps take preservation of material shift potential" into account.

7.2.3 Preserving Material Shift Potential

The proposed implementation of the spectral reflectance manipulation framework in FIGURE 7.5 defines identification, estimation, and modification steps that provide for either partial preservation of material shift potential or the minimization of color attribute differences.

As was demonstrated in Chapter 4, one partial approach proposed by Chau used a decomposition of spectral reflectance into the sum of two spectral reflectances [Chau, 1999]. This decomposition is represented in Eq. 7.8 as a sum of two spectral reflectances. Thus:

$$O = g\mathbf{I} + s\mathbf{O}_{\text{sat}} \tag{7.8}$$

where:
$\mathbf{O}$ is a matrix representing an arbitrary resulting spectral reflectance,
$\mathbf{I}$ is an identity matrix representative of a “white" reflects 100% of the light for all wavelengths,
$\mathbf{O}_{\text{sat}}$ is a matrix representing representing a maximally saturated reflectance (also referred to as a characteristic reflectance),
g is a scalar of spectral whiteness, and
s is a scalar of spectral saturation.

[Note: The maximally saturated reflectance matrix $\mathbf{O}_{\text{sat}}$ has a minimum reflectance of 0% and maximum reflectance of 100% only when the arbitrary spectral reflectance $\mathbf{O}$ is selective (meaning that it represents different reflectance factors for different wavelengths). Otherwise, if $\mathbf{O}$ is non-selective then the $\mathbf{O}_{\text{sat}}$ matrix is a zero (or null) matrix.]

Eq. 7.8 defines a plane in spectral vector space when $\mathbf{O}_{\text{sat}}$ is fixed and non-zero, and g and s are varied. Both Koenderink and Chau showed that for values of scalars g and s greater than or equal to zero, the resulting spectral reflectances in this plane can be described with a constant color description of hue (as defined by dominant wavelength) for arbitrary observers and illuminants [Koenderink, 1987; Chau, 1999]. This is accomplished by substituting the matrix representation of Eq. 7.8 into Eq. 1.3 resulting in a linear combination of cone excitations for white and the characteristic reflectance. The chromaticities of these cone excitations fall on a line containing the chromaticities of the white point and the characteristic reflectances thus preserving hue as defined by dominant wavelength.

As was demonstrated in terms of Wpt Shift Manifolds in Chapter 4, hue relationships are preserved for objects with reflectances that are defined by Eq. 7.8. Chau leveraged this principle to define a spectral gamut mapping strategy that results in a spectrally preferred reproduction. The spectral gamut mapping approach that Chau proposed can be described by defining specific implementations of the steps in the spectral manipulation framework in FIGURE 7.5 (hereafter known as the "Chau implementation") as follows:

1. The color identification step uses Eq. 1.3 with a CIE D50 illuminant, the starting reflectance, and the CIE 1931 standard 2° observer resulting in colorimetric tristimulus values that are converted to the CIELUV color space [CIE15, 1976]. The color description used by the Chau implementation is CIELUV along with a magnitude of u* and v* to define chroma (C_{uv}).

2. The starting spectral estimation step uses an identity transform of the source reflectance resulting in the modified spectral estimation step directly determining the modified reflectance.

3. The description modification step utilizes a conventional hue preserving gamut mapping technique adjusting L^* and C_{uv} relative to a gamut boundary for the printer in CIELUV space.

4. The modified spectral estimation step establishes a direct functional relationship between the modified color description's L^* and C_{uv} and Eq. 7.8 for the characteristic reflectance for the starting reflectance to determine modified s and g values. These values along with the starting reflectance's characteristic reflectance $\mathbf{O}_{\text{sat}}$ are applied in Eq. 7.8 to determine the modified estimated reflectance, which becomes the modified reflectance.

The following two observations can be made of the Chau implementation:

1. Constant hue as defined by CIELUV doesn't always correlate directly with constant perceptual hue [Fairchild, 2013]. Small changes in hue may be needed to preserve perceptual hue and larger changes in hue may be needed to achieve preferred reproduction objectives.

2. The use of CIELUV as a color description space for manipulation and entry for spectral estimation introduces computational complexities in that it requires a non-linear transformation going from colorimetry to the spectral estimation scalars s and g.

7.3 Proposed Wpt based Spectral Implementation

The proposed implementation addresses these two issues while providing for a more robust and efficient method of spectral manipulation that can be used in a spectrally preferred color reproduction system.

7.3.1 Proposed Spectral Estimation

The system utilizes spectral estimation based upon relationships between the polar representation of Wpt with coordinates W, C_{pt}, and h_{pt} and terms in Eq. 7.8. An empirical domain specific lookup based on h_{pt} is used to determine the characteristic reflectance $\mathbf{O}_{\text{select}}$.

The following approaches are proposed to determine this relationship. The first uses fixed hues while the remaining approaches utilize “a priori" determined empirical relationships between characteristic reflectances and h_{pt} values. As hue is a continuous function it is common to use a discrete set of hues with corresponding characteristic reflectances, and then interpolate between these reflectances to determine corresponding characteristic reflectances for arbitrary h_{pt} values. The proposed approaches include:

- If a starting reflectance is known and the associated Wpt hue remains constant then the characteristic reflectance can be the same as the characteristic reflectance of the starting reflectance (see Eq. 4.5). This ensures that the material shift potential is maintained with the change in Wpt lightness and/or chroma. This is identical to the way Chau approached hue.

- In some workflow domains there is only one characteristic reflectance associated with each hue – for instance an artist’s palette. In this case the characteristic reflectances can directly be assigned to each hue.

- In some workflow domains, multiple spectral reflectances are associated with the same concept of hue. A color order system is an example of such a domain. In this case, one of the specific characteristic reflectances associated with a hue can be selected as being representative of all objects with the similar hue. Criteria for establishing characteristic reflectances might include using the Object Hue Similarity Index (OHSI) as defined in Chapter 4 to find a characteristic reflectance that best matches the characteristic reflectances of all the objects in the domain that have similar hue. Additionally, minimization in the width of hue shift in the material shift manifolds for characteristic reflectances of

colors with related hues might be considered as a means of reducing the overall color inconstancy due to hue.

- In workflow domains involving a color gamut, the characteristic reflectances for hues can be defined by the spectral reflectances of the maximum chroma points for each hue.

- Though not pursued in this research, it is conceivably possible to use a model to approximate the shape of a “reference" characteristic reflectance. Such a model might include features like roundness, transition slopes, band pass width, and whether features shift in wavelength or simply select relative output levels in different wavelength regions. Once the parameters of a model are defined then it can be used to define a hue family that defines spectral reflectances for each hue. One problem with this approach is that generally the shape of the reflectance for one hue is not a very good predictor of the shape of a completely different hue. However, this may be provide an adequate approach for defining “nearby" hues. However, defining such model based characteristic hue definitions is beyond the scope of the present research.

The estimated reflectance is then determined using Eq. 7.8 with this characteristic reflectance and the scalars g and s that are determined directly from a linear relationship with the color identification W and C_{pt} values as follows:

$$\begin{bmatrix} g \\ s \end{bmatrix} = \mathbf{M}_{\text{select}} \begin{bmatrix} W \\ C_{pt} \end{bmatrix} \tag{7.9}$$

where:
$\mathbf{M}_{\text{select}}$ is a matrix associated with the characteristic reflectance $\mathbf{O}_{\text{select}}$ (associated with the Wpt hue h_{pt}) that converts polar Wpt coordinates W and C_{pt} to scalar values g and s to be used in Eq. 7.8,
g, s both represent spectral estimation scalars used in Eq. 7.8,
W represents the Wpt lightness used to define the spectral estimation, and
C_{pt} represents the Wpt chroma used to define the spectral estimation.

The matrix $\mathbf{M}_{\text{select}}$ is specific to each characteristic reflectance associated with a Wpt hue and can be determined by associating Eq. 7.9 with the W, C_{pt} for white ($\mathbf{I}$) and the characteristic reflectance ($\mathbf{O}_{\text{select}}$) and inverting as follows:

$$\mathbf{M}_{\text{select}} = \begin{bmatrix} W_{\mathbf{I}} & W_{\text{select}} \\ 0 & C_{\text{select}} \end{bmatrix}^{-1} \tag{7.10}$$

where:
$\mathbf{M}_{\text{select}}$ is the same as in Eq. 7.9,
$W_{\mathbf{I}}$ represents the Wpt W (lightness) value for a non-selective white reflectance (defined by identity matrix $\mathbf{I}$),
W_{select} represents the Wpt W lightness value for the characteristic reflectance $\mathbf{O}_{\text{select}}$ using Eq. 2.1 for the appropriate observing conditions, and

C_{select} represents the Wpt C_{pt} chroma value for the characteristic reflectance $\mathbf{O}_{\text{select}}$ using Eq. 2.1 and converting to polar notation for the appropriate observing conditions.

7.3.2 Proposed Spectral Manipulation

The proposed implementation of the workflow steps from FIGURE 7.5 based on the spectral estimation technique outlined in the previous section can be described as follows:

1. The color identification step is defined using the polar representation of Wpt coordinates as provided by application of a Wpt normalization matrix using Eq. 2.1.

2. The starting spectral estimation is determined using the procedure from Section 7.3.1 with the starting reflectance's $WC_{pt}h_{pt}$ determined from the previous step as described above.

3. The description modification step either modifies Wpt values directly or converts using the Wpt to WLab transform in Appendix B to get to the more perceptually uniform representation WLab for making changes to meet reproduction objectives followed by applying the reverse transform to get back to Wpt.

4. The modified spectral estimation is determined using the procedure from Section 7.3.1 with the modified characteristic reflectance associated with the hue of the modified Wpt values determined from the previous step.

7.4 Application of Proposed Methods

Examples of spectral estimation and spectral manipulation were performed using the proposed methods in the previous sections to demonstrate their applicability. The primary challenge in these cases was defining the methods to relate Wpt hues to characteristic reflectances.

7.4.1 Generating reflectances for Munsell Colors

Spectral reflectances for Munsell colors were generated using the proposed Wpt based spectral estimation approach described in Section 7.3.1. The association of Wpt hues to characteristic reflectances utilized the Munsell corrected reflectances found in Appendix A. A characteristic reflectance (CR) curve was determined for each of the spectral reflectances in this data set, and these CR were then analyzed to select a single representative CR for each of the 40 Munsell hue planes. This was done as follows:

1. It was found that the third (metameric black) term in Eq. 4.7 becomes an important factor when converting spectral reflectances to CR using Eq. 4.5. For very long and very short

wavelengths the visual system loses sensitivity to changes in spectral reflectance, and changes to reflectances in these regions act as metameric blacks. Thus the min and max functions used in CR generation were limited to only consider reflectance factor values for wavelengths in the range of 420nm to 680nm. The resulting CR were then clipped to the range of 0 to 1 to ensure that estimations of highly saturated colors using these CR also have reflectance factors in the range from 0 to 1.

2. Object WSMs were determined for the CR of the Munsell chips in each hue plane. The product of the standard deviation and the range (max-min) of the h_{pt} values of these manifolds was calculated and then associated with each chip in the plane. This product (hereafter referred to as a hue shift factor) is representative of the degree to which hue is inconstant for variation of the illuminants and observers used to define the Wpt shift manifold.

3. Hue shift factors and associated CR were then collected and sorted by hue shift factor for chips that have Munsell Chroma greater than six. The analysis was limited to Munsell chips with larger Munsell Chroma because it was felt that the larger chroma minimizes the effects of measurement noise and influence of the metameric black component of the neutrals.

4. The CRs of the resulting chips with the lowest hue shift factor for each hue plane were then considered as candidate CRs for the hue planes. An additional pass was then performed to ensure that perceptive reversals would not occur for changes in observer and illuminant. The h_{pt} values of the Object Wpt shift manifolds for successive hue CRs were compared and minimal hue differences were determined. If the minimal hue difference for any pair of CRs was less than 3 degrees then the succeeding CR for the hue having the next larger hue shift factor was used as a candidate to represent its hue plane. This process was repeated until successive CRs had minimal manifold hue differences of greater than 3 degrees.

The resulting CRs associated with the 40 Munsell hue planes therefore have the properties of having minimized hue inconstancy and guaranteed to be distinct and monotonically increasing for changes in the illuminants and observers used for Wpt shift manifold generation. The CRs used for Munsell reflectance estimation are plotted in FIGURE 7.6 and the actual reflectances used to define these CRs are plotted in FIGURE 7.7.

The spectral reflectances in FIGURE 7.7 represent the actual measurements from the University of East Finland spectral database for Munsell Glossy reflectances. Unlike most object reflectances that are usually smooth, these measurements have considerable noise which is further amplified by the process of scaling the spectral reflectances in FIGURE 7.7 to get the CRs in FIGURE 7.6. One other observation from these figures is that there is some clipping of spectral reflectances in the infrared and near-UV regions in order to get CRs that represent high chroma colors. If clipping were not performed then in some cases the maximum or minimum points of the spectral reflectances would largely be determined by wavelengths that have little visual impact.

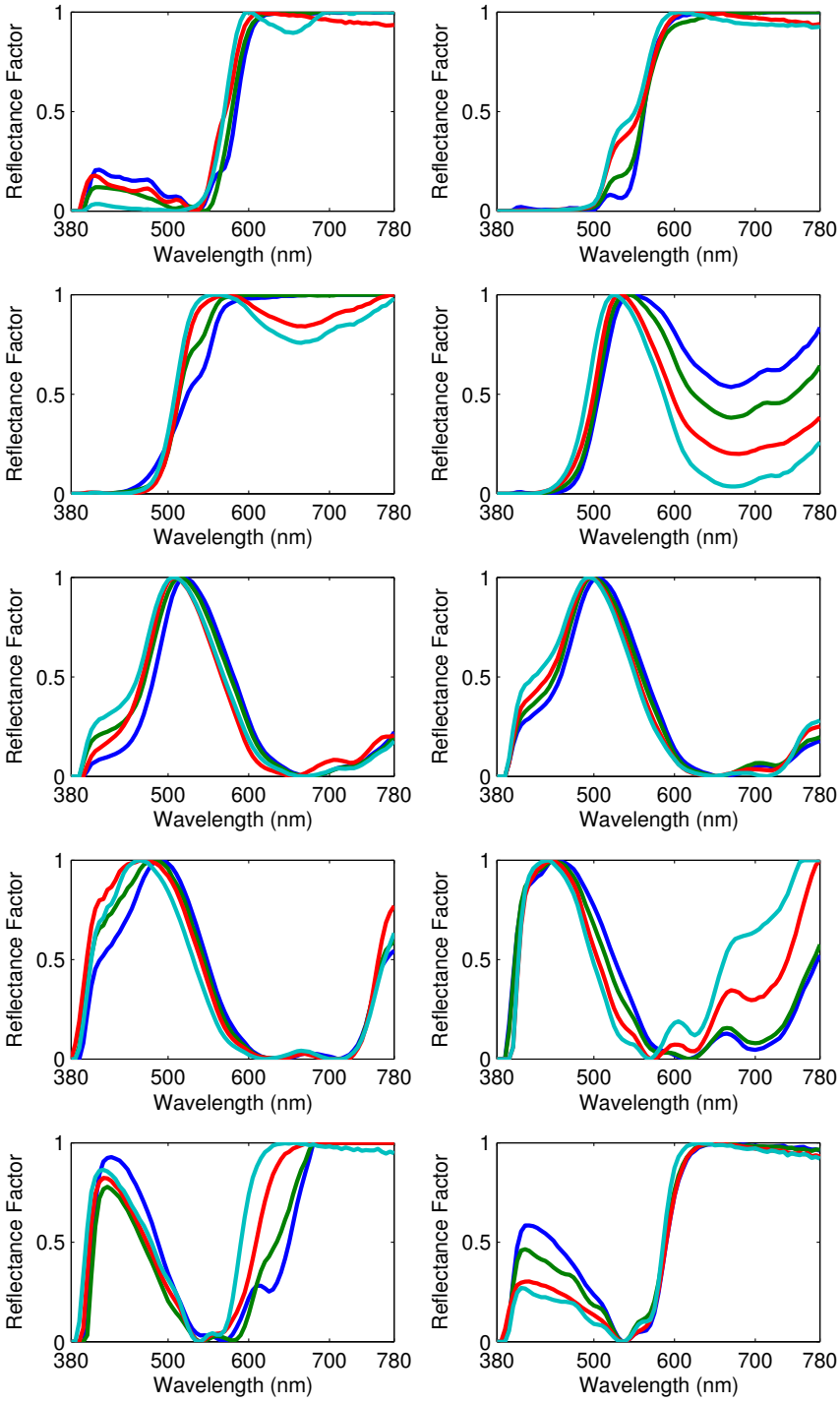

FIGURE 7.6. – Characteristic Reflectances (CRs) used for Munsell spectral estimation

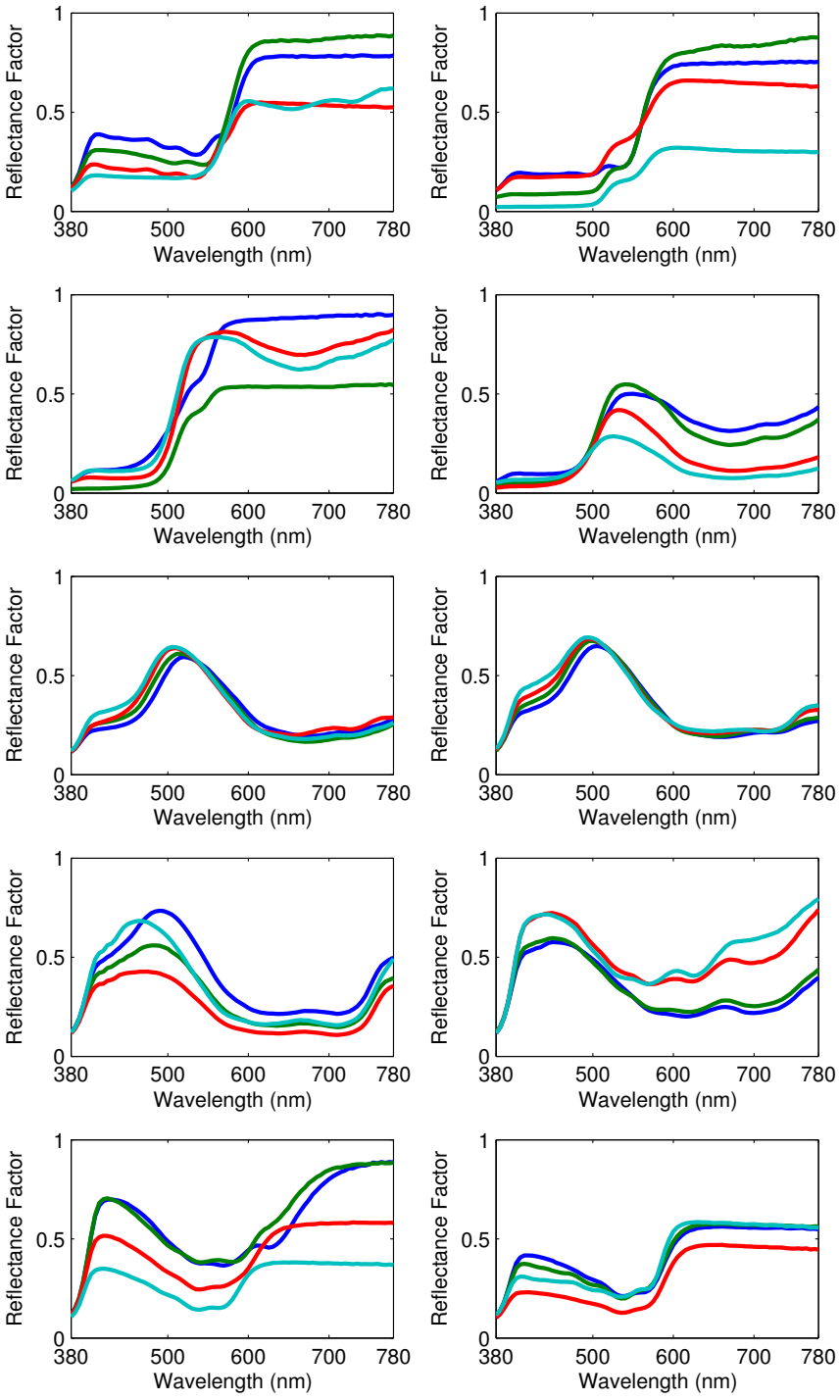

FIGURE 7.7. – Reflectances used to define Characteristic Reflectances (CRs) for Munsell spectral estimation

A decision was therefore intentionally made to clip these regions (not significantly changing the visual color).

The estimation of spectral reflectances for Munsell colors was performed by first determining $WC_{pt}h_{pt}$ values for each of hue plane CR of FIGURE 7.6 under Illuminant C as viewed by the 2° standard observer. Then associations between h_{pt} values and these CRs were established as a finely sampled hue lookup table using linear interpolation to define characteristic reflectances for intermediate hues. The use of this lookup table facilitated fast conversion of h_{pt} values to CRs.

Spectral estimation reflectances for the Munsell colors was then performed by first transforming Munsell Renotation colorimetry of each chip to Wpt using the observing condition specific Wpt Normalization matrix and then converting to $WC_{pt}h_{pt}$. Then h_{pt} was used as a lookup to identify the corresponding CR ($\mathbf{O}_{\text{select}}$) for the desired hue, and a corresponding s, g scalar estimation matrix was derived using Eq. 7.10 and applied to convert the W, C_{pt} values to s, g. Eq. 7.9 was then applied resulting in spectral reflectances with nearly identical colorimetry to the Munsell Renotation colorimetry. Example reflectances for two Munsell hue planes can be found in FIGURE 7.8 and FIGURE 7.9.

Two metrics from Chapter 4 were used to assess the effectiveness of using Wpt based spectral estimation for Munsell colors. These metrics were based only on spectral reflectances of the chips on the 40 hue planes. (Spectral reflectances for the neutrals and colors on intermediate planes were generated but not analyzed).

The metrics were arrived at by first computing a Wpt shift manifold for each chip in the 40 hue planes. The manifolds were determined using the same observers and illuminants used for Object Wpt shift manifold visualization used in Section 4.2 with 7128 points in each manifold. Mean Object Inconstancy Index (MOII) values were calculated from these manifolds, and an overall mean of the MOII values (MMOII) was determined to give an overall indication of the level of inconstancy for all the spectral reflectances analyzed. Additionally, Object Hue Similarity Index (OHSI) values were determined for each of the chips relative to the Value 5, Chroma 6 chip in each hue plane, and an overall mean of the OHSI values (MOHSI) was determined to give an overall indication of the level of hue similarity of chips in all the hue planes. The metric results for the actual measured reflectances and the Wpt Estimation reflectances using the characteristic hues in FIGURE 7.6 are found in TABLE 7.1.

TABLE 7.1. – Inconstancy and Hue Similarity Metrics for Munsell Reflectance Sets

	Mean Inconstancy (MMOII)	Mean Hue Similarity (MOSHI)
Actual Measurements	0.67	7.83
Wpt Estimation	0.55	2.67

These results are as expected in that the numbers for the actual reflectances are larger than the Wpt estimation reflectances. This is because the Wpt Estimation reflectances are based on

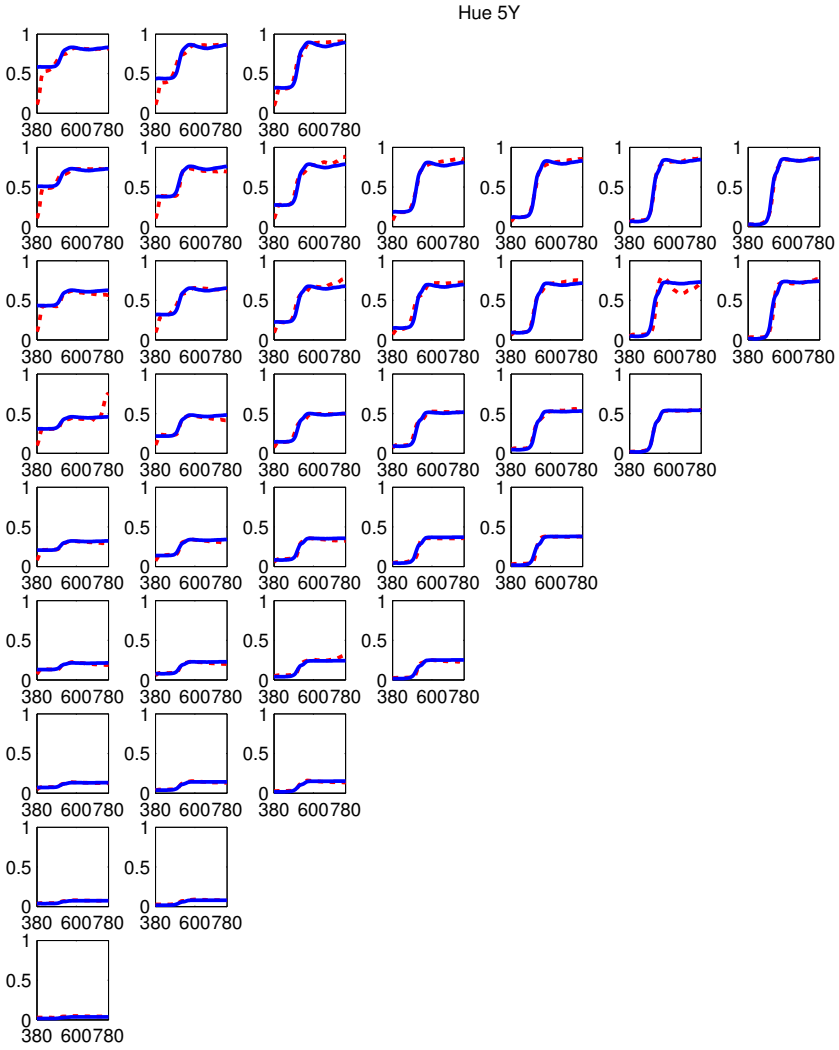

FIGURE 7.8. – Example Reflectances for Munsell 5Y Hue Plane – Actual Measured (red), Proposed Wpt based Spectral Estimation (blue)

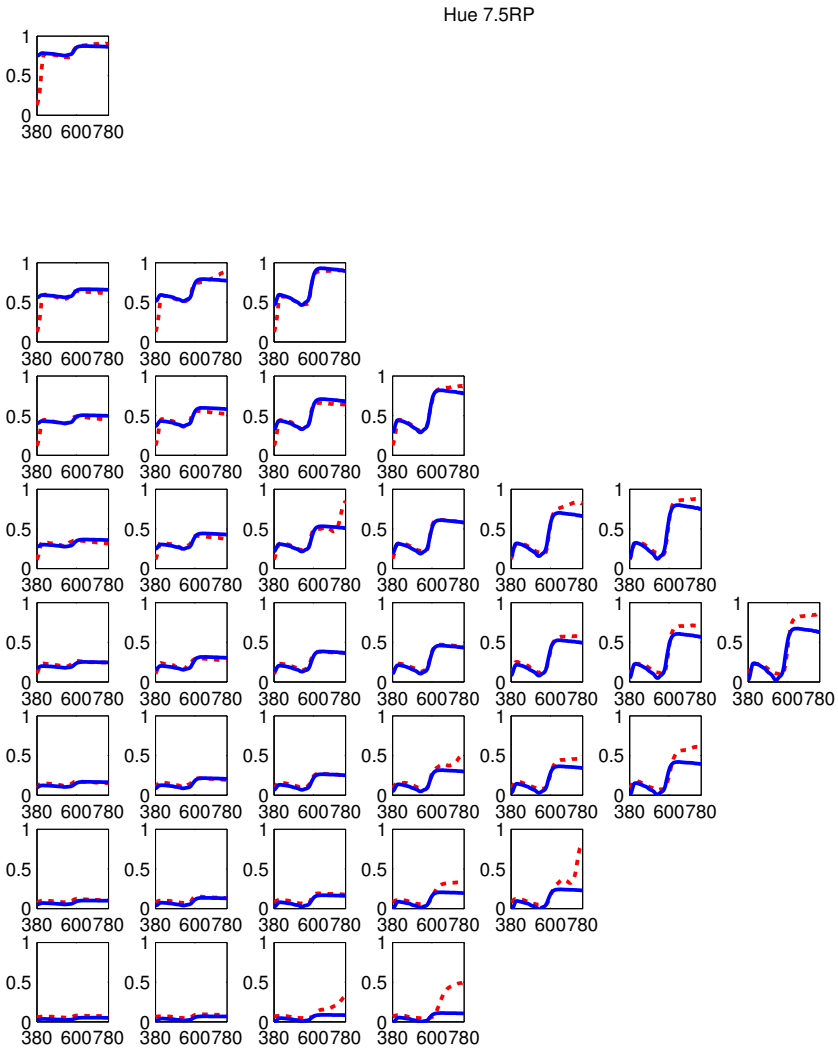

FIGURE 7.9. – Example Reflectances for Munsell 7.5RP Hue Plane – Actual Measured (red), Proposed Wpt based Spectral Estimation (blue)

nearly identical CRs for each hue plane, and each of the CRs were chosen to have low hue inconstancy.

Nevertheless, the reflectances of the two sets are still generally very close to one another. A visual example of the spectral reflectances is found in FIGURE 7.8 where only one chip in the 5Y hue plane, as well as in FIGURE 7.9 and several of the chips in the 7.5RP plane have significant differences. The differences are largely in the red and infrared regions of the spectrum where huge spectral differences are mostly imperceivable (except for cases where the illumination has a low CCT with high spectral power in those wavelengths).

7.4.2 Spectral Reflectance Manipulation

A standardized strategy for printing has been established that utilizes seven Reference Printing Conditions (RPC) used to define image exchange with associated colorimetry for virtual IT8.7-4 charts [ANSI-CGATS21-2, 2013]. These seven RPCs define progressively larger print gamuts for different printing conditions which are described in TABLE 7.2, and ICC color management is used to render to/from specific RPCs for the purpose getting more consistent results across all printing conditions [ANSI-CGATS21-1, 2013]. However, the RPCs are only defined colorimetrically, and spectral representations of these printing conditions are not available.

TABLE 7.2. – Reference Printing Condition data sets

Name	Description
RPC1	Universal ColdsetNews Small gamut printing (newsprint)
RPC2	Universal HeatsetNews Moderate gamut printing on improved newsprint type paper
RPC3	Universal PremUncoated Utility printing on a matte uncoated type paper
RPC4	Universal SuperCal General printing on super-calendared paper
RPC5	Universal PubCoated typical publication printing
RPC6	Universal PremCoated large gamut (typically commercial) printing
RPC7	Universal Extra large gamut printing processes

Spectrally defined printer characterization reflectances for the seven RPC were therefore generated for the purposes of this research by manipulating spectrally defined printer characterization reflectances from Actual CMYK Printing Conditions (APC) using an extension of the proposed Wpt based spectral manipulation approach described in Section 7.3.2. Both the RPC colorimetry as well as APC spectral measurement data from IT8.7-4 charts were provided to the author by M. Rodriguez (who established the colorimetry for the RPCs in the standard) [Rodriguez, 2013]. Rodriguez provided three APC data sets: “Hallmark" – representative of smaller uncoated gamut characterizations, “QuadSWOP3" – close to RPC4 and RPC5, and “MANRavg" – providing and average of several printed press sheets representative of RPC6 and RPC7. Plots of the IT8.7-4 spectral reflectances for these data sets are found in FIGURE 7.10. The reflectance curves for paper in both the “Hallmark" and “MANRavg" data sets have significant bumps near 440nm which is indicative of the use of optical brighteners [Bala and Zhao, 2007], while the paper reflectance curve for “QuadSWOP3" remains fairly flat.

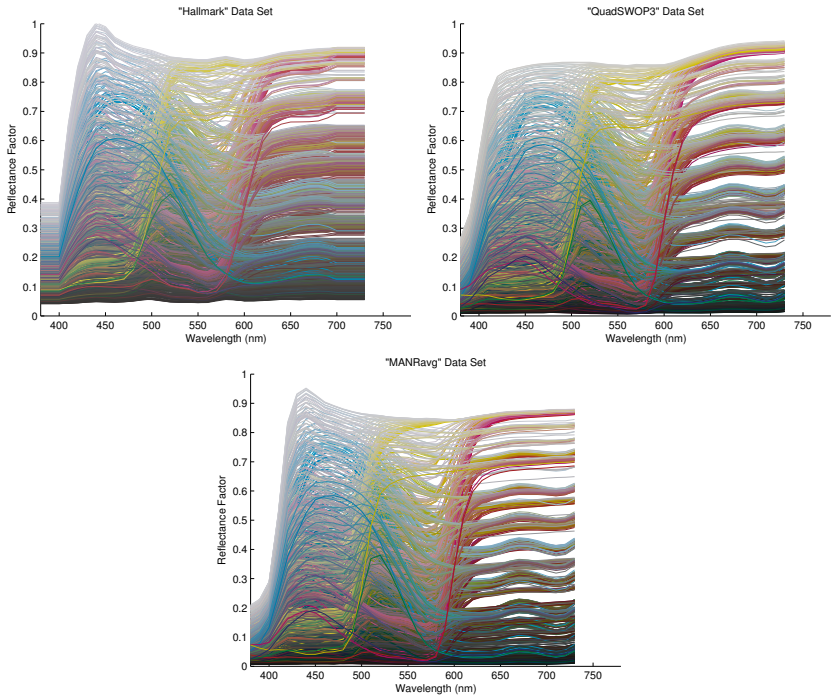

FIGURE 7.10. – Spectral Reflectances for Actual Printing Condtions provided by M. Rodriguez

The generation of spectral reflectances for RPC colorimetry can be accomplished in several ways depending upon the objectives set in place. A multi-stage approach was used to generate the reflectances in order to be faithful to the spectral characteristics of the papers involved as well as the basis reflectances. The first stage involved using a vonKries type scaling of spectral reflectances to adjust the reflectance of the paper to match that of the RPC conditions. A plot of typical spectral reflectances for each of the RPCs can be found in FIGURE 7.11. The second stage used a Chau-like Wpt based adjustment of these paper scaled spectral reflectances to match the lightness and chroma of the target colorimetry. The final stage adjusted hue by utilizing an association of Wpt hues to characteristic reflectances derived from the maximal chroma colors in the APC IT8.7-4 chart gamut or “gamut girdle." The combinations of characterization colorimetry, paper reflectance, and basis spectral reflectances used for generating for spectral reflectances for each RPC are outlined in TABLE 7.3.

The final two stages could possibly be performed as a single stage based solely upon gamut girdle CRs, but it was felt that the separation of hue adjustment from lightness and chroma adjustment allows for more of the spectral nature of the APC to be preserved. A more detailed description of the process is as follows:

1. Each of the APC spectral reflectances were scaled by multiplying by the representative spectral reflectances of the RPC paper and dividing by the spectral reflectances of the APC paper resulting in scaled APC reflectances.

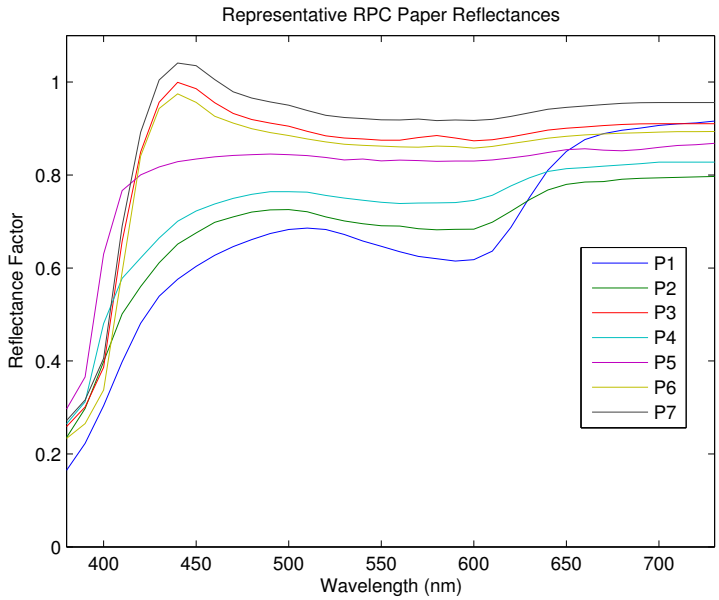

FIGURE 7.11. – Representative Spectral Reflectances for each RPC paper provided by M. Rodriguez

TABLE 7.3. – Combinations used to generate Reference Printing Condition spectral reflectances

Colorimetry	Paper	Basis spectral reflectances
RPC1	P1	QuadSWOP3
RPC2	P2	QuadSWOP3
RPC3	P3	Hallmark
RPC4	P4	QuadSWOP3
RPC5	P5	QuadSWOP3
RPC6	P6	MANRavg
RPC7	P7	MANRavg

2. The scaled APC reflectances were adjusted using the spectral gamut mapping framework to adjust only the lightness and chroma by defining the framework steps in the following manner. Wpt normalization is used as the means of defining color descriptions. The first spectral estimation step simply uses the starting spectral reflectance. The color description modification step uses the Wpt hue from the starting reflectance and the Wpt lightness and chroma of the target RPC colorimetry. The modified spectral estimation uses the CR of the starting reflectance curve and the target Wpt lightness and chroma with the Wpt based spectral estimation approach defined in Section 7.3.1.

3. The resulting spectral reflectances are further adjusted using the approach outlined in Section 7.3.1. The association of Wpt hue with CRs is based on the maximal chroma colors of the APC IT8.7-4 chart gamut or “gamut girdle" with interpolation of spectral reflectances used to define CRs for interim hues. Color descriptions and color description modification are both based upon Wpt Normalization. However, only the hue aspect of the spectral reflectance is adjusted based upon gamut girdle CRs. As a result, if hue is not adjusted then the final spectral reflectances are entirely determined by the CR of the paper scaled starting reflectances.

Resulting spectral reflectances for each of the RPCs are found in FIGURE 7.12. The colorimetry for each set of spectral reflectances is correct for the 2° observer under D50. The spectral reflectances for paper matches the general shapes in FIGURE 7.11, and the spectral reflectances are generally realistic matching the shapes of the basis reflectances in FIGURE 7.10. These RPC reflectances have been made available to M. Rodriguez for possible distribution.

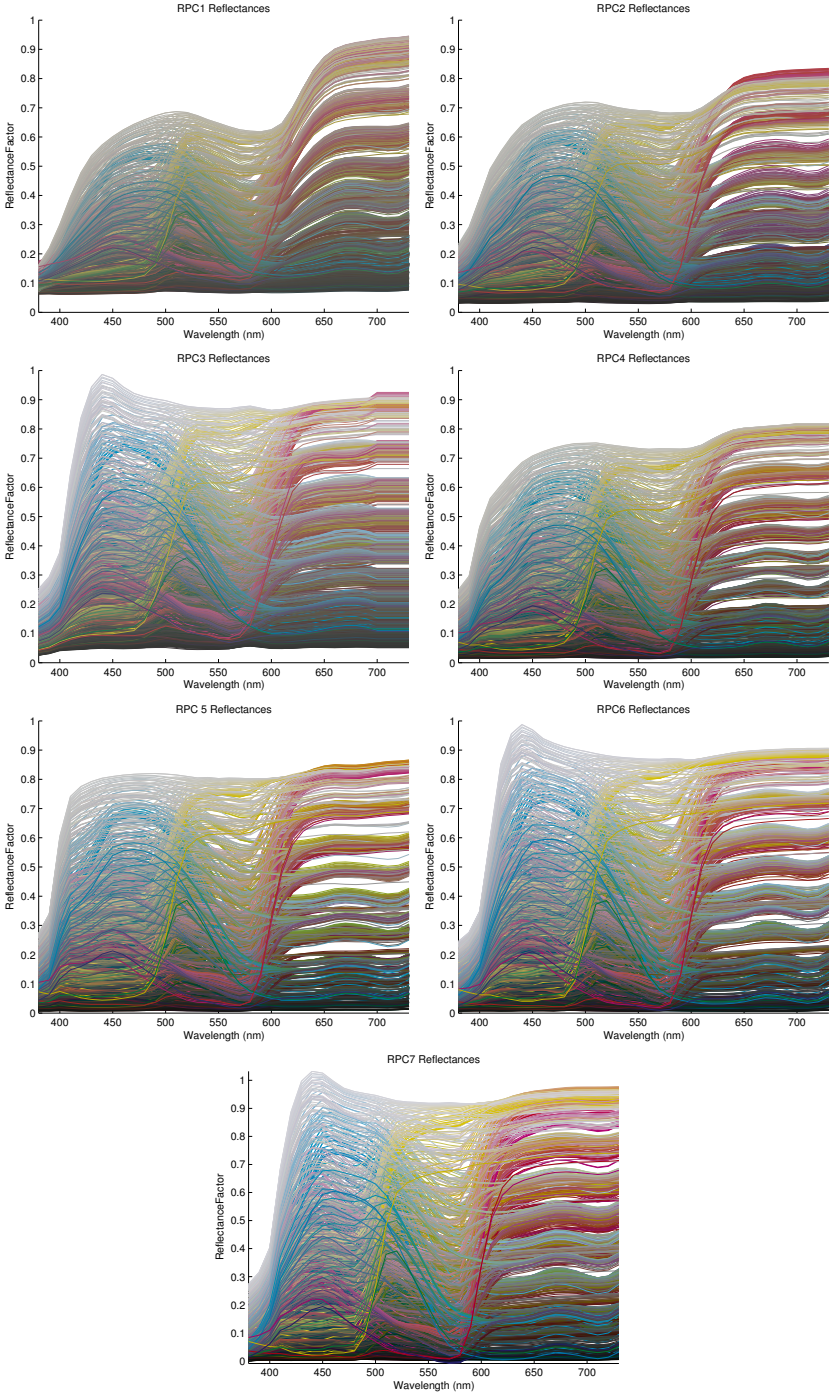

FIGURE 7.12. – Spectral Reflectances for each Reference Printing Condition (RPC) found by manipulating spectral reflectances from Actual Printing Conditions.

7.5 Applications using iccMAX

The International Color Consortium (ICC) is in the process of defining a new standard for encoding color profiles and defining color management workflows under the name “iccMAX" [ICC, 2015]. iccMAX provides a platform for defining spectrally based color management workflows with the ability to use spectrally based Profile Connection Spaces (PCSs) as well as flexibility to directly encode color transforms as programmable scripts. The reference implementation of iccMAX provides command line tools that allow for iccMAX profiles to be created and applied to TIFF images. Wpt normalization based techniques of spectral estimation and manipulation presented in this chapter as well as other Wpt based concepts defined throughout this dissertation are therefore directly applicable in the context of iccMAX based color profiles. The following is a (non-exhaustive) list of iccMAX based profiles and one legacy version 2 ICC profile that can be utilized in spectrally based image manipulation. (Note: Associated with each profile is an icon that will be used for describing sequences of profiles to apply in an iccMAX based workflow).

1.  An iccMAX input profile that is embedded in an image provides the transformational relationship between image pixel values and spectral or colorimetric PCS values. The examples provided in this section use an embedded iccMAX profile that provides an identity transform between the pixel values and spectral PCS values ranging from 400nm to 700nm in 10nm increments. Other input profiles (not presenty demonstrated) may provide modeling transforms that convert multi-spectral pixel capture data or pigment concentrations into spectral reflectance. Alternatively, spectral reflectance estimations from image pixel data could be encoded within the input profile. One example would be to use the spectral estimation technique from Section 7.3.1 where estimates of spectral reflectances for Munsell colors was performed.

2. 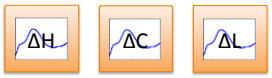

Several spectral manipulation iccMAX abstract profiles were created to manipulate spectral reflectances going from one spectral reflectance PCS to another. A CR was first determined within each profile for the incoming spectral reflectance vector, and Wpt coordinates are determined for the desired manipulation observing condition. These Wpt coordinates are converted to Wch, adjusted, transformed back to WCh and then used to adjust the spectral reflectances using the approach outlined in Section 7.3.2. Three separate spectral reflectance adjustment profiles were defined that independently adjust hue, chroma, or lightness.

3. 

Several abstract iccMAX profiles were generated that perform no change of color within a spectral reflectance PCS, and include Profile Connection Conditions (PCC) information that provides spectral data about the observer and illuminant for conversion of spectral reflectance to colorimetry as well as transforms

that convert to/from custom colorimetry to the standard PCS under a D50 illuminant for the 2° observer. The transforms to/from custom colorimetry were implemented using an identity matrix resulting in the illuminant specific colorimetry being utilized by the following profile.

4. 

Several other abstract iccMAX profiles were generated that also perform no change of color within a spectral reflectance PCS, and include PCC information that provides spectral data about the observer and illuminant for conversion of spectral reflectance to colorimetry as well as transforms that convert to/from custom colorimetry to standard D50/2° observer colorimetry. However, these transforms to/from custom colorimetry were implemented using Wpt based MATs that provide a material equivalency estimation of the changes in observing conditions.

5. 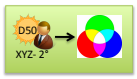

A legacy version 2 display profile was used that converts colorimetry from the standard PCS (D50 illuminant with 2° observer) to sRGB display values.

6. 
Alternatively, an iccMAX output profile can be used in an iccMAX color management workflow that takes spectral reflectance PCS values in and determines output device values that achieve spectral or spectrally preferred output objectives. (Note: Although an iccMAX output profile was not utilized as part of the spectral imaging visualization in this section it is important to note that the techniques presented throughout this chapter can be fully utilized in the creation and implementation of an iccMAX output profile).

The MetaCow image [Fairchild and Johnson, 2004], used for visualization in this research, is a synthetic spectral reflectance image that contains 3-dimensional renderings of cows in the form of a color checker that have metameric spectral reflectances under D65 for the Standard 2° observer for the head and the tail sections of each cow. The small format MetaCow image data was manipulated to enable various spectral manipulation visualizations by taking the pixel information and saving it as a multi-sample per pixel TIFF image with an embedded iccMAX profile that defines the relationships between the TIFF pixel samples and a spectral reflectance based iccMAX PCS. This spectral reflectance TIFF image was then used with the iccMAX reference implementation tools to create and apply various combinations of iccMAX and legacy ICC profiles for visualization purposes using the following illuminants: D65, Illuminant A, chromatic green, and chromatic blue. The illuminants were chosen to demonstrate the metameric nature of the MetaCows with the cows appearing uniform under D65, and non-uniform under the other the three other illuminants as they generally emphasize three different regions of the visible spectrum. The SPDs of these illuminants are plotted in FIGURE 7.13.

Five sets of visualizations were performed relative to the illuminants in FIGURE 7.13 using iccMAX profiles with the MetaCow image data to demonstrate various relationships between the methods

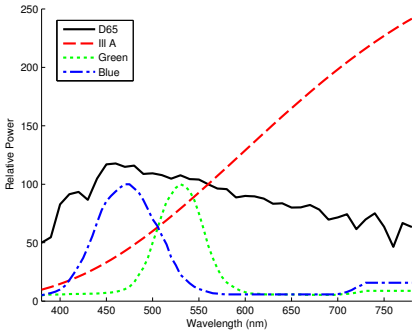

FIGURE 7.13. – Spectral reflectances of Metameric Blacks added using an iccMAX abstract profile.

proposed in this chapter. TABLE 7.4 contains the sequence of profiles used to get each of the images in FIGURE 7.14. In the process of applying iccMAX profiles to a spectral reflectance image, the illuminants were used to determine colorimetry that was passed into a version 2 ICC sRGB display profile to arrive at RGB values for visualization. This display profile uses a PCS based upon a D50 illuminant for the Standard 2° observer. Therefore the colorimetry resulting from applying the illuminants was determined by the Profile Connection Conditions used, and resulted in either direct illuminant relative colorimetry through the use of an identity conversion matrix (Absolute), or adjusted to D50 colorimetry using a Wpt based MAT (Wpt Normalized).

TABLE 7.4. – iccMAX profile sequences for images in FIGURE 7.14 with differences in PCC colorimetry adjustment between columns, and differences in illuminant between rows.

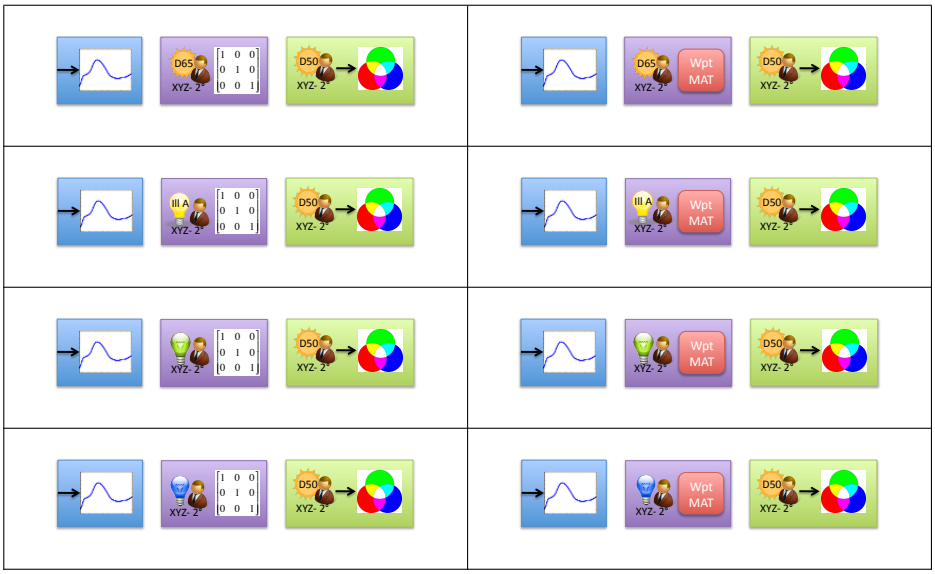

The following observations can be made of the profile sequences in TABLE 7.4 and the appearance of the cows in FIGURE 7.14:

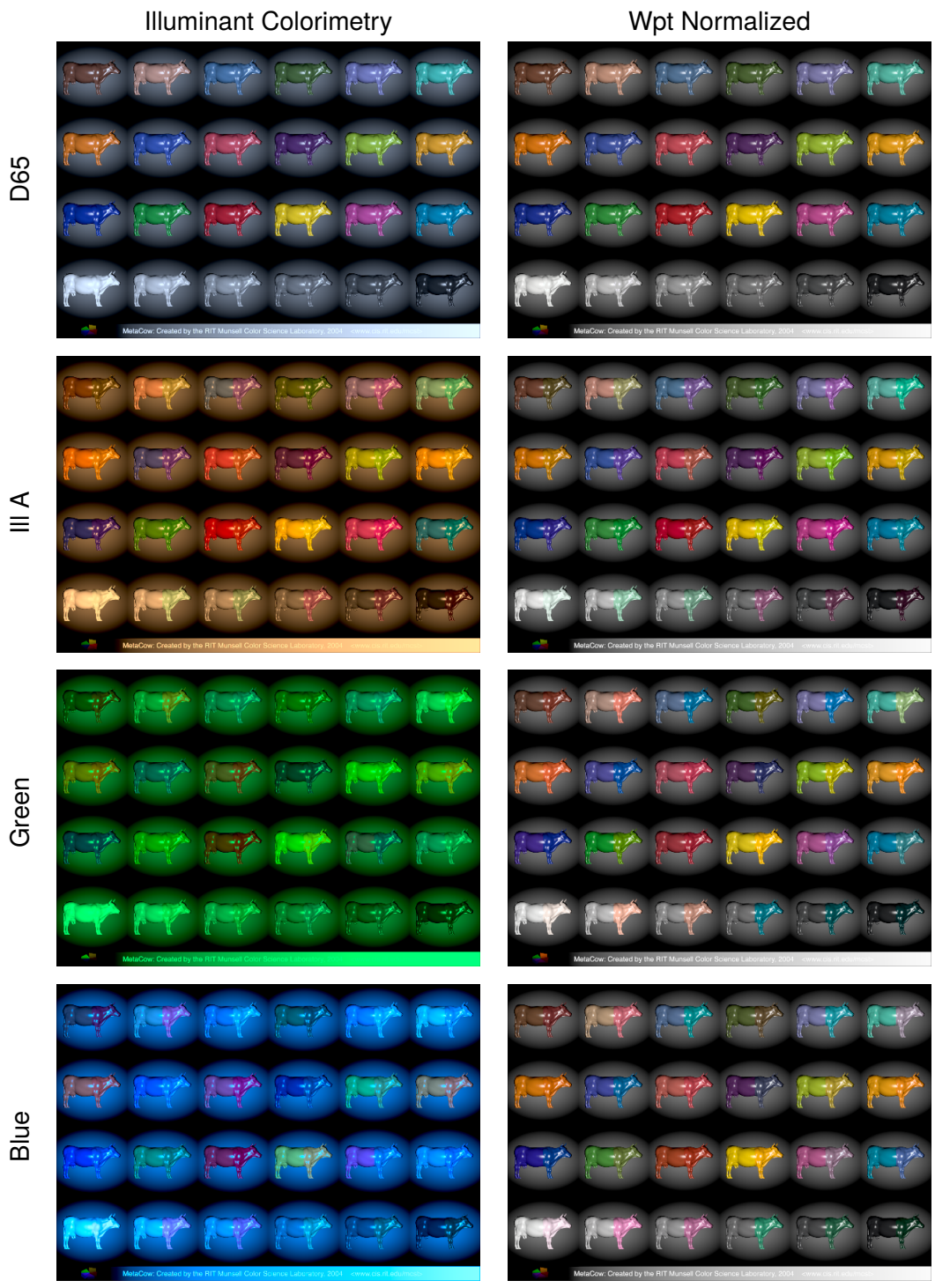

FIGURE 7.14. – Metacow visualizations under different illuminants using iccMAX. Using absolute colorimetry (left column), MAT adjusted to D50 (right column). Viewed under D65 (top row), Illuminant A (second row), chromatic green (third row), and chromatic blue (bottom row).

1. The eight different visualization images in the figure are all based on the same spectral reflectance image data. Differences occur as a result of applying the four illuminants as part of PCC processing and normalizing the colorimetry using a Wpt based MAT.

2. The metameric nature of the cows is clearly demonstrated as the apparent color of the head and tail sections of the cows changes under the different illuminants. There is no visible difference between the head and tail sections under D65, while many of the head and tail sections differ in appearance for the other three illuminants.

3. The relative relationship between the head and tail sections of the cows is generally preserved between the left and right images for each illuminant.

4. The normalization provided by the Wpt based MATs to adjust to D50 colorimetry results in a more uniform appearance of the images in the left column. This uniformity provides an easier means of comparing the relative inconstancies introduced by the application of the illuminants.

5. There is much greater consistency in the Wpt normalized images on the left between the tail sections of the cows than there is between the head sections of the cows. This may be indicative of the reflectances for the tails sections being closer to smooth shaped reflectances typical of real objects.

6. Some material color shifts occur due to color inconstancies of the spectral reflectances involved. This is especially true for the reddish or pinkish cows under the green and blue illuminants.

TABLE 7.5. – iccMAX profile sequences for images in FIGURE 7.15 representing different reflectance modifications under D65 illumination

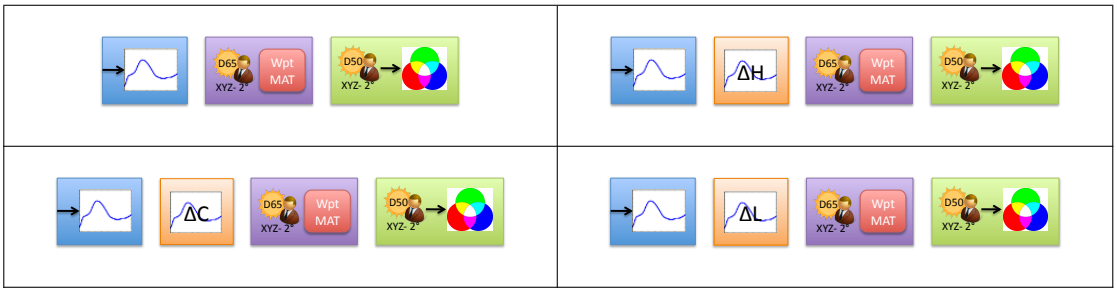

TABLE 7.5 contains the iccMAX profile sequences applied to achieve each of the images in FIGURE 7.15. These images provide a visualization of the original MetaCow image (upper right) compared to three spectral reflectance manipulations of the image provided by iccMAX abstract reflectance PCS profiles. In each case the modification to the spectral reflectances of the pixels has been made relative to D65 illumination under which the head and tail sections of the cows are metameric. Therefore, the changes apply equally to both sections of each of the cows. Additionally a D65 to D50 Wpt MAT was applied before applying the sRGB display profile for visualization in all four cases.

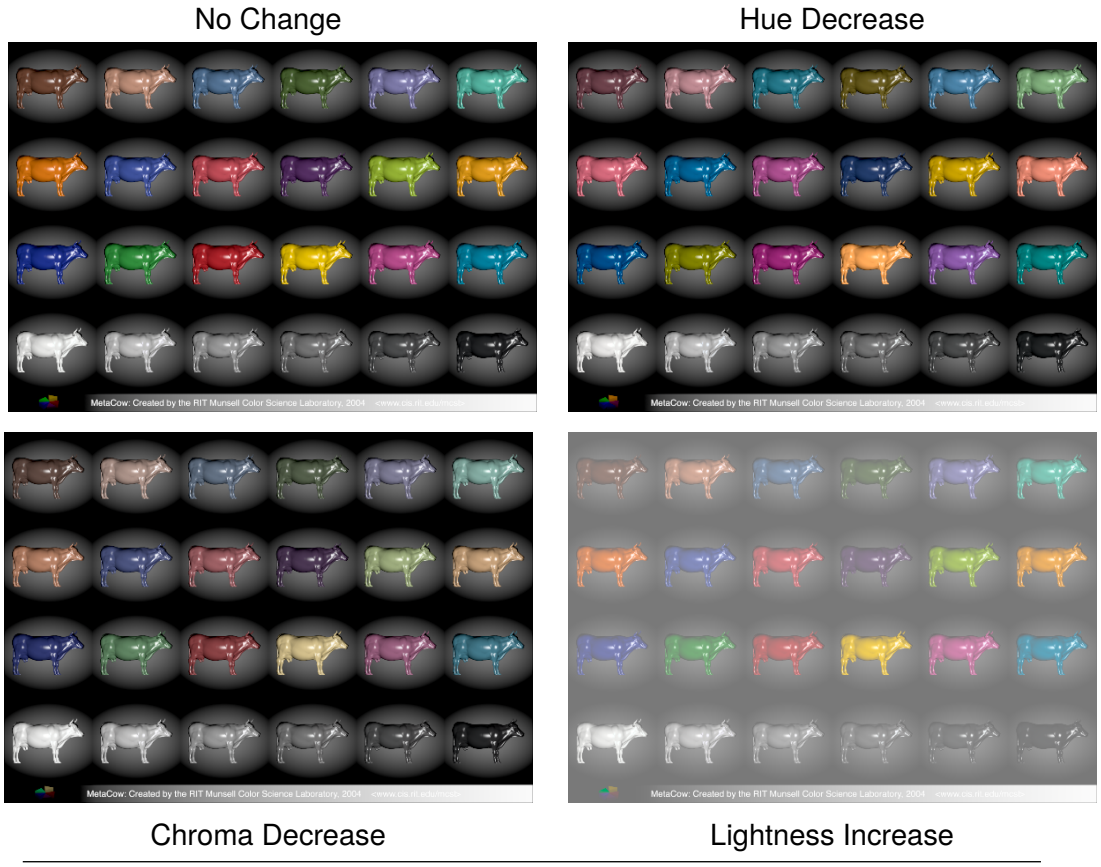

FIGURE 7.15. – MetaCow spectral manipulation visualizations under D65 with D50 Wpt MAT using iccMAX having no manipulation (upper left), decreasing hue (upper right), decreasing chroma (lower left), increasing lightness (lower right).

The upper right image had the spectral reflectances of the pixels modified by an abstract iccMAX profile that rotates the Wpt hue under D65 illumination counterclockwise by nine degrees. This results in the yellows becoming more orange, the oranges becoming redder, the reds becoming pinker, the pinks becoming more lavender, the purples becoming more blue, the blues becoming greener, and the greens becoming yellower. There is no change to the achromatic cows.

The lower left image had the spectral reflectances of the pixels modified by an abstract iccMAX profile that scales the chroma using the equation $C_{out} = 0.5C_{in}$ so that the chroma decreases under D65 illumination. As a result, the cows all appear to be less chromatic and closer to gray, and once again there is no change in the appearance of the gray scale cows.

The lower right image had the spectral reflectances of the pixels modified by an abstract iccMAX profile that scales the lightness using the equation $W_{out} = 0.8W_{in} + 0.2$ so that the apparent lightness under D65 illumination is uniformly increased. In this case the background along with all of the cows appear lighter, and there is a general decrease in overall contrast.

TABLE 7.6. – iccMAX Profile Sequences with spectrally based Hue adjustment for images in FIGURE 7.16 with differences in PCC colorimetry adjustment between columns, and differences in illumination between rows.

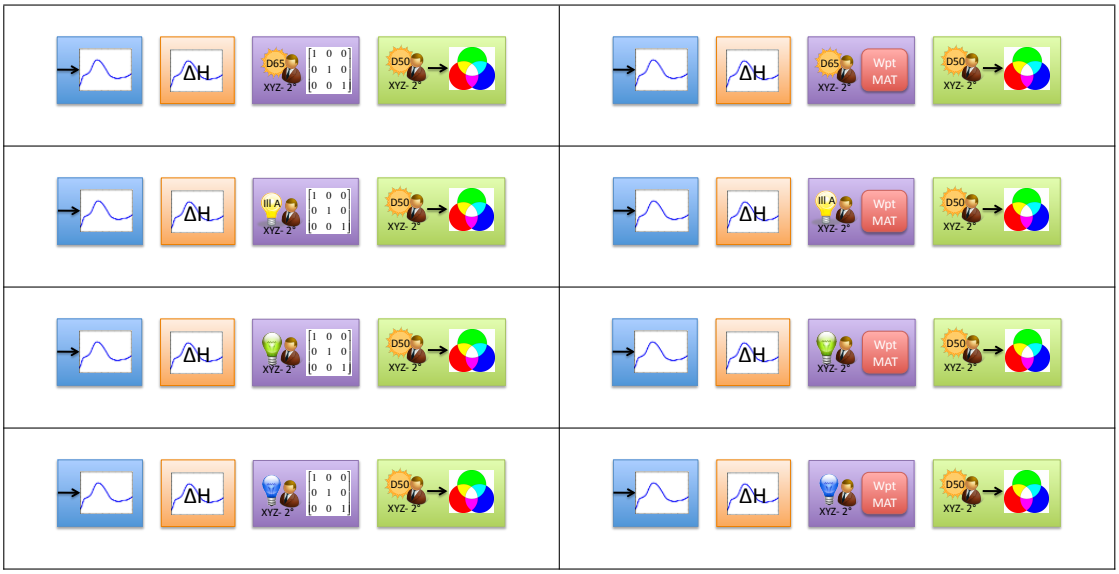

TABLE 7.6 contains the iccMAX profile sequences for each of the images in FIGURE 7.16 which represents various visualizations of the MetaCow spectral reflectance image with the same iccMAX profile that was applied in the upper right image of FIGURE 7.15. All of the images in FIGURE 7.16 therefore represent different visualizations of the same modified spectral reflectances that have decreased hue under D65 illumination.

It is evident in FIGURE 7.16 that the hue change is spectrally based (rather than colorimetric) because the general relationships of the apparent colors in FIGURE 7.16 are very similar to the relationships of the apparent colors in FIGURE 7.14. However, the tail sections of the cows in

the illuminant visualizations in the Wpt Normalized images on the left all appear to have the same hue adjustment as in the D65 visualization in the top row of the figure. The head sections maintain their distinct color shifts from the tail sections, and the hue adjustment does not seem to apply to shifts in color due to illuminant metamerism. This is exemplified by the fact that the color of the material shifts of the achromatic cows in FIGURE 7.16 is identical to the cows in FIGURE 7.14. In other words there is no hue change in any of the other illuminant visualizations where there is no hue change under D65 illumination.

TABLE 7.7. – iccMAX profile sequences with spectrally based modification of chroma for images in FIGURE 7.17 with differences in PCC colorimetry adjustment between columns, and differences in illumination between rows.

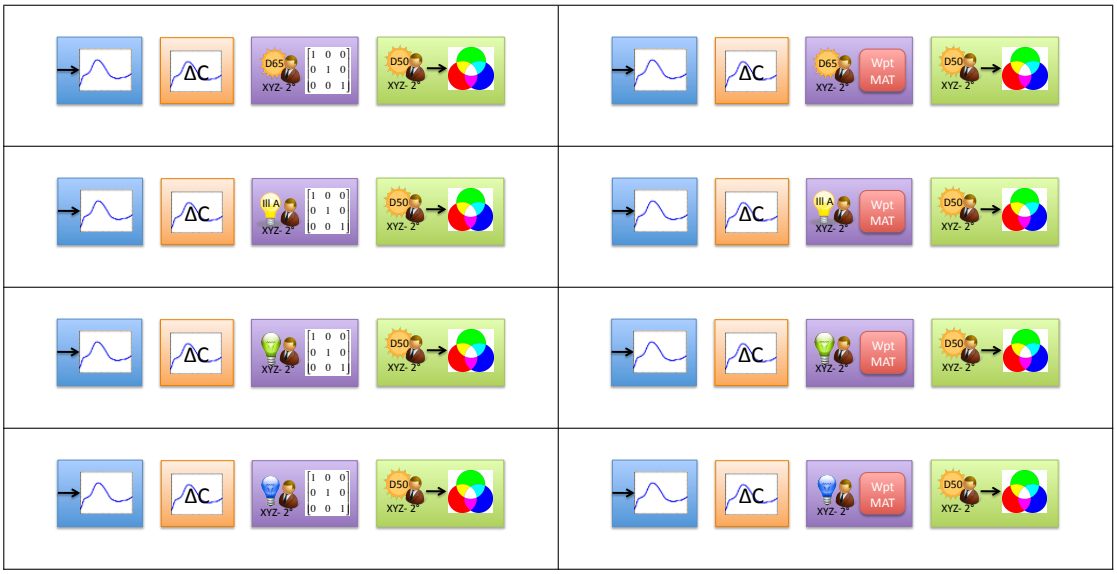

TABLE 7.7 contains the profile sequences for each of the images in FIGURE 7.17 which represents various visualizations of the MetaCow spectral reflectance image with the same iccMAX adjustment profile that was applied in the lower left image of FIGURE 7.15. All of the images in FIGURE 7.17 therefore represent different visualizations of the same modified spectral reflectances that have a decrease of chroma under D65 illumination.

It is evident in FIGURE 7.16 that the chroma change is spectrally based (rather than colorimetric) because the general relationships of the apparent colors in FIGURE 7.17 are very similar to the relationships of the apparent colors in FIGURE 7.14. However, the tail sections of the cows in the illuminant visualizations in the Wpt Normalized images on the left all appear to have the same chroma adjustment as in the D65 visualization in the top row of the figure. The head sections maintain their distinct color shifts from the tail sections, and the chroma adjustment does not seem to apply to shifts in color due to illuminant metamerism. This is exemplified by the fact that the color of the material shifts of the achromatic cows in FIGURE 7.17 is identical to the cows in FIGURE 7.14. In other words there is no chroma change in any of the other visualizations where there is no chroma change under D65 illumination.

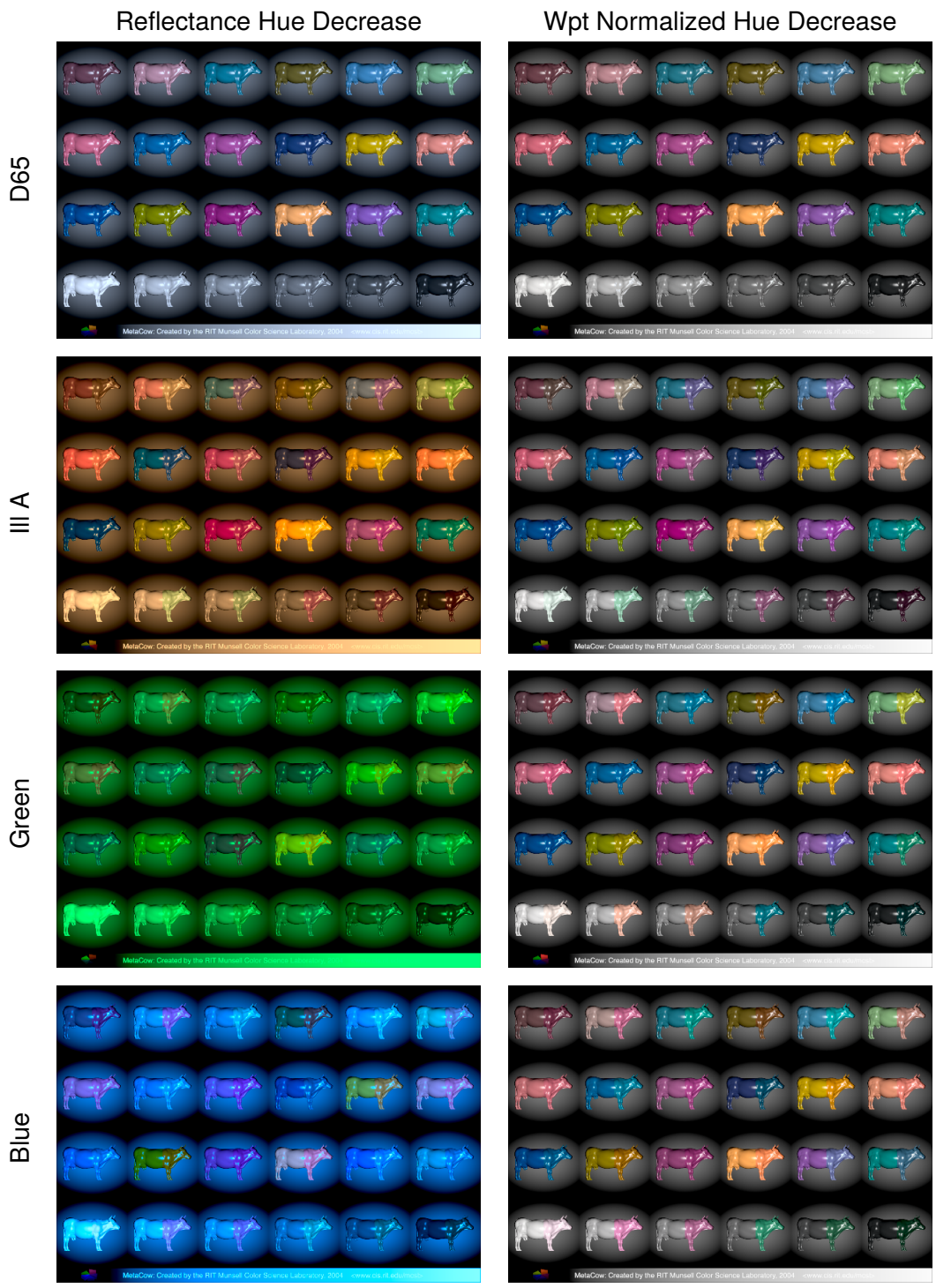

FIGURE 7.16. – MetaCow spectral reflectance hue decrease visualizations under different illuminants using iccMAX. Using absolute colorimetry (left column), MAT adjusted to D50 (right column). Viewed under D65 (top row), Illuminant A (second row), chromatic green (third row), and chromatic blue (bottom row).

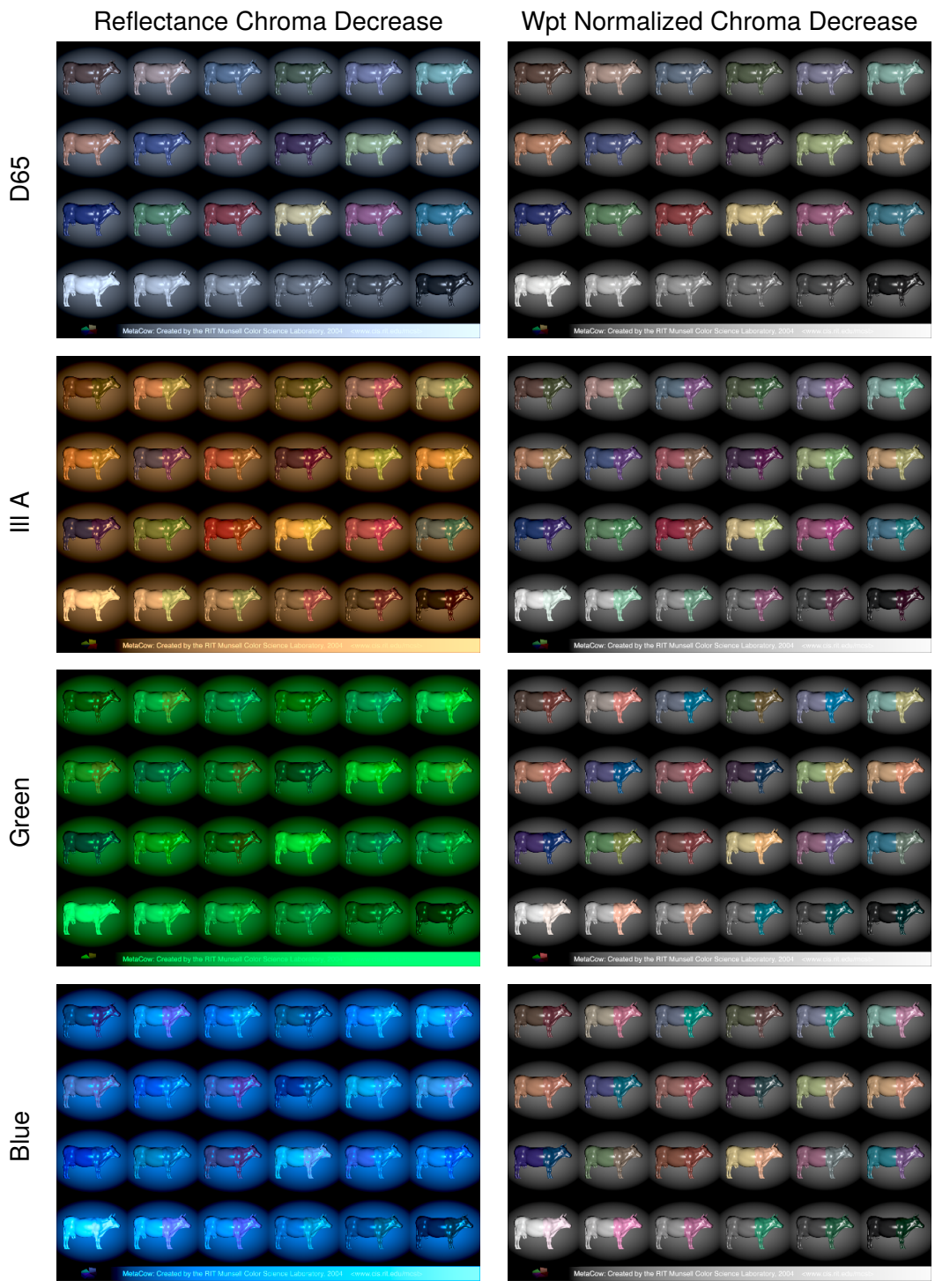

FIGURE 7.17. – MetaCow spectral reflectance chroma decrease visualizations under different illuminants using iccMAX. Using absolute colorimetry (left column), MAT adjusted to D50 (right column). Viewed under D65 (top row), Illuminant A (second row), chromatic green (third row), and chromatic blue (bottom row).

TABLE 7.8. – iccMAX profile sequences with spectrally based modification of lightness for images in FIGURE 7.18 with differences in PCC colorimetry adjustment between columns, and differences in illumination between rows.

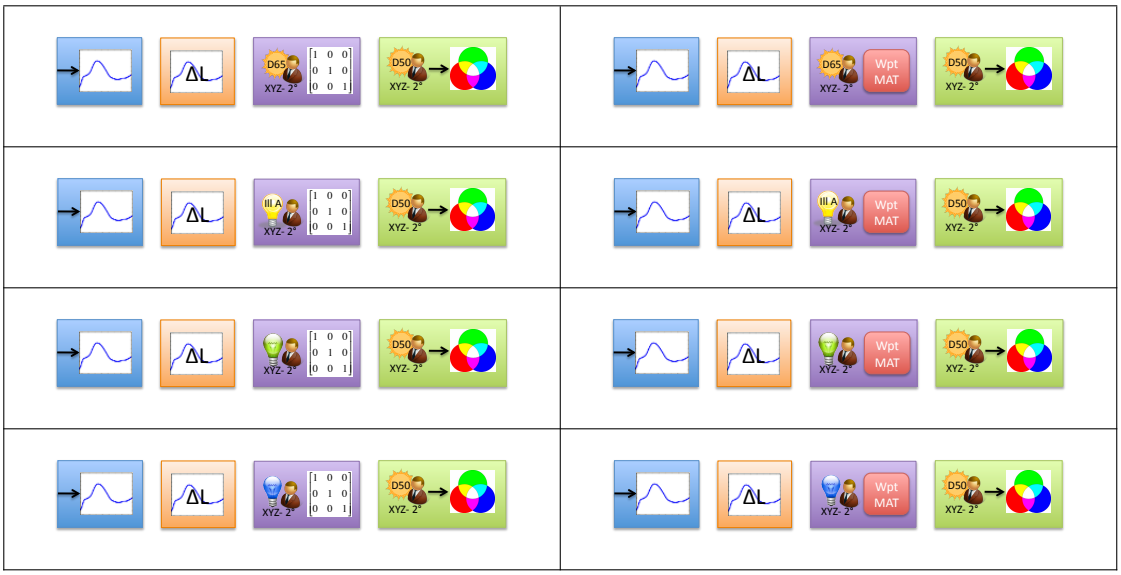

TABLE 7.8 contains the profile sequences for each of the images in FIGURE 7.18 which represents various visualizations of the MetaCow spectral reflectance image with the same iccMAX lightness adjustment profile that was applied in the lower right image of FIGURE 7.15. All of the images in FIGURE 7.18 therefore represent different visualizations of the same modified spectral reflectances that have an increase in lightness under D65 illumination. It is evident that the lightness changes are spectrally based (rather than colorimetric) because the general relationships of the apparent colors in FIGURE 7.18 are nearly identical to the relationships of the apparent colors in FIGURE 7.14.

The general conclusion from the figures and tables in this section is that the methods introduced in this chapter provide very useful tools for the purposes of implementing spectrally based color management systems using iccMAX. The realization of spectrally preferred color reproduction systems using iccMAX is therefore possible.

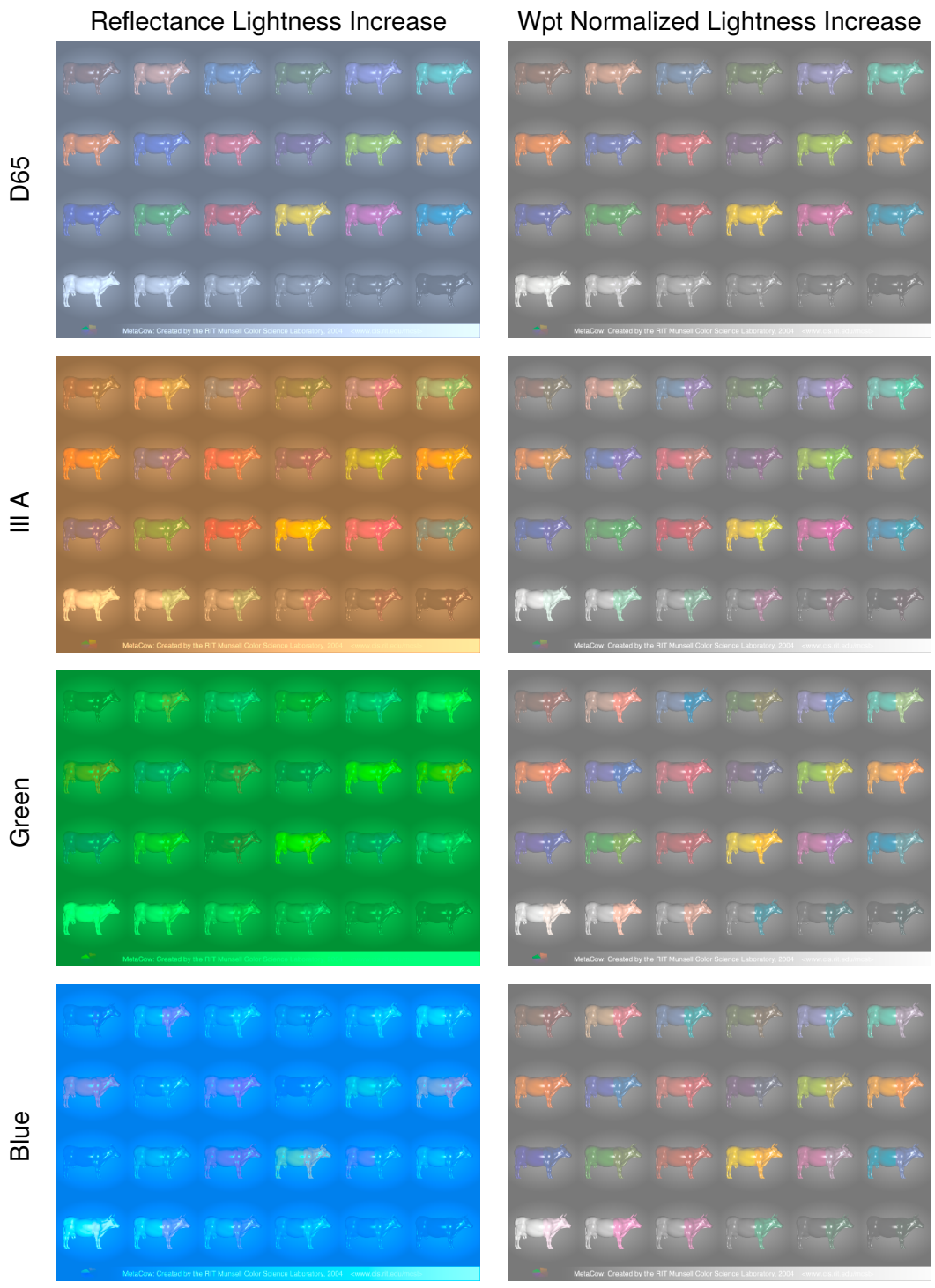

FIGURE 7.18. – MetaCow spectral reflectance lightness increase visualizations under different illuminants using iccMAX. Using absolute colorimetry (left column), MAT adjusted to D50 (right column). Viewed under D65 (top row), Illuminant A (second row), chromatic green (third row), and chromatic blue (bottom row).

7.6 Conclusions about Spectral Manipulation

As was mentioned in Chapter 1, the concept of spectral manipulation was the initial targeted focus of doctoral research in order to make key concepts of spectrally based color management (as represented by iccMAX) feasible. The general spectral manipulation framework outlined in this chapter can be applied to various approaches of spectral manipulation. However, Wpt based material color equivalency provides a means of defining relationships between perceptive aspects of color and spectral reflectance where both can be easily modeled and manipulated within the proposed spectral manipulation framework. As a result, several examples of spectral estimation and manipulation have been demonstrated – thus illustrating the feasibility and ease in which spectrally preferred image reproduction objectives can be accomplished.

8 Conclusions

The underlying basis of this dissertation is the concept of “Wpt Normalization", which represents an empirical approach to solving the problem of accounting for differences in sensor excitations of material colors due to changes in lighting and observer. It defines a material color equivalency representation that preserves the perceptive concepts of lightness, chroma, and hue. Thus, it provides a “Waypoint" for linearly adjusting sensor excitations of material colors from one observing condition to “equivalent" sensor excitations of other observing conditions. Resulting shifts in sensor excitations from such a transform are ascribed to non-linear relationships that exist between the surface reflectances, observer sensitivity functions, and spectral power distribution of the lighting.

Wpt is admittedly a poor predictor of the perceptual uniformity of material color differences because it is the result fo a linear transform of sensor excitations . Therefore, empirical non-linear modeling was applied to Wpt’s representation of colors to define invertible transforms into and out of a more perceptually uniform color representation designated as “WLab". Comparisons of colors with Euclidean WLab distances were shown to be statistically similar to existing color difference metrics like $\Delta E^{\star}{}_{94}$ and ΔE_{00}, and better predict "supra-threshold color difference experiments" under Illuminant A. However, since WLab is based on Wpt it inherits the property of also being a material color equivalency space. Thus, WLab distances are both meaningful and quantitative for describing differences in material color, observer color matching, illuminant rendering, and observing conditions.

The concept of a "Wpt shift manifold" was introduced which represents a set of Wpt points that vary due to differences in object, illuminant, and/or observer. Various color metrics were proposed comparing WLab points both within and between different manifolds. This resulted in the definition of various metrics of color including a color inconstancy index, paramer index, hue similarity index, illuminant color rendering index, observer color matching equivalency index, and observing condition equivalency index.

Methods of estimating appropriate Wpt normalization matrices based on sensor excitation values were proposed when a spectral understanding of the illuminant is not available or desired. The methods either use captured sensor excitations of training reflectances or model resulting Wpt sensor transforms for a variety of illuminants based on the sensor excitations of the illuminants. This allows for Wpt based operations to be utilized in cases where white balancing is normally utilized.

It was shown that Wpt normalization provides a prediction of the Luther-Ives condition which indicates the sameness of color matching of observers. Therefore, unlike other color spaces derived using standard observer Color Matching Functions, Wpt coordinates of material colors are the same regardless of whether Cone Fundamentals or Color Matching Functions are used to define the same observer. Therefore, the use of Wpt normalization based transforms was considered for the purposes of converting Cone Fundamentals into Color Matching Functions as compared to direct regression or preserving common color matching primaries. This is especially important when ascribing meaning to comparisons of sensor excitations from multiple observers with different color matching characteristics. An important question to keep in mind is "What is basis for defining the *sameness of color* from the sensor excitations?" It was shown that the basis for each of the methods reviewed varies, and Wpt is based on the "sameness of material color."

Because Wpt defines a material color equivalency space it provides an excellent starting point for defining relationships between spectral reflectance and sensor excitations. The works of Wyszecki and Chau were extended to define both a spectral estimation technique as well as a spectral reflectance manipulation approach using this technique within a generalized spectral reflectance manipulation framework. Domain specific knowledge is used to define characteristic reflectances for every possible Wpt hue. Conversion of Wpt coordinates to spectral reflectances use a linear transform of the hue based characterization reflectance based on Wpt chroma and lightness. Direct manipulation of spectral reflectance based upon manipulation of corresponding Wpt coordinates allows for the realization of a new color reproduction objective – Spectrally Preferred Reproduction. A demonstration of the proposed spectral estimation approach resulted in realistic spectral reflectances being defined for Munsell Renotation colors that have minimal overall color inconstancy with increased consistency of hue within Munsell hue planes. A demonstration of the proposed spectral manipulation strategy resulted in the manipulation of characterization spectral reflectances for actual printing conditions to derive characterization spectral reflectances for theoretical reference printing conditions. Finally, various Wpt based spectral image estimation, manipulation and adjustment techniques were presented within an iccMAX profile based color management system – thus demonstrating the power and flexibility which these techniques provide.

8.1 Future Work

The breadth of the material covered by this dissertation is admittedly large. As was asserted in the introduction, it represents the formulation of an entire ecosystem for defining, measuring and manipulating color based upon material color equivalency as provided by Wpt normalization. Therefore, many concepts have only been briefly touched upon with just introductory relationships established, and just mere thoughts expressed about how future research could be employed. The follow list is a summary of the concepts that can be further explored:

- Investigate various differences and applications between the use of existing CATs and MATs for sensor adjustment transformation, color system analysis, and color modeling (possibly using iccMAX based profiles).

- Investigate perceptual uniformity and application of WLab and LSWLab in relationship to actual imaging and color reproduction systems using visually based assessment.

- Investigate perceived differences in uniformity in areas where WLab and LSWLab make significantly different predictions of uniform steps from existing uniform color spaces (most notably for high chroma regions using visually based assesment).

- Investigate factors of color systems that result in material shifts, and how they cause shifts answering the question “What characteristics of spectral power distributions, reflectance curve shapes and observer sensitivities lead to material color shifts"?

- Investigate material color equivalency predictions and material shift manifolds for objects that exhibit fluorescence (since equations throughout this dissertation use a matrix to represent object reflectance).

- Investigate relationships between material color inconstancy metrics and visually perceived color inconstancy.

- Investigate relationships of proposed object shift manifold metrics and color difference tolerances in relation to imaging and applications of color reproduction.

- Investigate relationships and differences between existing illuminant color rendering metrics and the proposed Illuminant Shift Manifold based Illuminant Rendering Equivalency metric.

- Follow up on results found in FIGURE 4.16 indicating greater observing condition equivalency under mesopic conditions with rod sensor values included in Wpt normalization than photopic conditions without rods. Compare corresponding color results under mesopic and photopic viewing conditions.

- Generate physical realizations of the targets defined in Section 5.3 with special attention to ensure Wpt W value is accurately achieved.

- Utilize Generated Direct Wpt target to characterize/color correct cameras, and compare with other methods.

- Combine Direct Wpt normalization strategies with Computer Vision approaches to determine how Wpt Normalization improves/changes the results.

- Demonstrate differences in perceived experience and tristimulus values from adjusted cone fundamentals. Perform color matching experiments of high chroma colors for different observers' using their custom cone fundamentals found using on Asano's color categorization methods [Asano, 2015] to compare tristimulus values resulting from different methods of converting the cone fundamentals to XYZ-like color matching functions.

- Implement spectral reproduction iccMAX profile using Wpt based spectral manipulation to perform gamut mapping. Compare and contrast results with equivalent colorimetric based gamut mapping approaches.

From a conceptual standpoint, there is a fundamental question that has been hinted at, but has essentially not been addressed or explored to any great extent in this work. It is "What relationships can be established (if any) between Wpt normalization and the human visual system?" This can also be expressed as "What are the relationships between material color equivalency and visual appearance/corresponding color results"?

Wpt normalization is an empirical approach that normalizes spectrally derived sensor excitations of key material colors with assigned perceptive qualities for specific observing conditions. This has conceptual parallels to chromatic adaptation, color appearance, and perception modeling with differences being minimized due to changes in viewing conditions with the assignment of perceptive aspects of color. Additionally, “memory colors" are used as a means of determining the nature of the adjustment/adaptation.

There is some experimental basis behind Wpt and WLab which is found in the psychophysical work underlying the Munsell Renotation and definition of color difference equations, but the experimental basis for quantifying relationships between Wpt normalization and visual appearance has yet to be performed. A possible approach for experimentally determining such relationships between material color equivalency (as provided by Wpt) and appearance (as provided by corresponding color experiments) was envisioned in the process of preparing this dissertation for final publication, and therefore the actual realization of such an approach is left as a future research endeavor. The following general concepts are involved:

- Generate physical realizations of the targets defined in Section 5.3 with special attention to ensure Wpt W value is accurately achieved.

- Utilize these physical targets to perform corresponding color experiments.

- Use Asano's color categorization methods [Asano, 2015] to establish field size appropriate observer specific cone fundamentals.

- Use Wpt normalization of observer sensor excitations of targets (based on SPD of viewing conditions, reflectances of target, and observer specific cone fundamentals) to determine observer specific sensor excitation to Wpt normalization matrix for reference viewing conditions of corresponding color experiments.

- Experimentally establish sensor excitations of corresponding colors for each of the target colors. Use Wpt normalization of established corresponding color sensor excitation values to define an observing condition specific matrix that converts corresponding color sensor excitation data to Wpt coordinates. This should represent a conversion/correction between material color equivalency and corresponding color for the two viewing conditions witnessed by the observer.

- Concatenation of a Wpt normalization matrix providing transform from reference sensor excitations to an inverse of the matrix transform from corresponding color sensor excitations to Wpt should represent a CAT that predicts corresponding color data.

- Perform this experiment for lots of different viewing conditions, and for lots of different observers.

- Determine whether there is any generalizations that can be applied to the results.

- Compare this method with existing methods of defining Chromatic Adaptation Transforms.

One significant difference between Wpt normalization and existing vision and appearance models is in the relationship of normalization/adaptation and the definition of lightness and color opponency. Generally, vision and appearance models consider adaptation and the definition of lightness and color opponency as separate steps with a fixed definition of lightness and color opponency in relation to sensor excitations. However, with Wpt normalization, an adjustment process is applied separately to the perceptive concepts of lightness, chroma and hue resulting in the definition of lightness and opponency being both variable and defined by the observing conditions. Could this possibly be something that the visual system does as well? The proposed approach outlined above may provide insight into answering this question.

It is conceivably possible that various relationships could be identified, and then color appearance models could be defined based upon transformations of Wpt (or something similar) with non-linear transformations similar to those used to derive WLab to define appearance correlates. For now, such relationships and transformations can only be considered as possibilities. However, even without such relationships being firmly established, the concepts of material color equivalency provided by Wpt normalization and its applications are believed to be extremely useful and potentially profitable for imaging applications.

A Correcting Measured Spectral Reflectances to Match Munsell Renotation Data

A.1 Overview

The spectral reflectances for the Munsell glossy data found in the UEF spectral database were analyzed and compared to the Munsell Renotation data, and discrepancies revealed. Two methods of correcting these differences were implemented: one that compensated for sphere geometry and the second that corrected the spectra using principles of batch correction. The latter method was most successful and from these corrected spectra, analyses were performed to evaluate the color inconstancy of the Glossy MBC when viewed under real illuminants quite dissimilar from illuminant C. These analyses revealed that significant improvements are possible in developing a physically-based MBC with improved color inconstancy.

A.2 Background

The Munsell color system was developed (starting in 1905) by A. H. Munsell to define color perceptions using the terms Hue, Value, and Chroma. In 1915, the system was first produced as the Atlas of the Munsell Color System. Experiments performed during the 1920s both improved the Atlas' visual uniformity and expanded its color gamut resulting in the 1929 Munsell Book of Color (MBC). The MBC was defined by its physical samples and as such, was equivalent to a spectrally-based color order system [Berns and Billmeyer, 1985]. With usage, the 1929 MBC was found to still lack visual uniformity and further visual experiments were performed during the late 1930s and early 1940s. This resulted in the Munsell re-notations [Newhall et al., 1943]. Of particular importance was that the system changed from a spectral system to a colorimetric system. Chromaticities and luminance factor for CIE illuminant C and the 1931 standard observer defined the Munsell system. Since the colorimetry was published in the Journal of the Optical Society of America, the Munsell system became public domain. Producing a collection of samples, such as the MBC, is within the commercial world, and the spectral data are not made available.

Joni Orava of the Color Research Laboratory at the University of Eastern Finland (UEF – formerly Joensuu University) has measured matte finish and glossy finish MBCs manufactured in 1976.

The spectrophotometer was a Perkin-Elmer Lambda 18 with an integrating sphere attachment. Specular excluded mode was used, matching the MBC's reference geometry. These data have been made available online[Orava, 2012] and have been used extensively in color and imaging research. However, the Lambda 18 is not identical to a GE Recording spectrophotometer (initially used for quality control when manufacturing the MBC),[Berns, 1982] and it is unlikely that any specific book would have identical colorimetry to the Munsell re-notation data because of manufacturing variability. Therefore, the published spectral reflectance data in the UEF data sets may not match the Munsell system.

The purpose of this research was to compare how well the spectral reflectances of the UEF Munsell glossy spectral data set corresponded to the colorimetry defined by the Munsell re-notation data set, implement a simple method of correcting for any differences found, and analyze color appearance aspects of the corrected spectral reflectances.

A.2.1 Methodology

The UEF spectral reflectance measurements (UEFSRM) of the 1600 glossy Munsell color chips were transformed to colorimetry for the 1931 two degree standard observer under Illuminant C. Both the UEFSRM and the Munsell re-notation data (MRD) were converted to CIELAB and compared using the ΔE_{00}formula with overall results shown in Table 1, and a histogram of the color differences plotted in FIGURE A.1.

TABLE A.1. – ΔE_{00}Color difference statistics between UEFSRM and MRD

Minimum ΔE_{00}	Mean ΔE_{00}	Maximum ΔE_{00}	Standard Deviation
0.12	3.45	23.68	2.95

As can be seen from both Table 1 and Figure 1, there are significant colorimetric differences between the UEFSRMs and MRDs. A mean color difference of 3.45 indicates that the differences on the average will be noticeable with an extremely noticeable maximum difference. Only 43% of the color chips have a $\Delta E_{00}$of 2.0 or less.

To analyze how these differences affect the visual spacing, a visualization technique was developed to convert the colorimetry and color difference information into an understandable form. The colorimetric data were first chromatically adapted to D50 using CIECAT02[Moroney et al., 2002] and then rendered as a CIELAB tiff image ordered by both Munsell Value and Hue, shown in FIGURE A.2. For the Value slices, each gray background had the equivalent Value. Because our visual system has greater contrast sensitivity to luminance, we can see that certain regions have systematic differences in Value, e.g., the GY and Y region at Value 4 and 3.

False-color visualizations, ranging between 0 and 14+ in 1Δ unit-differences, were also made for ΔE_{00}, ΔL*, ΔC*ab, and ΔH*ab, shown in FIGURE A.3 and FIGURE A.4.

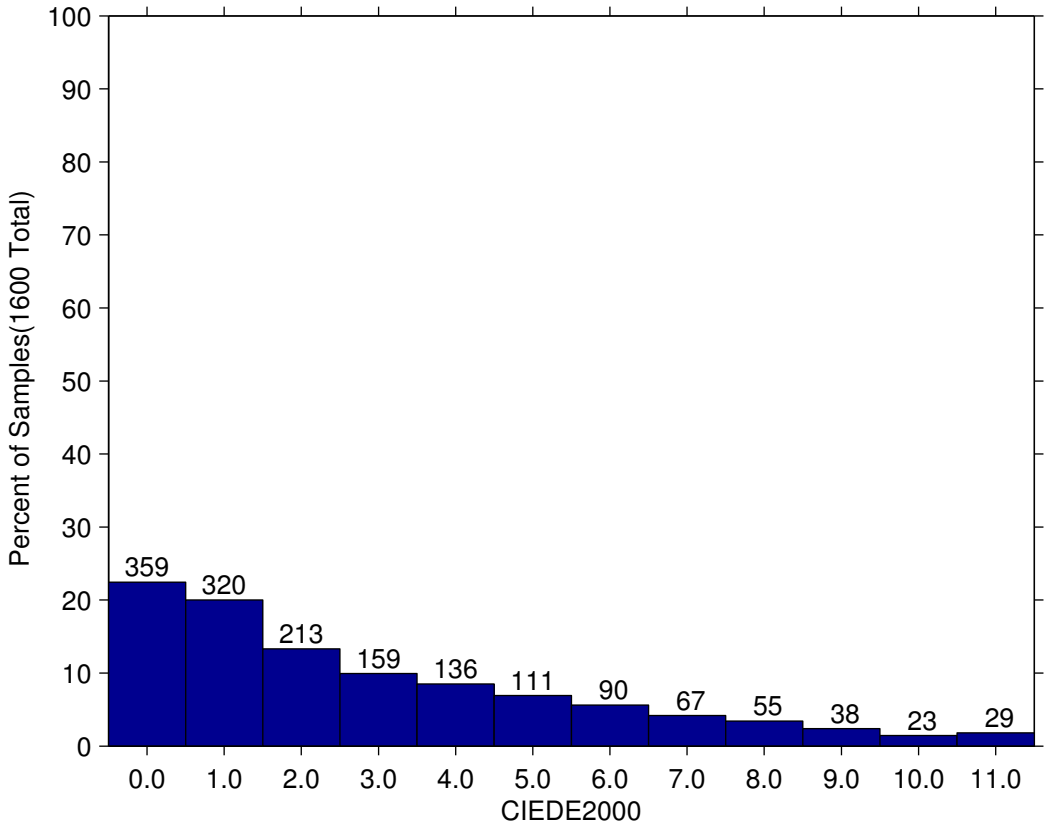

FIGURE A.1. – Histogram of ΔE_{00}color differences between UEFSRM and MRD

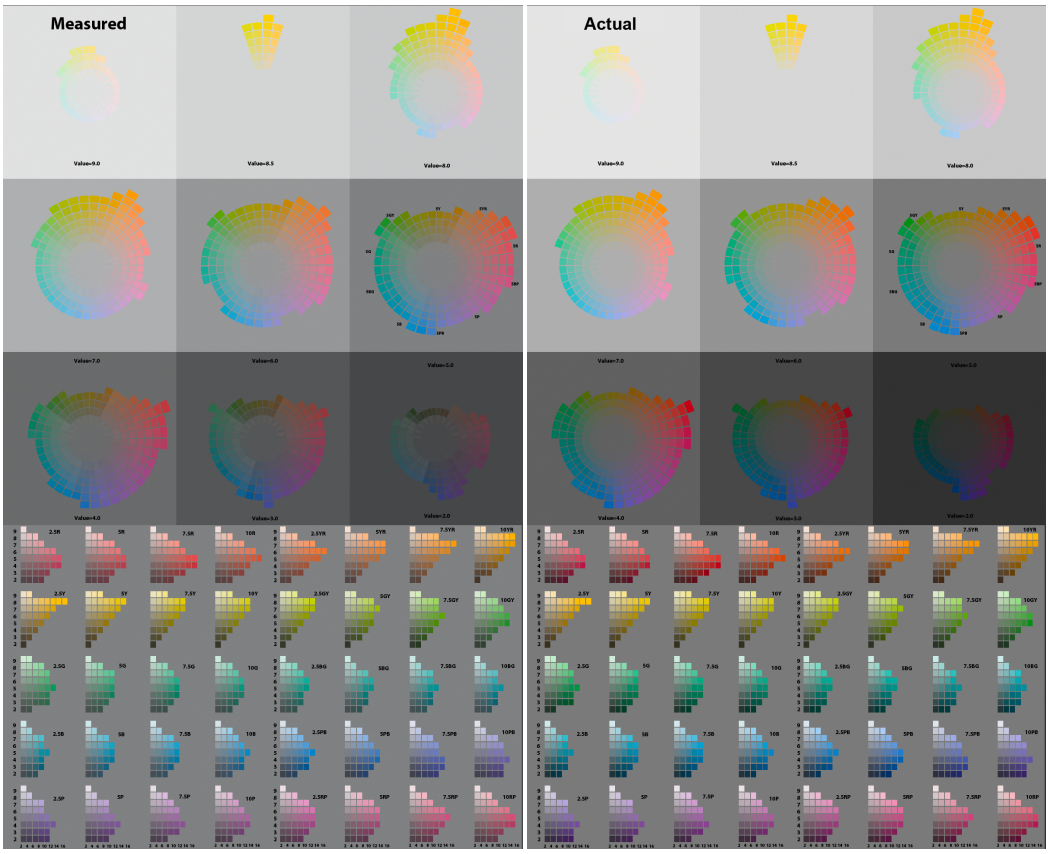

FIGURE A.2. – Image renderings using the UEF Spectral database (left) and Munsell re-notation data (right)

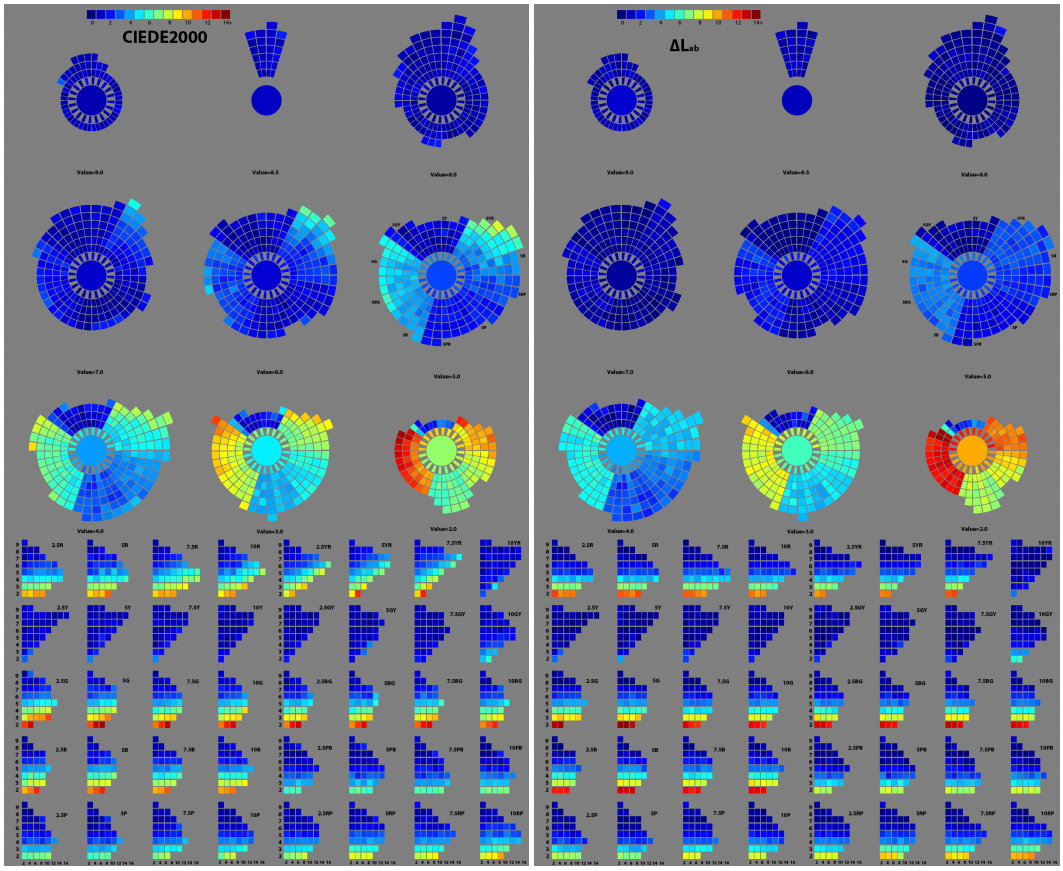

FIGURE A.3. – Color difference maps between UEFSRM and MRD with ΔE_{00}(left), ΔL*ab (right)

Most of the large color differences occurred for darker colors or more chromatic colors with small differences occurring as a result of hue shifts. Having large errors in lightness and chroma for dark colors is indicative of a difference in the specular port employed by the devices used to measure the colors and can be corrected by adding a small constant to the spectral reflectance [Berns and Peterson, 1988].

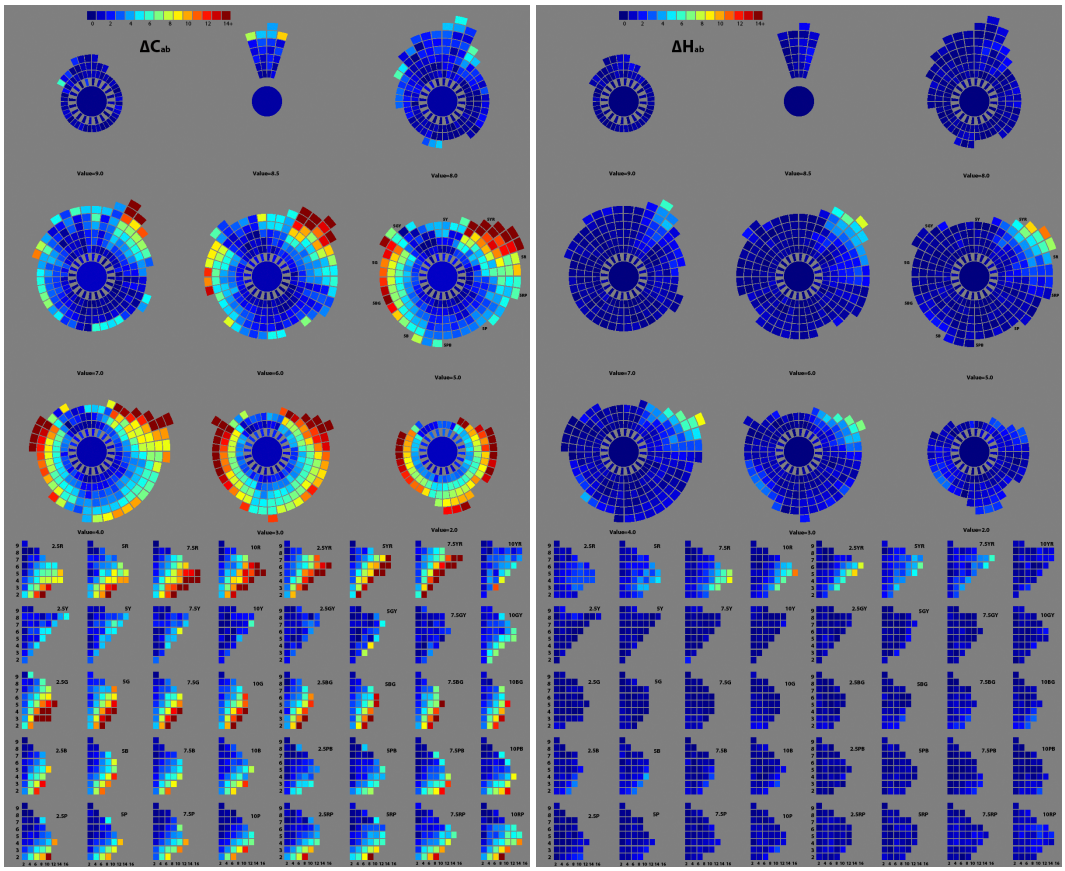

FIGURE A.4. – Color difference maps between UEFSRM and MRD with ΔC*ab (left), and ΔH*ab (right)

To test this, an optimization to find the best value for k in Eq. A.1 was performed (minimizing the average ΔE_{00}[Luo et al., 2001] between adjusted UEFSRM and MRD).

$$r_{adjusted,\lambda} = r_{measured,\lambda} + k \tag{A.1}$$

The optimization resulted in a k value of -0.0254, and the min, mean, max, and standard deviation of adjusted color differences to the MRD data are shown in TABLE A.2, and corresponding false-color visualization of the adjustments are shown in FIGURE A.5.

TABLE A.2. – Color difference statistics between adjusted UEFSRM and MRD colorimetry

Minimum ΔE_{00}	Mean ΔE_{00}	Maximum ΔE_{00}	STD
0.18	2.18	22.42	1.68

As can be seen from TABLE A.2 and FIGURE A.5, there is an appreciable improvement in the average color difference and standard deviation confirming that differences in sphere geometry was a large contributor. However, the maximum errors are still very large which is likely due to errors in manufacturing rather than other differences in spectrophotometers such as wavelength scale or bandwidth [Berns and Peterson, 1988].

A strategy was used that is similar to batch correction, commonly used in colorant formulation to completely correct for the differences [Allen, 1980]. The method involved deriving a pseudo-inverse-based matrix that estimates spectral reflectance from colorimetry:

$$\mathbf{E} = \mathbf{R}\mathbf{C}^{-1} \tag{A.2}$$

where $\mathbf{C}^{-1}$ represents the pseudo-inverse of a (3x1600) matrix of tristimulus values, $\mathbf{R}$ is a (401x1600) matrix of spectral reflectance, and $\mathbf{E}$ is the (401x3) estimated transformation matrix.

A plot of the $\mathbf{E}$ matrix is shown in Figure 6. The spectra are quite smooth, particularly at long wavelengths, and represent “pseudo-colorants."

The pseudo-colorants were used to batch correct the measured spectral data for each Munsell chip:

$$\mathbf{r}_{corrected} = \mathbf{r}_{actual} + \mathbf{E}\left(\begin{bmatrix}X\\Y\\Z\end{bmatrix}_{renotation} - \begin{bmatrix}X\\Y\\Z\end{bmatrix}_{actual}\right) \tag{A.3}$$

where $\mathbf{r}_{corrected}$ is a 401 element column vector representing the corrected spectral reflectance of the Munsell chip, $\mathbf{r}_{actual}$ is a 401 element column vector representing the actual UEFSRM of the Munsell chip, $\mathbf{E}$ is the (401x3) matrix derived using Eq. A.2, [XYZ]renotation is the MRD tristimulus values for the Munsell chip, and [XYZ]actual is the tristimulus values corresponding to $\mathbf{r}_{actual}$.

As can be seen from Eq. A.3, $\mathbf{r}_{corrected}$ will differ from the $\mathbf{r}_{actual}$ only by the amount that the renotation colorimetry differs from the actual colorimetry. Additionally, since $\mathbf{E}$ is derived directly from the UEFSRM data set it is believed that the characteristics of the estimated corrected

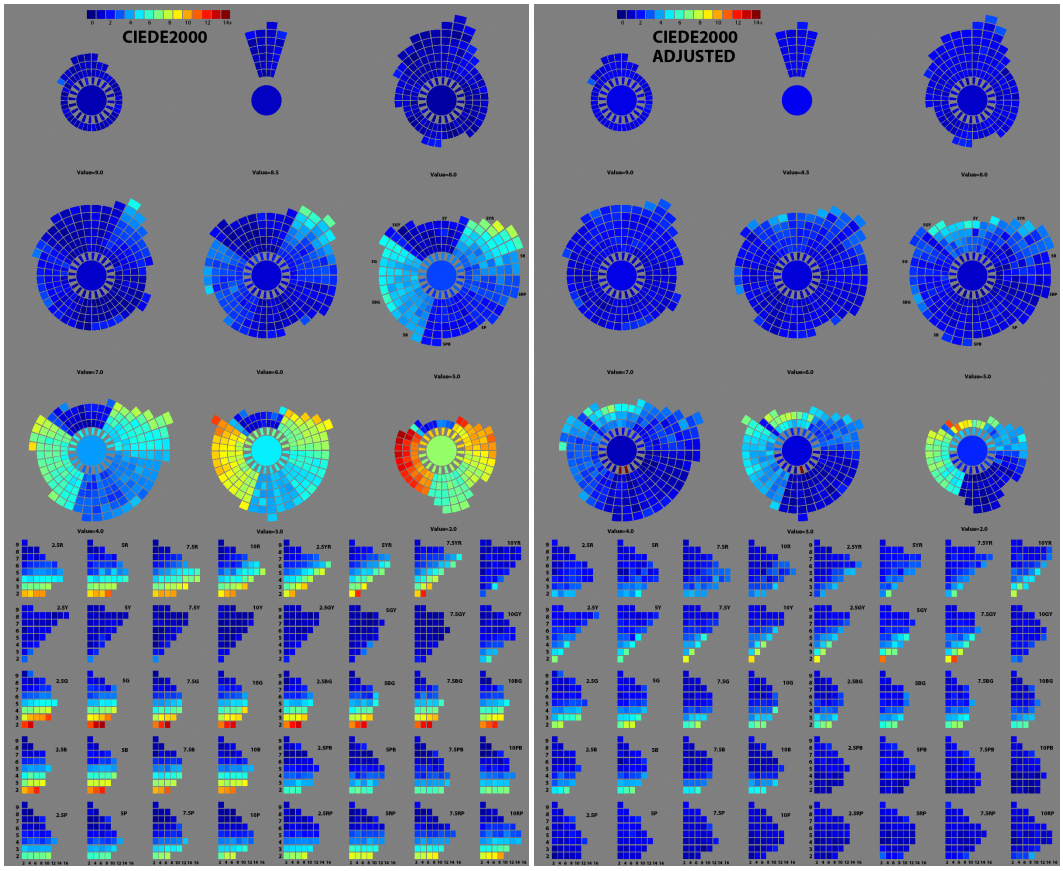

FIGURE A.5. – UEFSRM color difference (left), Adjusted UEFSRM color difference (right)

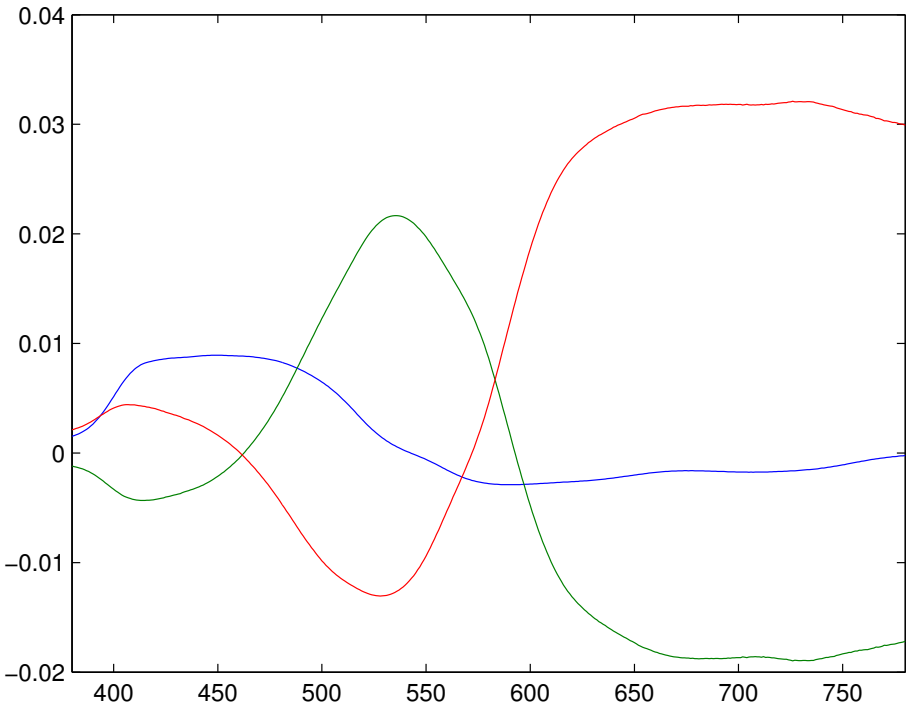

FIGURE A.6. – Pseudo “Colorants" associated with estimation matrix E from Eq. A.2

reflectances will correspond to realistic spectral reflectances. This method is similar to parameric corrections used for determining indices of metamerism [Li and Berns, 2007].

This is exemplified in FIGURE A.7 with UEFSRM and corrected spectral reflectance curves for a series of chips with a large variation in UEFSRM vs MRD colorimetric differences. In this plot curves corresponding to Munsell hue of 5G, chroma of 6 and varying value are depicted. (Note: These colors were picked because they exhibit the largest color differences in FIGURE A.5). Although a single correction factor is not implied by the corrections in FIGURE A.7, the bulk of the corrections have a magnitude of less that 0.05, and the general trends of the spectral reflectances are maintained.

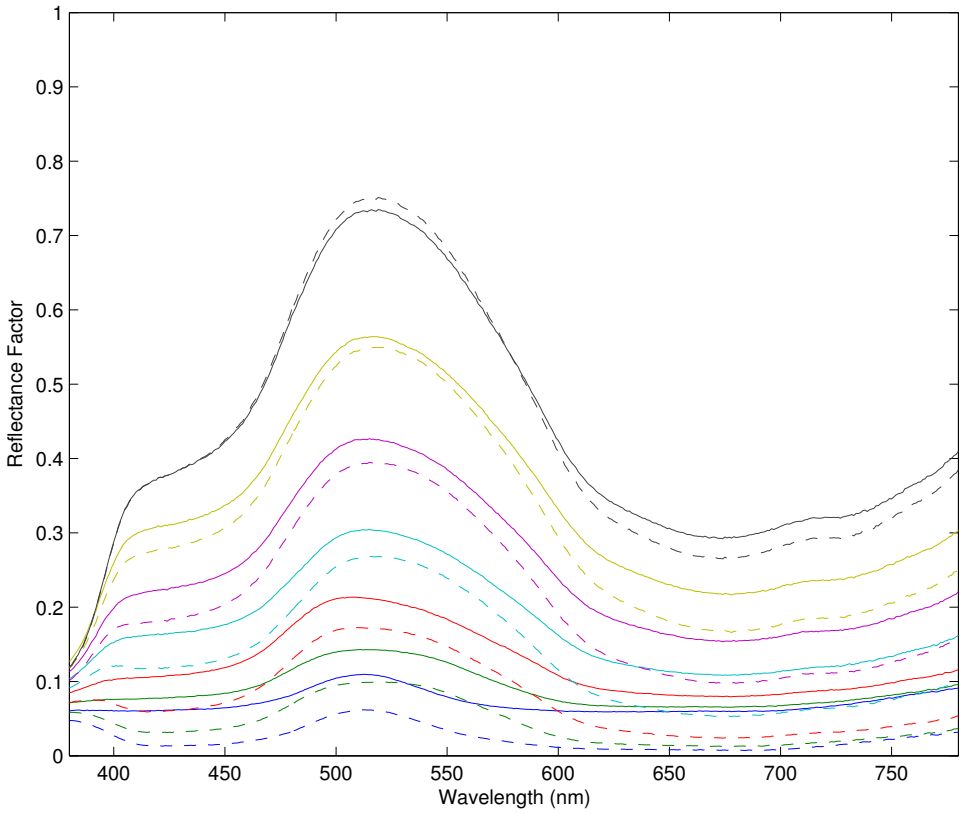

FIGURE A.7. – Spectral reflectance differences between UEFSRM data (solid) and corrected (dashed) for patches with Munsell hue of 5G and chroma of 6

With corrections to the UEFSRM result in spectral reflectances that match the MRD, however the next question one might ask is, "How well do these reflectances maintain the visual spacing of the MBC for sources other than illuminant C?" To answer this question, potential issues of color inconstancy for the corrected UEFSRM spectral reflectances were analyzed. Figure 8

contains a representation of the Munsell colors under 21 different illuminants (listed in Table 3) chromatically adapted to D50 using CIECAT02.

Each row represents chromatically adapted renderings of the Munsell colors with the same Munsell value for different illuminants. The illuminants used for rendering each column going horizontally from left to right across FIGURE A.8 are given in TABLE A.3.

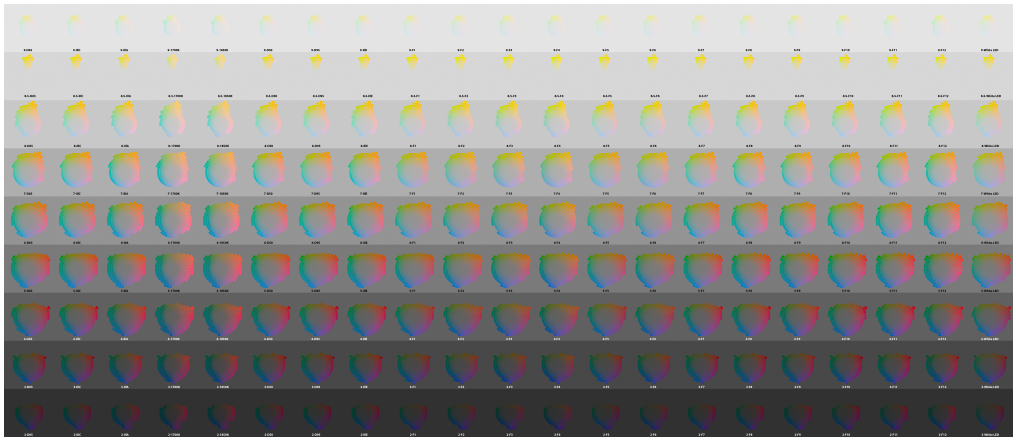

FIGURE A.8. – Adapted Representation of corrected UEFSRM data under 21 different illuminants

TABLE A.3. – Illuminants used to assess color inconstancy

1. D65	8. Illuminant E	15. F7
2. Illuminant C	9. F1	16. F8
3. Illuminant A	10. F2	17. F9
4. 1700K black body radiator	11. F3	18. F10
5. 1850K black body radiator	12. F4	19. F11
6. D50	13. F5	20. F12
7. D95	14. F6	21. Generic white LED

The normalized spectral power distributions for the illuminants used to render FIGURE A.8 are shown in FIGURE A.9.

In FIGURE A.10 an index of color inconstancy based on the corrected UEFSRM (using a CAT02 transform and $\Delta E^{\star}{}_{ab}$to calculate the CII)[Berns, 2000] for each color depicted in FIGURE A.8 was calculated (relative to D65) and rendered as a false-color map (with the same false color metric for steps as in FIGURE A.3).

As can be seen from FIGURE A.10 the illuminants that have a lower Correlated Color Temperature CCT[Wyszecki and Stiles, 2000] have the greatest CII factors for high chroma. There is some question as to whether this is an actual aspect of the color inconstancy or a limitation of the CAT used to accurately predict the corresponding color under the illuminant used to calculate color inconstancy.

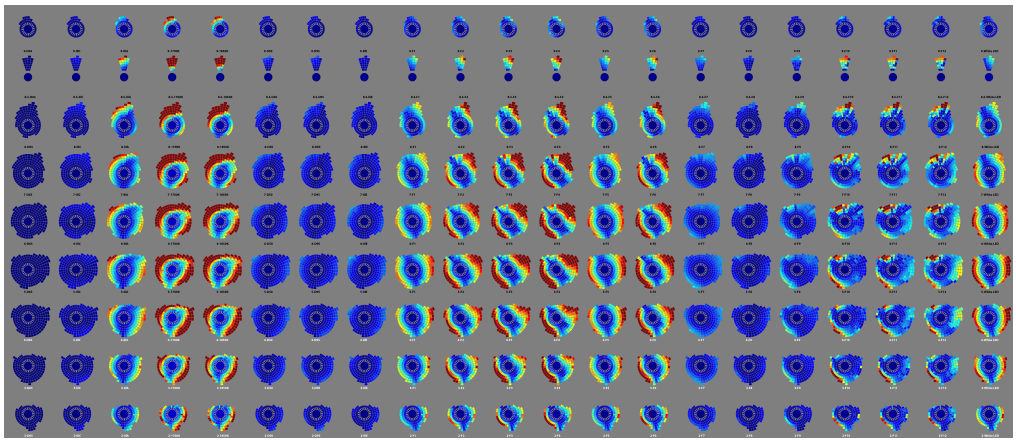

FIGURE A.9. – Normalized spectral power distributions used for calculating CII results

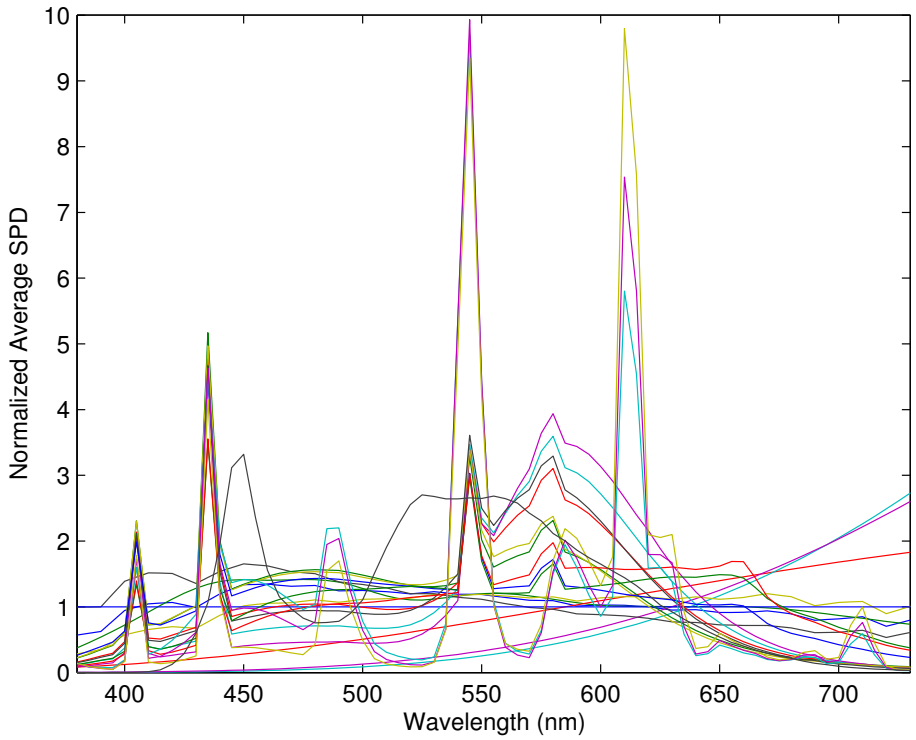

FIGURE A.10. – Color Inconstancy Index calculations for each color in FIGURE A.8

One area of concern from viewing FIGURE A.8 and FIGURE A.10 is the color inconstancy of the yellow and yellow-green regions. For some light sources (most noticeably F10 through F12) the color inconstancy doesn't have consistent transitions going from chip to chip. An example of this is depicted in FIGURE A.11.

As can be seen in this figure there is significant variability in the apparent hue for the spectral reflectances of the Munsell 5Y hue page under illuminant F11. Hue variability appears to be associated with variations in the general shape of the spectral reflectance curves. These relative shifts in hue are a result of changes in formulation of the 5Y page from this particular edition of the Glossy MBC. This is seen for 5Y 8/12 where its spectrum is very different from surrounding samples, resulting in an appreciable green caste compared with the other samples.

It is important to note that color constancy is generally not achievable for the MBC under all light sources using real colorants,[Berns et al., 1985] but if possible, it is desirable to have the relative relationships between the colors remain consistent with one another as their colors shift due to color inconstancy. An approach for this is discussed in Chapter 7.

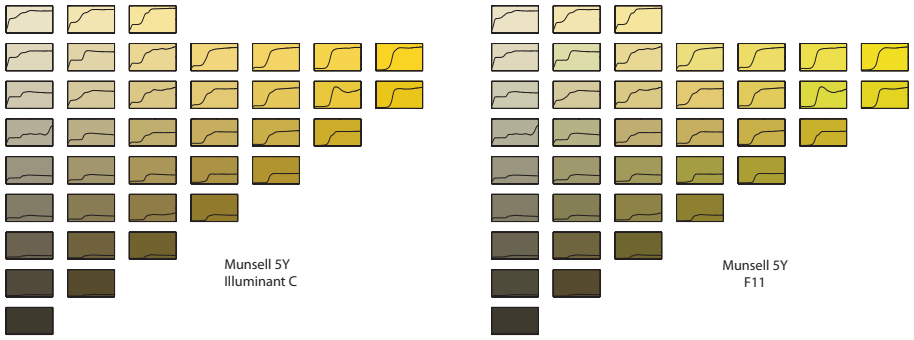

FIGURE A.11. – Appearance comparison of corrected UEFSRM curves for Munsell 5Y hue plane under Illuminant C (left), and F11 (right). Both were chromatically adapted to D65, with curves depicted for each Munsell chip ranging from 380nm to 780nm

Note:

The depicted figures as well as the corrected Munsell glossy spectral reflectances can be found at the following web location: http://www.cis.rit.edu/mcsl/research/CorrectedMunsellData.

B Conversions between Wpt and WLab

B.1 Conversions Introduction

The following equations provide the complete sequence of steps that can be used to convert between XYZ colorimetry and WLab. Excel spreadsheets and Matlab code that perform Wpt normalization in addition to these conversions, as well as visualization images with equally spaced WLab coordinates can be found at (http://www.rit.edu/cos/colorscience/re_WLab.php). Following these equations are numeric worked examples.

B.2 To convert from X, Y, Z to L_w, a_w, b_w:

First, determine/identify the observing condition specific Wpt normalization matrix **A** and use it in the following vector-matrix formulas to convert *X*, *Y*, *Z* to *W*, *p*, *t*:

1. Determine Wpt normalization matrix $\mathbf{A}$ for observing conditions

$$\mathbf{A} = T\left(\mathbf{C}, \mathbf{l}\right), \textit{(Defined in Chapter 2)}$$

2. Convert from XYZ to Wpt using Wpt normalization matrix $\mathbf{A}$

$$\begin{bmatrix} W \\ p \\ t \end{bmatrix} = \mathbf{A} \begin{bmatrix} X \\ Y \\ Z \end{bmatrix}$$

3. Convert W to L_w

$$\begin{aligned} W_n &= \tfrac{W}{100} \\ v &= \begin{cases} W_n^{1/3}, & \text{if } W_n > \left(\tfrac{6}{29}\right)^3 \\ \left(\tfrac{1}{3}\right)\left(\tfrac{29}{6}\right)^2 W_n + \tfrac{4}{29}, & \text{otherwise} \end{cases} \\ L_w &= 116v - 16 \end{aligned}$$

4. Convert p, t to polar notation c_{pt}, h

$$
\begin{aligned}
&c_{pt} = \sqrt{p^2 + t^2} \\
&h = \mathsf{tan}^{-1}\,(t, p)\,\tfrac{180}{\pi} \\
&\mathsf{if}\ \ (h < 0)\ \ \mathsf{then}\ h = h + 360
\end{aligned}
$$

5. Calculate chroma-lightness dependency coefficient based on L_w

$$
s = \frac{e^{(0.0267(L_w - 51.5762))}}{0.4589}
$$

6. Divide chroma-lightness dependency coefficient

$$
c_{mod} = \frac{c_{pt}}{s}
$$

7. Determine chroma adjustment coefficients based on h_{pt} and L_w

$$
\begin{aligned}
r_1 &= \begin{cases} [\mathsf{sin}\,(h-1)]^3\,, & \mathsf{if}\ h > 1\ \mathsf{and}\ h < 181 \\ 0, & \mathsf{otherwise} \end{cases} \\
r_2 &= \begin{cases} 0.39\,[\mathsf{cos}\,(h-14)]^2\,, & \mathsf{if}\ h > 104\ \mathsf{and}\ h < 284 \\ 0, & \mathsf{otherwise} \end{cases} \\
d_0 &= 62\,(r_1 + r_2 + 0.31) \\
d_1 &= 0.36\,(r_1 + r_2 + 0.19)
\end{aligned}
$$

8. Adjust chroma to have small-scale perceptual uniformity using chroma adjustment coefficients

$$
c_w = d_0 \left[\mathsf{ln}\left(\frac{c_{\mathsf{mod}}}{80} + d_1\right) - \mathsf{ln}\,(d_1)\right]
$$

9. *(Optional if LSWLab coordinates are desired) The following large-scale chroma difference conversion is performed*

$$
c_w = 80\left[e^{\left(\frac{C_w}{24.9523} + \mathsf{ln}(0.1104)\right)} - 0.1104\right]
$$

10. Convert from Polar coordinates to Cartesian coordinates

$$a_w = c_w \cos\left(h\frac{\pi}{180}\right)$$
$$b_w = c_w \sin\left(h\frac{\pi}{180}\right)$$

B.3 To convert from L_w, a_w, b_w to X, Y, Z:

1. Convert from Cartesian coordinates to Polar coordinates

$$c_w = \sqrt{a_w^2 + b_w^2}$$
$$h = \tan^{-1}(t, p)\frac{180}{\pi}$$
$$\text{if } (h < 0) \text{ then } h = h + 360$$

2. *(Optional if LSWLab coordinates being provided)* The following inverse large-scale chroma difference conversion is performed

$$c_w = 24.9523\left[\ln\left(\frac{c_w}{80} + 0.1104\right) - \ln(0.1104)\right]$$

3. Determine chroma adjustment coefficients based on h_{pt} and L_w (same as step 7 above)

$$r_1 = \begin{cases} [\sin(h-1)]^3, & \text{if } h > 1 \text{ and } h < 181 \\ 0, & \text{otherwise} \end{cases}$$
$$r_2 = \begin{cases} 0.39\,[\cos(h-14)]^2, & \text{if } h > 104 \text{ and } h < 284 \\ 0, & \text{otherwise} \end{cases}$$
$$d_0 = 62\,(r_1 + r_2 + 0.31)$$
$$d_1 = 0.36\,(r_1 + r_2 + 0.19)$$

4. Apply inverse of chroma adjustment to get small-scale perceptual uniformity using chroma adjustment coefficients

$$c_{mod} = 80\left[e^{\left(\frac{c_w}{d_0} + \ln(d_1)\right)} - d_1\right]$$

5. Calculate chroma-lightness dependency coefficient based on L_w

$$s = \frac{e^{(0.0267(L_w - 51.5762))}}{0.4589}$$

6. Multiply chroma-lightness dependency coefficient

$$c_{pt} = sc_{mod}$$

7. Convert L_w to W

$$v = \frac{L_w+16}{116}$$
$$W = \begin{cases} 100v^3, & \text{if } v > \frac{6}{29} \\ 300\left(\frac{6}{29}\right)^2\left(v - \frac{4}{29}\right), & \text{otherwise} \end{cases}$$

8. Convert from Polar coordinates to Cartesian coordinates

$$p = c_{\text{pt}}\cos\left(h\frac{\pi}{180}\right)$$
$$t = c_{\text{pt}}\sin\left(h\frac{\pi}{180}\right)$$

9. Determine Wpt normalization inverse matrix $\mathbf{A}^{-1}$ for observing conditions

$$\mathbf{A} = T\left(\mathbf{C}, \mathbf{l}\right), \textit{(Defined in Chapter 2)}$$

10. Convert from Wpt to XYZ using Wpt normalization inverse matrix $\mathbf{A}^{-1}$

$$\begin{bmatrix} X \\ Y \\ Z \end{bmatrix} = \mathbf{A}^{-1}\begin{bmatrix} W \\ p \\ t \end{bmatrix}$$

B.4 Worked example converting from X, Y, Z to L_w, a_w, b_w:

Starting values for D50 illuminant and 2° Standard Observer
X = 23.33, Y = 18.92, Z = 8.37

1. $\mathbf{A} = \begin{bmatrix} -0.06265 & 1.03839 & 0.02669 \\ 4.68561 & -4.82563 & 0.37293 \\ 0.28350 & 1.50053 & -2.15101 \end{bmatrix}$ (*Found using Wpt-Normalization.xlsx*)

2. W = 18.40, p = 21.14, t = 17.00

3. L_w = 49.99

4. c_{pt} = 27.12, h = 38.81

5. s = 2.0885

6. c_{mod} = 12.99

7. d_0 = 33.5053, d_1 = 0.1513

8. c_w = 24.42

9. (**LSWLab** c_w = 14.67)

10. a_w = 19.03, b_w= 15.31; (*LSWLab* a_w = 11.43, b_w = 9.19)

Resulting Values:

L_w= 44.99, a_w = 19.03, b_w = 15.31; (*LSWLab* L_w = 44.99, a_w = 11.43, b_w = 9.19)

B.5 Worked example converting from L_w, a_w, b_w to X, Y, Z:

Starting Values:

L_w = 44.99, a_w = 19.03, b_w = 15.31; (*LSWLab* L_w = 44.99, a_w = 11.43, b_w = 9.19)

1. c_w = 24.42, h = 38.81; (*LSWLab* c_w = 14.67, h = 38.81)

2. (*LSWLab* c_w = 24.42)

3. d_0 = 33.5053, d_1 = 0.1513

4. c_{mod} = 12.99

5. s = 2.0885

6. c_{pt} = 27.12

7. W = 18.41

8. p = 21.14, t = 17.00

9. $\mathbf{A}^{-1} = \begin{bmatrix} 0.96425 & 0.22325 & 0.05067 \\ 1.00000 & 0.10249 & 0.01458 \\ 0.82468 & 0.03814 & -0.44805 \end{bmatrix}$ (*Found using Wpt-Normalization.xlsx*)

10. X = 24.33, Y = 18.92, Z = 8.37

Resulting Values:

X = 24.33, Y = 18.92, Z = 8.37

Bibliography

[Adams, Parulski, and Spaulding, 1998]
Adams, Jim, Ken Parulski, and Kevin Spaulding (1998). “Color processing in digital cameras”. In: *IEEE micro* 6.6, pp. 20–30 (Cited on page 14).

[Alder, Chaing, Chong, et al., 1982]
Alder, C., K. P. Chaing, T. F. Chong, et al. (1982). “Uniform Chromaticity Scales - New Experimental Data”. In: *Journal of the Society of Dyers and Colourists* 98, pp. 14–20 (Cited on page 50).

[Alfvin and Fairchild, 1997]
Alfvin, Richard L. and Mark D. Fairchild (1997). “Observer Variability in Metameric Color Matches using Color Reproduction Media”. In: *Color Research and Application* 22.3, pp. 174–188 (Cited on page 111).

[Allen, 1966]
Allen, Eugene (1966). “Basic Equations Used in Computer Color Matching”. In: *J. Opt. Soc. Am.* 56.9, pp. 1256–1259 (Cited on page 3).

[Allen, 1980]
Allen, Eugine (1980). “Colorant Formulation and Shading”. In: vol. Optical Radiation Measurements, Volume 22. Academic Press, Inc. Chap. 7, pp. 289–336 (Cited on page 173).

[ANSI-CGATS21-1, 2013]
ANSI-CGATS21-1 (2013). *Graphic technology - Printing from digital data across multiple technologies - Part 1: Principles* (Cited on page 144).

[ANSI-CGATS21-2, 2013]
ANSI-CGATS21-2 (2013). *Graphic technology - Printing from digital data across multiple technologies - Part 2: Reference characterization data* (Cited on page 144).

[Arend and Reeves, 1986]
Arend, Lawrence and Adam Reeves (1986). “Simultaneous color constancy”. In: *J. Opt. Soc. Am. A* 3.10, pp. 1743–1751 (Cited on page 12).

[Arnold, Faruq, Savolainen, MCowan, and Chittka, 2010]
Arnold, Sarah EJ, Samia Faruq, Vincent Savolainen, Peter W. MCowan, and Lars Chittka (2010). “FReD: The Floral Reflectance Database - A Web Portal for Analyses of Flower Colour”. In: *PloS one* 5.2, e14287 (Cited on page 29).

[Asano, 2015]
Asano, Yuta (2015). “Individual Colorimetric Observers for Personalized Color Imaging”. PhD thesis. Rochester Institute of Technology (Cited on page 165).

[Asano, Fairchild, and Blonde, 2014]
Asano, Yuta, Mark D. Fairchild, and Laurent Blonde (2014). “Development of a vision model for individual colorimetric observers”. In: *Journal of Vision* 14.15, p. 52 (Cited on pages 61, 104, 108).

[Bala and Zhao, 2007]
Bala, Raja and Yonghui Zhao (2007). “Substrate Fluorescence: Bane or Boon”. In: *Fifteenth Color and Imaging Conference of the IS&T*. IS&T (Cited on page 144).

[Berns, 1982]
Berns, Roy S. (1982). *Personal communication between R. S. Berns and C. S. McCamy* (Cited on page 168).

[Berns, 1993]
Berns, Roy S. (1993). “The Mathematical Development of CIE TC 1-29 Proposed Color Difference Equation: CIELCH”. In: *AIC Color 1993 Proceedings* B.C19-1 (Cited on page 38).

[Berns, 2000]
Berns, Roy S. (2000). *Billmeyer and Saltzman’s Principles of Color Technology*. 3rd. John Wiley & Sons (Cited on pages 127, 130, 133, 177).

[Berns, 2014]
Berns, Roy S. (2014). “Extending CIELAB: Vividness, V*ab, Depth, D*ab, and Clarity, T*ab”. In: *Color Research and Application* 39.4, pp. 322–330 (Cited on page 16).

[Berns and Billmeyer, 1985]
Berns, Roy S. and Fred W. Billmeyer (1985). “Development of the 1929 Munsell Book of Color: A historical review”. In: *Color Research and Application* 10.4, pp. 246–250 (Cited on page 167).

[Berns and Peterson, 1988]
Berns, Roy S. and Kelvin H. Peterson (1988). “Empirical Modeling of Systemic Spectrophotometric Errors”. In: *Color Research and Application* 13.4, pp. 243–256 (Cited on pages 172, 173).

[Berns, Billmeyer, and Sacher, 1985]
Berns, Roy S., Fred W. Billmeyer, and Richard S. Sacher (1985). “Methods for generating spectral reflectance functions leading to color-constant properties”. In: *Color Research and Application* 10.2, pp. 73–83 (Cited on page 179).

[Berns, Alman, Reniff, Snyder, and Rosen, 1991]
Berns, Roy S., David H. Alman, Risa Reniff, Gregory D. Snyder, and Mitchel R. Rosen (1991). “Visual Determination of Suprathreshold Color-Difference Tolerances Using Probit Analysis”. In: *Color Research and Application* 16.5, pp. 297–316 (Cited on page 50).

[Brainard and Stockman, 2010]
Brainard, David H and Andrew Stockman (2010). “Handbook of Optics”. In: 10. Chap. Colorimetry (Cited on pages 106, 111, 115).

[Brill and Oleari, 2014]
Brill, Michael H. and Claudio Oleari (2014). “Chromatic Adaptation by Illuminant Matrix Products: An Alternative to Sharpened Von Kries Primaries”. In: *Color Research and Application* 39.3, pp. 275–278 (Cited on page 15).

[Chau, 1999]
Chau, Wing-Ki Wilkin (1999). “Colour Reproduction for Reflective Images”. PhD thesis. University of Waterloo (Cited on pages 9, 58, 124, 133, 134).

[Chen, 2011]
Chen, P. (2011). “Scanline Lightness Perception and Differences Above and Below Diffuse White and Modifying Color Spaces for High-Dynamic-Range Scenes and Images”. Masters Thesis for MS in Imaging Science. New York: Rochester Institute of Technology (Cited on page 50).

[CIE13, 1995]
CIE13 (1995). *Method of measuring and specifying colour rendering properties of light sources.* (Cited on page 74).

[CIE15, 1976]
CIE15 (1976). *Official Recomendations on Uniform Color Spaces, Color-Difference Equations, and Metric Color Terms* (Cited on page 134).

[CIE15, 2004]
CIE15 (2004). *Colorimetry* (Cited on pages 35, 38, 40, 45, 104).

[CIE170, 2006]
CIE170 (2006). *Fundamental Chromaticity Diagram with Physiological Axes - Part 1* (Cited on pages 7, 61, 104).

[Cohen, 2001]
Cohen, Jozef (2001). *Visual Color and color mixture: the fundamental color space*. Univerity of Illinois Press (Cited on pages 56, 57, 133).

[Derhak and Berns, 2012]
Derhak, Maxim and Roy S. Berns (2012). “Analysis and Correction of the Joensuu Munsell Glossy Spectral Database”. In: *Twentieth Color and Imaging Conference: Color Science and Engineering Systems, Technologies, and Applications*, pp. 191–194 (Cited on pages 4, 132, 133).

[Derhak and Rosen, 2004]
Derhak, Maxim and Mitchell Rosen (2004). “Spectral Colorimetry Using LabPQR - An Interim Connection Space”. In: *IS&T/SID Twelfth Color Imaging Conference*, pp. 246–250 (Cited on page 57).

[Donaldson, 1954]
Donaldson, R. (1954). “Spectrophotometry of fluorescent pigments”. In: *British Journal of Applied Physics* 5.6, p. 210 (Cited on pages 3, 34).

[Fairchild, 2013]
Fairchild, Mark D (2013). *Color appearance models*. Third Edition. John Wiley & Sons (Cited on page 134).

[Fairchild and Heckaman, 2013]
Fairchild, Mark D. and Rodney L. Heckaman (2013). “Metameric Observers: A Monte Carlo Approach”. In: *21st Color and Imaging Conference Final Program and Proceedings*. Society of Imaging Science and Technology, pp. 185–190 (Cited on pages 55, 61, 81, 104, 111, 116).

[Fairchild and Johnson, 2004]
Fairchild, Mark D. and Garrett M. Johnson (2004). “METACOW: A Public-Domain, High-Resolution, Fully-Digital, Noise-Free, Metameric, Extended-Dynamic-Range, Spectral Test Target for Imaging System Analysis and Simulation”. In: *Proceedings of the 12th Color Imaging Conference: Color Science and Engineerig, Scottsdale, AZ, USA*. Vol. 239-245. 1, p. 7 (Cited on page 150).

[Finlayson, Funt, and Jiang, 2003]
Finlayson, Graham D., Brian Funt, and Hao Jiang (2003). “Predicting Cone Quantum Catches Under Illuminant Change”. In: *Color and Imaging Conference*. Society of Imaging Science and Technology, pp. 170–174 (Cited on page 14).

[Finllayson, Hordley, and Hubel, 2001]
Finllayson, G. D., S. D. Hordley, and P. M. Hubel (2001). “Colour by Correlation: A Simple, Unifying Approach to Colour Constancy”. In: *IEEE Transactions on Pattern Analysis and Machine Intelligence* 23.11, pp. 1209–1221 (Cited on page 94).

[Foss, Nickerson, and Granville, 1944]
Foss, Carl E., Dorothy Nickerson, and Walter C. Granville (1944). “Analysis of the Ostwald Color System”. In: *J. Opt. Soc. Am.* 34.7, pp. 361–381 (Cited on page 59).

[Foster, 2011]
Foster, David H (2011). “Color constancy”. In: *Vision Res* 51.7, pp. 674–700 (Cited on pages 12, 13).

[Garcia, Huertas, Melgosa, and Cui, 2007]
Garcia, Pedro A., Rafael Huertas, Manuel Melgosa, and Guihua Cui (2007). “Measurement of the relationship between perceived and computed color differences”. In: *J. Opt. Soc. Am. A* 24.7, pp. 1823–1829 (Cited on pages 49, 50).

[Hotelling, 1936]
Hotelling, Harold (1936). “Simplified calculation of principal components”. In: *Psychometrika* 1.1, pp. 27–35 (Cited on page 57).

[Hou, 2010]
Hou, Bingxin (2010). “Extending the RIT-DuPont Suprathreshold Data Set: Weighted Individual Discriminaiton Pair Data and New Chroma Dependency Visual Data”. MS Imaging Science. Rochester, New York: Rochester Institute of Technology (Cited on page 50).

[Huang, Liu, Cui, and Luo, 2012]
Huang, Min, Haoxue Liu, Guihua Cui, and M. Ronnier Luo (2012). “Testing Uniform Colour Spaces and Colour-Difference Furmulae Using Printed Samples”. In: *Color Research and Application* 37.5, pp. 326–335 (Cited on page 50).

[Hunt, 2005]
Hunt, Robert W. G. (2005). *The Reproduction of Colour*. Sixth Edition. John Wiley & Sons (Cited on page 126).

[ICC, 2015]
ICC (2015). *Introducing iccMAX*. URL: http://www.color.org/iccmax.xalter (visited on May 9, 2015) (Cited on page 149).

[ISO, 2007]
ISO (2007). *Colorimetry* (Cited on page 104).

[Ives, 1915]
Ives, H. E. (1915). "The transformation of color-mixture equations from one system to another"". In: *J. Franklin Inst.* 16, pp. 673–701 (Cited on pages 25, 77, 106).

[Jiang, Liu, Gu, and Susstrunk, 2013]
Jiang, Jun, Dengyu Liu, Jinwai Gu, and Sabine Susstrunk (2013). "What is the space and spectral sensitivity functions for digital color cameras?" In: *Applications of Computer Vision (WACV), 2013 IEEE Workshop on*. IEEE, pp. 168–179 (Cited on pages 7, 82, 90).

[Kang, 2006]
Kang, Henry R. (2006). *Computational Color Technology*. SPIE Press (Cited on pages 14, 88).

[Klein, 2010]
Klein, Georg A. (2010). *Industrial Color Physics*. Springer (Cited on page 45).

[Koenderink, 1987]
Koenderink, Jan J. (1987). "Color atlas theory". In: *J. Opt. Soc. Am. A* 4.7, pp. 1314–1321 (Cited on page 134).

[Kohonen, Parkkinen, and Jääskeläinen, 2006]
Kohonen, Oili, Jussi Parkkinen, and Timo Jääskeläinen (2006). "Databases for Spectral Color Science". In: *Color Research and Application* 31.5, pp. 381–390 (Cited on pages 4, 29).

[Krantz, 1975]
Krantz, David H. (1975). "Color Measurement and Color Theory: 1. Representation Theorom for Grassmann Structures". In: *Journal of Mathematical Biology* 12, pp. 283–303 (Cited on page 104).

[Li and Berns, 2007]
Li, Zhaojian and Roy S. Berns (2007). "Comparison of methods of parameric correction for evaluating metamerism". In: *Color Research and Application* 32.4, pp. 293–303 (Cited on pages 130, 176).

[Logvinenko, 2009]
Logvinenko, Alexander D (2009). "An object-color space". In: *J Vis* 9.11, pp. 5.1–5.23 (Cited on pages 14, 26).

[Logvinenko, 2013]
Logvinenko, Alexander D. (2013). "Object-Colour Manifold". In: *International Journal of Computer Vision* 101.1, pp. 143–160 (Cited on pages 1, 13, 25, 26, 54, 55, 60).

[Logvinenko and Beer, 2012]
Logvinenko, Alexander D and Anja Beer (2012). "Color constancy investigated via partial hue-matching". In: *J Vis* 12.4 (Cited on pages 8, 33, 35, 52).

[Logvinenko and Tokunaga, 2011]
Logvinenko, Alexander D and Rumi Tokunaga (2011). “Colour constancy as measured by least dissimilar matching”. In: *Seeing Perceiving* 24.5, pp. 407–452 (Cited on pages 13, 26, 33, 88).

[Luo, 2000]
Luo, M. Ronnier (2000). “A review of chromatic adaptation transforms”. In: *Review of Progress in Coloration and Related Topics* 30.1, pp. 77–92 (Cited on pages 12, 88).

[Luo, Cui, and Rigg, 2001]
Luo, M. Ronnier, G. Cui, and B. Rigg (2001). “The Development of the CIE 2000 Colour-Difference Formula: CIEDE2000”. In: *Color Research and Application* 26.5, pp. 340–350 (Cited on pages 38, 172).

[Luo, Cui, and Li, 2006]
Luo, M. Ronnier, Guihua Cui, and Changjun Li (2006). “Uniform Colour Spaces Based on CIECAM02 Colour Appearance Model”. In: *Color Research and Application* 31.4, pp. 320–330 (Cited on pages 35, 45).

[Luther, 1927]
Luther, R. (1927). “Aus dem Gebiet der Farbreizmetrik (On color stimulus metrics)”. In: *Zeitschrift für technische Physik* 8, pp. 540–558 (Cited on pages 25, 77, 106).

[McCann, 2006]
Ideal Illuminants for Rod /L-Cone Color (2006). Vol. 6058, pp. 605801–605801–8 (Cited on page 85).

[McLaren, 1976]
McLaren, K. (1976). “The Development of the CIE 1976 (L*a*b*) Uniform Colour Space and Colour-difference Formula”. In: *Journal of the Society of Dyers and Colourists* 92.9, pp. 338–341 (Cited on page 6).

[Mintz, 2009]
Mintz, Eliezer (2009). “A Physicalist Relationist Theory of Color”. PhD thesis. Rutgers University-Graduate School-New Brunswick (Cited on pages 3, 54).

[Mirzaei and Funt, 2011]
Mirzaei, Hamid and Brian Funt (2011). “Gaussian-metamer-based predictoin of colour sitmulus change under illuminant change”. In: *AIC 2011 Miterm Meeting - Interaction of colour & light in the arts and sciences*. Zurich, pp. 585–588 (Cited on page 14).

[Moroney, Fairchild, Hunt, et al., 2002]
Moroney, Nathan, Mark D. Fairchild, Robert W. G. Hunt, et al. (2002). “The CIECAM02 Color Appearance Model”. In: *Proceedings of the IS&T/SID 10th Color Imaging Conference*, pp. 23–27 (Cited on pages 14, 35, 45, 168).

[Morovic, 2008]
Morovic, Jan (2008). *Color gamut mapping*. John Wiley & Sons (Cited on page 128).

[Nayatani, Yano, and Ihara, 2002]
Nayatani, Yoshinobu, Tadashi Yano, and Masamori Ihara (2002). “Analyses of Methods for Predicting Corresponding Colors of LUTCHI data”. In: *Color Research and Application* 28.5, pp. 335–348 (Cited on page 29).

[Nemcsics, 2002]
Nemcsics, Antal (2002). “Coloroid Colour System”. In: *HEJ: ARC-03520-A* (Cited on page 59).

[Newhall, 1940]
Newhall, Sidney M. (1940). “Preliminary Report of the O.S.A. Subcommittee on the Spacing of the Munsell Colors”. In: *J. Opt. Soc. Am.* 30.12, pp. 617–645 (Cited on pages 18, 35).

[Newhall, Nickerson, and Judd, 1943]
Newhall, Signey M., Dorothy Nickerson, and Deane B. Judd (1943). “Final Report of the O.S.A Subcommittee on the Spacing of the Munsell Colors”. In: *J. Opt. Soc. Am.* 33.7, pp. 385–411 (Cited on pages 4, 35, 167).

[Nickerson, 1960]
Nickerson, Dorothy (1960). “Light Sources and Color Rendering”. In: *J. Opt. Soc. Am.* 50.1, pp. 57–69 (Cited on page 74).

[Oleari, 2005]
Oleari, Claudio (2005). “Hypotheses for Chromatic Opponency Functions and Their Performance on Classical Psychophysical Data”. In: *Color Research and Application* 30.1, pp. 31–41 (Cited on page 14).

[Oleari, 2014]
Oleari, Claudio (2014). “Corresponding color datasets and a chromatic adaptation model based on the OSA-UCS system”. In: *J. Opt. Soc. Am. A* 31.7, pp. 1502–1514 (Cited on pages 15, 16).

[Oleari, Melgosa, and Huertas, 2009]
Oleari, Claudio, Manuel Melgosa, and Rafael Huertas (2009). “Euclidean color-difference formula for small-medium color differences in log-compressed OSA-UCS space”. In: *J. Opt. Soc. Am. A* 26.1, pp. 121–134 (Cited on pages 15, 89).

[Oleari, Melgosa, and Huertas, 2011]
Oleari, Claudio, Manuel Melgosa, and Rafael Huertas (2011). “Generalization of color-difference formulas for any illuminant and any observer by assuming perfect color constancy in a color-vision model based on the OSA-UCS system”. In: *J. Opt. Soc. Am. A* 28.11, pp. 2226–2234 (Cited on pages 15, 29).

[Orava, 2012]
Orava, Joni (2012). *The reflectance spectra of 1600 glossy Munsell color chips*. URL: `http://www.uef.fi/en/spectral/munsell-colors-glossy-all-spectrofotometer-measured` (visited on Nov. 22, 2014) (Cited on pages 57, 64, 168).

[Peyvandi and Amirshahi, 2011]
Peyvandi, Shahram and Seyed Hossein Amirshahi (2011). “Generalized spectral decomposition: a theory and practice to spectral reconstruction”. In: *J. Opt. Soc. Am. A* 28.8, pp. 1545–1553 (Cited on page 56).

[Pridmore, 2010]
Pridmore, Ralph W. (2010). “Color Constancy from Invariant Wavelength Ratios: III. Chromatic Adaptation Theory, Model and Tests”. In: *Color Research and Application* 35.6, pp. 425–442 (Cited on pages 16, 20).

[Rea and Freyssinier, 2010]
Rea, M.S. and J.P. Freyssinier (2010). “Color Rendering: Beyond Pride and Prejudice”. In: *Color Research and Application* 35.6, pp. 401–409 (Cited on page 74).

[Riemann and Clifford, 1873]
Riemann, Bernhard and William Kingdon Clifford (1873). “On the Hypotheses which lie at the Bases of Geometry”. In: *Nature* 8.183,184, pp. 14–17, 36, 37 (Cited on page 54).

[Rodriguez, 2013]
Rodriguez, Michael (2013). *Personal communication between M. W. Derhak and M. Rodriguez* (Cited on page 144).

[Royer, Houser, and Wilkerson, 2012]
Royer, M. P., K. W. Houser, and A. M Wilkerson (2012). “Color Discrimination Capability Under Highly Structured Spectra”. In: *Color Research and Application* 37.6, pp. 441–449 (Cited on page 74).

[Sarkar, Autrusseau, Vienot, Callet, and Blonde, 2011]
Sarkar, Abhijit, Florent Autrusseau, Francoise Vienot, Patrick Le Callet, and Laurent Blonde (2011). “From CIE 2006 Physiological Model to Improved Age- Dependent and Average Colorimetric Observers”. In: *J. Opt. Soc. Am. A* 28.10, pp. 2033–2048 (Cited on pages 61, 104).

[Shamey, Sedito, and Kuehni, 2010]
Shamey, Renzo, Michael G. Sedito, and Rolf G Kuehni (2010). “Comparison of Unique Hue Stimuli Determined by Two Different Methods Using Munsell Color Chips”. In: *Color Research and Application* 35.6, pp. 419–424 (Cited on page 16).

[Smithson, 2005]
Smithson, H E (2005). “Sensory, computational and cognitive components of human colour constancy”. In: *Philos Trans R Soc Lond B Biol Sci* 360.1458, pp. 1329–1346 (Cited on page 89).

[Stockman and Sharpe, 2000]
Stockman, A and L T Sharpe (2000). “The spectral sensitivities of the middle- and long-wavelength-sensitive cones derived from measurements in observers of known genotype”. In: *Vision Res* 40.13, pp. 1711–1737 (Cited on page 55).

[Stockman, Sharpe, and Fach, 1999]
Stockman, A, L T Sharpe, and C Fach (1999). “The spectral sensitivity of the human short-wavelength sensitive cones derived from thresholds and color matches”. In: *Vision Res* 39.17, pp. 2901–2927 (Cited on page 55).

[Stockman and Sharpe, 1999]
Stockman, Andrew and Linsay T. Sharpe (1999). “Cone spectral sensitivities and color matching”. In: *Color vision: From genes to Perception*. Cambridge U. Press, Cambridge, UK, pp. 53–88 (Cited on page 55).

[Susstrunk, 2005]
Susstrunk, Sabine (2005). “Computing Chromatic Adaptation”. PhD thesis. University of East Anglia, Norwich: School of Computing Sciences (Cited on page 6).

[Tonnquist, 1986]
Tonnquist, Gunner (1986). “Philosophy of Perceptive Color Order Systems”. In: *Color Research and Application* 11.1, pp. 51–55 (Cited on pages 16, 34, 35).

[vonKries, 1970]
vonKries, Johannes (1970). “Sources of Color Science”. In: The MIT Press. Chap. Chromatic Adaptation, pp. 145–158 (Cited on pages 5, 33).

[Vos, 1978]
Vos, J. J. (1978). “Colorimetric and photometric properties of a 2-degree Standard Observer”. In: *Color Research and Application* 3, pp. 125–128 (Cited on page 78).

[Wright, 1981]
Wright, W. D. (1981). “Why and How Chromatc Adaptation Has Been Studied”. In: *Color Research and Application* 6.3, pp. 147–152 (Cited on pages 13, 89).

[Wright, 1982]
Wright, W. D. (1982). “The Golden Jubilee of Colour in the CIE 1931-1981*”. In: *Color Research and Application* 7.1, pp. 12–15 (Cited on pages 105, 106).

[Wyszecki, 1953]
Wyszecki, Gunter (1953). ““Valenzmetrische Untersuchung des Zusammenhanges zwischen normaler und anomaler Trichromasie (Psychophysical investigation of relationship between normal and abnormal trichromatic vision)”. In: *Die Farbe* 2, pp. 39–52 (Cited on pages 9, 56, 124).

[Wyszecki and Stiles, 2000]
Wyszecki, Gunter and W. S. Stiles (2000). *Color Science - Concepts and Methods, Quantitative Data and Formulae*. second. Wiley Interscience (Cited on pages 1, 3, 56, 57, 61, 78, 104, 116, 177).